Seismic analysis of the Niger Delta gravitational detachment system

DOMINIC PETER MALONEY

Department of Earth Sciences, Durham University

Seismic analysis of the Niger Delta gravitational detachment system

Submitted to Durham University for the degree of Doctor of Philosophy in the Faculty of Science

Dominic Maloney

2011

Abstract

Ductile deformation of overpressured, fine-grained, argillaceous sediments ("mobile shale") is commonly invoked to explain the deformation style at the base of thin-skinned, gravitational detachment systems. The usage of "mobile shale" arose as a consequence of poor imaging on seismic reflection data, where low-resolution seismic intervals appeared ductile on a seismic scale (a thickening and thinning of the seismic interval). Acquisition of high-quality seismic reflection data from the Niger Delta provides an opportunity to investigate the internal structures within a basal detachment succession that is commonly referred to as the "mobile shale."

Deformation within the basal detachment succession in down-dip compressional settings is characterised by brittle deformation. Thickening of the basal detachment succession occurs through contractional duplexes and stacked imbricates that have formed within the cores of detachment folds. In up-dip extensional settings, the formation of stacked master detachment faults and detachments, which splay off the pre-existing master detachment fault, incorporates structures that formed in the hanging wall of older, structurally lower detachment faults into the basal detachment succession. Plastic deformation that involves a complete loss of shear strength within the deforming sediment probably does occur. Such processes are invoked to explain the lateral redistribution of strata leading to the formation of a "shale weld" in down-dip compressional settings.

The recognition of fault-related folding within detachment fold cores and the deformation imaged beneath a major listric fault system highlights the fact that end-member structural models do not always adequately capture the structural complexity at the base of gravitational detachment systems. Despite the overpressured signature of basal detachment successions composed of argillaceous sediments, overpressure is not synonymous with a wide-spread ductile deformation style. Therefore, the term "mobile shale" – although widely used – inaccurately represents the styles and types of the deformational processes that occur within basal detachment successions composed of overpressured, argillaceous sediments.

Table of Contents

List of figures

Chapter 1

Chapter 2

Chapter 3

Chapter 4

Chapter 5

Chapter 6

Appendices

List of tables

Appendices

Acknowledgements

First and foremost I would like to thank my supervisors Richard Davies, Jonathan Imber and Steve King. Their enthusiasm, motivation and guidance have been inspirational in helping me complete my time here at Durham University. I am entirely grateful to Richard Davies for setting up the project with BG Group as without his initial efforts this project would not exist. I would also like to thank BG Group who allowed a substantial amount of research to be done at their offices in Reading. In particular, I am extremely grateful to Steve King, Rishiraj Gupta, Allan Foum and Javier Cortes of BG Group who helped organise and setup the project at BG Group, which was not part of the original Ph.D. plan.

In addition I am grateful to those who reviewed copies of manuscripts and provided helpful discussions. I am grateful to Joe Cartwright, Richard Groshong, Lorena Moscardelli, Chris Morley and Nancye Dawers who all gave their time to review copies of papers.

I am thankful for my funding provided by NERC (reference number NE/F008015/1) Open CASE Studentship with BG Group, and to those who provided the data on which this study was based. Petroleum Geo-Services (PGS), CGGVertitas and BG Group provided the seismic data, and Landmark and BG Group provided the seismic interpretation software.

Finally, I would like to thank all my family and friends especially Gloria and Calum who have always supported and backed all of my decisions.

Declaration

No part of this thesis has previously been submitted for a degree at this or any other university. The work described in this thesis is entirely that of the author, expect where reference is made to previously published or unpublished work.

1 Introduction

1.1 Rationale

Large deltas are widely distributed over passive and active continental margins and can exhibit deformation styles typical of gravity-driven deformation (e.g. Morley, 2003; Rowan et al., 2004). Deformation can be driven by an interaction between differential loading, gravity gliding and gravity spreading (Schultz-Ela, 2001; Morley; 2003; Rowan et al., 2004) (see appendix 1, glossary). Gravity-driven deformation results in the horizontal translation of sediments that are being deformed with an associated loss of gravitational potential energy within the deforming sedimentary strata (Schultz-Ela, 2001; Rowan et al., 2004). At the base of these laterally sliding sediments lies a basal detachment succession (also referred to as basal detachment unit) (see appendix 1, glossary), which is either composed of salt or overpressured, fine-grained argillaceous sediments (Rowan et al., 2004). Basal detachment successions composed of salt are found in the Gulf of Mexico (Rowan, 1997), offshore Angola (Fort et al., 2004) and the Nile deep sea fan (Gaullier et al., 2000; Loncke et al., 2004). Basal detachment successions composed of overpressured, argillaceous sediments occur in the Niger Delta (Morley and Guerin, 1996; Corredor et al., 2005; Briggs et al., 2006), the Amazon Fan (Cobbold et al., 2004), parts of the Gulf of Mexico (Weimer and Buffler, 1992), offshore Trinidad and Venezula (Moscardelli et al., 2006) and in many other regions (see Fig. 1.1). Despite extensive hydrocarbon exploration activities over large deltas, few studies have focussed on the internal architecture and the spatial and temporal evolution of basal detachment successions composed of overpressured, argillaceous sediments. Understanding the internal architecture and the types of processes that operate within basal detachment successions is currently a major challenge. Although numerous seismic surveys have been shot over large deltas research into basal detachment successions themselves has been, and continues to be, hampered by poor seismic imaging. As a consequence, many uncertainties and unanswered questions remain with regards to the types of deformational processes and structural styles that occur within basal detachment successions composed of overpressured, argillaceous sediments.

This study focuses on a basal detachment succession composed of fine-grained, argillaceous sediments using multiple, marine seismic data sets from the gravitational detachment system of the Niger Delta (see section 2.1 for geological setting). It uses high-quality three-dimensional (3D) and two-dimensional (2D) seismic reflection data to analyse 1) the structural architecture of a basal detachment succession, 2) how basal detachment successions evolve and interact with overlying sediments being deformed by gravitational processes, 3) the deformational mechanisms and processes that control and influence the rheology of a basal detachment succession composed of argillaceous sediments.

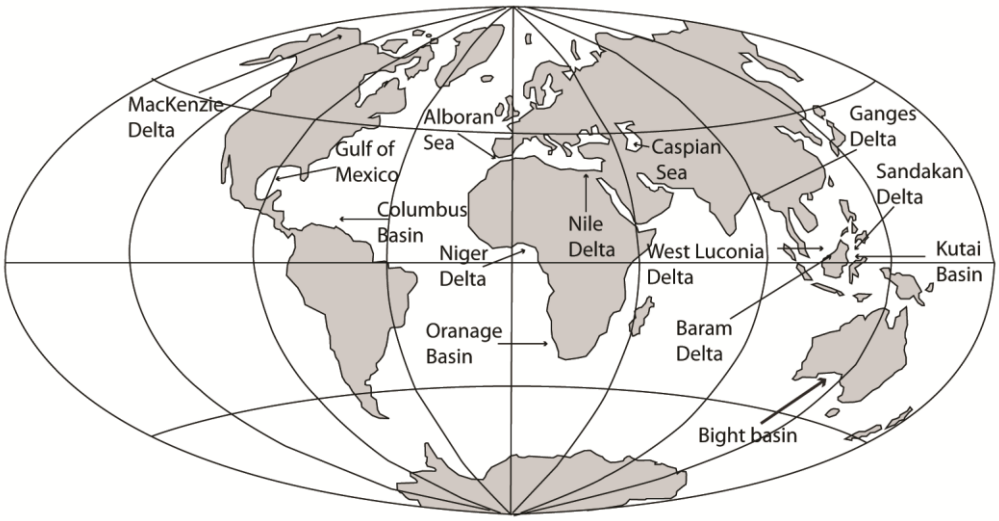

Fig. 1.1. Location map showing the global locations of major shale tectonic provinces associated with deltas (from Morley, 2003).

1.2 Thesis aims

- To analyse the types and styles of deformational processes that operate within an argillaceous, overpressured basal detachment succession in up-dip extensional and down-dip contractional settings in the Niger Delta. Does a basal detachment succession composed of fine-grained, overpressured, argillaceous sediments conform to the concept of "mobile shale"?
- To determine the structural style of an overpressured basal detachment succession composed of argillaceous sediments and to analyse the interaction

and influence that such a succession has on deformation styles within an overlying sedimentary overburden.

- To constrain the relative timings of deformation that occurs within the basal detachment succession and deformation within the sedimentary overburden.
- To provide insights and reveal, where possible, the deformational mechanisms and processes by which argillaceous basal detachment successions are able to thicken and thin, providing an explanation for the apparent ductility of these successions.
- To determine, where possible, the structural architecture of the basal detachment succession.
- To determine whether structural models developed for gravitational systems that involve having a ductile succession at their base are always applicable to gravitationally-driven detachment systems.

1.3 Terminology

1.3.1 "Mobile shale"

Shales are defined as mud-rich, fine-grained, laminated sedimentary rocks that are fissile, and are deposited under suspension in quiet depositional settings (Potter et al., 1980; Gutierrez et al., 2008) (see appendix 1, glossary). In the case of the commonly used term "shale tectonics," however, we are dealing with the deformation of argillaceous and siliciclastic sediments including clays, muds, silts and sandstones. "Shale tectonics" and "mobile shale" (see appendix 1, glossary) are convenient terms used to capture the large-scale deformation of thick accumulations of overpressured, argillaceous sediments (see appendix 1, glossary). The term "mobile shale" is commonly applied to an amalgamation of siliciclastic sediments that are dominantly argillaceous and show apparent ductility at the scale of seismic observation (i.e. on a metre or kilometre-scale). The terms "ductile" and "ductility" (see appendix 1, glossary) are used as defined by Rutter (1986) who states: "ductility only describes the capacity of a material to deform to a substantial strain without the tendency to localise the flow into faults", and as such does not state a deformational mechanism. The terms "shale tectonics" and "mobile shale" are those that have been used in the literature over the past five decades and therefore rather than derive alternative

terminology, the terms are employed to some extent in this thesis. In this thesis "shale" refers to successions that are likely to represent argillaceous, fine-grained siliciclastic sediments.

The study of shale tectonics has led to the development of a plethora terms used to describe structural features associated with the withdrawal and rise of what is considered to be mobile shale (these are dealt with in section 1.11). One of the most commonly used terms is "shale diapir," ("diapiric structure") (see appendix 1, glossary), which is often applied to domal structures characterised by areas of low reflectivity on seismic reflection data (e.g. Morley, 2003). The interpretation of "shale diapirs" is open to some subjectivity (section 1.11.2) and numerous uncertainties are linked to the actual processes that form "diapiric structures" (e.g. liquefaction, fluidized flow (section 1.9.1) unconfined cataclastic flows (section 1.9.3) (see appendix 1, glossary)) (e.g. Maltman and Bolton, 2003).

1.3.2 Basal detachment succession (basal detachment unit)

The gross architecture of deltas on passive margins can be separated into two main components: 1) an upper sedimentary succession that is undergoing gravitational failure (Rowan et al., 2004), which is referred to as the sedimentary overburden (see appendix 1, glossary); 2) an underlying, relatively undeformed (passive) sedimentary succession, which may or may not display evidence of ductility (thickening and thinning of the succession) (Fig. 1.2). This underlying sedimentary succession is referred to as the basal detachment succession (or basal detachment unit). Basal detachment successions composed of thick accumulations of overpressured, fine-grained sediments form an effective mechanical discontinuity, which facilitates the horizontal translation of strata undergoing gravitational failure in the sedimentary overburden. The weak mechanical strength of basal detachment successions allows them to act as effective structural detachments for thin-skinned deformation (see appendix 1, glossary), which is characteristic of the sedimentary overburden (Fig. 1.2). "Detachment system" (see appendix 1, glossary) is a term that describes the large-scale, thin-skinned deformation style and architecture of a gravity-driven tectonic province where the majority of deformation detaches upon or within the

basal detachment succession. "Thin-skinned" deformation means that the basement is not involved in deformation.

1.4 Review of shale tectonic detachment systems

1.4.1 Introduction

Since the 1970s the concept of mobile shale, the ductile deformation of fine-grained argillaceous sediments, has been used in close association with the interpretation of seismic reflection data from basins where thin-skinned detachment occurs on a basal detachment succession of overpressured shale (Bruce, 1973; Buryakovsky et al., 1995; Van Rensbergen et al., 2003; Brown et al., 2004; Deville et al., 2006; Stewart and Davies, 2006). Shale tectonics occurs in a variety of settings. These include deltaic provinces, such as the Niger (Corredor et al., 2005; Cobbold et al., 2009); Baram (Tingay et al., 2009) and Nile (Badri et al., 2000) deltas, regions of compressional stress (e.g. Van Rensbergen et al., 2003), such as accretionary prisms (e.g. Deville et al., 2006), and sag basins, such as the Caspain Sea (e.g. Davies and Stewart, 2005; Stewart and Davies, 2006) (e.g. Fig. 1.1). Direct evidence for the presence of overpressured, fine-grained argillaceous sediments deep within the subsurface comes from 1) mud volcanoes (e.g. Graue, 2000; Stewart and Davies, 2006; Roberts et al., 2010), 2) pressure tests taken during drilling (Fig. 1.3), 3) drilling blowouts caused by the intersection of overpressured successions that could not be controlled. Indirect evidence comes from significant reductions in seismic stacking velocities recorded in velocity-depth profiles deep within the subsurface (e.g. sections 1.8 and 2.5), wireline logging and on occasions a low-resolution seismic facies on seismic reflection data (e.g. section 1.8). In the literature the term mobile shale is used interchangeably as both an interpretation, to imply a type of ductile deformational process, and as a description for a particular type of seismic facies. On seismic reflection data what is described as mobile shale is characterised by seismic intervals of limited or no reflectivity which internally contain chaotic and discontinuous reflections (e.g. Cohen and McClay, 1996; Morley, 2003; Corredor et al., 2005).

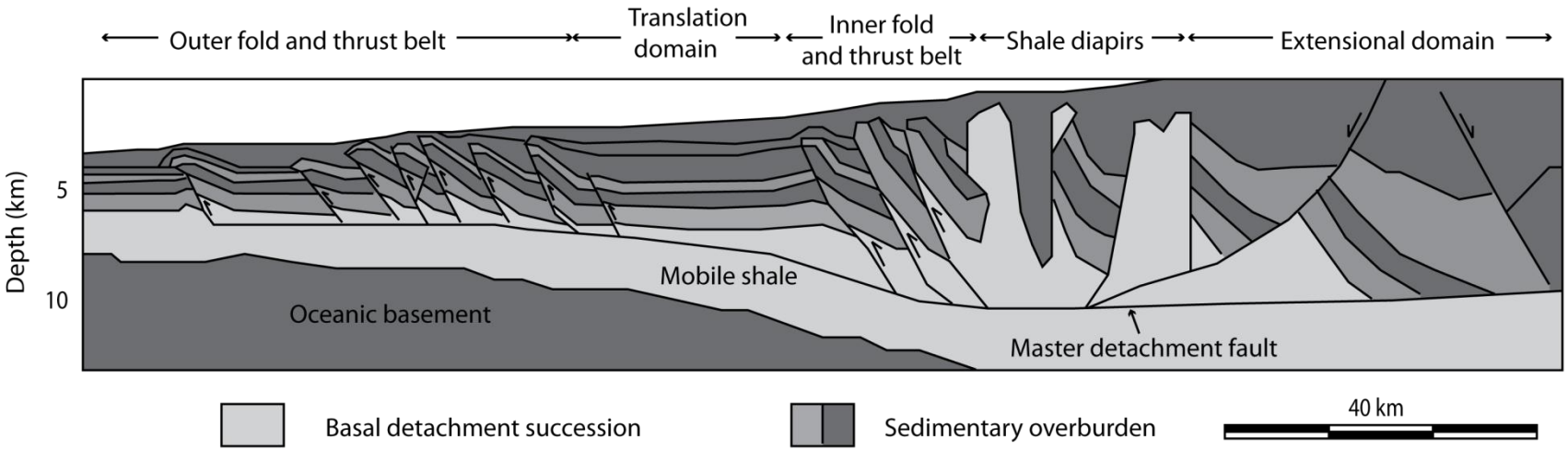

Fig. 1.2. Cross-section through the Niger Delta showing the gross architecture and structural style that is typical to large deltas situated on passive margins. In the case of the Niger Delta the basal detachment succession is dominantly composed of overpressured, fine-grained, argillaceous sediments (labelled mobile shale). The sedimentary overburden lies above the basal detachment succession and is heavily deformed with structural detachment occurring both upon and within the basal detachment succession (from Corredor et al., 2005). Vertical exaggeration = 2x.

The pioneers of shale tectonic studies worked on describing deformation styles from the Gulf of Mexico and the Niger Delta (e.g. Musgrave and Hicks, 1966; Morgan et al., 1968; Pennebaker, 1968; Bruce, 1973; Evamy, 1978) and many of the original ideas and concepts that they proposed are entrained in the literature. Although the usage of mobile shale as an interpretation is widespread the semantics of what mobile shale actually means (the deformational connotations it implies or alludes to) are still not clearly defined. This has enabled the label "mobile shale" to be applied ubiquitously to areas of low seismic reflectivity in shale tectonic provinces globally. Our understanding of the deformational processes associated with mobile shale in the deep subsurface is still relatively unconstrained and so many uncertainties surrounding mobile shale remain. Pioneering works on mobile shale inferred rheological similarities with salt due to the similar deformation styles of salt and shale tectonic provinces observed on seismic reflection data (e.g. Bruce, 1973; Evamy, 1978). Consequently, due to the entrainment of these original ideas in the literature, some still consider the rheology between mobile shale and salt to be similar despite studies later highlighting the differences (e.g. Weijermars et al., 1993; Morley and Guerin, 1996; Deville et al., 2010). Currently, mobile shale is considered to move in some form of sediment-water mixture where the moving sediment particles are supported by displaced pore-fluids (e.g. Einsele et al., 1974; Maltman, 1994; Deville et al., 2010).

The following sections of this chapter provide a review on the following aspects of shale tectonics: 1) the deformation of shale; 2) overpressure generation mechanisms; 3) deformational styles and characteristics associated with mobile shale; 4) how the presence of a basal detachment succession composed of overpressured, fine-grained argillaceous sediments can influence deformation styles within large deltas.

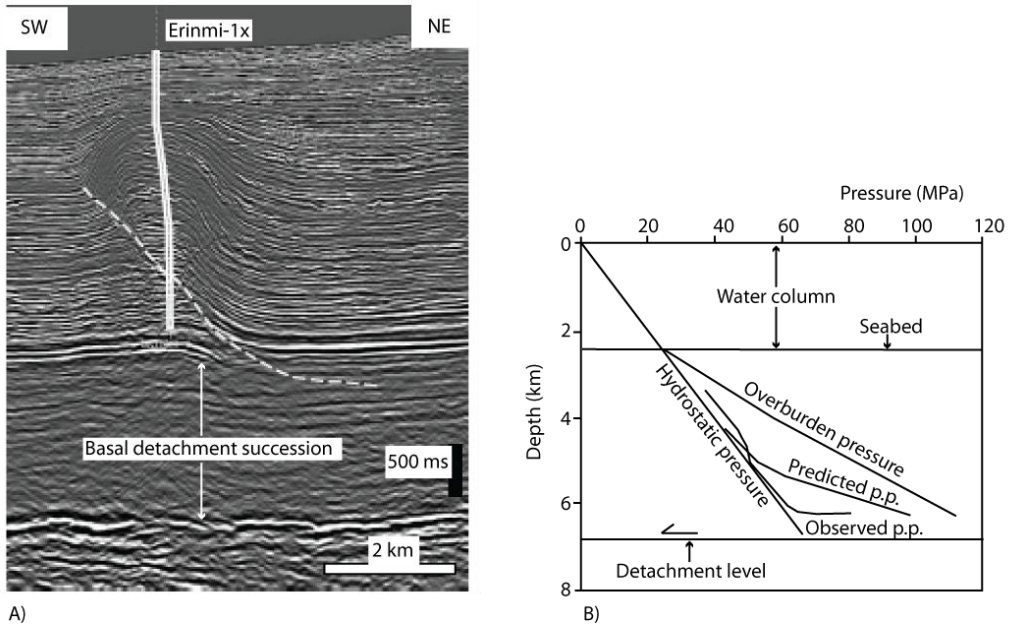

Fig. 1.3. A) Seismic line showing the pathway of borehole Erinmi-1x through a fault-related anticline in the deep-water fold and thrust belt of the Niger Delta (VE = 1.5x) and B) pressure-depth plot for well Erinmi-1x. The pressure data compares direct (observed pore-fluid pressures from pressure tests) and indirect (predicted pore-fluid pressures from seismic stacking velocities) evidence for the presence of overpressured sediments within the basal detachment succession (from Cobbold et al., 2009, their figure 9). The observed pore-fluid pressure increases significantly just before the onset of the basal detachment succession. p.p. = pore-fluid pressure.

1.5 Deformation of shale

The deformational response of shale is controlled by its mineralogy, shear strength, the degree to which pore-fluids are overpressured and the effective confining pressure it is subjected to (e.g. Einsele et al., 1974; Potter et al., 1980; Ibanez and Kronenberg, 1993; McClay et al., 2003; Nygard et al., 2006) (Figs. 1.4 and 1.5) (see appendix 1, glossary). Shale will deform when its shear strength is exceeded by an applied shear stress (see appendix 1, glossary). The shear strength of shale is a function of its frictional coefficient and cohesion, and the effective stress (section 1.5.1) (see appendix 1, glossary). The magnitude of shear stress that can be sustained by sediments is limited by their shear strength as shear failure serves to maintain the shear stress below the failure condition (Maltman, 1994). Therefore sediments cannot sustain shear stresses that exceed the shear strength. During

deposition and compaction (section 1.6) sediments gain resistance to an applied shear stress. As sediment particles are deposited electrostatic bonds are generated and a physical cohesion is imparted to the sediment and so grain to grain movement involves intergrain friction (Maltman, 1994). The peak shear strength is the maximum shear stress sediment can sustain at the point failure occurs. The relationship between these parameters can be expressed with the Mohr-Coulomb equation (Equation 1.1)

$$\tau = C + \sigma_n \tan \phi \qquad \text{Equation 1.1}$$

where τ is the maximum shear stress sustained at the point of maximum resistance, σ_n is the component of stress acting normal to the plane of failure, C the cohesion and ϕ the angle of internal friction. The strength parameter of ϕ and C can be determined through laboratory experiments under a range of effective pressures allowing a failure criterion to be established (Nygard et al., 2006).

Fracture formation is characterised by hydraulic (tensile), shear or mixed tensile-shear fractures and their formation is governed by the fracture criterion (e.g. Jaeger et al., 2007) (Fig. 1.4.). Hydraulic fracture (see appendix 1, glossary) occurs when the pore-fluid pressure exceeds the minimum stress and tensile strength of the rock (Sibson, 2003; Yassir, 2003; Jaeger et al., 2007) (Fig. 1.4, point A).

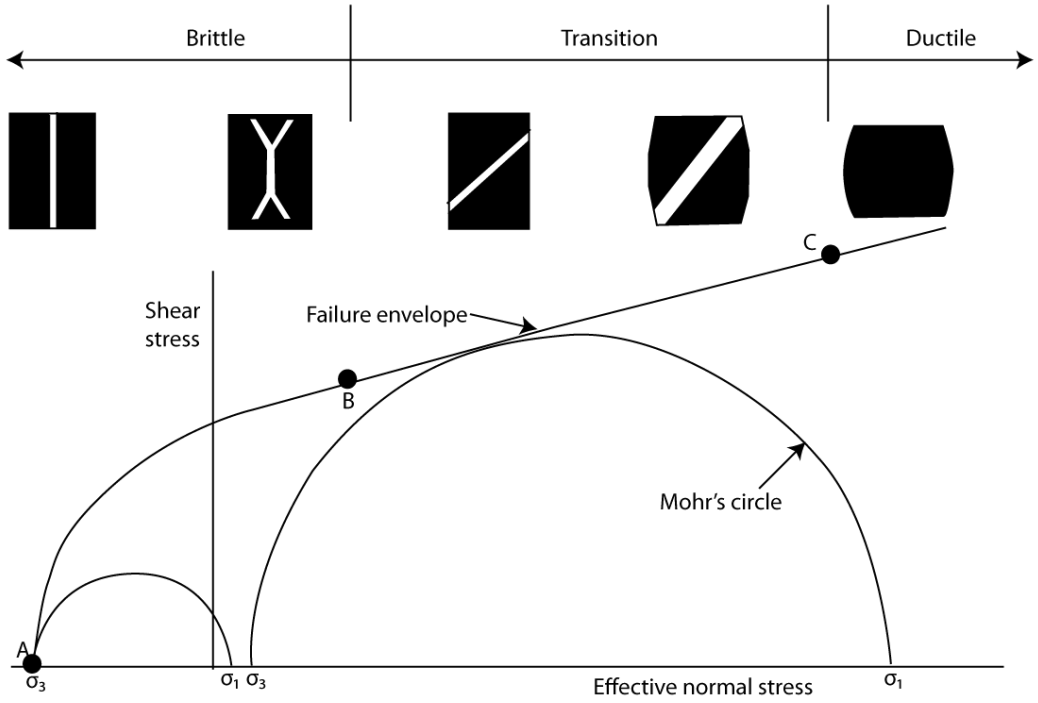

Fig. 1.4. Mohr diagram depicting the possible modes of failure (from Nygard, 2006). At high confining stresses shear strain becomes pervasive and diffusive (see text for explanation).

Shear failure occurs when loading creates shear stresses of a great enough magnitude to overcome the shear strength of the rock (Nygard et al., 2006). However, shear failure does not always result in the formation of a distinct fracture surface. Fracture formation is also controlled by the material's tendency to deform in a plastic or brittle manner in addition to the magnitude of the effective confining stress (Jaeger et al., 2007). Brittle failure is likely to occur when a lithology is stiff, having a high shear strength (Nygard et al., 2006). Ductile failure is characterised by diffusive deformation which penetrates throughout the deforming body without the formation of a distinct fracture surface (Rutter et al., 1986; Jaeger et al., 2007). At high effective confining pressures fracture formation can be retarded, as higher differential stresses (Equation 1.7) are required to induce fracture and so the rock will show a tendency towards ductile failure, as shown schematically in figure 1.4 (Nygard, 2006; Jaeger et al., 2007). In contrast, shear failure is characterised by a dilative response and sudden failure at a peak shear strength (Nygard et al., 2006; Jaeger et al., 2007). In the case of mobile shale the deforming shale is considered as

a purely plastic material (see appendix 1, glossary) whose rheological behaviour is independent of strain rate (Rowan et al., 2004). Sediments behaving as plastic materials undergo permanent changes in shape without fracturing (Maltman, 1994).

The influence of effective confining stress on the mode and style of deformation is shown by the Mohr diagram in figure 1.4 (from Nygard et al., 2006), which shows the forms of tensile and shear failure surface for sedimentary rocks. Three types of fracture are shown 1) tensile fractures at point A, which form when the minimum effective stress becomes negative as the pore-fluid pressure exceeds the tensile strength of the rock and the minimum effective stress, 2) mixed tensile-shear fractures between points A to B at low confining stresses, and 3) shear fractures between points B to C at higher confining pressure. At high effective confining stresses (above point C in Fig. 1.4) shear surfaces become less distinct as the material prefers to deform in a ductile manner.

1.5.1 The role of pore-fluids in the mobility of argillaceous sediments

When a vertical load is applied to a rock volume the resultant stress that acts through that volume can be separated into its effective and pore-fluid pressure components (Terzaghi, 1923; Dickinson, 1953) (see appendix 1, glossary). The proportion of an applied load that is sustained by the mineral skeleton is the effective stress, whereas the portion of the load that is sustained by the pore-fluids is the pore-fluid pressure (Terzaghi, 1923). The vertical stress (S) acting on sediments at a specific depth is given by Equation 1.2 (Terzaghi, 1923):

$$S = z \cdot \rho \cdot g \qquad \text{Equation 1.2}$$

Where z represents the sediment thickness, ρ the rock density and g the acceleration due to gravity. Where pore-fluids are likely to be overpressured (see appendix 1, glossary) as in shale tectonic provinces the effective stress should be taken into consideration. As rocks are compressed vertically with burial the resulting change in

rock porosity is controlled by the change in the effective vertical stress (Terzaghi, 1923). Terzaghi's principle (Terzaghi, 1923) is defined by: (Equation 1.3).

$$\sigma' = S - Pp \qquad \text{Equation 1.3}$$

Where σ′ is the effective stress and Pp is the pore-fluid pressure. If pore-fluids are able to escape during burial sediments will compact as a function of an increase in the effective vertical stress and maintain hydrostatic equilibrium (Maltman and Bolton, 2003). Such sediments are described as normally compacted (also referred to as normally consolidated) (Maltman and Bolton, 2003) (see appendix 1, glossary). Mechanical compaction cannot occur efficiently if pore-fluids are unable to escape and sediments become harder to compact as the effective vertical stress remains low (Nygard et al., 2006). When a burial load is sustained by pore-fluids sediments attain a fixed porosity irrespective of any further increase in burial depth (Maltman and Bolton, 2003). The rock volume therefore has elevated porosities and pore-fluids and is described as undercompacted (see appendix 1, glossary). As detachment successions lie at the base of a sedimentary overburden the effective vertical stress is defined by the lithostatic pressure at the base of the sedimentary overburden minus the overpressure (Rowan et al., 2004).

The mobility of argillaceous, fine-grained sediments is dependent on numerous factors: the degree of overconsolidation (the ratio between the maximum effective vertical stress that a sediment has been subjected to and the present effective vertical stress) (see appendix 1, glossary) (Nygard et al., 2006; Gutierrez et al., 2008), mineralogy, undercompaction, cementation and the presence of overpressured pore-fluids (Morley and Guerin, 1996; Osborne and Swarbrick, 1997; Rowan et al., 2004; Nygard et al., 2006). Sediments have little elasticity (Maltman and Bolton, 2003) therefore mechanisms that can lead to a reduction in effective stress (i.e. by an increase in pore-fluid pressure causing overpressure) causes sediments to become overconsolidated, as prior to the mechanism that caused a reduction in the effective stress the sediments were subjected to a higher effective stress (Maltman and Bolton,

2003). The higher the degree of overconsolidation the weaker the sediments are as a greater proportion of the burial load is sustained by the pore-fluids therefore increasing the possibility that sediments can mobilise and behave as a fluid (Maltman and Bolton, 2003). Overpressure is defined as pore-fluid pressure that exceeds the hydrostatic pressure (Dickinson, 1953). Of the contributing factors listed the degree of overconsolidation, undercompaction and presence of overpressured pore-fluids are thought to be critical to shale mobility (Maltman, 1994; Morley and Guerin, 1996; Maltman and Bolton, 2003; Deville et al., 2010). The fine-grained nature of clays, muds and siltstones makes them susceptible to the development of pore-fluid overpressure as a consequence of their low permeabilities. The amount of excess pressure over the normal fluid pressure is expressed as the fluid pressure ratio (λ) (Equation 1.4) (see appendix 1, glossary) (Maltman, 1994; Bilotti and Shaw, 2005).

$$\lambda = \text{pore fluid pressure} / \text{total burial pressure} \qquad \text{Equation 1.4}$$

The higher the fluid pressure ratio the greater likelihood that shale can effectively behave as fluid and liquefaction of sediments (section 1.9.1) may occur (Bilotti and Shaw, 2005).

Overpressure generation can significantly reduce the shear strength of sediments by decreasing the magnitude of cohesion (c) and intergrain friction (tan ϕ) between grains (Maltman and Bolton, 2003) (Figs. 1.4 and 1.5) (Equation 1.1). As overpressured pore-fluids are supporting an extra portion of the total stress acting though a mineral framework, in comparison to normally pressured sediments, the effective stress will be low (Equation 1.3). The reduction in shear strength as a consequence of overpressure development in shale is represented by varying values of λ (Fig. 1.5) (Equation 1.4). Shale with a high value of λ have a much lower shear strength in comparison to the shear strength of shale whose pore-fluids are at hydrostatic pressure (where λ=0.42 approximates shale at hydrostatic pressure in Fig. 1.5). The Mohr-Coulomb relationship (Equation 1.1) can be modified with respect to the effect stress (Equation 1.5).

$$\tau = C' + \sigma'_n \tan \phi' \qquad \text{Equation 1.5}$$

The prime symbol (´) indicates that the effective stress (Equation 1.3) has been taken into consideration (Maltman, 1994 nomenclature).

1.5.2 Laboratory experiments on argillaceous sediments

Triaxial laboratory experiments on illite-rich shale have shown that under low effective stresses where pore-fluids are normally pressured (shallow crustal conditions) shale typically fractures, showing a peak shear strength and strain weakening to a residual shear strength (Swan et al., 1989; Ibanez and Kronenberg, 1993; Petley, 1999; Nygard et al., 2006). Under high confining pressures shale tends to deform in a ductile manner (sections 1.5.2.1 and 1.9.1) with the maintenance of peak strength to large strains without fracturing (Petley, 1999). This change in deformation response is partly due to the increase in magnitude of shear and normal stress that occur with burial, and is also dependent on whether pore-fluids have been preserved (Einsele et al., 1974; Maltman, 1987; Ibanez and Kronenberg, 1993; Petley, 1999). At high confining pressures (approximately >15 MPa) sediment-water mixtures occur, but critically only if the water content is high enough (e.g. Einsele et al., 1974; Maltman, (1987). Triaxial experiments on argillaceous sediments performed by Maltman (1987) revealed that specimens with a water content of 15% or less fractured.

Swan et al. (1989) documented changes in the deformational response of shale under variable strain rates and demonstrated that under low strain rates macroscopic fault planes form, whereas distributed shear microstructures formed at higher strain rates. Nygard et al. (2006) deformed a variety of shales from the North Sea in a series of triaxial tests. They demonstrated that under normal compaction conditions shale exhibited a ductile response to an increasing load, but in cases where chemical

diagenesis (typically >100º C) (Mondol et al., 2007) and/or uplift occurred shale responded to loading by faulting and fracturing.

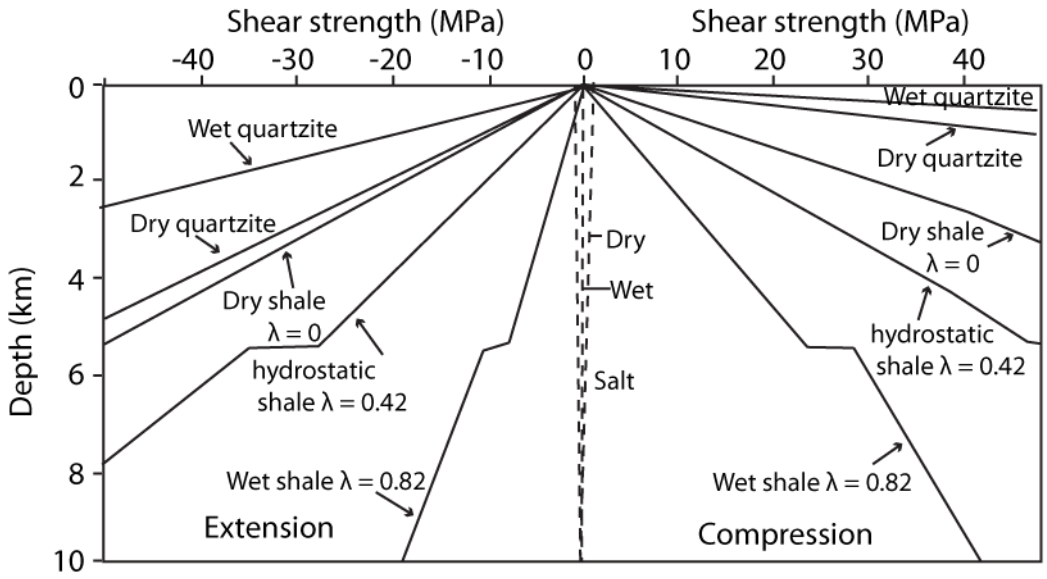

Fig. 1.5. Upper crustal shear strength profiles for sedimentary rock including dry, overpressured and normally pressured shales. Where λ=0 for dry shales, λ=0.42 approximates hydrostatically pressured shales (where λ=0.46 is for hydrostatically pressured shales, (Jackson and Vendeville, 1994) and λ= 0.82 for overpressured shales (from McClay et al., 2003 originally from Jackson and Vendeville, 1994).

Petley (1999) has shown at a transitional regime exists between brittle and ductile failure though a series of undrained (where pore-fluids are prevented from escaping) triaxial tests. He demonstrated that on a micro-scale shale samples were undergoing pervasive micro-fracturing; thus, behaving ductile on a macro-scale and brittle on a micro-scale. This was in agreement with Maltman's (1987) earlier studies where micro-scale shear zones where found to form in specimens containing up to 60% water content. In summary the deformational response of shale is dependent on whether pore-fluids are overpressured, the magnitude of overpressure and the magnitudes of the effective confining pressures that they are subjected to.

1.5.2.1 Critical state deformation

Critical state deformation (plastic shear deformation at a constant differential stress with no change in volume of the deforming body) (see appendix 1, glossary) (Roscoe, 1970; Yassir, 1989; Petley, 1999) can provide an additional explanation for when a succession of homogeneous shale is able behave in a ductile manner. Critical state differs from plastic rheological flows that involve a complete loss of shear strength (e.g. section 1.9.1), as sediments deforming at critical state retain some strength, but are still capable of large shear displacements (Yassir, 1989; Maltman and Bolton, 2003). Critical state deformation represents continuous shear failure for homogeneous sediments that behave in a perfectly plastic manner at a particular combination of porosity, pore-fluid pressure (effective stress) and differential stress (Maltman, 1994; Maltman and Bolton, 2003). Attaining critical state is dependent on shale consolidation, the time-dependent mechanical reduction in sediment volume (e.g. section 1.9.1). Shale consolidation is related to sediment permeability, the ability to expel pore-fluids with burial, the mean effective stress (p') (Equation 1.6) and the differential stress (q) (Equation 1.7) (see appendix 1, glossary) (Yassir, 1989; Maltman and Bolton, 2003).

$$p' = (\sigma'_1 + \sigma'_2 + \sigma'_3) / 3 \qquad \text{Equation 1.6}$$

$\sigma'_1 + \sigma'_2 + \sigma'_3$ are the effective maximum (σ'_1), intermediate (σ'_2) and minimum (σ'_3) principal stresses respectively.

$$q = \sigma'_1 - \sigma'_3 \qquad \text{Equation 1.7}$$

The attainment of fine-grained sediments deforming at critical state was demonstrated by Yassir (1989). He deformed a series of clay samples from mud volcanoes in a series of undrained triaxial experiments in confining pressures of up to

57 MPa (Fig. 1.6A). He revealed that for a mean effective stress (where $\sigma'_2 = \sigma'_3$) the samples deformed in an inherently ductile manner with shear failure occurring at a constant differential stress and constant mean effective stress.

The samples were deformed at different effective confining pressures to define a failure envelope: the critical state line (Fig. 1.6B) (Yassir, 1989; Petley, 1999). Stress-path diagrams of differential stress plotted against mean effective stress show the relationship between differential, mean effective stress and shear failure at the critical state line. This can be represented on a 3D yield surface diagram, which consists of two surfaces that intersect at the critical state line; the Roscoe surface and the Hvorslev surface (Fig. 1.7). The yield surface diagram represents the deformation pathway that sediments may take during their burial and subsequent deformational history in terms of pore volume, differential stress and mean effective stress (Maltman, 1994). Undercompacted, overpressured shales deform within the Hvorslev surface and trend towards the critical state line.

In this very specific stress condition perfectly plastic, homogeneous successions of shale can undergo large amounts of shear and deform in a ductile manner. In the case of overpressured, argillaceous basal detachment successions, if they attain plastic shearing at critical state then ductile deformation could occur until the causative forces dissipate, or the change in shape of the deforming body caused a change in the shale's strength (Maltman, 1994). Due to the undercompacted and overpressured nature of basal detachment successions low effective stresses are maintained and so low differential stresses could potentially drive large shear displacements (Maltman and Bolton, 2003). Therefore, basal detachment successions composed of overpressured, homogeneous, argillaceous sediments could possibly attain critical state deformation even though the total stresses acting upon the detachment system as a whole are large.

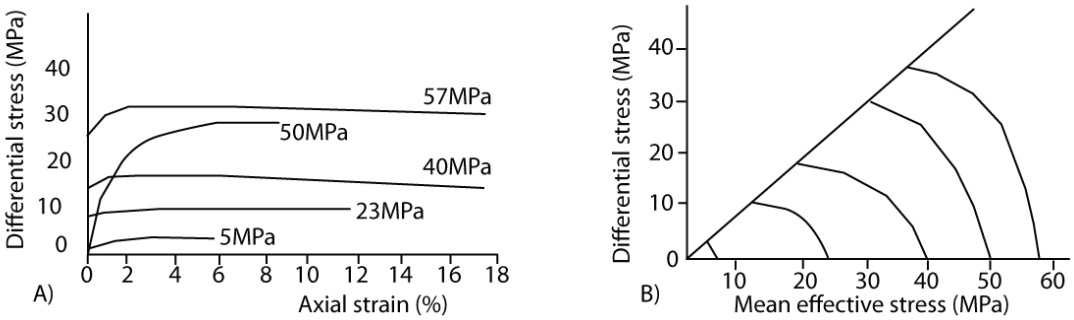

Fig. 1.6. A) Stress-strain curves for mud volcano clay where critical state deformation is achieved at differential a constant differential stress and a mean effective stress. B) Stress path diagrams for the experiments performed in A) defining the critical state line (modified from Maltman, 1994 originally from Yassir, 1989).

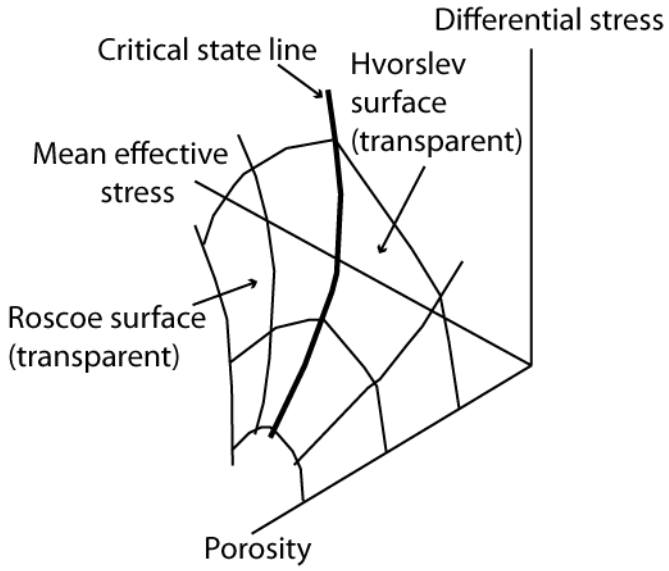

Fig. 1.7. Yield surface diagram representing the deformation pathways that overpressured, uncompacted shales can take to trend towards critical state deformation (modified from Maltman, 1994).

1.6 Compaction of argillaceous sediments

Compaction encompasses the mechanical and chemical processes that change the physical properties of sediments that occur during progressive burial (Mondol et al., 2007). During deposition clays and mudstones have permeabilities that range between 10^{-23} and 10^{-17} m^2 (approximately between 1.01^{-10} and 1^{-4} D) (Nygard et al., 2006) and porosities between 65-80% (Swarbrick and Osborne, 1998) (Fig. 1.8), which is significantly higher than other types of sediment (Mondol et al., 2007). As a consequence they are highly susceptible to physical changes during burial (increasing pressure with depth). At low confining pressures the early stages of compaction are controlled by the mechanical rearrangement of grains (down to 80°C–100°C) (Mondol et al., 2007). Compaction curves for clays and mudstones from a variety of basins worldwide, compiled by Mondol et al. (2007) (Fig. 1.8), show that clays and mudstones expel their pore-fluids rapidly during the first 2-2.5 km of burial. Below depths of 2 km the rate of dewatering decreases (Fig. 1.8). This change in the rate of dewatering is thought to reflect a change from mechanical to chemical dominated compaction and to possibly indicate the onset of diagenesis, which has a prominent role at these depths (Mondol et al., 2007). Chemical compaction is generally dominant in the deep subsurface, between depths of 2-5 km (>100°C), where cementation of the rock volume may occur through the dissolution and precipitation of minerals (Mondol et al., 2007). The influence of cementation is critical when considering the likelihood of a ductile response of argillaceous sediments, as the development of any mineral cement would reduce the ability of such successions to deform in a ductile manner.

1.7 Overpressure generation mechanisms

Mechanisms that cause overpressure within a rock volume involve increasing the pore-fluid pressure above the hydrostatic pressure (see appendix 1, glossary). Overpressure generation mechanisms fall into three categories. Mechanisms that 1) reduce the pore-space within a rock volume, which includes tectonic loading (increasing a lateral compressive stress) and sediment loading (i.e. disequilibrium compaction), 2) increasing the volume of pore-fluids, 3) involve fluid migration and buoyancy effects (Swarbrick and Osborne, 1998) (Fig. 1.9).

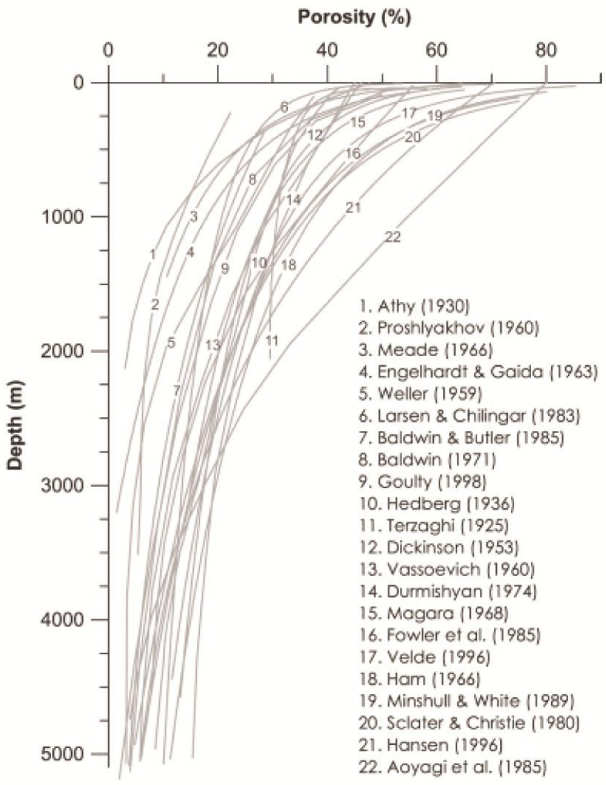

Fig. 1.8. Compaction curves for shales compiled worldwide. Initial porosity at deposition decreases rapidly with first 1-2 km of burial (from Mondol et al., 2007).

Disequilibrium compaction (see appendix 1, glossary) is the most common mechanism for generating large pore-fluid pressures within fine-grained sediments (Dickenson, 1953; Chapman, 1980; Swarbrick et al., 2002) and is the most frequently advocated mechanism for overpressure generation in the Niger Delta (e.g. Doust and Omatasola, 1990; Morley and Guerin, 1996; Bilotti and Shaw, 2005). Additional mechanisms listed above are thought to be secondary (e.g. Fig. 1.9). In the 1960s disequilibrium compaction was discovered as being the primary mechanism for overpressure generation in the Gulf of Mexico by Pennebaker (1968) and was rapidly applied to geological settings where argillaceous sediments are rapidly buried (e.g. Osborne and Swarbrick, 1997; Van Rensbergen and Morley, 2000). If pore-fluids are unable to escape during burial and become trapped or if they are unable to escape fast enough, pore-fluid pressures rise above hydrostatic pressure and become overpressured, as the lithostatic load is imposed onto the pore-fluids (Osborne and Swarbrick, 1997). This is the process of disequilibrium compaction. Rapid burial of fine-grained, low permeability sediments increases the

likelihood of overpressure development, as sediments have to be able to expel their formation-fluids at a greater rate.

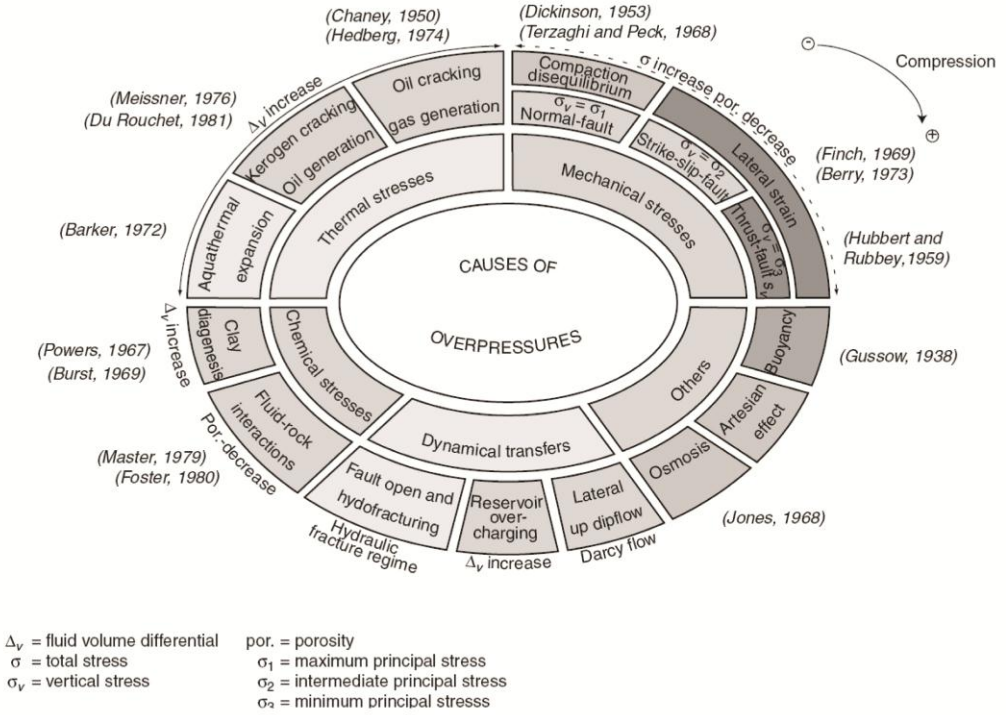

Fig. 1.9. The causal mechanisms that can generate overpressured pore-fluids (from Grauls, 1999).

1.8 Seismic evidence for overpressured argillaceous sediments

Criteria for interpretation of overpressured, argillaceous successions on seismic reflection data follow a specific set of geophysical characteristics. These include 1) the absence of acoustic impedance contrasts on seismic reflection data, 2) laterally discontinuous chaotic seismic reflections and 3) a significant reduction in the seismic velocity of a propagating seismic wave once the top of the overpressured section has been intersected (Fig. 1.10).

The lack of acoustic impedance (see appendix 1, glossary) contrasts within a seismic interval has long been used as primary evidence for the presence of overpressured

argillaceous sediments (e.g. Musgrave and Hicks, 1966; Pennebaker, 1968; Bruce, 1973; Evamy, 1978) (Fig. 1.10). However, the lack of acoustic impedance could be caused by numerous factors (these are detailed in section 2.5). It is considered that the preservation of porosity and pore-fluids that then become overpressured and structural complexity are the dominant contributing factors. Preserved porosity and pore-fluids within a succession deep within the subsurface can impede the generation of acoustic impedance contrasts as there are few grain to grain contacts leaving the impression of a seismically transparent interval (see section 2.3).

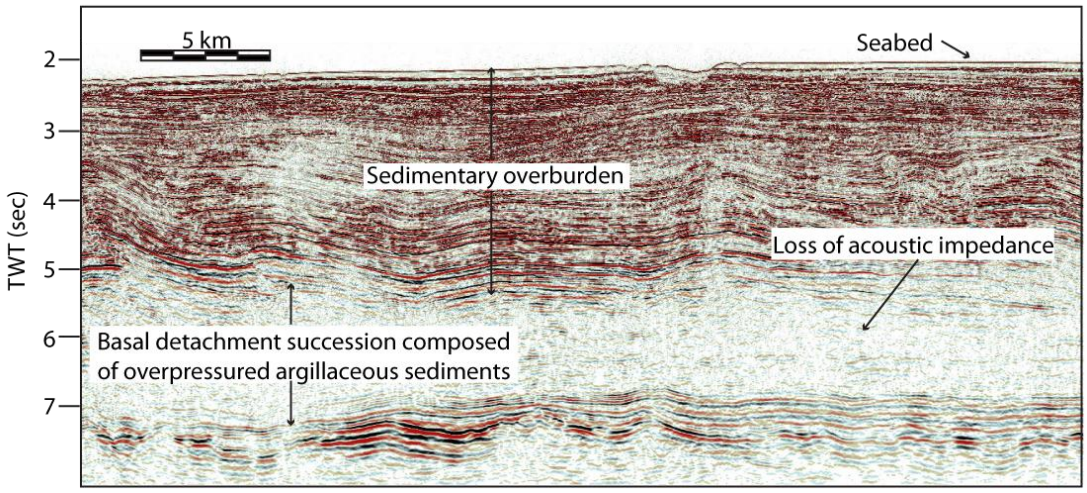

Fig. 1.10. Seismic line showing the loss of acoustic impedance and all reflectivity within the basal detachment succession of the Niger Delta.

Within standard velocity-depth profiles seismic velocity increases with increasing depth as a consequence of normally compacted sediments being able to expel their pore-fluids with burial. A sharp reduction in stacking velocities at the onset of a deeply buried siliciclastic succession is used as strong evidence for the presence overpressured pore-fluids (e.g. Morgan, 2003; Bilotti and Shaw, 2005; Corredor et al., 2005; Cobbold et al., 2009) (section 2.5). A large reduction in stacking velocities implies that the succession has a low bulk density, which could be due to a high porosity, abundant fractures, the presence of a light fluid within the pore space, or combinations of the above (Cobbold et al., 2009). Overpressured and

undercompacted sediments are likely advocates for sustaining such low densities within deeply buried sediments (Morgan, 2003; Cobbold et al., 2009).

1.9 Ductile deformational processes of overpressured sediments

The deformation of overpressured sediments in the deep subsurface partly draws its kinematic parallels with types of plastic flows (i.e. flows with no shear strength that deform immediately once a shear stress is applied) (Maltman, 1994). As the exact kinematic behaviour of mobile shales is unknown the possibilities of how mobile shale deforms and moves are discussed below.

1.9.1 Liquefaction and fluidization

The driving force for liquefaction is often shaking of sediments due to earthquakes, which reduces the effective stress (section 1.5.1) (Equation 1.3), generating pore-fluid overpressure (Mills, 1983; Maltman, 1994). As the pore-fluid pressure increases, the sediments shear strength decreases as grain to grain contacts separate and so the effective stress lowers (Terzaghi, 1956; Maltman, 1994). When sediments completely support an applied load through their pore-fluids then they have lost their ability to transmit a shear stress and can effectively behave as a fluid (Maltman and Bolton, 2003; Rowan et al., 2004). When sediments are in this state they are referred to as liquefied and will flow as they are now subject to fluid pressure gradients (Mills, 1983; Maltman and Bolton, 2003). Sediments will remain liquefied until dewatering is able to take place and some frictional strength is restored (Mills, 1983; Maltman and Bolton, 2003).

Fluidization is the entrainment of sediments within a flow where the moving sediment particles are supported by the upward motion of pore-fluids (Maltman, 1994). Fluidization occurs in conjunction with a rapid dewatering of sediment through movement of interstitial fluids (Maltman and Bolton, 2003). Dewatering induces a drag on sediment particles, which is greater than or equal to the gravitational component of the vertical stress and so sediment particles move upward

(Mills, 1983; Maltman, 1994). Fluidization is a localised process restricted to vertical fluid conduits whereas liquefaction occurs homogeneously throughout the bed (Mills, 1983).

1.9.2 Creep

Creep is the response of sediments subjected to high stresses that are continuously below the yield strength of the sediment so it does not reach shear failure. This accumulation of strain results in slow continuous deformation of the sediment typically at the rate of a few centimetres per year (Maltman, 1994).

1.9.3 Cataclastic flows

Cataclasis is a deformation process that involves fracturing and shearing of the rock. Breaking of the rock particles occurs via rotation and mechanical moving of the particles (Ramsey and Huber, 1997). It may involve microfracturing of every grain within the rock or break the rock into fragments on the scale of a few centimetres (Rutter, 1986).

1.10 Gravitational processes operating upon overpressured basal detachment successions

Margin failure on passive continental margins is often characterised by intense thin-skinned deformation driven by gravitational instability. The gravitational processes of gravity gliding and gravity spreading are detailed.

1.10.1 Gravity gliding

Gravity gliding (see appendix 1, glossary) refers to sedimentary strata sliding above a detachment level (see appendix 1, glossary) where the majority of deformation is by translation as opposed to accommodation of strain (i.e. changes in shape) (Schultz-Ela, 2001; Rowan et al., 2004) (Fig. 1.11). Gravity gliding refers to a rigid or coherent body in which internal deformation is restricted to accommodating

horizontal motion over an irregular detachment level (e.g. Schultz-Ela, 2001). Gravity gliding is limited by the shear strength of the detachment level relative to the shear stresses acting through the sliding body, which act parallel to the underlying detachment level (Schultz-Ela, 2001). A steep detachment dip means that shear stress acting upon the detachment is greater, in comparison to a detachment with a shallower dip, and therefore it is easier to overcome resistance to slip (Rowan et al., 2004). Passive margins often have an oceanward tilt induced by passive margin uplift, which enhances the conditions for gravity gliding to operate (Schultz-Ela, 2001). In cases where the basal detachment succession is overpressured the detachment has a very low resistance to slip enabling gravity gliding to be an effective process (Schultz-Ela, 2001).

1.10.2 Gravity spreading

Gravity spreading (see appendix 1, glossary) refers to sedimentary strata that are collapsing vertically and extending laterally above a detachment level that is horizontal or uphill in the direction of spreading (Schultz-Ela, 2001). It is the failure of a sediment body under its own weight and internal distortion is driven by gravitational stresses that are greater than the yield strength of the sediment body (Rowan et al., 2004). During deformation the rock volume thins vertically and extends horizontally (Fig. 1.11) (Schultz-Ela, 2001).

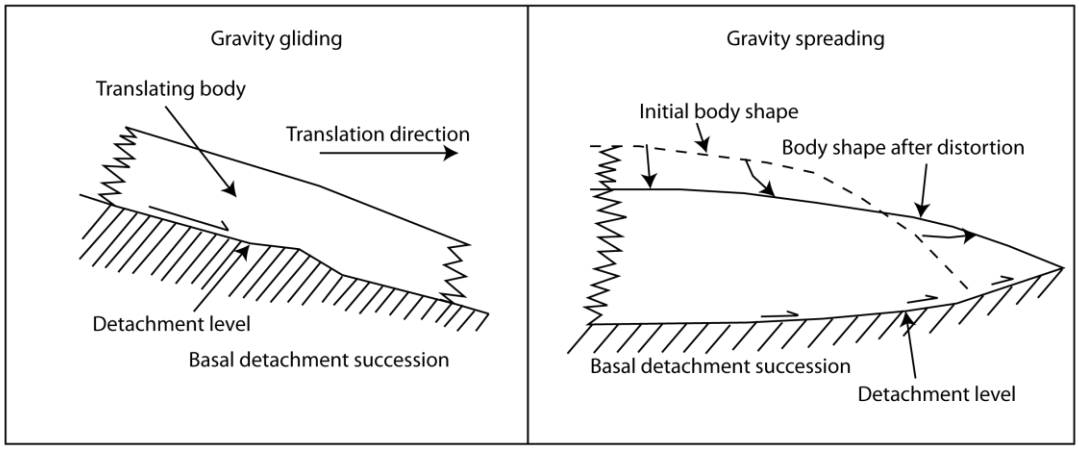

Fig. 1.11. The two types of gravity-driven processes that deform sedimentary strata on delta slopes. Gravity gliding is the translation of strata above a detachment surface whereas gravity spreading induces deformation internally within the body (from Schultz-Ela, 2001).

1.10.3 Large deltaic systems

The first-order geometry and kinematics of large deltaic systems follow critical taper wedge models originally developed to explain the deformation of accretionary wedges that form at convergent plate boundaries (e.g. Davis et al., 1983; Dahlen et al., 1984), but have since been adapted to passive margins (e.g. Bilotti and Shaw, 2005). Critical taper wedge theory can be applied to any overall wedge shaped geometry that is deforming by brittle processes (Bilotti and Shaw, 2005). The geometry of the sliding deltaic wedge is an interaction between 1) the internal strength of material deforming within the wedge, 2) the strength of the detachment surface on which the wedge slides, 3) the dip of the basal detachment layer, 4) the surface slope of the deforming wedge. The dip of the detachment surface and the dip of the surface slope together form the wedge taper. For the deformation front to continue migrating seaward the shear strength of the basal detachment must be weaker than the shear stresses operating through the propagating wedge (Bilotti and Shaw, 2005).

1.11 Structural styles associated with overpressured argillaceous sediments

An overview of conventional structural styles associated with shale tectonics is provided. Pioneering works identified that the critical factor in inducing ductile deformation of mobile shale is related to the rapid loading of sediments above a basal detachment succession composed of undercompacted, fine-grained argillaceous sediments (Bruce, 1973; Evamy et al., 1979). Sediment loading is considered to trigger the ductile movement of mobile shale, which is involved in the development of listric faults and shale diapirs. These models are detailed below (sections 1.11.1 to 1.11.2) and the limitations and uncertainties associated with these models are discussed throughout chapters within this thesis.

1.11.1 Listric faults

Listric normal faults (see appendix 1, glossary) are a common component of gravitationally-driven detachment systems (e.g. Bally et al., 1981) (Fig. 1.12). In gravitational systems the development of large regional and counter regional listric normal faults is associated with a basinward progradation of the sedimentary overburden (e.g. Knox and Omatsola 1989; Morley, 2003). Accommodation space in the hanging walls of listric normal faults is created coevally with the mobilisation of underlying argillaceous sediments. This allows thick accumulations of sediments to collect in their hanging walls as the accommodation space is filled. The additional weight of overburden sediments in the hanging wall creates a differential load, which is considered to cause overpressure and subsequently liquefy and induce ductile movement of the underlying mobile shale.

Knox and Omatsola (1989) proposed an escalator model to represent the continued basinward translation of deltaic sediments and the rapid burial of mobile shale for the Niger Delta. As differential loading overpressures and mobilises underlying fine-grained successions they flow basinwards and upwards, creating collapse structures associated with large listric faults and the rise of shale diapirs (e.g. Cohen and McClay, 1996; Morley and Guerin, 1996). Diapiric structures, and associated domal

structures, created by the buoyant rising of mobile shale then deform sediments in the distal parts of the hanging walls of major listric faults. The process then repeats itself in a more distal position as progradation of deltaic sediments continues.

Once complete evacuation of overpressured mobile sediments has taken place touchdown occurs (section 1.11.3) and the creation of accommodation space ceases. Once the accommodation has been filled the process repeats itself in a more distal position as continued episodes of deltaic progradation loads a new part of basal detachment succession.

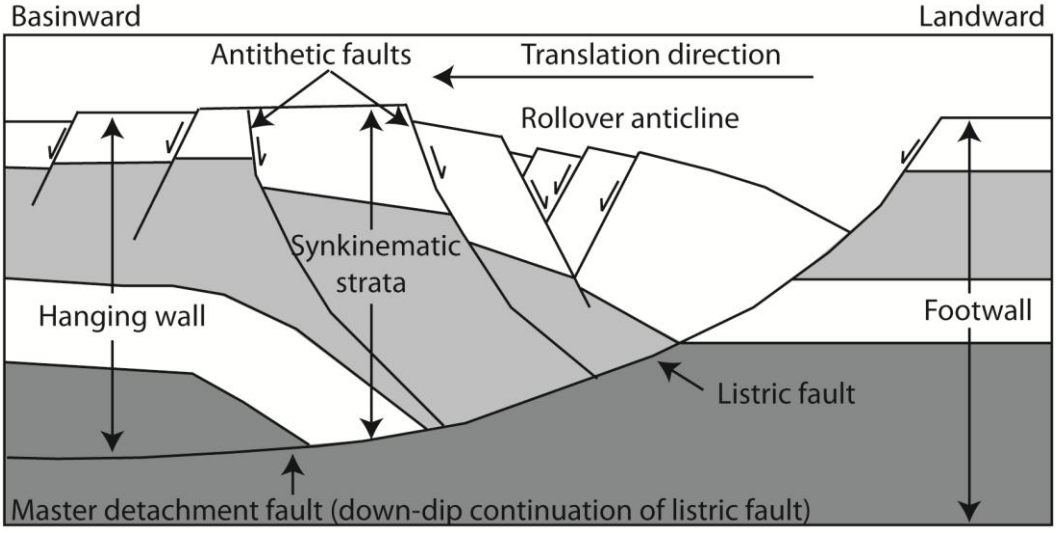

Fig. 1.12. Geometry of a listric normal fault with associate synthetic and antithetic faults in the adjacent hanging wall strata.

1.11.2 Shale diapirs

Diapirs (see appendix 1, glossary) have long been associated with gravitationally-driven deformation and have been regularly associated with overpressured deltas and accretionary prisms (Doust and Omatsola, 1990; Cohen and McClay, 1996; Morley and Guerin, 1996; Van Rensbergen and Morley, 2000; Morley, 2003; Van Rensbergen and Morley, 2003) (Fig. 1.13). Historically, shale diaprism has been described in four stages: 1) passive, 2) active, 3) reactive, 4) diapiric collapse (Vendeville and Jackson 1992; Cohen and McClay, 1996; Morley and Guerin, 1996;

Morley, 2003; Van Rensbergen and Morley, 2003), where each stage relates to a separate stage of diapiric development. Emplacement of shale diapirism originally drew parallels with salt diapirism where a bulbous body of overpressured shale was considered to actively rise from a high-pressured succession at depth. The four stages of diapiric growth identified with salt diapirs were applied to shale diapirs (e.g. Morey and Guerin, 1996; Morley, 2003). Diapir identification is related to the presence of low reflectivity, chaotic discontinuous seismic reflections that on mass appear to rise into overlying laterally continuous reflections (Figs. 1.13 and 1.14). In addition, fault-related folds have also been described as having diapric cores in some seismic data sets leading to some subjectivity in what is termed a diapir (e.g. Doust and Omatsola, 1990; Van Rensbergen and Morley, 2003) (Fig. 1.13). A historical overview of the four stages of diapir growth is presented, which is followed by more recent insights into what may exactly constitute a shale diapir.

1) Reactive diapirism

Reactive diapirism describes the initial stage of diapiric growth where the ductile succession begins to flow upwards, but does not penetrate overlying reflections (Van Rensbergen and Morley, 2003). Reactive diapirism signifies the development of relief at the top of the ductile succession by movement of mobile shale from a high to low pressure area (Morley and Guerin, 1996). Thinning of the sedimentary overburden (through faulting, erosion or depositional variation) effectively creates a pressure gradient, which begins to drive ductile movement of underlying mobile shales. This is thought to promote diapir growth as a consequence of the reduction in the vertical stress within thinned areas of the sedimentary overburden.

2) Active diapirism

Active diapirism describes the phenomenon of overpressured mobile shale actively rising, pushing and deforming the overlying sedimentary overburden as a consequence of the pressure exerted by the diapiric body (Vendeville and Jackson 1992). For diapiric rise to occur the brittle shear strength and the tensile strength of overlying sediments has to be overcome (Morley, 2003B). The source for the pressure that is acting to deform the sedimentary overburden is thought to come from

differential loading and buoyancy forces of the low density, undercompacted mobile shale (Van Rensbergen and Morley, 2003). The active phase of diapirism is indicated by symmetrical thinning of reflection packages towards the diapir crest, which form local depocentres in the sedimentary overburden (Morley and Guerin, 1996) (Fig. 1.14).

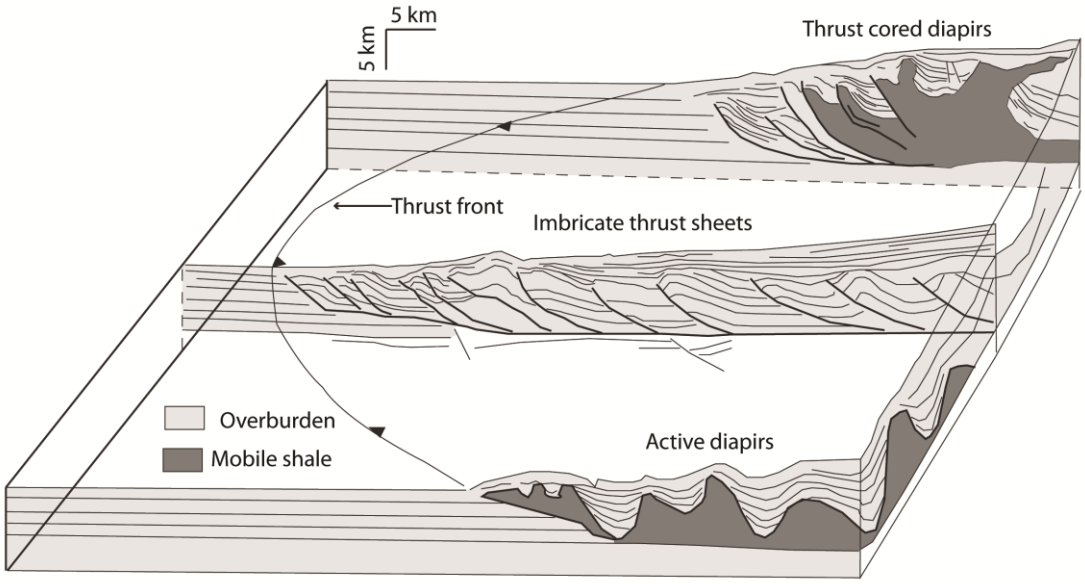

Fig. 1.13. Diagram showing the end-members associated with the range of geometries interpreted to be shale diapirs, which ranges from conventional active diapirs through to thrust cored diapiric imbricates (from Morley, 2003).

3) Passive diapirism

Passive diapirism is used to describe the growth of diapirs that develop through a sediment downbuilding of their flanks when they reach shallow subsurface levels. As diapirs rise overpressured sediments expel their pore-fluids. This causes a reduction in pressure within the diapiric body and cessation of diapiric rise (Morley and Guerin, 1996).

4) Diapiric collapse

The collapse of a diapir is related to the complete expulsion of pore-fluids trapped within the overpressured succession. As a diapir dewaters it shrinks due to the loss in volume and ceases growing. This final stage of diapirism is associated with the development of a sag basin at the diapir crest. Diapiric collapse may also occur if the

diapir crest continues to grow by the formation of extensional faults at its crest. Collapse may lead to the formation of radial faults or arrays of conjugate minor faults at the crestal region (Morley and Guerin, 1996).

Direct field evidence for large-scale shale diapirs is lacking (e.g. Maltman, 1994). More recent studies are beginning to question whether models that portray the rise of a bulbous mass of overpressured sediments (diapir) are a realistic representation of the types of processes involved in the rise of overpressured sediments (e.g. Stewart and Davies, 2006). Insights into what a shale diapir maybe composed off can be drawn from mud volcanoes (Stewart and Davies, 2006; Deville et al., 2010). Studies on mud volcanoes have revealed that large bodies of overpressured mud are absent and the terms developed to describe diapir growth (e.g. sections numbered 1-4) may not accurately reflect the emplacement of overpressured mobile shale (Stewart and Davies, 2006). A process now associated with the rise of large volumes of overpressured fine-grained sediments is the entrainment of sediment particles that are supported by the upward motion of displaced pore-fluids within localised, vertical conduits, and through hydraulic failure (Davies and Stewart, 2005). The process is akin to fluidization (section 1.9.1) and differs from the conventional interpretation of a diapiric rise of buoyant mud.

1.11.3 Touchdowns

Shale touchdowns (also known as shale welds) (see appendix 1, glossary) have been drawn from geometric parallels with the salt literature, where Jackson and Cramez (1989) first described a variety of salt welds, which were then applied to similar geometric features seen in shale tectonic provinces. Shale touchdowns occur when mobile shale withdraws from between two lithological successions, leaving the two originally separate lithologies juxtaposed against each other, forming what is described as the touchdown (weld) (e.g. Morley, 2003) (Fig. 1.15). The Niger Delta has been cited as a province where large-scale withdrawal of overpressured sediments takes place (Cohen and McClay, 1996; Morley and Guerin, 1996; Morley, 2003). Touchdowns are thought to form within the Akata Formation (section 2.2.1) and at the Akata-Agbada Formation boundary (section 2.2.2) as a consequence of

differential loading from the sedimentary overburden inducing the withdrawal of overpressured sediments.

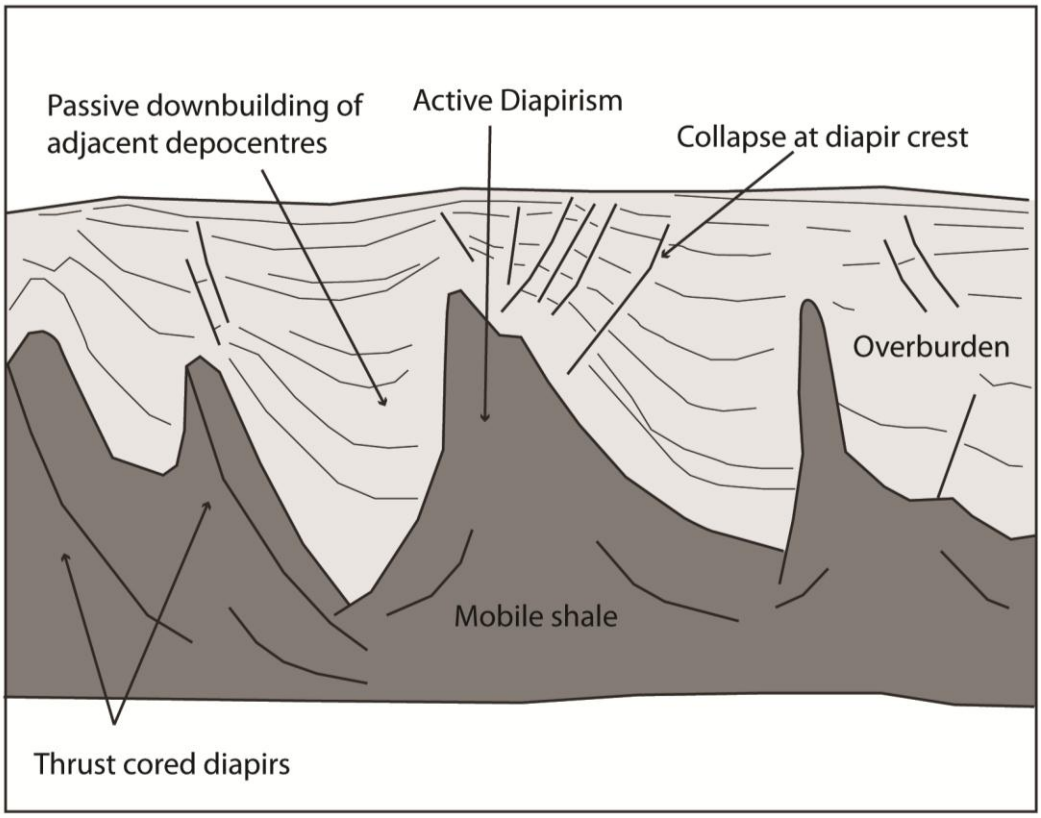

Fig. 1.14. Schematic cross section of active diapirism where mobile shale rises and deforms overlying sediments (from Van Rensbergen and Morley, 2003).

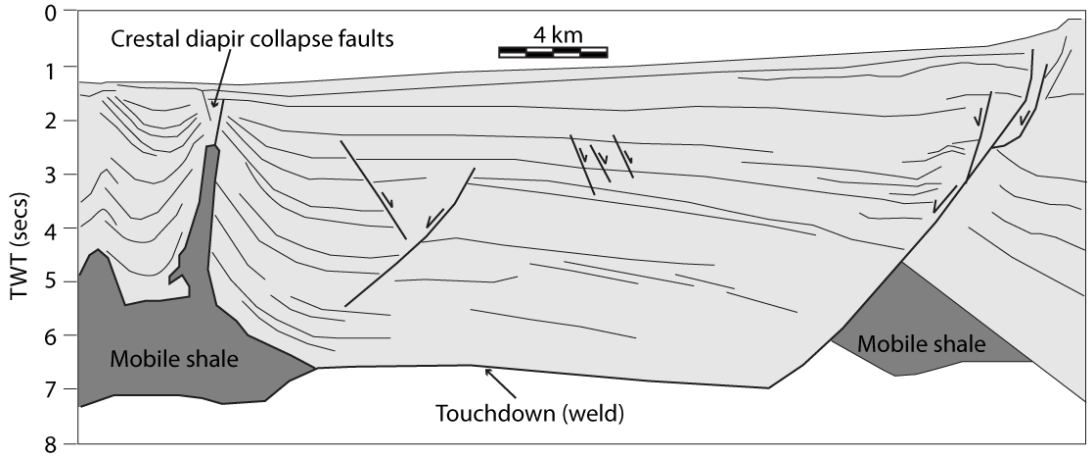

Fig. 1.15. Geometry of a shale touchdown which has formed as a consequence of mobile shale evacuating the intervening interval leaving two units that were not deposited adjacently juxtaposed against each other (from Morley, 2003).

1.12 Fault-related folding

Three end-member models have been used to characterise the deformation style of fault-related folds in fold and thrust belts: 1) fault-bend folds; 2) fault-propagation folds; 3) detachment folds (Suppe, 1983, 1985; Mitra; 1990; Suppe and Medvedeff, 1990; Shaw et al., 2004) (see appendix 1, glossary) (sections 1.12.2 to 1.12.4 respectively). Fault-related fold growth either can be represented by kink-band or limb rotation models (e.g. Suppe, 1983; Suppe et al., 1992; Shaw et al., 2004). Kink-band models require fold limbs to widen while maintaining a fixed limb dip, which is attained instantly at the initiation of fold amplification (Suppe, 1983; Suppe, et al., 1992). Folds amplify by the migration of kink-bands (marked by axial surfaces) where a single, or both kink-band pairs migrate through strata causing a widening of axial surface pairs (fold limbs) (Fig. 1.16). Kink-bands are identified by changes in the dip of strata at axial surfaces. Axial surfaces that move with respect to pre-kinematic strata are termed active axial surfaces and those that do not are termed inactive or fixed axial surfaces (Suppe et al., 1992). Material is incorporated into the fold limb by migrating through active axial surfaces (Shaw et al., 2004). For descriptive purposes axial surfaces are referred to with respect to their position relative to synclines or anticlines (e.g. Fig. 1.16). Suppe et al. (1992) identified five possible kinematic combinations of fold amplification involving kink-band migration based upon which axial surfaces are active and the direction that axial surface migrate with respect to each other (Fig. 1.16).

1.12.1 Growth folds

The synkinematic stratal architecture, which flanks fold limbs, is in part dependent on the kinematic mechanism by which the fold amplified (Fig. 1.17). The idealised synkinematic architecture that develops for the five combinations of kink-band migration are summarised in figure 1.17, which shows that complex depositional patterns can develop in the synkinematic strata (Suppe et al., 1992). In these models sedimentation rate is constant relative to fold amplification rate and sedimentation keeps ahead of deformation (Suppe et al., 1992). The inactive axial surface within the synkinematic strata is termed the growth (or synkinematic) axial surface, which is

the locus of particles that were deposited along the active axial surface and were then incorporated into the fold limb (Suppe et al., 1992; Shaw et al., 2004). The growth axial surface is identified by a change in dip from the inactive axial surface. It no longer bisects the angle between the fold limbs due to a change in bed thickness across the growth axial surface (Suppe et al, 1992). The growth axial surface migrates towards the active axial surface forming a "growth triangle" within the synkinematic strata due to a change in sedimentation rate across the active axial surface (Suppe et al, 1992). The end of fold growth is marked by the apex of the "growth triangle" (Suppe et al., 1992) (Fig. 1.17).

In deep-water fold and thrust belts the rate of uplift can periodically exceed the rate of sedimentation. The idealised growth architectures that develop in this case are summarised for kink band migration and limb rotation models (Fig. 1.18). In the case where the anticlinal axial surface is active the synkinematic strata are undeformed and onlaps migrate towards the fold hinge with each increment of folding (Shaw et al., 2004) (Fig. 1.18). When the synclinal axial surface is active, synkinematic strata are rotated and incorporated into the fold limb. Onlaps progressively step back, away from the fold crest, and are displaced with each increment of fold amplification (Fig. 1.18).

Limb rotation models require fold limbs to rotate during fold amplification (Hardy and Problet, 1994; Problet and McClay, 1996; Shaw et al., 2004). The rotation is distributed across the entire fold limb as the fold limb steepens with every increment of fold amplification. Onlaps and stratigraphic pinch-out occur between the synclinal and anticlinal axial surfaces and synkinematic strata display and upward shallowing of dips (Shaw et al., 2004) (Fig. 1.18).

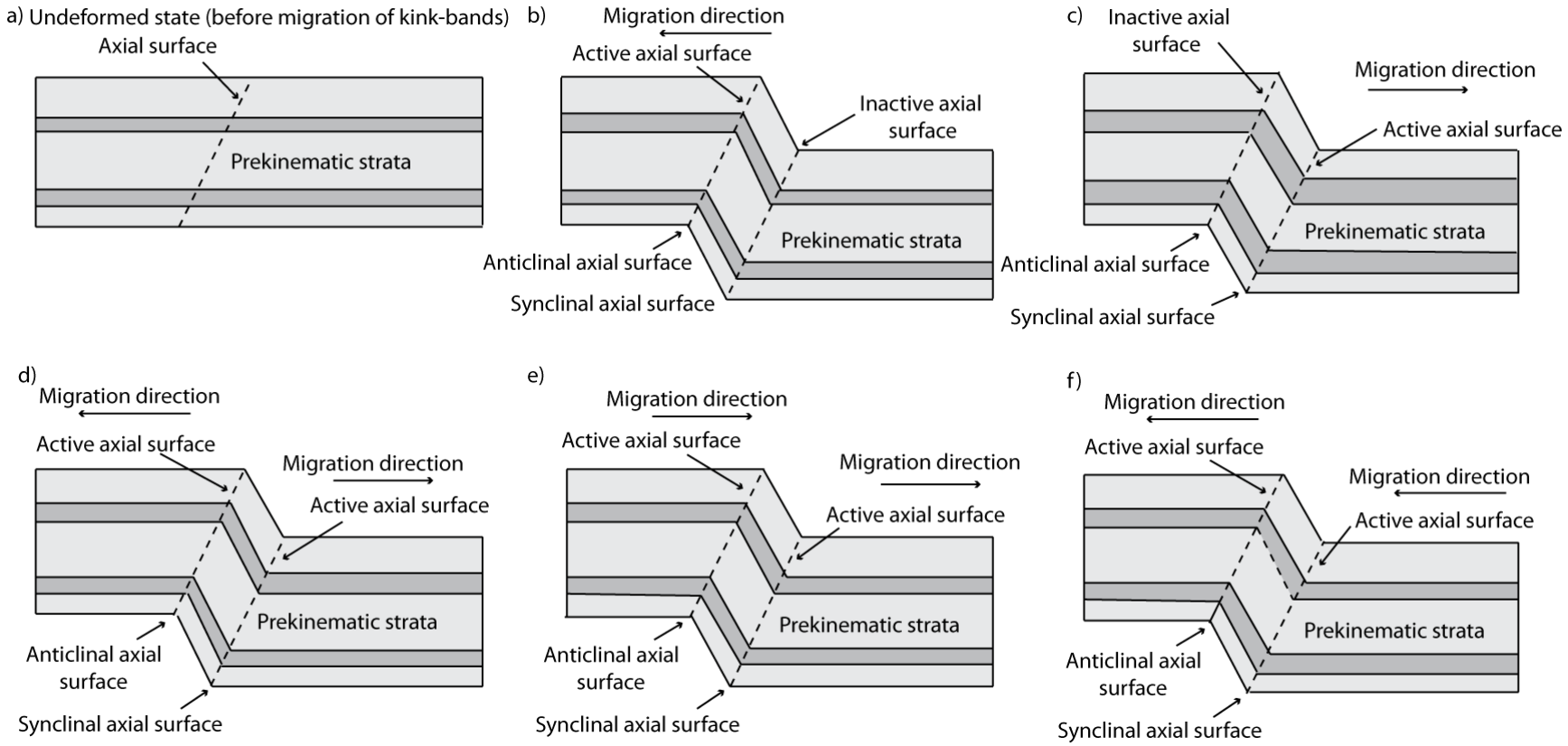

Fig. 1.16. The five kinematic classes of hinge migration based on which axial surfaces are inactive and active and migration direction of the active axial surface (from Suppe et al., 1992).

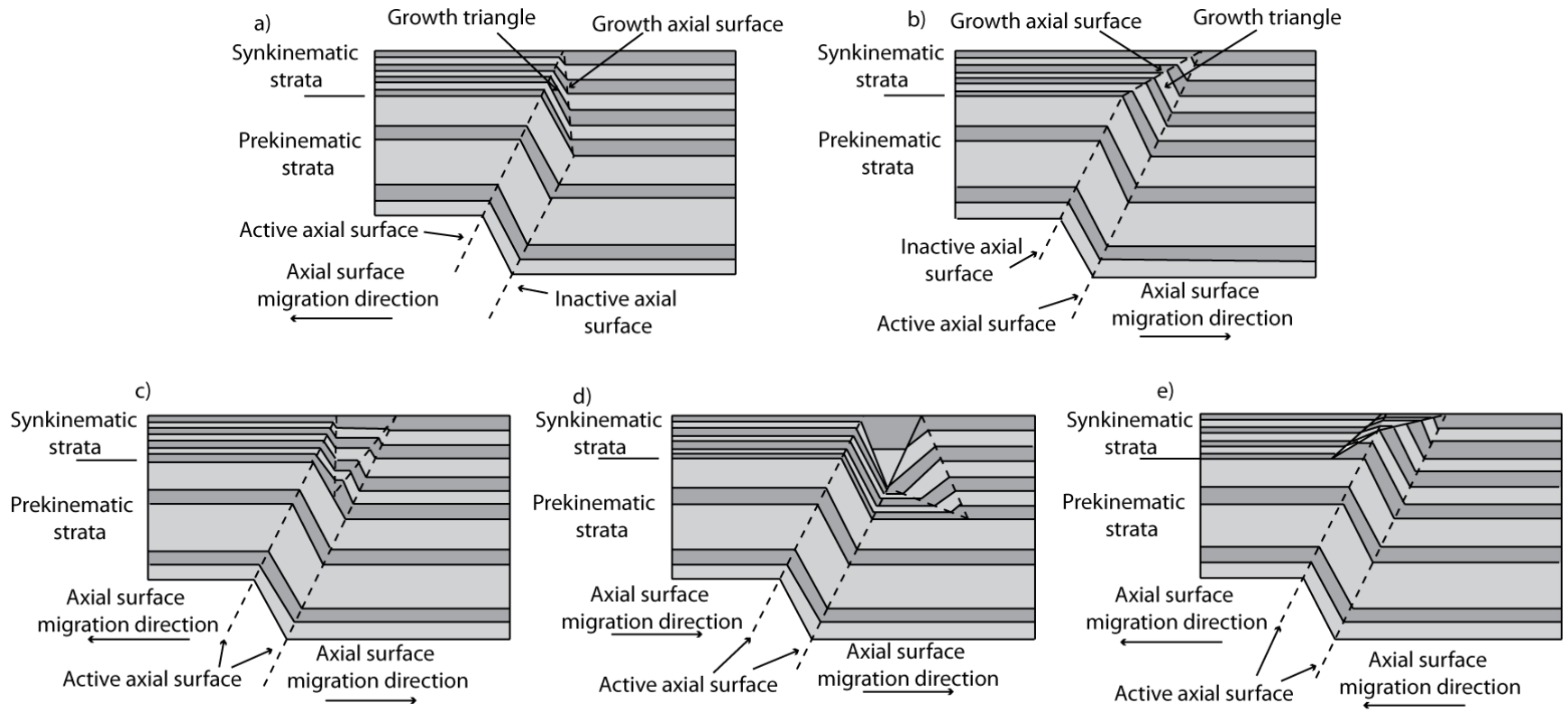

Fig. 1.17. The styles of synkinematic architecture that can form through the five kinematic classes of hinge migration. The synkinematic strata in A to E relate to the kinematic classes of B to F shown in figure 1.13 respectively. In these models sedimentation rate is constant relative to fold amplification rate however sedimentation keeps ahead of deformation so no relief develops (from Suppe et al., 1992).

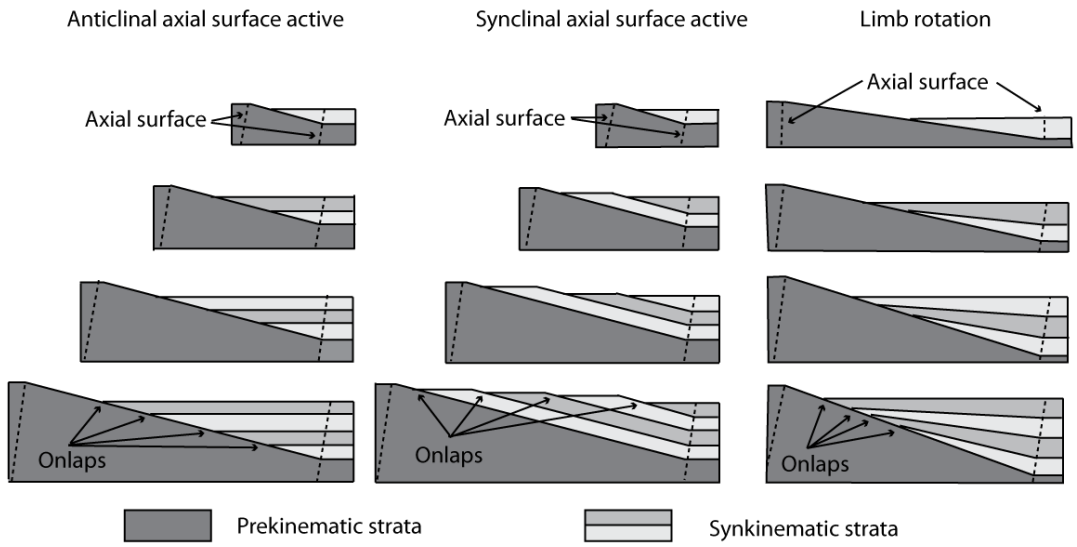

Fig. 1.18. Growth architectures associated with active anticlinal, synclinal axial surfaces on the flanks of folds that amplify by kink-band migration and limb rotation. In the limb rotation model the sedimentation rate is held constant while the amplification rate decreases with each increment of folding (from Shaw et al., 2004).

1.12.2 Fault-propagation folds

A distinguishing geometric feature of fault-propagation folds, in relation to their fault-bend fold counterparts (section 1.12.3), is that the propagating fault plane does not form a through going upper detachment level. Displacement at the upper tip line of a propagating fault tip is accommodated by folding, which amplifies as the underlying fault propagates (Suppe and Medvedeff, 1990). Geometrically, fault-propagation folds are characterised by short forelimbs and relatively long back limbs that have the same dip as the underlying fault plane (Suppe and Medvedeff, 1990) (Fig. 1.19A). Kinematic models developed for fault-propagation folding show that the back limb amplifies by migrating hinges (self similar fold growth) (e.g. Fig. 1.16), whereas the forelimb may amplify by hinge migration and/or limb rotation (Mitra, 1990; Suppe and Medvedeff, 1990; Problet and McClay, 1996) (Fig. 1.18).

1.12.3 Fault-bend folds

In contrast to fault-propagation folds, fault-bend folds are characterised by an upper and lower detachment level as a consequence of the propagating fault plane cutting-up section to the next mechanically incompetent layer (Suppe, 1983; Chester and Chester, 1990) (Fig. 1.19B). The upward stepping (ramping) component of the thrust plane occurs through relatively competent beds (mechanically stronger) and bedding parallel components of the fault plane (flats) occur in incompetent beds (mechanically weak). It is the movement of the overriding hanging wall over these ramps and flats in the fault plane geometry that causes strata in the hanging wall to fold (Suppe, 1983). Suppe (1983) proposed a kinematic model for the formation of fault-bend folds, which is used as the current end-member model for the interpretation of thrust faults in many fold and thrust belts. The main kinematic difference between fault-bend and fault-propagation folds is that both forelimbs and backlimbs amplify solely by hinge migration in the fault-bend fold model (Suppe, 1983; Suppe and Medvedeff, 1990).

1.12.4 Detachment folds

Detachment folds form at the tips of bedding parallel thrust faults as displacement is transferred from the thrust tip into overlying stratigraphy (Jamison, 1987). Detachment folds form in sedimentary successions where there are significant competency contrasts (Mitra, 2003). A characteristic geometric requirement of detachment folds is that buckling occurs within competent strata (mechanically strong, e.g. sandstone or limestone), which overlie incompetent strata (mechanically weak, e.g. overpressured sediments or salt) (Jamison, 1987; Epard and Groshong, 1995; Problet and McClay, 1996; Stewart, 1996; Atkinson and Wallace, 2003) (Fig. 1.19C). A wide range of kinematic and geometric models have been developed to explain amplification of detachment folds. The competent units, those which buckle, have been shown to grow by a variety of kinematic mechanisms. Fold limbs may grow by hinge migration, limb rotation and/or combinations of both (Dahlstrom, 1990; Problet and McClay, 1996; Mitra, 2002).

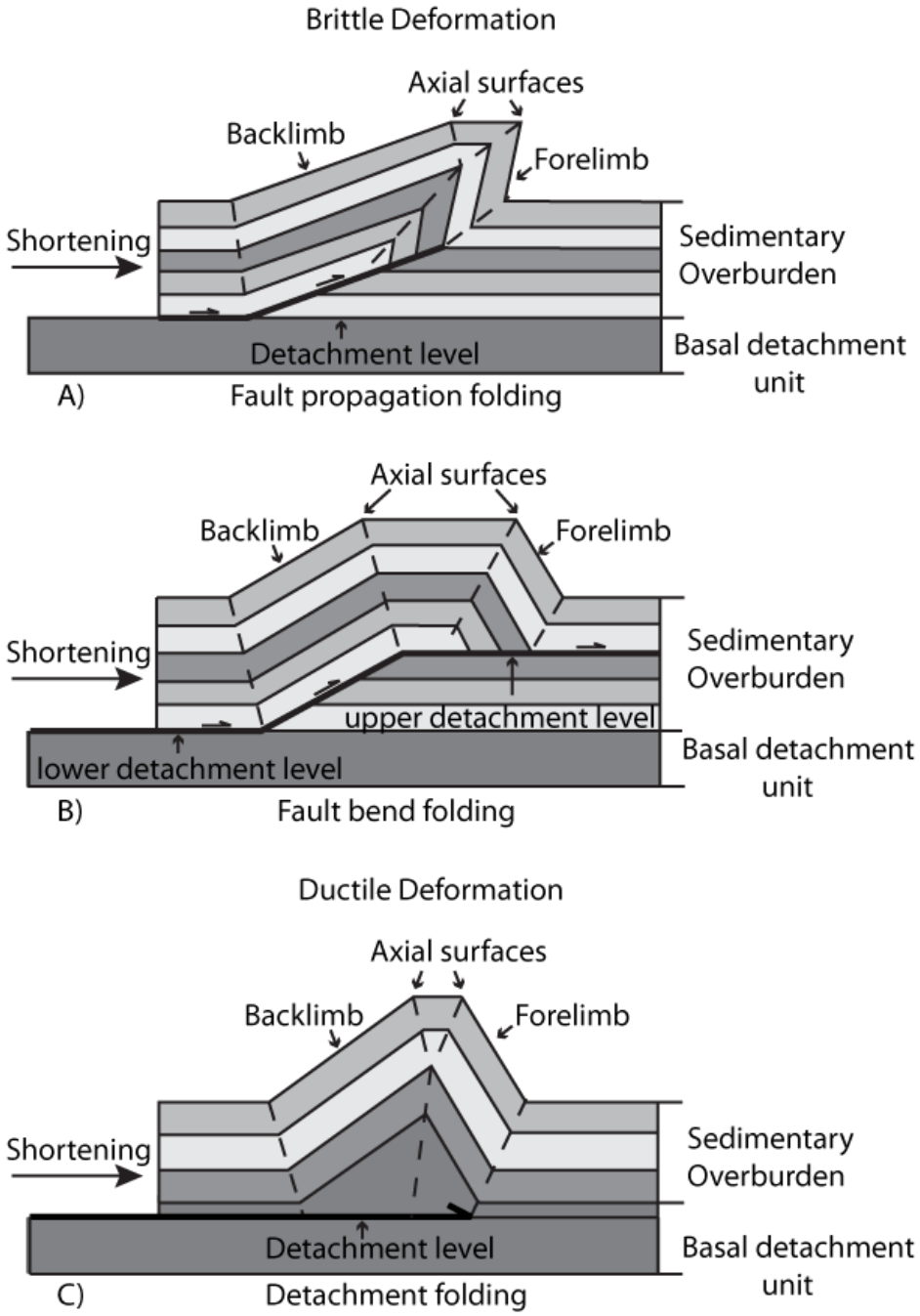

Fig. 1.19. The three conventional types of fault-related folding found in fold and thrust belts. A) fault-propagation fold (Suppe, 1985), B) fault-bend fold (Suppe, 1983), and C) detachment fold (Jamison, 1987).

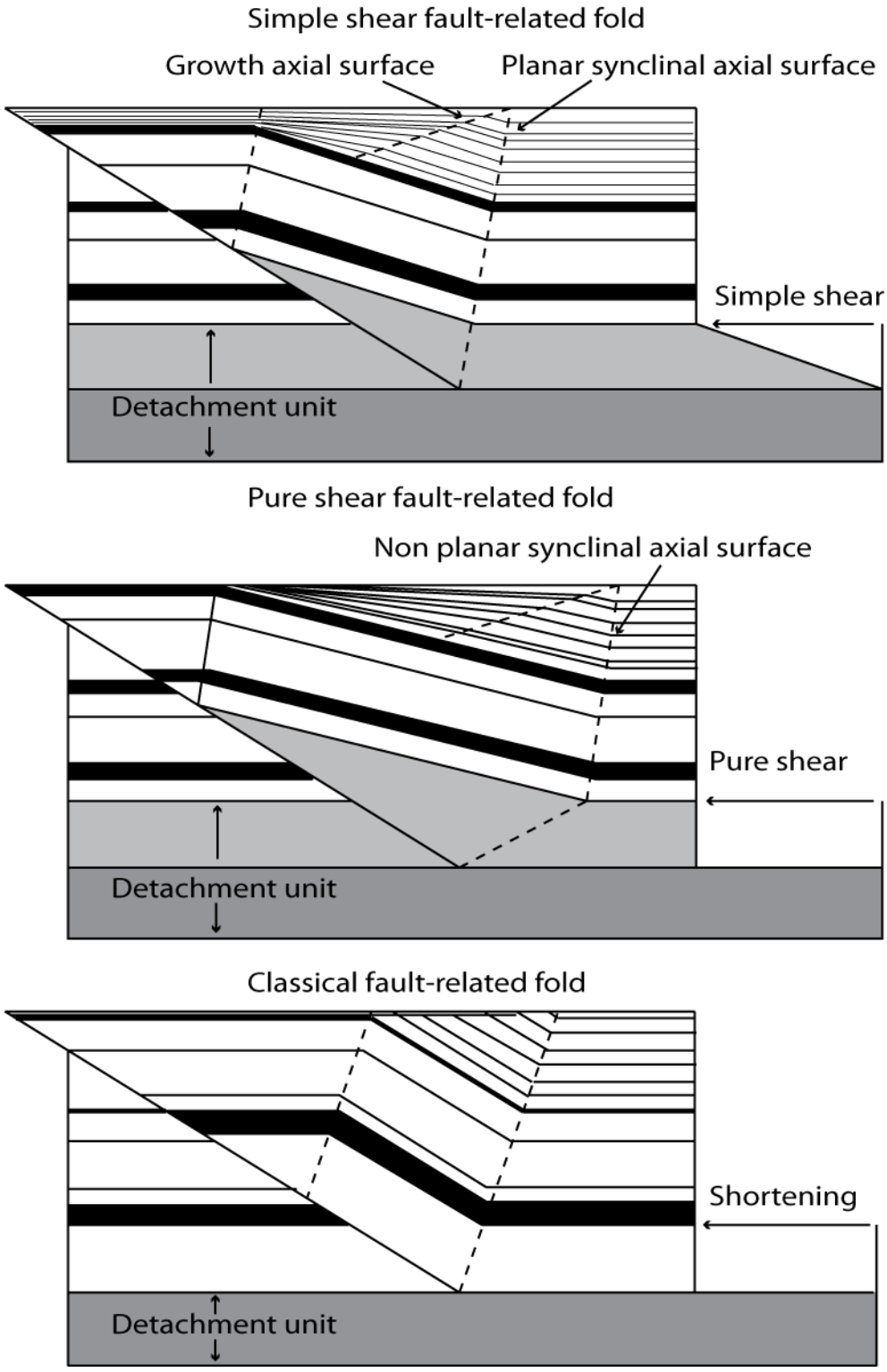

Fig. 1.20. Examples of simple and pure shear fault-related folding with comparison to a classical model of a fault-related fold (from Suppe et al., 2004).

1.12.5 Shear fault-related folds

Imbricate thrust faults can be subjected to externally applied shear and undergo internal deformation (Suppe et al., 2004; Corredor et al., 2005; Morley, 2009). Suppe et al. (2004) documents the two end-member types of shear (pure and simple shear) thrust-related folds. In cases where a thrust fault lies above a weak basal detachment succession deformation is distributed throughout the basal detachment succession at the base of the fault ramp. Shear fault-related folding produces fold backlimbs that differ geometrically from standard fault-bend and fault-propagation folds as the backlimbs dip significantly shallower than the underlying fault ramp (Suppe at al., 2004; Corredor et al., 2005) (Fig. 1.20).

In simple-shear fault-related folding the detachment succession undergoes externally imposed, bedding-parallel simple shear with no basal fault slip (Suppe et al., 2004). Layer-parallel shortening and thickening of the detachment succession is minimal. In pure-shear fault-related folding, the basal detachment succession shortens and thickens up the base of the fault ramp as some slip occurs along the basal detachment fault. The detachment succession shortens parallel to bedding and thickens normal to bedding above the fault ramp (Suppe et al., 2004; Corredor et al., 2005) (Fig. 1.20).

The application of these kinematic models to the gravity-driven deformation style of the Niger Delta will reveal insights into the evolution of the gravitational detachment system. Understanding fault-related kinematics will provide information on the progressive style of deformation that rocks have undergone during deformation. Kinematic analysis will allow for existing models to be improved, validated or invalidated within a particular structural setting or for a style of deformation (e.g. Problet et al., 2004). With the access to high-resolution seismic data additional information can potentially be gathered to further our understanding of how fault-related folds amplify.

1.13 Thesis Layout

This thesis is separated into seven chapters with the core research chapters (chapters 3-5) presented as a series of stand-alone manuscripts, which have been published, accepted or are currently in review in international journals. This thesis only contains manuscripts for which I am the first author and therefore was responsible for 90% of the data collection, interpretation and writing. These have been recast where appropriate for this thesis. Simon Higgins while completing his Ph.D. at Cardiff University provided the initial observations for the shale weld as detailed in the research outlined in chapter 4.

During the completion of the Ph.D. new data sets were acquired at during different stages. The data set used for the research detailed in chapter 4 was acquired at the start of the Ph.D. Access to the data used for the research detailed in chapter 3 was granted in the second year of the Ph.D. and the research was completed at BG Group offices. The data set used for the research in chapter 5 was acquired later, in the final year of the project.

- Chapter one (this chapter) outlines the thesis aims and rationale and provides a review of shale tectonics. It includes information on the deformation styles of argillaceous sediments (mobile shale), overpressure generation mechanisms and the range of deformation styles associated with gravitationally-driven shale tectonic provinces.
- Chapter two introduces the geological setting and stratigraphy of the Niger Delta and details the data sets and methodologies used for the analysis of the gravitational detachment system.
- Chapter three focuses within the up-dip extensional domain of the Niger Delta and highlights that deformation can be controlled by more than one master listric detachment fault, with the progressive shallowing of detachments. The evolution of the detachment fault system and its interaction, and influence, with sedimentary overburden deformation styles is

documented. Chapter three is currently in press in Basin Research: Maloney, D.P., R.J. Davies, J. Imber, and S. King, 2011, Structure of the footwall of a fault system revealed by 3D seismic data from the Niger Delta.

- Chapter four analyses the large-scale deformational processes that operate within a basal detachment succession composed of argillaceous sediments in contractional settings of the Niger Delta. In addition, how deformation within a basal detachment succession influences deformation styles within the sedimentary overburden. Chapter four is published in AAPG Bulletin: Maloney, D.P., R.J. Davies, J. Imber, S. Higgins, and S. King, 2010, New insights into deformation mechanisms in the gravitationally-driven Niger Delta deep-water fold and thrust belt (a copy is provided in the digital appendix).
- Chapter five analyses the brittle deformation styles, and structures, within the cores large-scale detachment-style folds close to the north-western, strike-slip margin of the Niger Delta. It is currently in review in the Journal of Structural Geology.
- Chapter six is a discussion chapter and places the principle results in context with other shale tectonic provinces. It draws upon field and modelling analogues in an attempt to assign deformational processes to succession interpreted to be occupied by mobile shale. Advances and recommendations for future research are highlighted.
- Chapter seven summarises the conclusions of this thesis.

2 Geological setting of the Niger Delta, data and methodology

This chapter outlines the geological setting of the Niger Delta together with the data sets and research methodologies used for analysing deformation mechanisms and processes within the gravitational detachment system. Analysis of deformation styles was dependent on the accurate interpretation of multiple marine based 3D and 2D seismic data sets. Four 3D seismic data sets and parts of four 2D regional seismic surveys were utilised, which combined provided high-resolution imaging of the sedimentary overburden and on occasions within the underlying basal detachment succession. The 3D seismic data sets traverse the delta providing imaging of the following structural domains that form within this gravitational detachment system: the up-dip extensional domain, a structurally segmented strike-slip domain on the north-western deltaic margin and the down-dip compressional toe. This chapter provides an introduction to the geology of the delta, seismic interpretation techniques, details the research methodologies used and summarises the seismic data sets used in this study.

2.1 Geological setting

The Niger Delta is a wave and tide dominated delta in the Gulf of Guinea on the West African margin that is fed by the Niger River (Doust and Omatsola, 1990; Hooper et al., 2002). It lies at the southern end of the Benue Trough, the failed arm of a triple rift junction, which formed during the opening of the Equatorial Atlantic in the Early Jurassic-Cretaceous with the breakup of African and South American plates (Burke, 1972; Lehner and De Ruiter, 1977; Doust and Omatsola, 1990). The two rift arms that followed the south-western and south-eastern coast lines of Nigeria and Cameroon developed into the passive continental margin of West Africa, while the third arm became the Benue Trough (Doust and Omatsola, 1990). During the Cretaceous, the Benue Trough became progressively filled with sediments of Albian age and by the Eocene a delta had begun to prograde over the passive margin (Burke,

1972; Doust and Omatsola, 1990). The delta is arcuate in form, covers an area of approximately 140,000 km^2 and is characterised by successions of deltaic sediments that can reach a maximum thickness of 12 km (Doust and Omatsola, 1990; Cohen and McClay, 1996; Hooper et al., 2002). Geometrically, it can be separated into its southern and western progradational lobes (Fig. 2.1). These deltaic lobes are separated by the Charcot oceanic fracture zone, a major basement structural high, which has served to compartmentalise the delta into its two dominant depositional lobes (Fig. 2.1).

The delta has been subdivided into five deformational zones, each characterised by a different thin-skinned structural style that formed as a consequence of gravitational instability. Corredor et al. (2005) identified: a) a proximal zone of extension dominated by regional and counter regional growth faults; b) a diapiric zone consisting of passive and active mud diapirs and shale ridges; c) an inner fold and thrust belt comprising of a series of regional imbricate thrusts; d) a translational zone between the inner and outer thrust belt where it is thought that sediments are subjected to relatively small quantities of deformation and only detachment folds develop; e) an outer fold and thrust belt characterised by regional and counter regional verging thrust faults (Fig. 1.2). The extension generated in up-dip proximal parts of the delta is mechanically linked to contractional structures that develop in the down-dip deltaic toe (Corredor et al., 2005).

2.2 Deltaic (seismic) stratigraphy

The deltaic stratigraphy of the Niger Delta can be separated into three lithological units: the Akata, Agbada and Benin Formations (Short and Stäuble 1967; Doust and Omatsola, 1990). These lithologic units can be identified by distinct acoustic properties on seismic reflection data, which are specific to each lithologic unit. The acoustic properties of each lithogical unit are detailed in the following sections below.

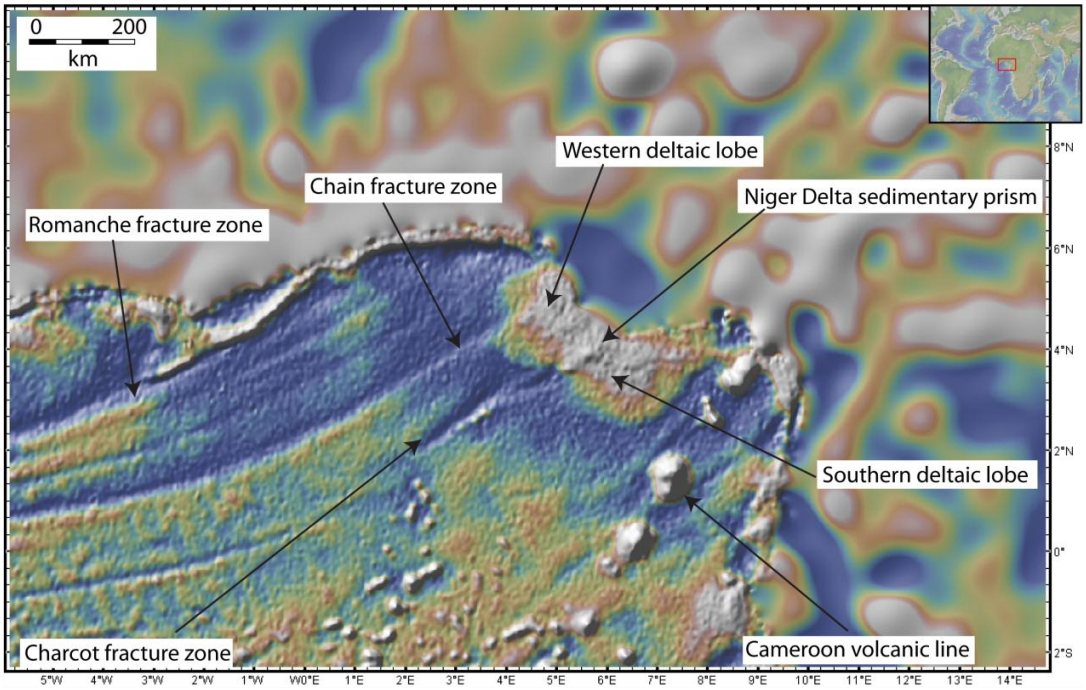

Fig. 2.1. Free air gravity map of the Niger Delta (downloaded from GeoMapApp). Gravity data overlay is from Sandwell and Smith (1997).

2.2.1 Akata Formation

The Akata Formation is the basal detachment succession of the delta and in the study area is mostly considered to be composed of fine-grained, pro-delta marine shales with subordinate amounts of silt, sand and carbonaceous interbeds (Doust and Omatsola, 1990; Cohen and McClay, 1996; Corredor et al., 2005). The Akata Formation is overpressured, considered to undergo ductile deformation and is often referred to as the mobile shale (e.g. Morley, 2003; Bilotti and Shaw, 2005) (e.g. Fig. 1.2).

The Akata Formation facilitates structural detachment and the horizontal translation of strata undergoing gravity-driven deformation. Overlying deforming strata in the sedimentary overburden decouple and gravitationally slide upon detachment levels at the Akata-Agbada Formation boundary and within the Akata Formation where the magnitude of overpressure is considered to be close to lithostatic pressure (Morgan, 2003; Cobbold et al., 2009). Multiple detachment levels are present within the Akata

Formation, which serve to separate brittle from ductile deformation styles, or undeformed strata (Corredor et al., 2005; Briggs et al., 2006). On seismic data the Akata Formation is represented by a dominantly acoustically transparent seismic interval within which a few laterally continuous and discontinuous, chaotic reflections are evident. The actual thickness of the Akata Formation is still uncertain with thickness estimates of up to 7000 m in the central deltaic lobes (Doust and Omatsola, 1990). Lateral and vertical thickness changes are common with up to 5 km thickening and thinning from proximal to distal regions (Corredor et al., 2005). A prominent high-amplitude reflection is evident within the lower half of the Akata Formation, which has been interpreted a major structural detachment fault in deep-water regions (Corredor et al., 2005; Briggs et al., 2006) (Fig. 2.2).

2.2.2 Agbada Formation

The Agbada Formation diachronously overlies the Akata Formation and consists of deep-water channel complexes and debris flows. On seismic data the Agbada Formation is represented by well imaged acoustic impedance contrasts representing alternative successions of deltaic sands and shales (Fig. 2.2). The Agbada Formation is heavily deformed by a series of regional and counter regional extensional faults in proximal settings and by fault-related folds in contractional settings.

2.2.3 Benin Formation

In landward (proximal) regions the Agbada Formation is in turn diachronously overlain by gravels, backswamp deposits and a series of fluvial continentally sourced sands known as the Benin Formation (Short and Stäuble, 1967). The Benin Formation is the thinnest of the three lithological units, reaching a maximum thickness of 2500 m and is absent in deep-water regions. On seismic data the Benin Formation is represented by canyons in shelfal settings and deep-water channel complexes off the shelf. The acoustic properties of the Benin Formation consist of high seismic amplitudes and well imaged acoustic contrasts, characteristic of the alternating successions of channel sands and interbedded fine-grained sediments.

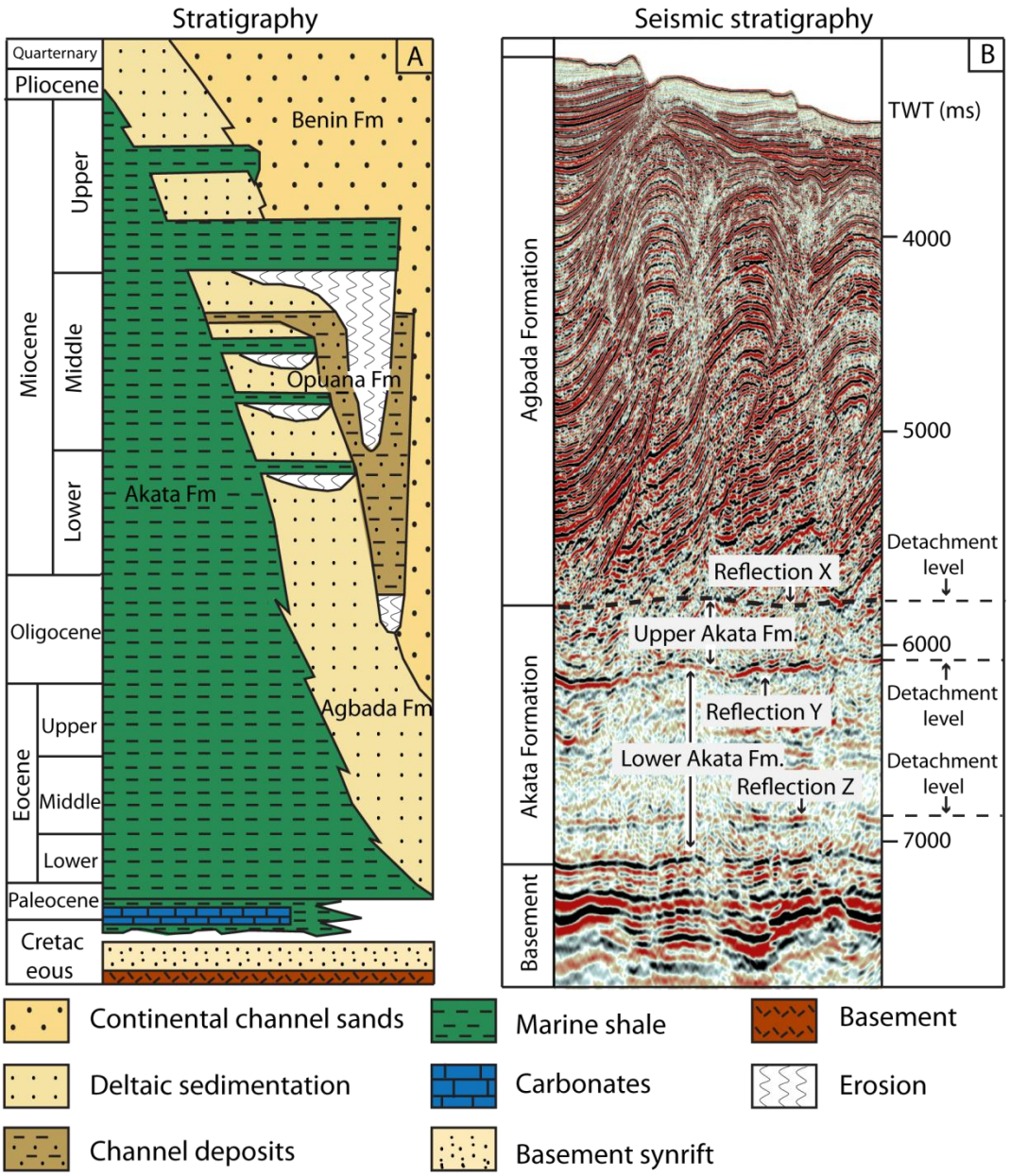

Fig. 2.2. A) Regional stratigraphy of the Niger Delta, depicting the three main diachronous lithological units of the Akata, Agbada and Benin Formations (from Corredor et al., 2005). B) Seismic profile from the deep-water, southern Niger Delta displaying the difference in acoustic impedance between the seismic facies that represent the Agbada and the Akata Formations.

2.3 Introduction to 3D seismic data and seismic interpretation techniques

The primary sources of data are marine seismic reflection surveys, which have a vertical scale in seconds two-way-travel-time (TWT). During marine acquisition seismic waves are generated by an acoustic pulse from an air or watergun (the seismic source), which propagates through the underlying water column and subsurface (e.g. Brown, 2004). Some of the energy within these acoustic pulses is then reflected and refracted at geological interfaces. These include geological boundaries (e.g. lithology changes, diagenetic events), where a change in fluid occurs (e.g. from water to hydrocarbons) and fault planes. This reflected and refracted energy is then detected by hydrophones and the arrival times of the seismic waves are measured (Kearey et al., 2002). At an interface between two different lithologies a change in rock properties and bulk rock density can occur (Brown, 2004). A change in rock density can induce a change in the velocity of the propagating seismic P-wave, which in turn creates a change in acoustic impedance (Z) across the interface between the two lithologies with differing properties. The acoustic impedance of a contact between two different lithologies is a product of rock density (ρ) and the velocity (v) of the propagating seismic P-wave (Equation 2.1).

$$Z = \rho v \qquad \text{Equation 2.1}$$

The velocity of a propagating seismic wave is affected by numerous factors including the composition, porosity, fluid content, texture and the elastic modulus of the lithology (Kearey at al., 2002). In order to determine the amplitude of a recorded wavelet the amplitude of the incoming wave is multiplied by the reflection coefficient (R), which is determined by the acoustic impedance contrast between the two interfaces with differing properties.

$$R = (v_2/ \rho_2 - v_1/ \rho_1) / (v_1/ \rho_1 - v_2/ \rho_2) \qquad \text{Equation 2.2}$$

Where v_1 and ρ_1, and v_2 and ρ_2 is the velocity of the propagating seismic wave and the rock density of the overlying (first) and underlying (second) lithologies encountered by a propagating P-wave (e.g. Fig. 2.3).

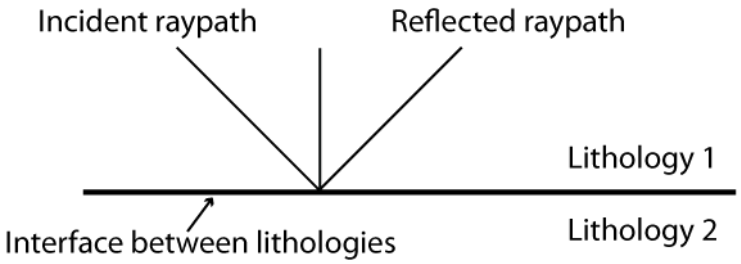

Fig. 2.3. Incident and reflected P-wave associated with change in acoustic impedance at the interface between two lithologies (modified from Kearey et al., 2002).

It then follows that if a change in acoustic impedance is not recorded, i.e. if the layered stratigraphy has homogeneous or near homogeneous rock properties, then a seismic interval will contain little or no reflectivity in the final TWT profile. A change in acoustic impedance induces a change in the amplitude of the recorded wavelet. Variations in the magnitude of the acoustic impedance boundary determine the amplitude response of the recorded wavelet. A large difference in acoustic impedance leads to a high-amplitude reflection and the opposite will generate a low-amplitude reflection or no reflection at all.

The amplitude response of the wavelet across an interface where there is an increase in acoustic impedance defines the polarity of the seismic data (Simm and White, 2002). To describe the seismic wavelet the phase of the data needs to be considered. Seismic reflection data are commonly either minimum or zero phase. Zero phase means the wavelet is symmetrical with the maximum amplitude situated on the geological interface that caused the reflection event (Brown, 2004) (Fig. 2.4). All the data used in this study are zero phase migrated. In European convention 'normal polarity' an increase in acoustic impedance causes a negative amplitude response (a tough displayed in red). A decrease in acoustic impedance causes a positive amplitude response (a peak displayed in black) (e.g. Brown, 2001; Simm and White,

2002) (Fig. 2.4). In American convention 'normal polarity' the inverse is true, i.e. an increase in acoustic impedance causes a positive amplitude response. The seismic reflection data used in this study are of both European and American polarity.

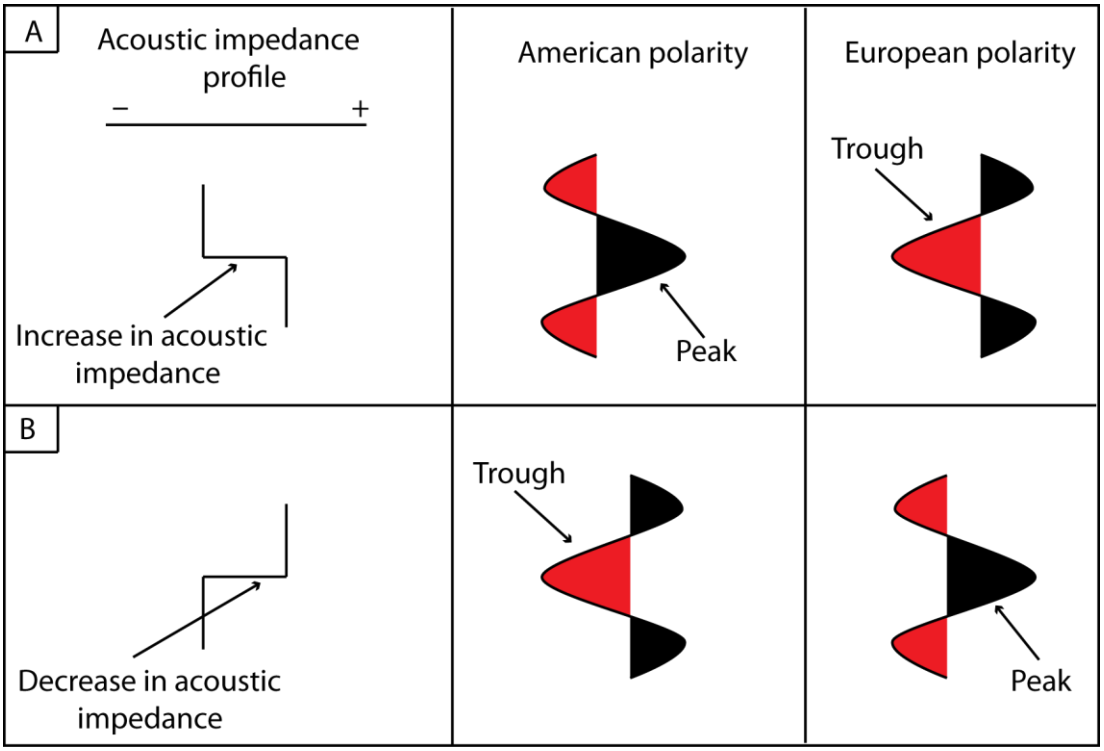

Fig. 2.4. Illustration of American and European polarity for A) an increase in acoustic impedance and B) a decrease in acoustic impedance for zero phase seismic migrated reflection data. Peaks are displayed in black and troughs in red (modified from Simm and White, 2002).

Acquisition of 3D seismic data acquires a tight grid of inlines (lines orientated normal to strike of structures) and crosslines (orientated parallel to strike of structures) at regularly spaced intervals. Typically, 3D seismic data sets have an inline and crossline spacing of 12.5 m. 2D acquisition is similar to 3D acquisition, but instead of acquiring a tight grid a loose set of inlines and crosslines is acquired. Line spacing may range between 300 m and 1000 m in 2D surveys and are they are focussed in capturing the geometry of large-scale regional structures.

2.3.1 Seismic attribute analysis

Seismic attribute maps were generated and used to aid structural and stratigraphic interpretation of the subsurface. Amplitude maps and coherency data were used to highlight discontinuities within a seismic volume that in this case represented structural features (faults), which may have been difficult to identify on a normal reflectivity volume. Seismic amplitude corresponds to a change in acoustic impedance so a greater seismic amplitude relates to a large increase or decrease in acoustic impedance. Root mean squared (RMS) amplitude is an average amplitude that can be calculated on a horizon, across a horizon or summed over window, and is useful for highlighting discrete changes (Brown, 2004). Coherency serves to highlight discontinuities within a seismic volume. Seismic reflections that have been offset by faults and structural features have a different seismic character to adjacent continuous reflections and these zones of discontinuous seismic character, which become apparent in a coherency volume (Brown, 2004).

2.4 Seismic resolution

Ductile successions have historically been difficult to image using seismic reflection data and have been, and on occasions still are, represented by seismic intervals that contain little or no internal coherent reflectivity (e.g. section 1.8). Understanding the spatial limits of the horizontal and vertical resolution within a seismic data set is critical to constructing a valid interpretation through seismic intervals where coherent reflectivity is limited. The vertical resolution of seismic data is a measure of the ability to recognise individual, closely spaced reflections and is measured with respect to the reflected wavelet (λ) (Kearey et al., 2002). The vertical resolution is equal to one-quarter of the seismic wavelength ($\lambda/4$) (Brown, 2004) and gives a representation of the thinnest bed thickness that can be imaged. The seismic wavelength (λ) is defined by:

$$(\lambda = v/f) \qquad \text{Equation 2.3}$$

where v is the velocity and f is the dominant frequency of the propagating seismic wave (Brown, 2004). Thus, the shorter the wavelength the higher the frequency, which in turn gives a higher vertical resolution. However, when the thickness of a bed is exactly one-quarter of the dominant wavelength the amplitude of the reflected wavelet can be increased due to the tuning effect (e.g. Brown, 2004). Tuning arises due to constructive interference of wavelets reflected from both the top and the base of a bed. If beds continue to thin past this point they are increasingly tuned, until the limit of resolution is reached and the reflection is no longer visible (Brown, 2004). The resolution of a bed is also dependent on the depth at which the bed is being imaged. As rocks commonly become more compacted with increasing depth the velocity of propagating seismic waves also increases, as seismic waves are able to propagate faster through indurated, consolidated beds than poorly lithified ones. Conversely, the frequency of a propagating seismic wave decreases with depth as higher frequencies become attenuated, which has the effect of reducing seismic resolution. As a result seismic wavelength increases with depth resulting in a lower-quality image (Brown, 2004).

The horizontal resolution of seismic data is controlled by two dominant factors: 1) the detector (hydrophones for marine surveys) spacing; 2) the intrinsic limit imposed by actual processes of reflection (Kearey et al., 2002). The horizontal resolution of 3D surveys is controlled by the line spacing. If one considers any flat lying reflection the horizontal resolution is limited to being half the length of the receiver sampling, therefore a closer detector spacing will enable reflections from the same acoustic interface to be correlated with greater confidence (Kearey et al., 2002). The second factor is inherent to the actual process of reflecting seismic wavelets at geological interfaces as they propagate through the subsurface. Acoustic energy sent from a source spreads out over large areas. Wavelets are not reflected as singular paths as commonly depicted (e.g. Figs. 2.3 and 2.5A) rather the reflection interface is actually an infinite number of point scatters where each scatter contributes to the final energy of the reflected signal (Kearey et al., 2002). The energy that is returned to a detector within half a wavelength of the initial reflected arrival interferes constructively and forms the Fresnel Zone (Kearey et al., 2002) (Fig. 2.5A). The width of the Fresnel Zone represents the absolute limit of horizontal resolution

within a seismic survey as reflections separated by a smaller distance than this cannot be individually resolved. The radius of the Fresnel Zone is expressed as:

$$v/2(t/f)^{0.5} \qquad \text{Equation 2.4}$$

where the Fresnel zone is a function of the velocity (v), frequency (f) of a wave and the TWT (t) to the reflection (Sheriff and Geldart, 1995; Brown, 2004). The radius of the Fresnel zone determines the horizontal resolution, which can be improved by migration techniques. Migration serves to reposition out of place reflections, focus energy dispersed across the initial unmigrated Fresnel zone, minimise diffraction patterns and ultimately reduces the size of the Fresnel Zone (Brown, 2004) (Fig. 2.5B). As the frequency of a propagating wavelength decreases with depth the size of the Fresnal Zone increases with reflection depth and so horizontal resolution also degrades with depth (Kearey et al 2002).

2.5 Interpretation problems

The interpretation of deep subsurface geology can be problematic, especially when mapping low resolution seismic intervals. Within a vertical TWT profile the seismic resolution of stratigraphic intervals within the Niger Delta can vary dramatically. The basal detachment succession marks a distinct change in seismic facies within which seismic resolution is significantly reduced (Fig. 2.6). The majority of seismic data sets suffer from imaging problems through the basal detachment succession (especially notable within 2D seismic surveys) making interpretations in some places problematic (Figs. 2.6 and 2.7) (see appendix 2, Figs. A1-A3).

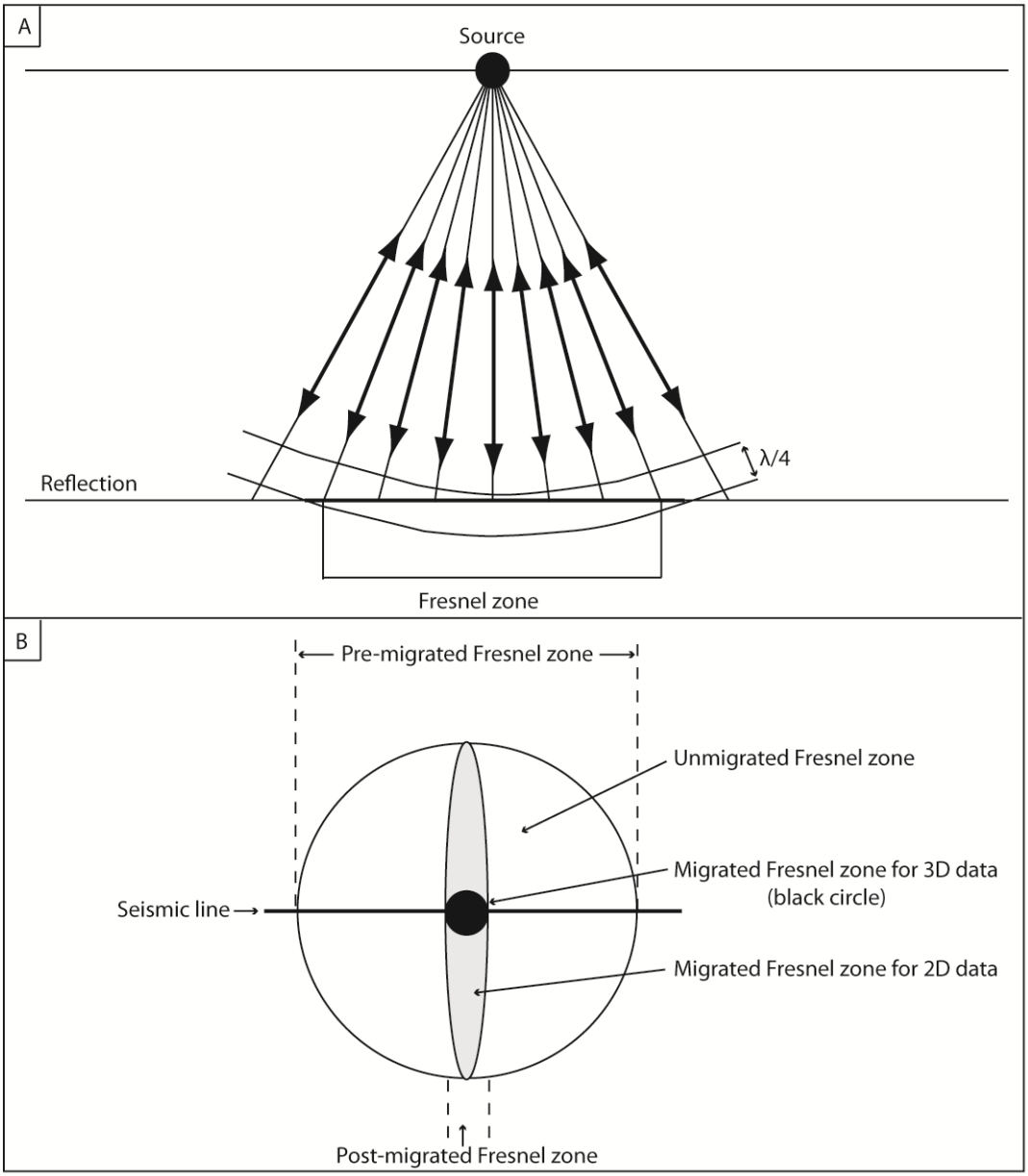

Fig. 2.5. A) The part of the reflection from which energy is returned to the source within half a wavelength makes the Fresnal zone (after Kearey et al., 2002). B) The Fresnal zone before and after migration. The unmigrated Fresnel zone is represented by the large circle which is then reduced to the oval after 2D migration and the black circle for 3D migration (after Brown, 2004).

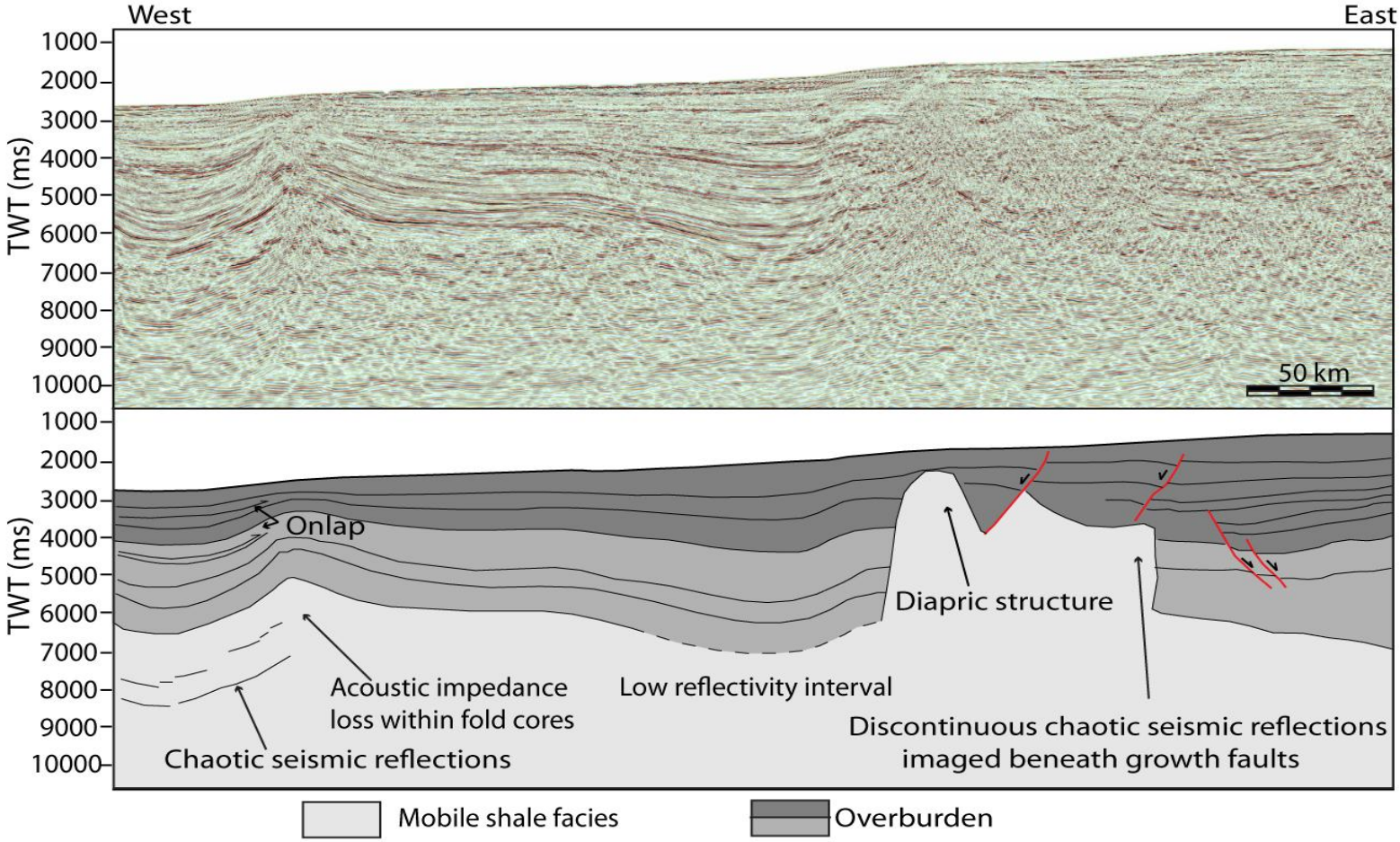

Fig. 2.6. Seismic cross-section from a 2D seismic survey from the Niger Delta showing the loss of acoustic impedance contrasts associated with the presence of gas, structural complexity and overpressured sediments at the base of the delta. Vertical scale is 1.5x the horizontal scale.

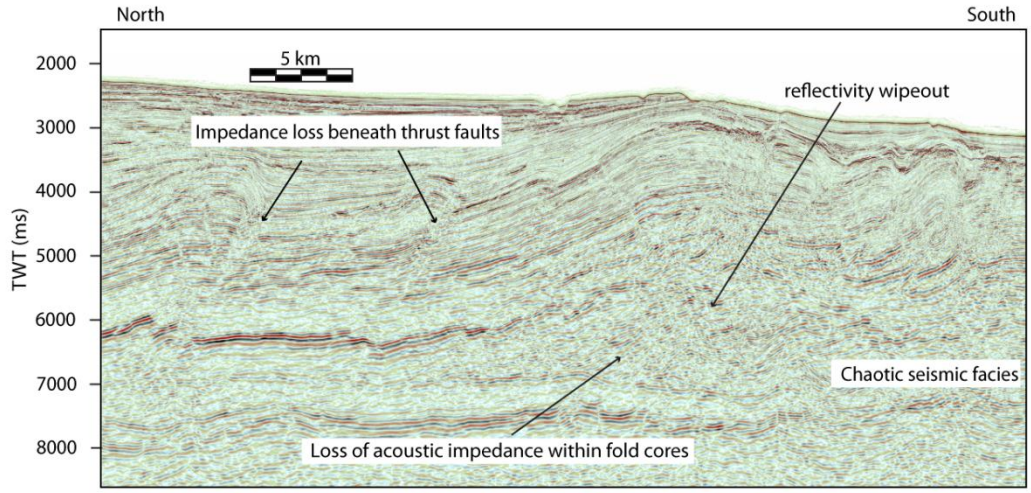

Fig. 2.7. Seismic cross-section from a 2D seismic survey showing two distinct seismic facies, which are representative of the Agbada and Akata Formations. The loss of seismic resolution occurs within the basal detachment succession (the Akata Formation). The reduction in resolution is associated with overpressured, argillaceous sediments, which here thicken in the core of a large-scale anticline. Vertical scale is approximately 2.5x the horizontal scale.

The lack of resolution within a seismic interval occupied by overpressured sediments can be caused by numerous reasons. Within the Niger Delta these include 1) a lack of acoustic impedance contrasts due to the homogeneous nature of the basal detachment succession, i.e. no corresponding change in rock density and therefore the velocity of a propagating seismic wave, 2) pore-fluids that have become overpressured with burial, which has the effect of reducing grain to grain contacts hindering the generation of acoustic impedance contrasts, 3) the basal detachment succession is on the limit of seismic resolution as propagating seismic waves are attenuated with increasing depth and so the majority of detail could be on a sub-seismic scale, 4) acoustic impedance contrasts are masked below features that can cause strong heterogeneities in vertical impedance e.g. beneath faults and gas traps.

Of primary importance when interpreting seismic intervals occupied by overpressured sediments is the seismic velocity of the overpressured interval in comparison to the seismic velocity of overlying, and underlying seismic intervals.

As the vertical scales of all the seismic data sets are in TWT the apparent thickness of a particular seismic interval is dependent on the time it takes for a propagating seismic wave to travel through it. The presence of overpressured, fine-grained sediments can cause a velocity inversion in a velocity-depth profile, which is marked by a significant reduction in the velocity of propagating P-waves. In the Niger Delta the Akata Formation exhibits low P-wave seismic velocities at the top of the overpressured interval (approximately 2000 ms^{-1}) (Morgan, 2003; Corredor et al., 2005) (Fig. 2.8) with a velocity inversion of up to 1000 ms^{-1} (Morgan, 2003) (Fig. 2.8). This velocity inversion can cause distortions in the apparent dips of reflections viewed in a TWT profile. A velocity "push down" is caused when an overlying seismic interval has a slower seismic velocity than an underlying seismic interval. This effect is present within some seismic reflection profiles from the Niger Delta (e.g. Fig. 2.9) (appendix 2, Figs. A1-A3). Velocity "pull up" of reflections is caused by the opposite scenario. In addition, the apparent dip of reflections viewed in TWT can also be perturbed by lateral changes in the velocity of the reflection interval.

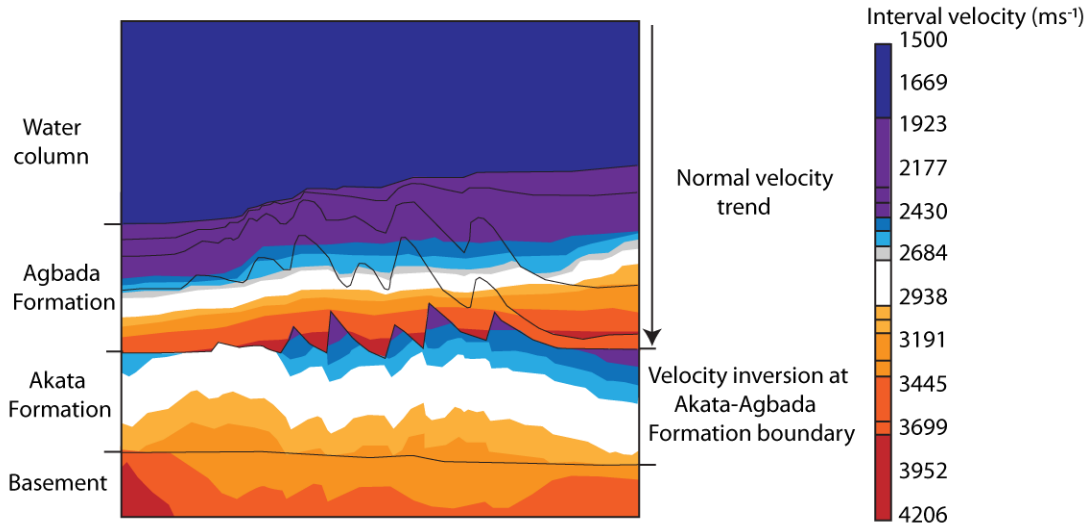

Fig. 2.8. Velocity model compiled from 2D seismic stacking velocities that reveal the inversion in the velocity gradient at the Agbada-Akata Formation boundary. This inversion is in excess of 1000 ms^{-1} indicative of undercompaction and overpressured sediments (modified from Morgan, 2003).

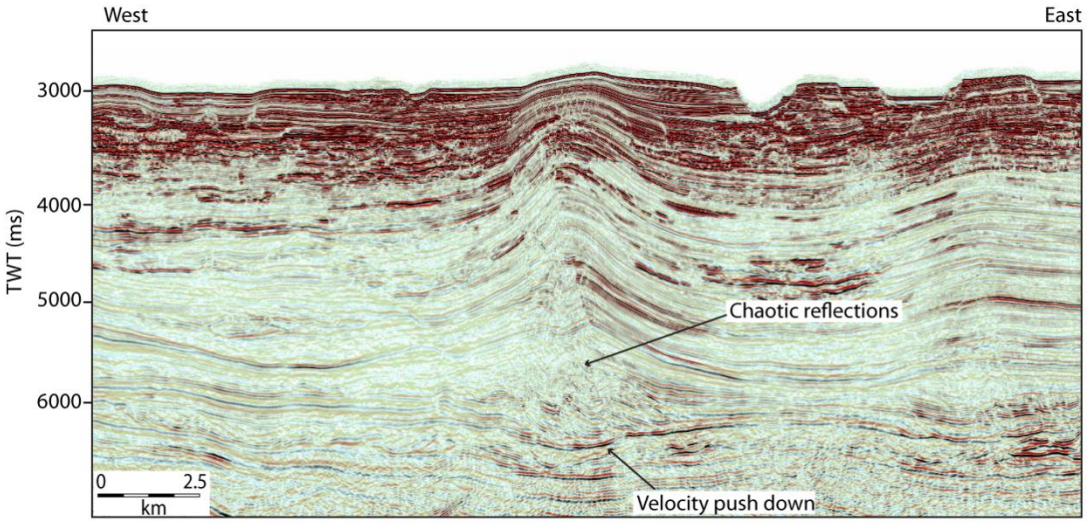

Fig. 2.9. Seismic profile showing an example of "push down." Reflections directly beneath the large-scale anticline have been warped downwards. The anticline is interpreted to be cored by overpressured, argillaceous sediments, which have a low seismic velocity and have caused the "push down". Adjacent parts of the same reflections in the synclinal regions of the anticline appear to be at a shallower depth. Vertical scale is 2.5x the horizontal scale.

2.6 Key structural and stratigraphic reflections

There are several key reflections that mark important structural and stratigraphic boundaries within the Niger Delta (see appendix 2, Figs A1-A3). As deposition within the Niger Delta was diachronous no age dates were assigned to individual horizons unless well control was available, which provided biostratigraphical data and age constraint. The seismic characteristics of the key laterally extensive horizons, which can be correlated throughout the whole delta, are recorded in Table 2.1 (also see appendix 2, Figs A1-A3). In addition, reflections that could only be correlated over part of the delta, i.e. local unconformities and reflections that defined seismic facies, were interpreted within each seismic data set to define structural geometries, determine relative timing relationships of structural features and to define seismic facies. On 3D seismic data horizons were interpreted in regular inline and crossline intervals, which were then autotracked (zapped) to generate a spatially continuous surface (horizon).

Horizon	Amplitude of reflection	Reflection continuity
Seabed	Positive and negative, strong	Laterally continuous.
Upper-Akata reflection	Positive and negative, weak in places.	Laterally continuous not always a single coherent reflection. Changes stratigraphic level continuously in places.
Mid-Akata reflection	Positive fluctuates from moderate to weak.	Laterally continuous, areas of little to no reflectivity. Absent in places.
Basement	Positive fluctuates from strong to weak.	Laterally continuous, areas of little to no reflectivity.

Table 2.1. Seismic characteristics of the main reflections present throughout the Niger Delta from all seismic surveys with differing polarities.

2.7 3D seismic data sets

2.7.1 BG Group in-house 3D data

The in-house BG Group 3D seismic survey covers an area of 1523 km^2 and is situated within the up-dip extensional domain of the Niger Delta (Fig. 2.10) (the survey name is not included as per a confidentiality request from BG Group). The seismic survey is a pre-stack time migrated volume with a line spacing of 12.5 m in inline and crossline directions. The data are zero phase migrated and an increase in acoustic impedance is displayed as a red-black-red reflection combination. The maximum vertical resolution is 14 m (33 Hz) in shallow sections (the first 0.5 s TWT of stratigraphy imaged below the seabed). Stacking of seismic records enhances the signal-to-noise ratio by adding reflections that occur from the same subsurface point (Kearey et al., 2002). Pre-stack time migration refers to seismic data that is migrated before the stacking process occurs. Interpretation of BG Group's in-house data was done using GeoFrame, BG Group's in-house seismic interpretation software

package. The horizons chosen to be interpreted were based upon biostratigraphic age dates, unconformities and key structural features which usefully define the structural geology of this region (only seismic data and horizon maps that have been released for publication by BG Group are included within this thesis). Biostratigraphic age data and interval velocities for sedimentary packages were constrained by a nearby unreleased well and stacking velocities where used for the sedimentary packages within the basal detachment succession (Note that well locations and data are not shown in this study as per a confidentiality request from BG Group).

2.7.2 OPL 314

OPL 314 lies approximately 25 km down-dip from OPL 332 (Fig. 2.10) and is situated upon the north-western margin of the Niger Delta. OPL 314 covers an area of 1878 km^2 and is a pre-stack time migrated volume with a line spacing of 12.5 m in inline and crossline directions. The data are zero-phase migrated and an increase in acoustic impedance is displayed as a black-red-black reflection combination. The maximum vertical resolution is 12 m the initial 0.5 s TWT below the seabed.

2.7.3 MC3D JDZ

The MC3D JDZ seismic data set provides imaging of the toe of slope, down-dip compressional domain within the southern Niger Delta and covers an area of approximately 3000 km^2 (Fig. 2.10). It is a post-stack time migrated volume with an inline and cross line spacing of 12.5 m and is zero phase migrated. An increase in acoustic impedance is displayed as a red-black-red reflection combination. Post-stack time migration refers to seismic data that has been stacked before the data is migrated. The maximum vertical resolution is 8 m (50Hz) in shallow sections, which decreases to approximately 25 m (23Hz) at the base of the Agbada Formation with the onset of the overpressured sediments. Interval velocities used for depth conversions (section 2.9) were provided from an unreleased commercial borehole, which are not included as per a confidentiality request from BG Group.

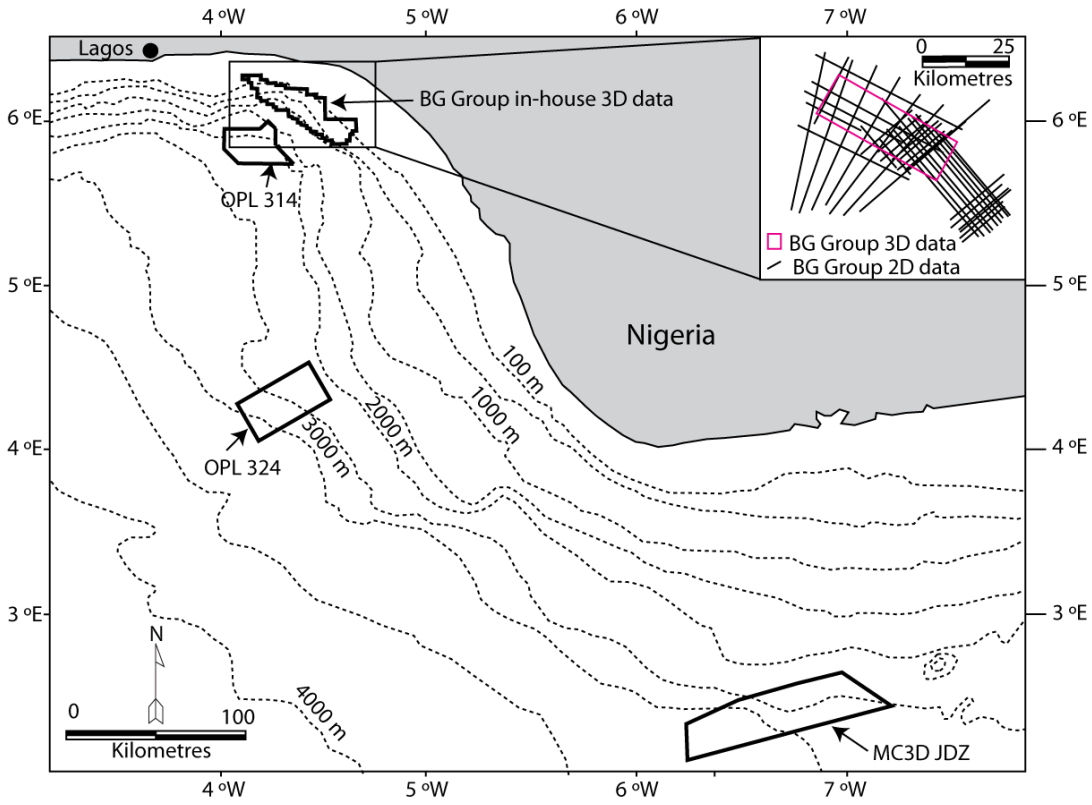

Fig. 2.10. Map of the Niger Delta showing the locations of the 3D seismic surveys and of BG Group's in-house 2D and 3D seismic data.

2.7.4 OPL 324

The OPL 324 3D seismic survey is situated in the western Niger Delta and images a section of the deep-water contractional domain (Fig. 2.10). The survey covers an area of 1630 km^2 with an inline and crossline spacing of 25 m and is a post-stack migrated volume. The maximum vertical resolution is 8 m in shallow sections, which deteriorates to approximately 20 m at the depth of the basal detachment succession. The data are zero phase migrated. An increase in acoustic impedance is displayed as a black-red-black reflection combination (European polarity).

Interpretation of the OPL 324, 314 and the MC3D JDZ seismic survey were done using Landmark Seisworks software interpretation package (courtesy of Halliburton).

2.8 2D Seismic surveys

The 2D seismic surveys were used to supplement, and in conjunction with, the 3D seismic volumes to place the 3D seismic data in structural context with relation to the large-scale regional geology of the Niger Delta.

2.8.1 VER98NG2D and VER99NG2D

VER98NG2D and VER99NG2D data sets were acquired by CGGVeritas in 1998 and 1999 respectively. Acquisition used an airgun array with a shotpoint interval of 50 m. These two surveys mainly image the deep-water contractional toe of the Niger delta with a few north-east-south-west orientated lines imaging the translational and small sections of the up-dip extensional domain. In the southern Niger Delta north-south trending seismic lines image cross sections perpendicular to the strike of structures within the subsurface (cross lines). The locations of the 2D seismic surveys are provided on individual study maps in later chapters (Figs 3.2 and 4.2).

2.8.2 BG Group in-house 2D data

The in-house BG Group 2D seismic surveys (Fig. 2.10) image a region of extension in the north-western Niger Delta. North-east-south-west trending seismic lines are orientated approximately perpendicular to the strike of structures within the subsurface. (Survey names and acquisition details are not included as per a confidentiality request from BG Group).

2.9 Depth conversion

Structures imaged in TWT may undergo geometric changes when depth converted due to seismic velocity increasing with increasing depth or through lateral variations in seismic velocity (Brown, 2004). As such, potential geometric changes that may occur during the depth conversion process were explored and analysed (e.g. Fig. 2.11). Selected cross-sections from both 2D and 3D seismic surveys were depth converted within the software 2DMove (courtesy of Midland Valley). To convert TWT into metres 2DMove uses the depth conversion function:

$$Z = V° (e^{kt} - 1) / k \qquad \text{Equation 2.5}$$

where Z is the depth in metres, V° is the initial velocity (ms), k is the rate of change in velocity with increasing depth and t is the one-way travel time. To convert TWT to metres in 2DMove a 2D TWT seismic cross-section is interpreted and digitized. Average interval velocities are then assigned to each reflection interval. 1480 ms^{-1} was used for the velocity of seawater and extrapolated interval velocities for underlying sedimentary packages from the closest available well for the BG Group seismic data and the MC3D JDZ surveys were used. Where no well data were available a 2D velocity model of the deltaic stratigraphy published by Morgan (2003) was used, or a constant velocity of 2000 ms^{-1} was used for sediment. A depth converted TWT profile is illustrated in figure 2.11, which allows the geometric differences that arose with using different velocities for depth conversions to be compared. The most significant change in geometry occurs at the depth of the basement reflection, which takes on an irregular appearance in the various depth profiles. Depth conversions of selected TWT profiles were performed within all 3D seismic surveys and selected 2D regional seismic lines to validate and improve initial structural interpretations.

Although a useful workflow the depth conversion function in 2DMove has inherent limitations. As the depth conversion process does not incorporate a heterogeneous 3D velocity model, lateral heterogeneities in seismic velocity are not incorporated into the depth conversion process. In addition, the process only allows an average seismic velocity to be assigned to each digitized reflection interval. Velocity is assumed to be vertically homogeneous through each seismic interval until a new seismic interval occurs and a different bulk velocity is assigned. As such, where depth conversions were implemented using homogeneous velocities the final depth converted geometries are considered only representative approximations.

2.10 Decompaction

Decompaction is a technique designed to remove the effects of volume loss (compaction) that occurs within a rock volume as it is progressively buried (Sclater and Christie, 1980). Decompaction of depth converted cross-sections was run in parallel with sequential restorations (section 2.11) in 2DMove. Before a stage of restoration could be completed the overlying water column and growth strata and were removed and the remaining underlying section was allowed to vertically expand. This expansion attempts to correct for reduction in porosity that occurs with burial in normally compacted sediments (Sclater and Christie, 1980). In 2DMove the relationship between porosity and depth is expressed as an exponential (Equation 2.7):

$$f = f_{\circ}, e^{-cz} \qquad \text{Equation 2.7}$$

where f is the present day porosity, $f_{\circ}$ is the surface porosity, c is the porosity-depth coefficient (km^{-1}) and z is the depth (m) (after Sclater and Christie, 1980).

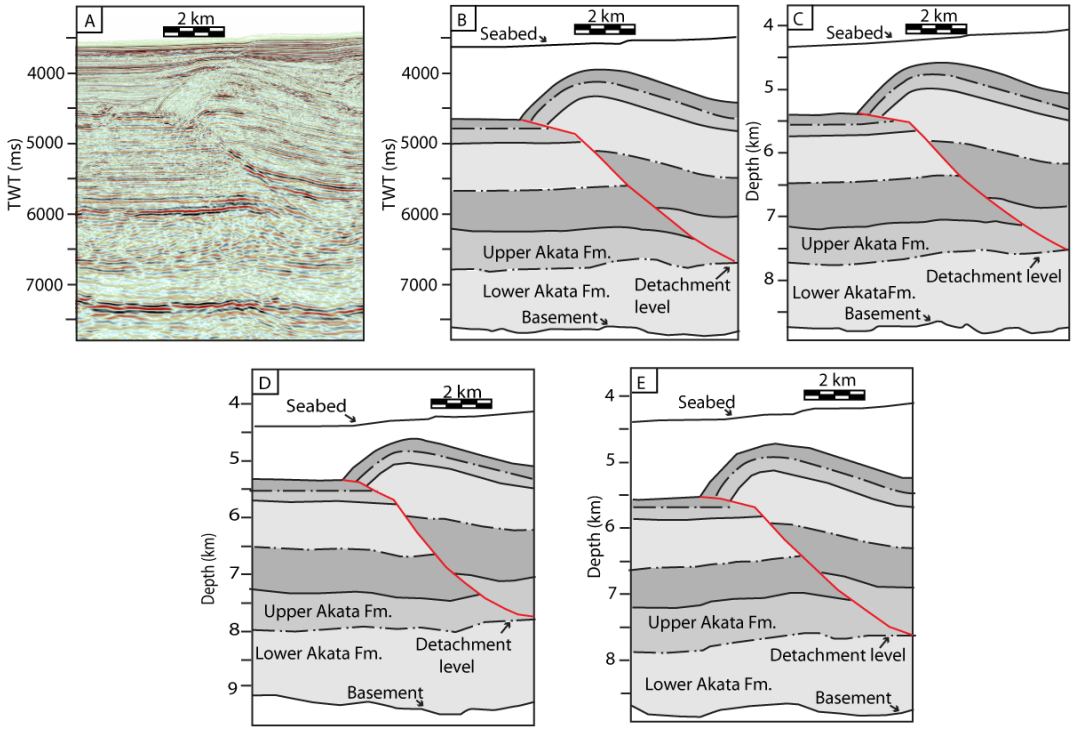

Fig. 2.11. Depth converted fault-related fold showing the geometric variation that can arise as a consequence of the velocity model used. A) The time section is interpreted and digitized (shown in panel B). Interval velocities were assigned to every seismic interval and the section was depth converted. Comparisons between apparent geometries in the TWT profile are compared with the corresponding geometries shown in depth. C) Depth conversion using confidential interval velocities extrapolated from a nearby borehole. D) Depth conversion using the 2D velocity model published in Morgan (2003) (shown in Fig. 2.9). E) Depth conversion using a constant velocity of 2000 ms^{-1}. Vertical scale is approximately 2x the horizontal scale.

As overpressured basal detachment successions are undercompacted the decompaction function was decoupled at the top of the basal detachment succession. Where a structural interpretation involved successions having undergone ductile deformation the overpressured succession was treated as incompressible, as overpressured sediments attain a fixed porosity despite any further increases in burial depth (Maltman and Bolton, 2003). In 2Dmove incompressible units are assigned a porosity-depth coefficient of 0.001, which allows the overpressured interval to undergo greater vertical expansion when decompacted relative to adjacent seismic

intervals. However, how to exactly deal with overpressured successions during the decompaction process was problematic.

Some uncertainty was introduced with the decompaction workflow as average porosity values are needed for the accurate expansion of the section being decompacted. As no porosity data were available the default values provided within 2DMove, which are based on data collected from the North Sea were used (e.g. Sclater and Christie, 1980).

2.11 Structural restoration

Selected structural interpretations were tested and validated and estimates of horizontal shortening were attained through structural restoration techniques within the software 2DMove. Restoration involves taking the geometry of a deformed structure and restoring it to a horizontal or regional datum (Dahlstrom, 1990). There is no unique method for the restoration of a particular geological structure as multiple methods and techniques can provide valid restorations of the same structure. The methods used for the restoration of geological cross-sections within the Niger Delta involved using both kinematic and non kinematic techniques based on the interpreted structural style present within a particular survey area. Kinematic methods use geometric constraints to define material pathways for the purpose of restoring deformed prekinematic successions back to their predeformed state (e.g. Suppe, 1983; Dahlstrom, 1990), which are typically related to the coeval movement of material with slip on a fault plane ("move-on-fault algorithms"). Non-kinematic restorations do not require geometric constraints (Mitra and Namson, 1989). The kinematic restoration techniques used were trishear folding (e.g. Erslev, 1991) and fault parallel flow. Non kinematic techniques involved flexural slip (section.2.112.1) and area balancing (section 2.112 .3) (Mitra and Namson, 1989).

2.11.1 Kinematic techniques

2.11.1.1 Trishear folding

The trishear model is based on the basis that instead of strain being concentrated on a singular discontinuity (i.e. a fault plane) a triangular zone of distributed strain is situated in front of a propagating fault tip (Erslev, 1991). The apex of the triangular zone of strain is situated at the fault tip and is symmetrical about the fault plane in order for volume to be maintained (Erslev, 1991) (Fig. 2.12). Shear within the trishear zone is related to the width of the triangular zone. Near the apex strain is concentrated in a narrow band, which becomes more progressively more diffusive away from the apex. Within the trishear zone the velocity of the hanging wall fluctuates in magnitude and orientation relative to the underlying stationary footwall along a line normal to the fault plane. Material next to the hanging wall must have the same velocity as the material in that block outside the triangular shear zone. Material within the shear zone towards the bottom boundary experiences a rotation as the velocity must rotate toward being parallel with the base of shear zone (Fig. 2.12). These are the boundary conditions required to maintain constant volume within a trishear zone. The trishear model has the advantage of explaining fault-related folds which do not follow kink band models (i.e. fault-bend and fault-propagation folding) (Erslev, 1991).

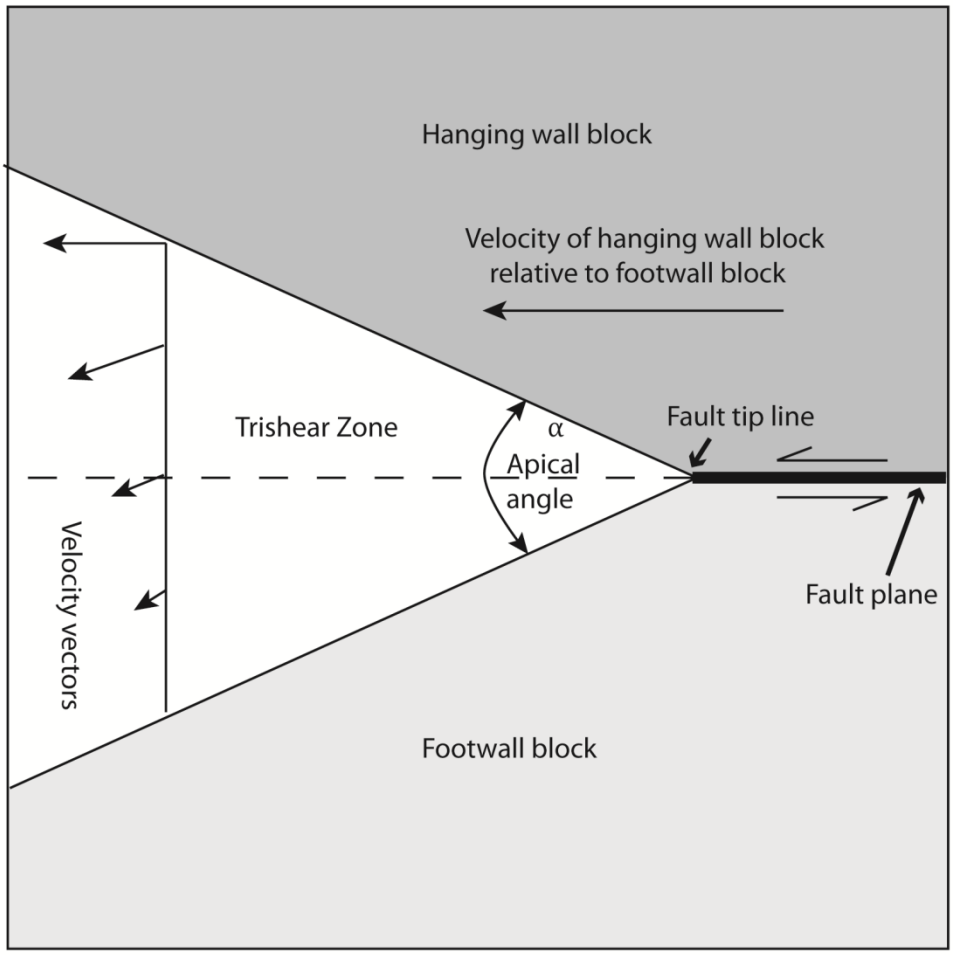

Fig. 2.12. Illustration of trishear (from Twiss and Moores, 1992)

2.11.1.2 Fault parallel flow

Fault parallel flow as the name suggests is the movement of an overriding hanging wall block that has been displaced by fault parallel shear (Fig. 2.13). The workflow for restoring fault-related folds using fault parallel flow is shown in figure 2.13. The restoration process involves the creation of flow pathways that are aligned parallel to the geometry of the fault plane (Fig. 2.13B). The hanging wall block is then subsequently resorted by material 'flowing' along the constructed flow paths. Fault parallel flow is widely applied to contractional fold and thrust belts.

2.11.2 Non-kinematic techniques

2.11.2.1 Flexural slip

Flexural slip unfolding restores a folded layer to a horizontal or inclined datum by slip acting parallel to the folded layers. Typically, the uppermost layer is chosen to be the template bed (the bed which is actively chosen to be unfolded), and additional folded layers are unfolded passively during the restoration process (Fig. 2.14). Flexural slip maintains thickness variations between beds and the line-length of passive beds and is commonly applied to contractional fold and thrust belts.

2.11.2.2 Area balancing

Cross-sections that are characterised by thickness changes in multiple strata units need to be area balanced (Mitra and Namson, 1989). Equal-area balancing involves an area restoration of beds to their undeformed geometries assuming plane strain (Chamberlin, 1910; Mitra and Namson, 1989).

Area balancing involves calculating the area of the deformed shape (A_x) and the original undeformed thickness (z) of the unit. The average restored bed length (la) can then be determined by Equation 2.6.

$$la = A_x/z \qquad \text{Equation 2.6}$$

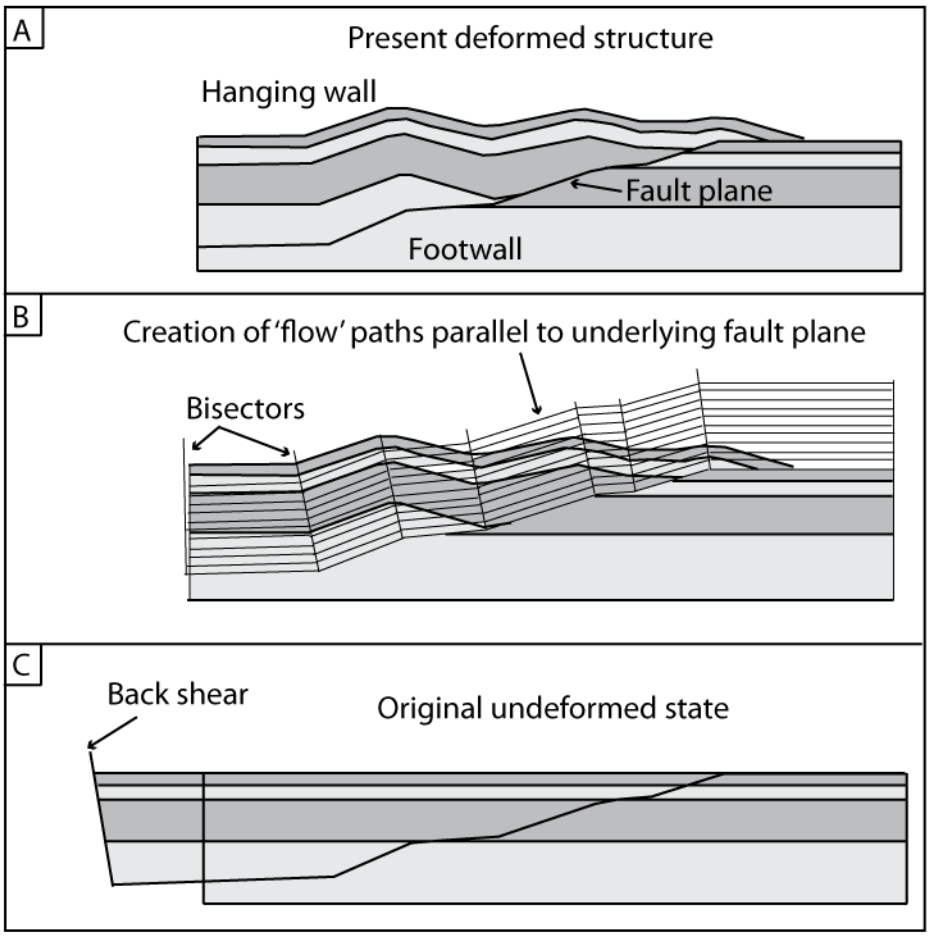

Fig. 2.13. Diagram illustrating the methodology used for fault parallel flow. A) An initial structure is digitised and imported into 2DMove. B) Flow lines and bisectors are created, which constrain the paths through which material in the hanging wall will move. C) The final undeformed restored geometry (from Midland Valley 2D Move training manual, 2010).

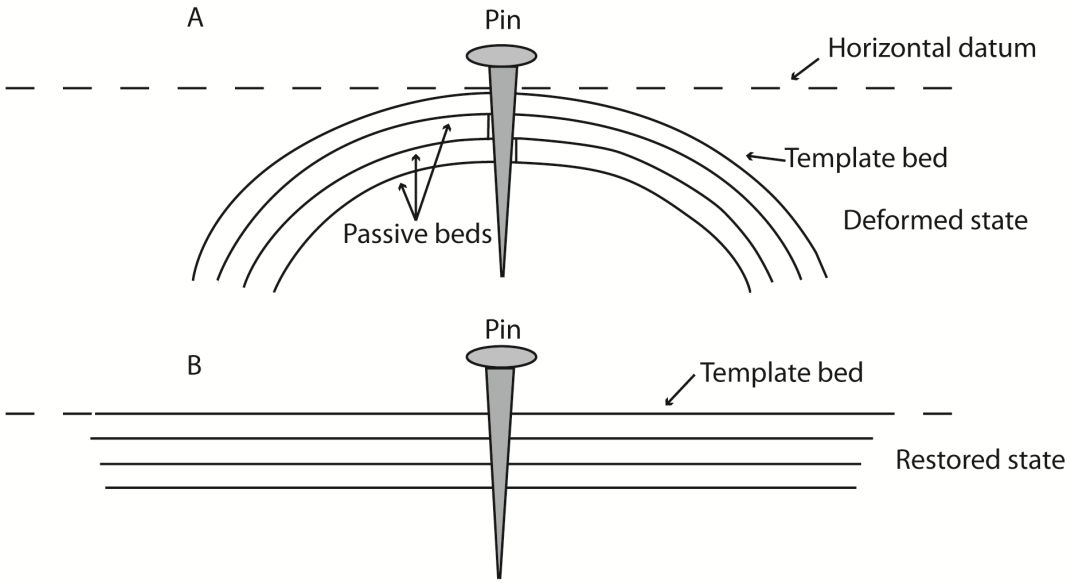

Fig. 2.14. Flexural slip unfolding. A) Deformed folded strata are pinned through the anticlinal hinge line and restored to a horizontal datum. B) The template bed is unfolded around the pin and underlying beds are unfolded passively till a representative undeformed state is reached.

3 Structure of the footwall of a listric fault system revealed by 3D seismic data from the Niger Delta

3.1 Abstract

3D seismic reflection data was used to analyse the architecture of the footwall of a listric fault in a gravitationally-driven extensional system, in the north-western Niger Delta. In contrast to conventional listric normal fault models with a single master listric fault plane the level of detachment switches from a deeper to shallower level. The footwall evolves through the generation of a new master detachment fault and detachments, which transfer hanging wall rocks into the footwall. New detachments form by branching off pre-existing detachment levels, cutting-up through stratigraphy to the next mechanical weakness, separating discrete sections of extended strata. As a consequence a deeper, older array of seaward-dipping, tilted extensional fault blocks becomes incorporated into the footwall beneath the master listric detachment fault. The structural complexity located below the master detachment fault highlights extensional episodes on separate detachment faults that are not captured in conventional listric models. Changes in the level of the detachment are thought to be caused by mechanical weaknesses controlled by lithology, pore pressure and episodes of sediment loading related to deltaic progradation.

Note a published version of this chapter can be found in the digital appendix.

3.2 Introduction

Listric fault systems have long been recognised in extensional terranes (Gibbs, 1984; Shelton, 1984) and commonly form during continental rifting (e.g. Wernicke, 1981), formation of oceanic crust (Salisbury and Keen, 1993**)** and due to gravity-driven tectonics (e.g. Bally et al., 1981). Conventional models for listric faults comprise of a curved fault plane with a dip that decreases with increasing depth and a geometrically necessary rollover anticline, with associated synthetic and antithetic faults situated in the adjacent hanging wall strata (Dula, 1991; McClay et al., 1991; Matos, 1993; Imber et al., 2003) (Fig. 3.1).

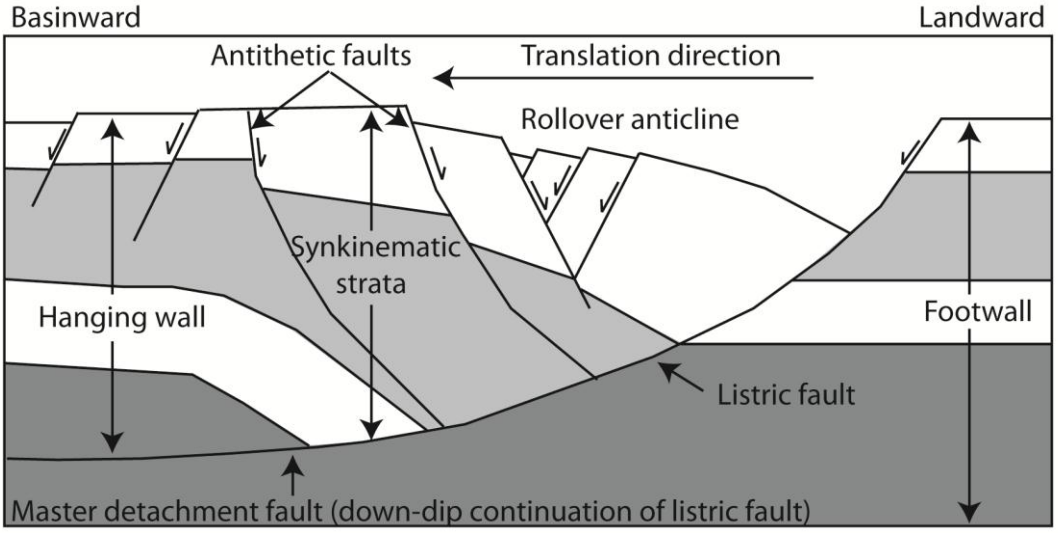

Fig. 3.1. Characteristic model of a listric normal fault with fault plane shallowing with increasing depth a geometrically necessary rollover situated in the hanging wall and no deformation within the footwall region (modified from Imber et al., 2003).

While numerous authors have focused on deformational style and variability in the hanging walls of listric systems (White et al., 1986; Wheeler, 1987; William and Vann 1987; Withjack and Peterson, 1993) the footwall regions are often understudied. This is probably because the footwall is poorly resolved on seismic reflection data and the simplistic perception or assumption that the footwall is thought to be passive (not being deformed) as evidenced in many analogue models (e.g. Groshong, 1989; McClay, 1990). Within the underlying footwall region and at the footwall-hanging wall interface deformation is poorly constrained and often

overlooked in current studies (Problet and Bulnes, 2005). In analogue modelling of listric systems the footwall is usually fixed (e.g. Groshong, 1989; Yamada and McClay, 2003A; Yamada and McClay, 2003B) and as a consequence all the deformation is focussed within the hanging wall. This has served to develop valid, well constrained models of hanging wall deformation. However, the footwalls of natural systems may not be static through time and so deformational processes that operate within the footwall are not necessarily captured in modelling studies.

Here high-quality 2D and 3D seismic reflection data were used that provide excellent imaging of deformation in the footwall and at the hanging wall-footwall interface of a listric fault system in the north-western Niger Delta. The structural style at the base of a listric fault system is described and analysed. This allows for an analysis of the interaction between footwall and hanging wall deformational processes and insights into how natural gravitational listric fault systems evolve.

3.3 Geological setting

The regressive Tertiary stratigraphy of the Niger Delta is represented by three diachronous upward coarsening clastic units of the Akata, Agbada and Benin Formations (section 2.2). The Niger Delta is undergoing gravitational collapse and it is generally accepted that a major regional detachment level occurs close to the Akata-Agbada Formation boundary (Morgan, 2003; Corredor et al., 2005; Briggs et al., 2006). Based upon this, and long range seismic correlation on 2D data, the base of the deltaic succession and the footwall of the up-dip listric fault system is a pro-delta marine shale, probably the Akata Formation. The overlying Agbada Formation consists of deep-water channel complexes, mass transport complexes and hemi-pelagic sediments (e.g. Deptuck et al., 2003). The uppermost Benin Formation represents the youngest depositional cycle and is dominantly composed of fluvial sand deposits of a continental origin. These three clastic-dominated Formations can reach a maximum thickness of up to 12 km (Doust and Omatsola, 1990).

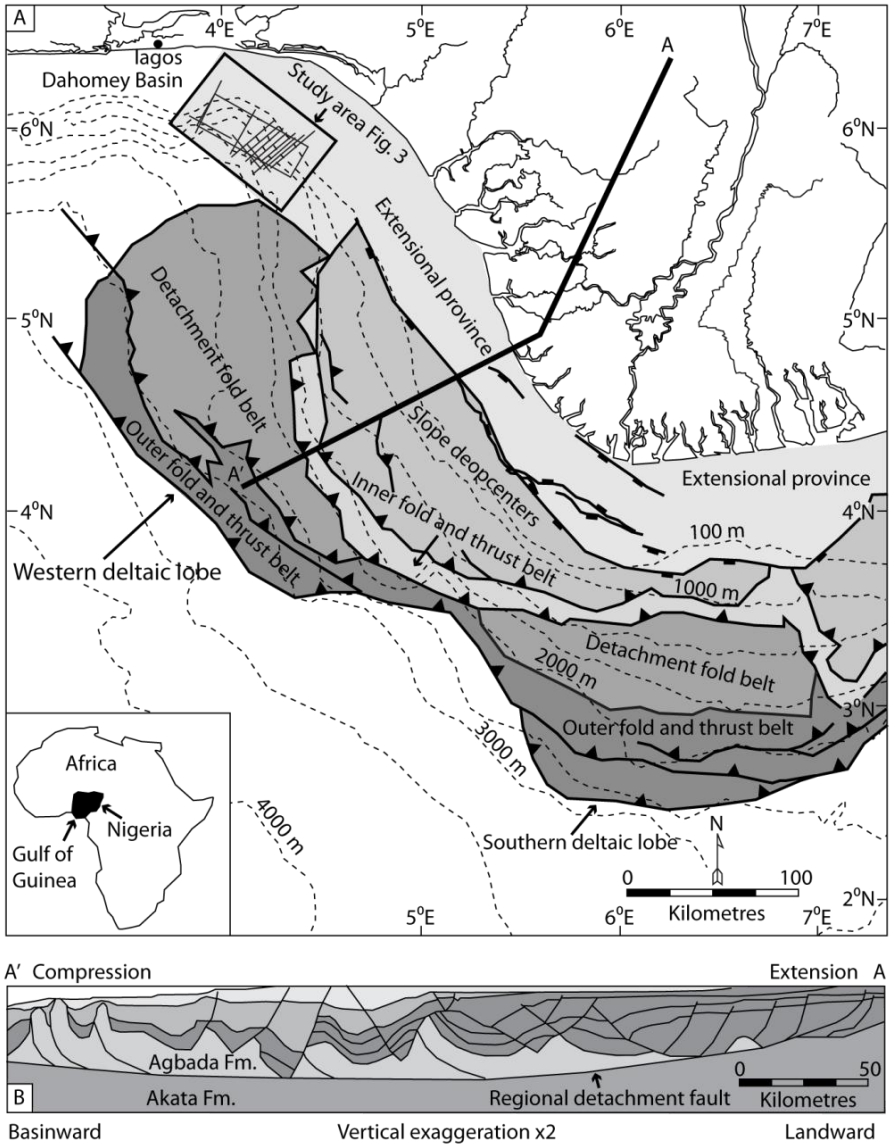

Fig. 3.2. Map of the Niger Delta depicting the main structural domains (modified from Briggs et al., 2006). The location of the 3D seismic survey and 2D lines are shown. Cross-section after Heiniö and Davies (2006).

The structural style of the Niger Delta is similar to most gravitationally-driven tectonic provinces; an up-dip zone of extension followed by a translational zone situated over the outer continental shelf and a contractional zone in deep- and ultra-deep-water down-dip regions (Figs. 3.2A and 3.2B). These three structural zones are characterised by seaward and landward dipping growth faults, detachment folds and seaward and landward thrust faults moving from up-dip extension to down-dip compression respectively (Fig. 3.2B).

The south-eastern margin of the study area is approximately 50 km offshore of the northwest coast of Nigeria, seaward of the shelf break (approximated by the 100 m bathymetric contour, Figs. 3.2A, 3.3 and 3.4) and is structurally complex. The survey area itself lies in a zone of up-dip extension (Figs. 3.2 and 3.3), but locally deformation is strongly influenced by the presence of two strike-slip faults situated approximately 12.5 km down-dip of the survey area (Fig. 3.3). These strike-slip faults have segments that strike oblique to the major axis of deltaic progradation, which has led to structurally controlled segmentation of the passive margin. Buckle folds have developed as the strike of down-dip tear faults makes them an effective buttress to gravitationally driven translation and progradation (Fig. 3.4). This study will not focus on the influence of structural segmentation created by these tear faults, but highlights their importance as they create compressional features in the seismic sections used here (see Clement et al., 1997 for a review on structural segmentation along the African passive margin).

The study area is located 15 km north-west of the main western progradational deltaic lobe (Fig. 3.2). In contrast to the western and southern deltaic lobes, where sedimentation rates are consistently high up to 100 m/m.y. (Davies, 2003), the northern margin has experienced lower sedimentation rates. Deltaic progradational episodes have deposited large volumes of sediment rapidly, but these periods of high sediment input have been followed by intervals of reduced sediment supply; hence the northern margin has a thinner sedimentary column (Cohen and McClay, 1996; Morley and Guerin, 1996, their Figure 4). Deltaic progradation began over the African passive margin in the Eocene, with the onset of wave dominated sedimentation and deposition of paralic siliciclastics (Burke, 1972). Continued deposition and progradation of deltaic sediments has lead to the development of structurally bound depobelts, which are dominated by specific age ranges of sediment that progressively young oceanward (Evamy et al., 1978; Doust and Omatsola, 1990; Cohen and McClay, 1996). The age of the stratigraphy imaged in the sections shown here is Early Cretaceous to the Holocene. The age dates of mapped seismic reflections (Fig. 5) are derived from biostratigraphy from a nearby

unreleased commercial borehole and approximated from stratigraphic dates in Ajakaiye and Bally (2002) where biostratigraphic data was unavailable.

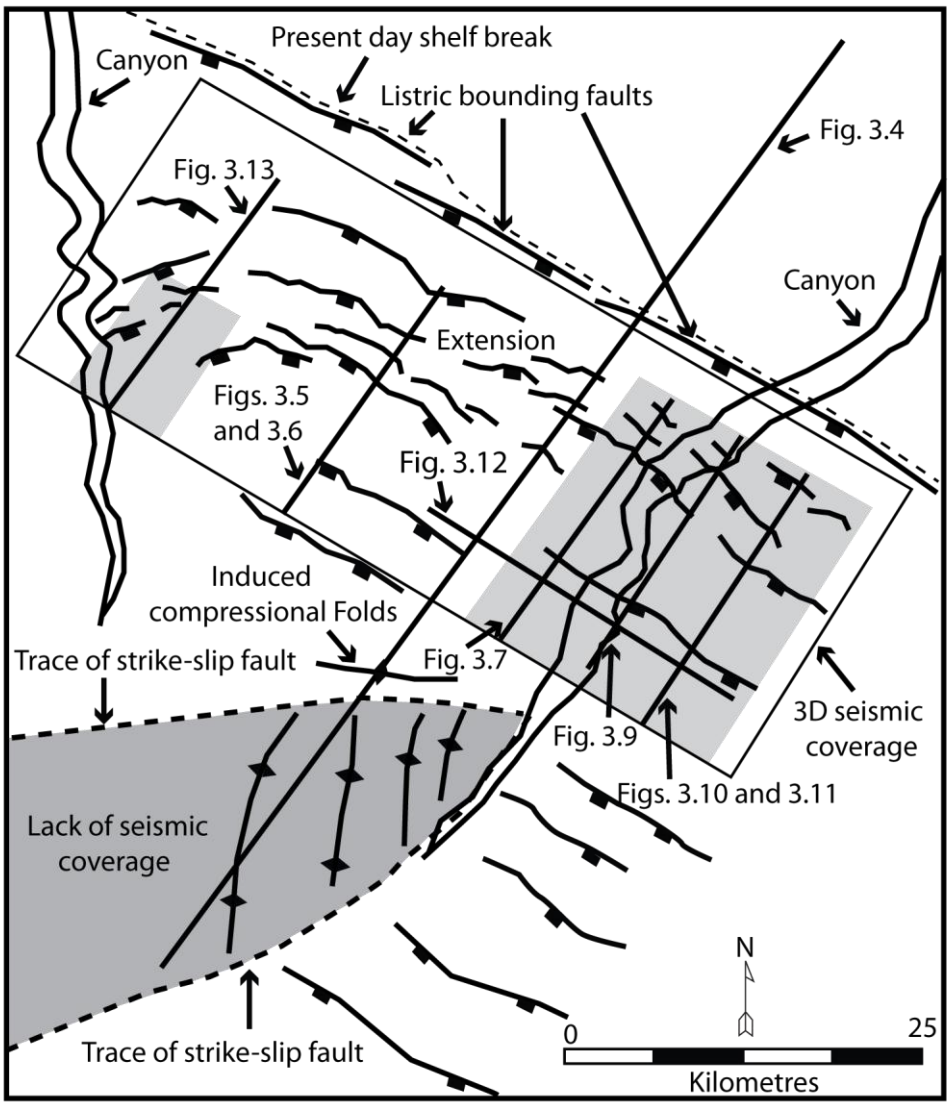

Fig. 3.3. Structural map of the study area highlighting the main deformation features. The approximate strike of two strike-slip faults situated down-dip of the survey area are shown, which act as buttresses to the prograding delta inducing compressional folds. Shaded boxes with the area imaged by 3D seismic data are the locations of footwall deformation.

3.4 Gravitational detachment tectonics

Detachment is a term used to describe the apparent depth that brittle deformation ceases to penetrate within a sedimentary succession (Lister and Davis, 1989; Briggs et al., 2006), or to mark the separation of brittle-ductile regimes in lithospheric crustal models (Davis; 1983b; Lister et al., 1986; Lister and Davies, 1989). The

depth that detachment occurs is indicated by numerous fault planes soling to a well defined detachment level (a décollement surface or detachment fault). Detachment can occur within either a sedimentary succession on a ductile layer (salt or overpressured shale), or within basement rocks involving the formation of metamorphic core complexes (Lister and Davies, 1989; Smith et al., 2006).

In gravitational settings a detachment fault separates hanging wall from footwall (detachment unit) strata and can be the down dip bedding parallel continuation of a major listric fault plane (e.g. Fig. 3.1). A master detachment fault is a kilometre-scale detachment fault that exerts the main control on deformation within its hanging wall and can accommodate over tens of kilometres of displacement (Lister et al., 1986). In gravitational tectonics a detachment fault is a shallow dipping (<30°) fault that accommodates or transfers strain (i.e. mechanically links up-dip extension to down-dip contraction). A detachment fault has also been interpreted to act as ductile shear zone, which serves to make strain compatible between overlying brittle and underlying ductile deforming (or passive) rock types at the point of the fault plane (Lister and Davies, 1989). In this paper the term "regional hanging wall" is used to refer to all strata lying above the active master detachment fault, and "regional detachment fault" to refer to the major Palaeocene age detachment level that is present throughout the survey area.

On the West African margin gravitationally-driven detachment systems occur within overpressured shale (Briggs et al., 2006), or salt (Brun and Mauduit, 2007) where multiple detachment levels are common. The following areas are under investigation: 1) the rheological and mechanical properties of the footwall (Morley and Guerin, 1996; Costa and Vendeville, 2002); 2) the deformation style in an overlying sedimentary hanging wall (Guy 2009); 3) kinematic reconstructions of fault histories (Verschuren et al., 1996); 4) structurally balancing extensional and contractional domains (de Vera et al., 2010). Exactly how all these components interact and affect footwall evolution and hanging wall deformation is still poorly constrained, especially in gravitational detachment fault systems.

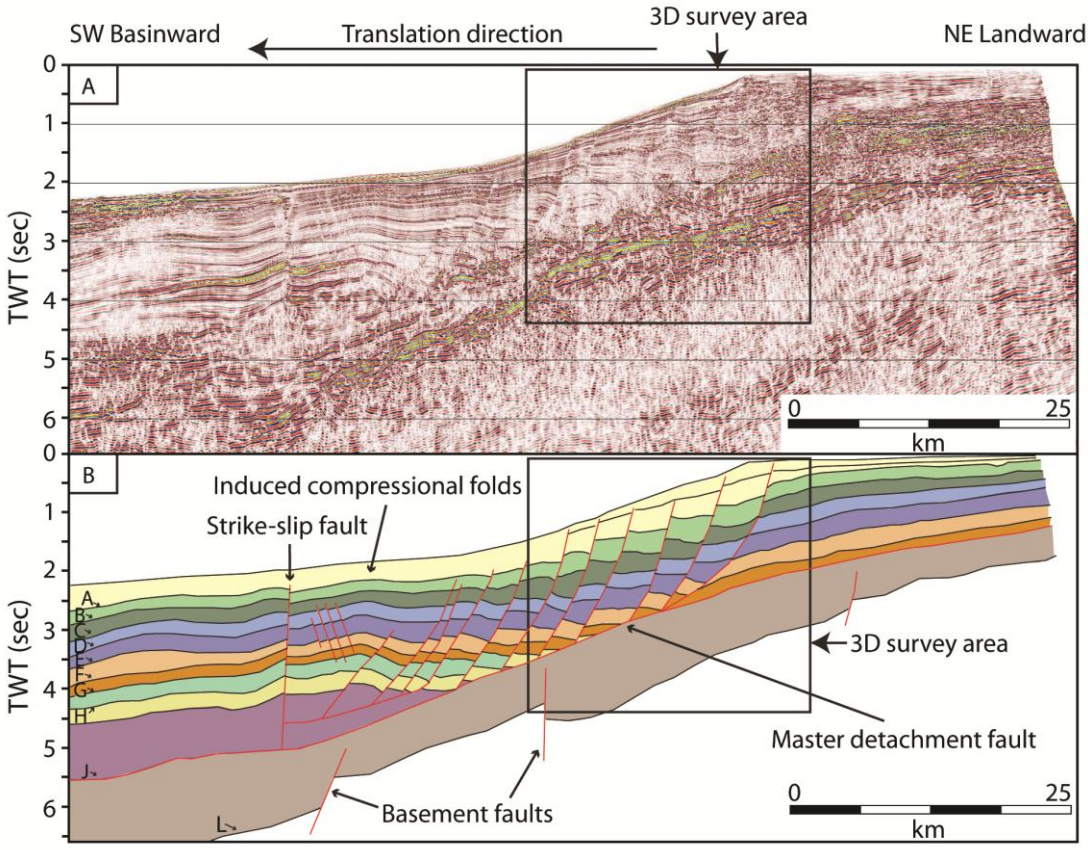

Fig. 3.4. A) Uninterpreted and B) interpreted regional 2D seismic dip line depicting buckling within the hanging wall induced by down-dip strike-slip faults. Note the dominant structural trend of basinward verging listric normal faults. Vertical scale is approximately 2.5x horizontal scale.

3.5 Data and methodology

The 3D seismic survey covers an area of 1523 km^2 (29 km in dip line orientations and 52.5 km along strike) and was combined with 2D seismic lines that image up-dip regions of the north-western Niger Delta (Fig. 3.2). The 3D survey is a pre-stack, time-migrated volume with a line spacing of 12.5 m. These data are zero-phase migrated and an increase in acoustic impedance is characterised by a red (trough)-black (peak)-red (trough) reflection line. The maximum vertical resolution is 15 m (frequency 33 Hz), a quarter of the dominant wavelength in shallow sections, and the data are displayed in seconds (s) two-way travel time (TWT). These data enabled accurate mapping of seismic reflection packages, unconformities and structural

features, which were used in conjunction with seismic attribute analyses to interpret the internal structure of the underlying footwall region.

A series of reflections (A-L) were mapped, which allowed for the definition of seismic units. For the purposes of this paper seismic units may be composite (i.e. span multiple seismic units, e.g. A to C or A to D). It was assumed that differences in the thickness of synkinematic strata between the hanging wall and footwall of individual fault planes were related to active periods of fault slip. This assumption is based on the sedimentation rate being equal to or greater than the rate of fault slip during synchronous periods of deposition and fault activity (e.g. Cartwright et al., 1998). Thickened, or additional seismic reflections within the hanging walls of individual fault planes form wedge shaped geometries, which have allowed us to correlate synkinematic strata to activity on individual growth faults. The assumption that sedimentation rate is equal to or greater than the rate of fault slip is reasonable in shelf environments where progradation rates are high (e.g. Cartwright et al., 1998; Back et al., 2006; Boudin and Cartwright, 2008). Even though sedimentation rates have not been consistently as high as rates within the central deltaic lobes growth faulting is likely to coincide with periods of deltaic progradation and rapid sediment loading (Cohen and McClay, 1996; Morley, 2003) and so it is still reasonable to make this assumption.

Major faults in the regional hanging wall are numbered in the seismic sections shown (1-24) (note that numbered faults do not correlate between figures). Fault traces are interpreted on the basis of numerous, regularly spaced breaks in lateral continuity of seismic reflections that constitute straight, or curved high angle vertical discontinuities in the seismic profiles. Fault analysis on coherency data was used to aid structural interpretation deep within the subsurface (>4 s TWT). A coherency volume was derived from the reflectivity volume, which highlights discontinuities in the local coherence of reflections that are offset by faults. A coherency analysis generates low coherency lineaments that represent a fault plane surface.

Structures imaged in TWT may experience geometric changes when depth converted due to lateral and vertical changes in seismic velocity associated with lithology (e.g. Brown, 1999). To convert from TWT into metres interval velocities were extrapolated from the nearest confidential commercial borehole for corresponding stratigraphic packages. These were used for depth converting selected TWT profiles for determining geometric fault and displacement data. In TWT profiles the measured inclination of a surface is referred to as apparent dip and fault displacements are measured in TWT. A depth converted section shows that the geometric effect of converting TWT to depth is minimal (*cf.* Fig. 3.5 and Fig. 3.6). Importantly, fault planes have similar geometries to their corresponding time sections. As the geometric effect of depth conversion is minimal all further seismic profiles are shown in TWT. In the following sections the deformational structures in the regional hanging wall and then the footwall region are described.

3.6 Observations

3.6.1 Hanging wall deformation

The deformational style of the regional hanging wall is characterised by a series of closely-spaced normal faults (fault spacing ranges between 0.25 km and up to 2 km for larger faults) that form an array where most faults dip in a basinward (south-western) direction (Fig. 6). Some small scale antithetic (northeast dipping) and conjugate fault pairs are present in the south-western part of the survey area (Fig. 7), but these are subordinate and not characteristic of the main deformational style. In plan view fault planes are cuspate in form over a kilometre-scale (Fig. 3), whereas in cross-section fault planes display planar through to listric geometries with fault plane curvature typically increasing with depth. Fault planes strike approximately parallel to the continental margin (largest faults strike for approximately 15 km) and dip between 55° and 65° (Fig. 6). The presence of fault planes coincides with anticlinal or synclinal geometries in adjacent individual hanging wall stratal reflections, which are interpreted to be, faulted, rollover anticlines upon listric faults (Figs. 5 and 6, faults 4-11).

Faults situated immediately seaward of the shelf break in the north-eastern area of the survey are approximately 3 km (about 2.5 s TWT) high in cross-section and have the largest throws (vertical displacements) (Figs. 3.5 and 3.6, faults 5, 6, 9, 10 and 11). Significant wedging of hanging wall reflection packages occurs towards these fault planes indicating substantial across fault stratal thickening (Figs. 3.5 and 3.6, seismic units A to F). This observation places fault activity coeval with sediment deposition during periods within the Upper Pliocene to the Lower Miocene and identifies them as growth faults. The seismic unit A to F displays varying degrees of thickening into hanging wall rollovers (Figs. 3.5 and 3.6), with the most pronounced thickening occurring within the seismic unit C to E (Miocence age stratigraphy), indicative of increased accommodation created during fault activity.

Typically, but not always, seismic units A to F thicken towards the south-west from the position of the shelf break, reflecting the individual activity on separate growth faults (see appendix 3, Fig. A4). The upper tip points of major growth faults (Figs. 3.5 and 3.6, faults 4-11) terminate at either the seabed reflection or within the seabed to reflection A seismic unit. In contrast, the upper tip points of faults 1-3 situated in the south-western part of the survey area terminate within seismic unit A to B, which suggests that faults 1-3 became inactive before faults 4-11. The throws on major growth faults vary from approximately100 m at the top of mapped hanging wall succession, increase to 400 m in the centre and remain at about 400 m at the base of the hanging wall succession (between the seabed to reflection H on Figure 3.6). Horizontal displacement (heave) is 51 m on major growth faults in seismic unit A to B, which increases to a maximum of 117 m at the centre of fault planes (seismic units D to E). Fault displacement does not decrease towards the base of fault planes indicating that some extension is likely to be accommodated upon an underlying basal detachment fault (Stewart and Argent, 2000).

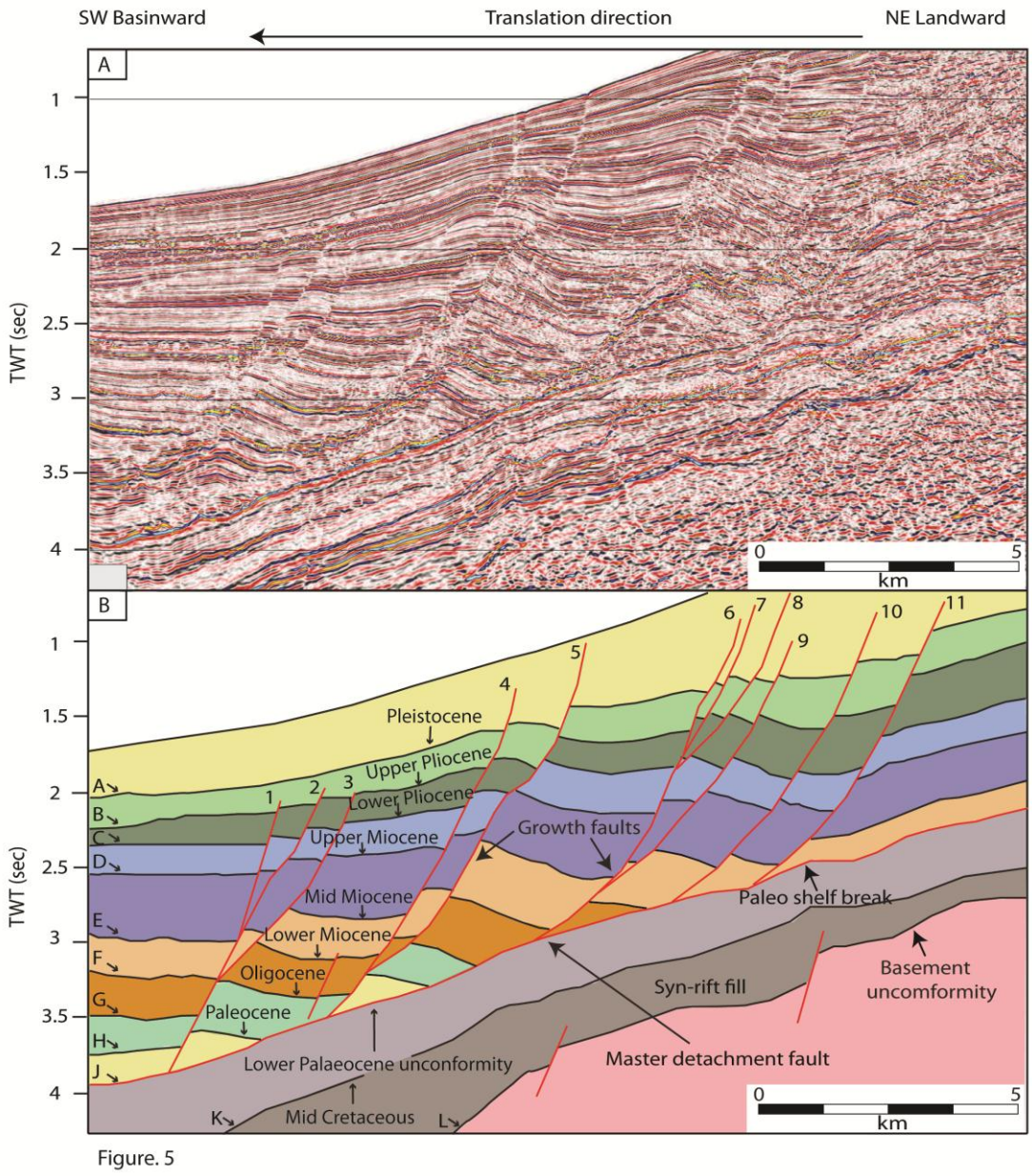

Figure. 5

Fig. 3.5. A) Uninterpreted and B) interpreted seismic dip line illustrating the typical listric deformation style. Regional hanging wall deformation detaches upon the master detachment fault (reflection J) that marks the top of the detachment unit. Vertical scale is approximately 2.5x horizontal scale.

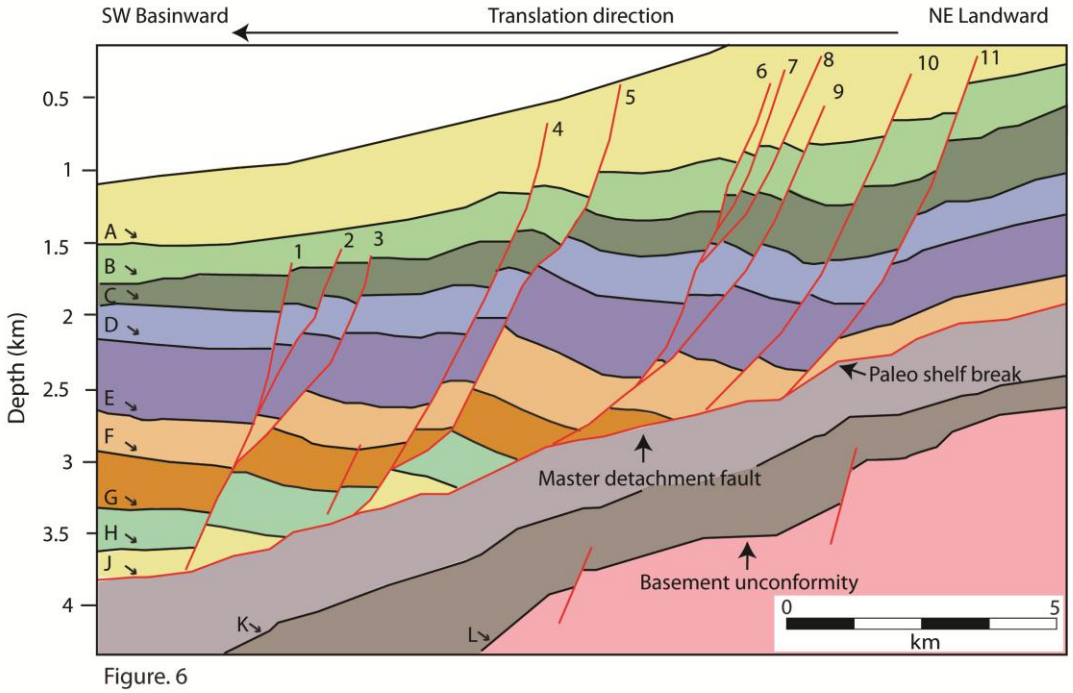

Fig. 3.6. Depth converted schematic of a TWT seismic profile. The equivalent time section for this profile is shown in figure 5B. Vertical scale is approximately 2.5x horizontal scale.

Deformation in the south-western section of the survey area is typically characterised by small-scale normal fault arrays (Fig. 3.7). Fault planes 1-5 (and smaller unnumbered faults) range between 0.5 s and 1.1 s (TWT) high in cross-section with apparent dips of approximately 70°. The absence of across fault thickness variations indicates that movement of faults 1-5 was post depositional. This observation marks these small normal fault arrays as the youngest deformational features in the survey area. The upper tip points of these faults typically terminate within the seismic unit A to C, but occasionally penetrate reflection A. Fault throw is approximately 40 m and heave is minimal.

The majority of growth and post depositional faults in the regional hanging wall sole to a single, high-amplitude negative impedance reflection indicated by a black red black seismic reflection line, possibly indicative of a transition into lower density or velocity sediment (Figs. 3.5 and 3.6, reflection J). A map of reflection J in TWT shows it is dipping basinward (with an apparent dip of 20°-25° towards the

southwest) with a strong southerly rotation (Fig. 3.8). This differs from reflections within the regional hanging wall that typically dip at approximately 10° (Fig. 3.6). Hanging wall stratal reflections both onlap and terminate against reflection J (Figs. 3.4, 3.5, 3.6 and 3.7). Seismic units G to H pinch out and terminate against reflection J in basinward (south-western) sections of the survey area, but are present, albeit thinner, in up-dip regions in other parts of the survey area (as identified on regional 2D seismic lines, Fig. 3.4).

The lateral distribution of seismic units G to H may be explained by depositional variation or alternatively seismic units G to H may have become incorporated into the footwall through faulting; hence they are not well imaged within some north-eastern parts of the survey area. Structurally these observations indicate that reflection J is a major detachment fault and an onlap surface, which separates overlying regional hanging wall from the underlying footwall strata. Basinward translation of the hanging wall occurs on this detachment level.

Reflection J also correlates with a distinct change in seismic facies, and structural style, as it separates overlying seismic reflections that are coherent and continuous from underlying low frequency, discontinuous seismic reflections. Reflection J can be correlated over 150 km to the down-dip compressional structural domain and is the major regional detachment level for overlying fault systems in both extensional and compressional regions. Stratigraphically reflection J probably marks the regional Akata to Agbada Formation boundary and the intersection between regional hanging wall and footwall stratigraphy. Due to the change in seismic facies across reflection J and reflection terminations reflection J is also interpreted as an unconformity dated as Lower Paleocene in age.

3.6.2 Footwall deformation

The footwall region of the listric fault system can be separated into a series of packages that characterise the deformation style. Within this region two seismic facies can be broadly distinguished on the seismic reflection data. Underlying

reflection J (the regional hanging wall-footwall interface) is an interval of low seismic reflectivity. Low-frequency, laterally discontinuous seismic reflections typically characterise seismic unit J to K; however, some continuous moderate- to high-amplitude reflections that lie parallel, or sub parallel to reflection J can be resolved (Fig. 3.5). Seismic unit J to K is Upper to Mid Cretaceous in age. The thickness of the seismic unit J to K varies from 0.75 s to 0.4 s (TWT) respectively and is bound at its base by a triplet of high-amplitude reflections that lie sub-parallel to reflection J (collectively labelled reflection K).

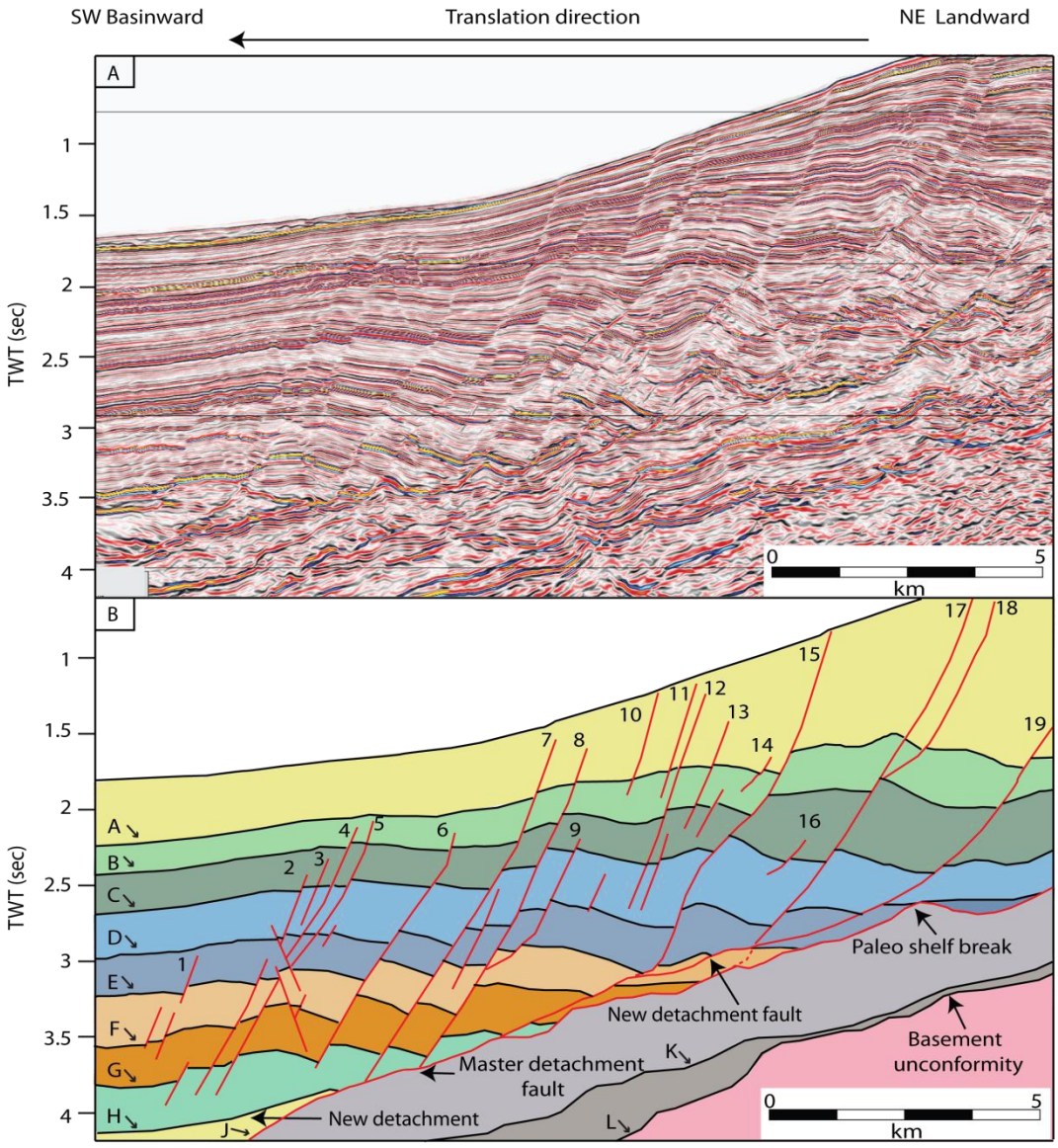

Fig. 3.7. A) Uninterpreted and B) interpreted seismic dip line showing the formation of a new detachment fault. A major listric fault detaches at a shallower depth within the stratigraphy and induces decoupling from the regional master detachment fault. Vertical scale is approximately 2.5x horizontal scale.

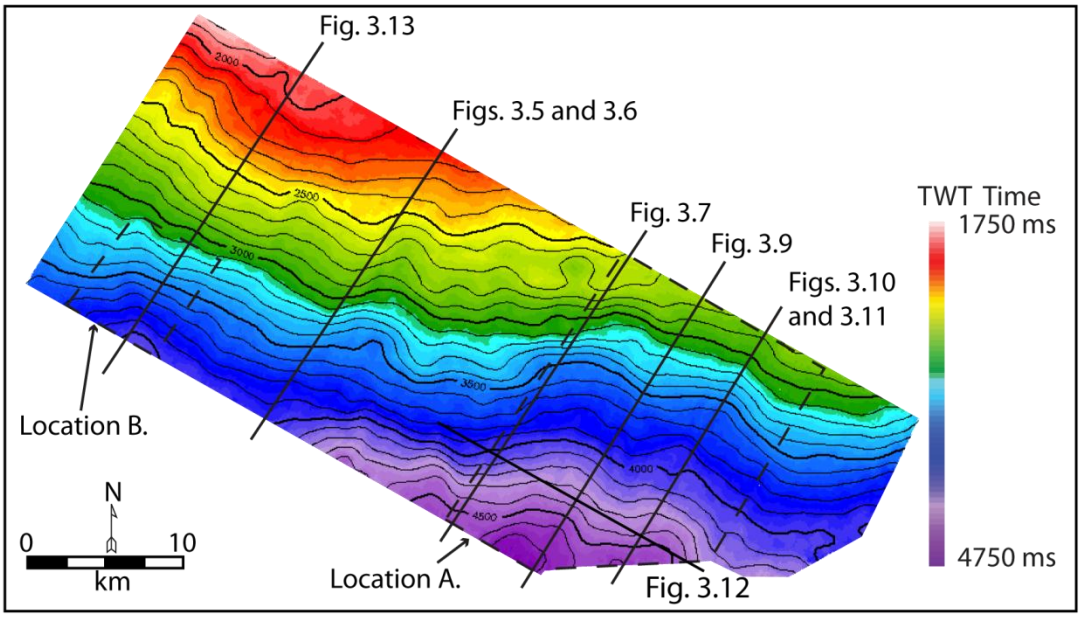

Fig. 3.8. TWT map of the regional master detachment fault (reflection J) displaying the inclination of the footwall region and areas of footwall strain.

The onset of this reflection combination coincides with a change in seismic characteristics between the seismic unit J to K and the seismic unit K to L (Fig. 3.5). Beneath reflection K is a seismic unit composed of laterally continuous high- to moderate-amplitude reflections that are bound by reflection L at its base. Reflection L is highly irregular, steeply dipping and in places significantly offset by planar normal faults, and is interpreted to mark the top of the extended crystalline basement. Beneath reflection L the seismic data are dominated by seismic noise and no further structures are resolvable. The laterally continuous high- to moderate-amplitude reflections overlying the top basement reflection (Fig. 3.5, seismic unit K to L) are interpreted to represent the syn-rift succession, which probably consists of Lower Cretaceous shales and carbonate material deposited on syn-rift basement highs. A prominent, 2 km wavelength, low amplitude monocline lies within reflections above

the top basement reflection (L), beneath growth fault 11 and above a basement normal fault (Figs. 3.5 and 3.6), within seismic unit J to K and extends vertically to reflection J. This is interpreted to be the paleoshelf break, which has undergone very little lateral movement since the Cretaceous migrating only ~10 km landwards to its present day position. The thickness of seismic unit K to L thins and thickens along strike, but in particular thins dramatically landward (north-eastward) (Figs. 3.5 and 3.6).

Two areas where the detailed geometry of the detachment fault system is particularly well imaged within the footwall region are highlighted (Fig. 3.8, locations A and B, see Fig. 3.3 for structural context). Location A marks the position of a 29 km (down-dip direction) by 20 km (strike direction) corridor where major growth faults do not detach upon reflection J, but instead sole to a stratigraphically younger reflection (Fig. 3.7, faults 15, 17 and 19). The lateral margin of this corridor shows that major up-dip growth faults sole to a similar negative acoustic impedance reflection combination, again indicative of a transition into sediment with a low density and/or low seismic velocity. This stratigraphically younger reflection becomes coincident with reflection H and is interpreted to be the down-dip continuation of a listric fault plane, directly basinward of the present day shelf break. Faults 1-5 (Fig. 3.7) represent older post depositional faults, or alternatively they could be growth faults that had low ratios of sedimentation to fault slip (e.g. Childs et al., 2003).

Moving along strike (in a south-eastern direction) through location A (Figs. 3.3 and 3.8) there is evidence for complete decoupling at the level that detachment occurs. All growth faults in the regional hanging wall detach on reflection H rather than reflection J (Fig. 3.9). Growth faults 13-21 sole out at reflection H, which has an apparent basinward dip of ~14°. Post depositional faults 1-11 detach within the seismic unit F to G. This indicates that in places reflection H is a major detachment level, and is the interface between hanging wall and footwall strata across location A (Fig. 3.8), rather than a component of faulted synkinematic stratigraphy. Elevation of the hanging wall-footwall interface has incorporated seismic unit H to J into the footwall region.

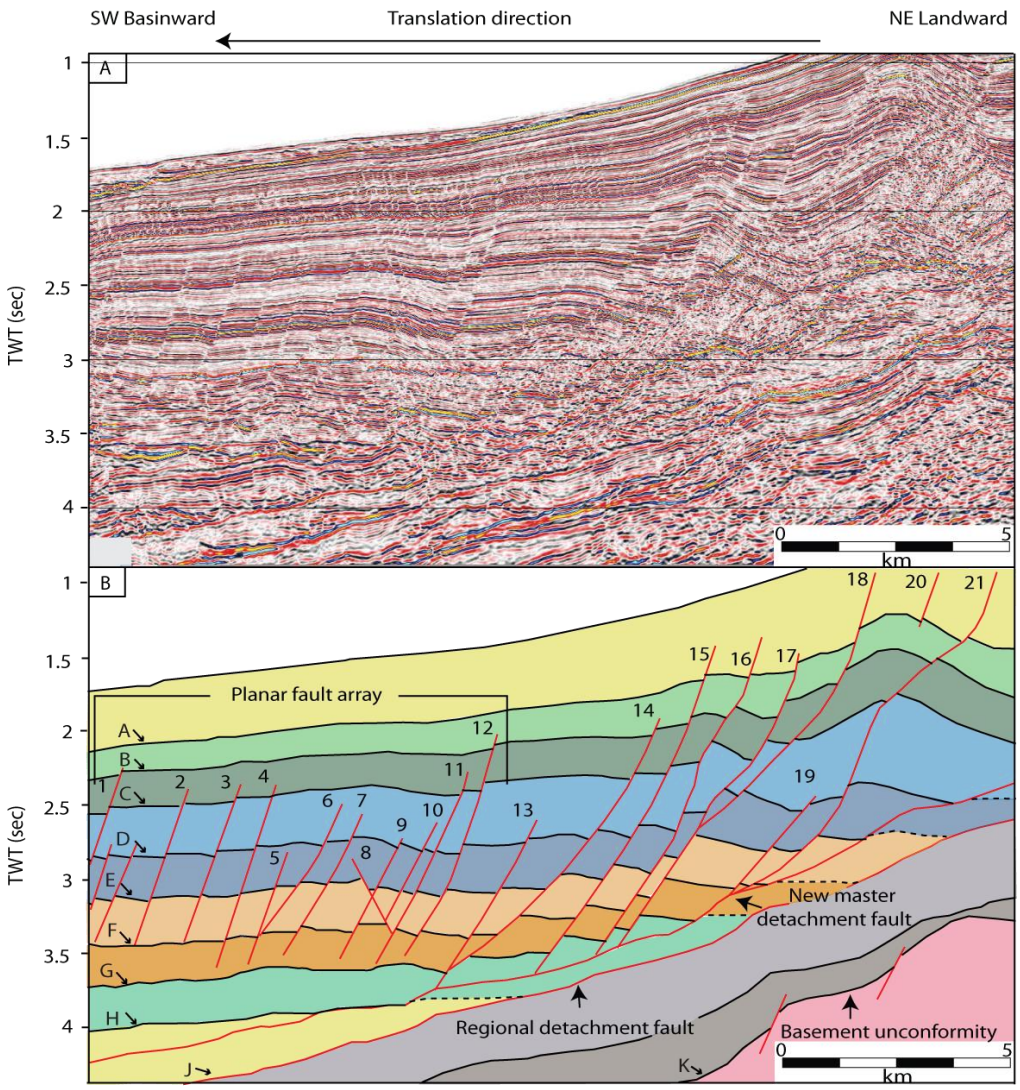

Fig. 3.9. A) Uninterpreted and B) interpreted seismic dip line showing complete separation of the regional hanging wall from the original master detachment fault (reflection J). Deformation is controlled by the new master detachment fault (reflection H). Strata located between reflections H and J have been transferred into the footwall region. Vertical scale is approximately 2.5x horizontal scale.

Within location A across the thickened footwall region a series of rotated reflections are imaged within the seismic unit H to J (Fig. 3.10). These rotated reflectors are also highlighted in the coherency volume (Fig. 3.11) and are situated directly beneath reflection H and bound by reflection J at their base. They are composed of variable seismic amplitudes that display breaks in horizontal continuity and coincide with the presence of sub-vertical discontinuities (Figs. 3.10 and 3.11). Stratal reflections thicken adjacent to where breaks in lateral continuity and sub-vertical discontinuities occur.

Reflection offsets are also observed across these sub-vertical discontinuities as indicated by reflection I (Fig. 3.10). A strike line through location A (northwest-southeast trending) (Fig. 3.12) highlights the stratigraphic thickening and thinning within the regional footwall. The shallower detachment level branches off reflection J and becomes stratigraphically coincident with reflection H in south-eastern sections of the survey. From the elevated hanging wall-footwall interface down to reflection K the footwall thickens from ~0.5 s (TWT) in the north-western section of the survey, where a single detachment level dominates, to 0.8 s (TWT) in the south-western section of the survey area.

Fig. 3.10. A) Uninterpreted interpreted seismic dip line depicting the structural complexity at the base of the hanging wall and within the footwall region. A two tier extensional system is imaged with an extensional fault array situated within the regional footwall. B) Interpreted seismic profile of A. C) Close up uninterpreted seismic profile of the fault array imaged in A). Vertical scale is approximately 2.5x horizontal scale.

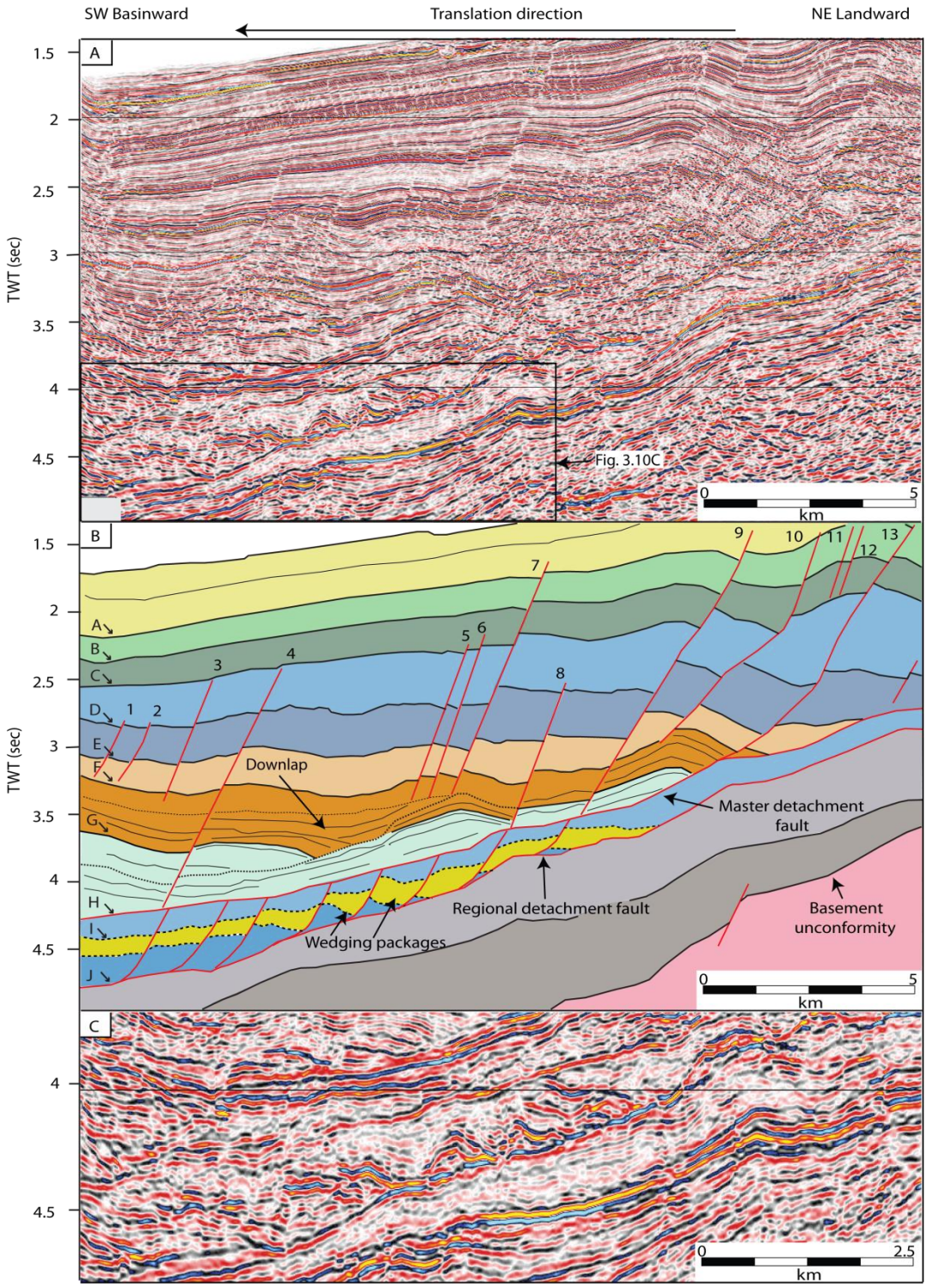
SW Basinward
Translation direction
NE Landward
A
B
C
TWT (sec)
1.5
2
2.5
3
3.5
4
4.5
Fig. 3.10C
0
5
km
1
2
3
4
5
6
7
8
9
10
11
12
13
A
B
C
D
E
F
G
H
I
J
Downlap
Master detachment fault
Regional detachment fault
Basement unconformity
Wedging packages
0
2.5
km

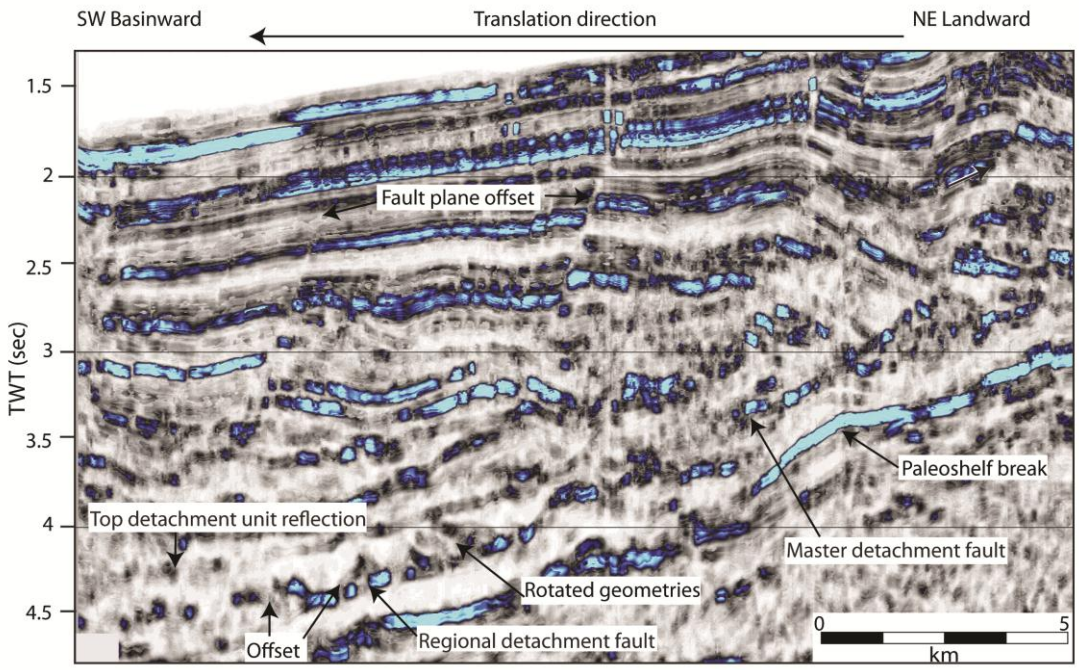

Fig. 3.11. Coherency image of the seismic line shown in figure 3.10A. The coherency image captures the two tier master detachment fault system and rotated geometries situated within the footwall region. Vertical scale is approximately 2.5x horizontal scale.

Location B (Figs. 3.3 and 3.8) displays a similar structural style described above; however, the south-western section of location B displays deformation that does not conform to the typical style (Fig. 3.13). Overlying reflection J in the south-western part of the survey area is a series of rotated high-amplitude reflections. These rotated geometries are discordant with respect to the dip of overlying and adjacent basinward stratal reflections and truncate against the reflection J. The base of the seismic unit F to G is composed of disturbed reflections, which drape the contact with the underlying rotated high-amplitude reflections (Fig. 3.13). The contact between concordant reflections representative of the dominant deformation style in the regional hanging wall and the underlying rotated interval is marked by reflection G.

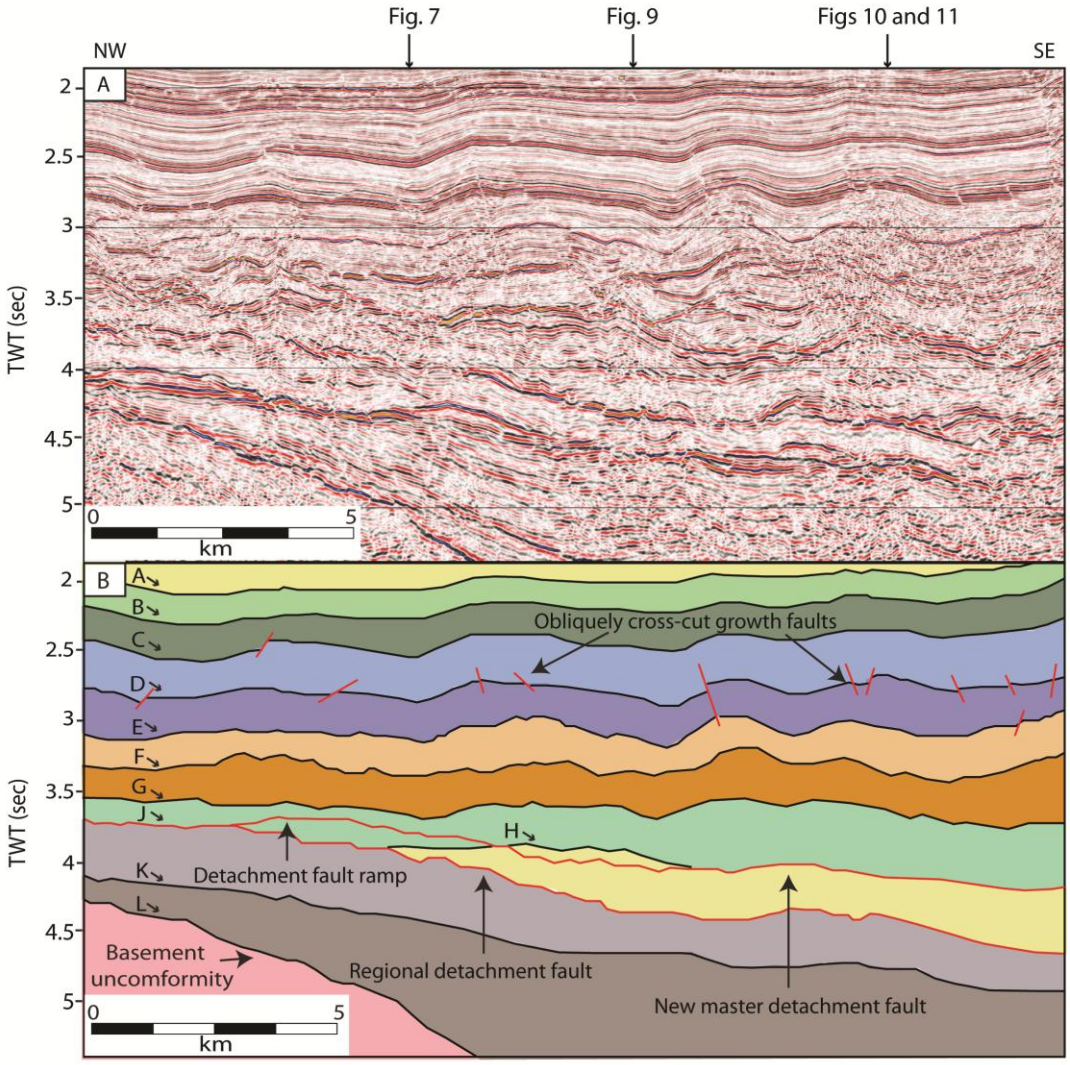

Fig. 3.12. North-west-south-east trending seismic line showing the thickening within the footwall associated with the formation of a new shallower master detachment fault. The onlapping nature of reflection J is clear. Locations of intersections are shown. Vertical scale is approximately 2.5x horizontal scale.

Directly down-dip from this package of rotated geometries is a triangular shaped wedge of seismic reflections. Reflections within this wedge are chaotic, locally truncate and terminate against adjacent reflections within the wedge. An additional high-amplitude reflection branches off reflection J that has an apparent basinward dip of 17° (marked by an inflection point in Fig. 3.13, reflection X).

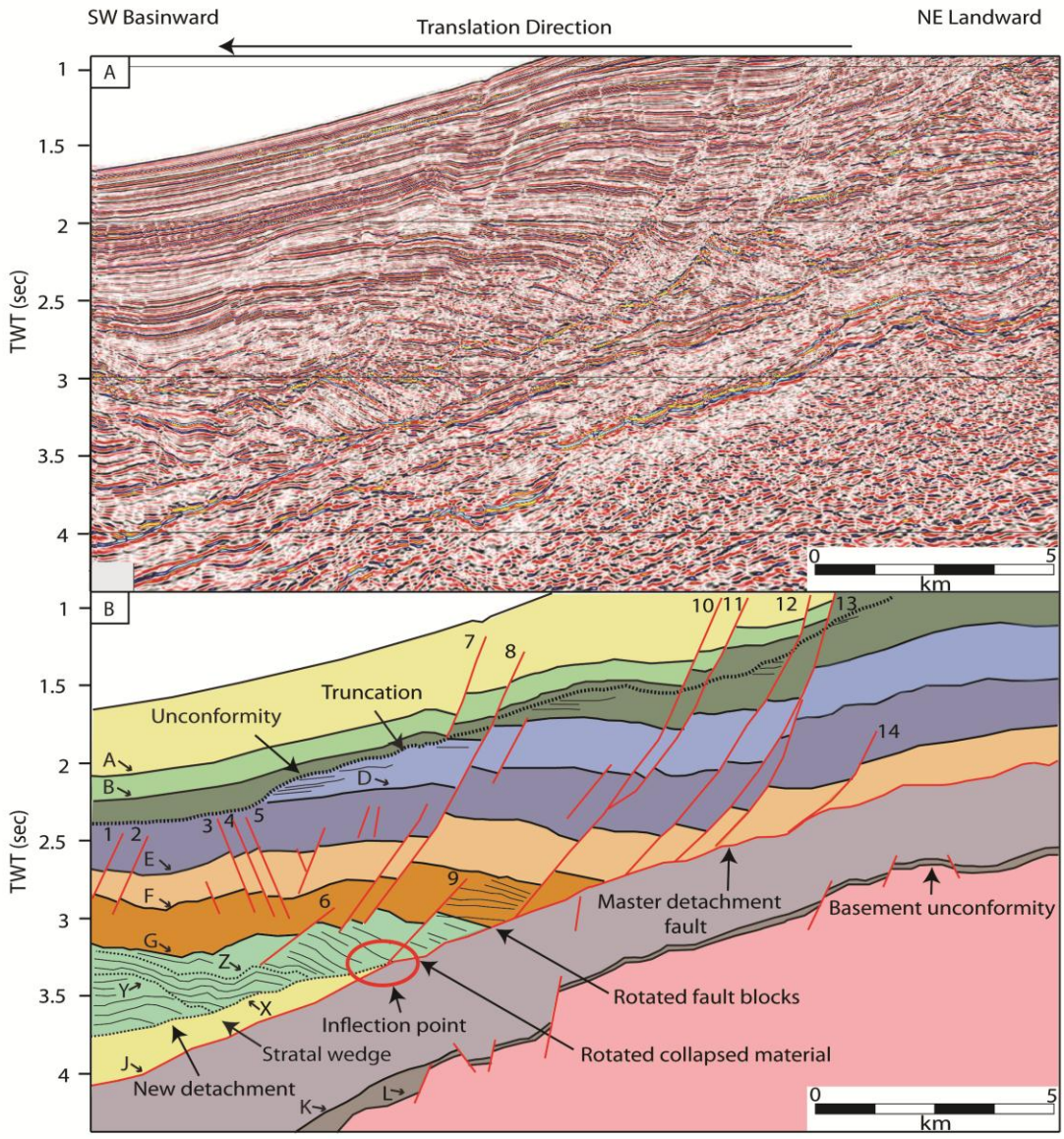

Fig. 3.13. A) Uninterpreted and B) interpreted seismic dip line capturing the formation of a new detachment, which splays off the master detachment fault (reflection X). Rotational fault blocks are situated above the inflection point at the hanging wall-footwall intersection. Vertical scale is approximately 2.5x horizontal scale.

Overlying rotated reflections truncate and terminate against reflection X. Reflection X separates rotated reflections from those detaching on reflection J in the south-western section of the survey area and as a consequence strata preferentially translate down reflection X rather than reflection J. Through the upper section of this stratal wedge are two distinctive reflections that branch off reflection X, and appear to cut-up through stratigraphy (Fig. 3.13, reflections Y and Z). Rotated reflections appear

to contain steep segments (ramps) that terminate against reflection Y and Z, which may have caused preferential thickening of this section.

3.7 Interpretation

3.7.1 Footwall structures

It is observed that the intersection between the footwall and the regional hanging wall cuts-up through stratigraphy from reflection J to a new detachment level, which becomes coincident with reflection H. As a consequence the seismic unit J to H becomes incorporated into the regional footwall (Figs. 3.9, 3.10, 3.11 and 3.12). Detachment of regional hanging wall growth faults occurs on reflection H, which coincides with the basal continuation of an up-dip listric fault. This fault plane is actively accommodating present day gravitational collapse directly basinward of the shelf break. It is interpreted that slip and propagation of fault 13 (Fig. 3.10), coupled with the presence of a mechanically weak stratal discontinuity, has influenced separation and decouplement of hanging wall deformation from reflection J level to reflection H.

As the primary level of detachment has stratigraphically shallowed reflection J no longer acts as the master detachment fault as translation and deformation is focused within the hanging wall of the new detachment fault across location A (Figs. 3.7, 3.9, 3.10 and 3.12). However, reflection J is still a mechanical weakness (approximately the Akata-Agbada Formation boundary) within the layered stratigraphy. The rotated geometries located within seismic unit H to J are interpreted to represent fault blocks and the sub-vertical discontinuities are interpreted as fault planes (Figs. 3.10 and 3.11). Fault planes within this lower fault array have a regular spacing, apparent dips of 60° that get progressively steeper (approaching apparent dips of 70°) in the basinward part of the survey area. This footwall fault array is bound by reflection J at its base and by reflection H at its upper surface. Critically, the dip of fault planes decreases with depth and faults take on a listric profile in cross section. Seismic package I (Fig. 3.10, yellow package) has been mapped throughout this lower fault array and displays numerous offsets and breaks in lateral continuity, which marks the

location of numerous fault planes. In addition, stratal reflections within this fault array thicken and wedge into the hanging walls of individual fault plane reflections. This lower fault array is significantly smaller than regional hanging wall growth faults, reaching a maximum height of 1 s (TWT) in cross-section and a maximum basinward throw of up to 0.2 s (TWT). As a consequence of the master detachment level stratigraphically shallowing a stacked extension detachment system developed with the lower fault array situated within the footwall of the listric fault.

Propagation of a detachment fault is unlikely to be restricted to one mechanical or stratigraphic horizon. Fault geometry will likely both contain steep segments (ramps) and horizontal segments (flats) as it propagates through the stratigraphy localising on mechanical weaknesses. Linkage of discrete lateral fault segments during propagation may lead to the ramp-flat geometry of the master detachment fault (Figs. 3.12 and 3.14), which in this example formed through two separate episodes of detachment fault activity. Parallels between this ramp-flat detachment fault geometry may be drawn with the kinematics of thrust faults where the generation of multiple detachment levels is common (Corredor et al., 2005; Briggs et al., 2006). Thrust belts that have multiple detachment levels often have master detachment faults that ramp up through stratigraphy connecting upper and lower detachment levels (Corredor et al., 2005). However, within thrust systems the thickness of the hanging wall does not change. Repetition of stratal units occurs as a consequence of hanging wall blocks being forced over non planar segments of a fault plane. In both of these possibilities ramping of a detachment fault is the result of a kinematic function of fault propagation; however, the possibility that fault propagation may still be influenced by local distributions in pore pressure cannot be discarded.

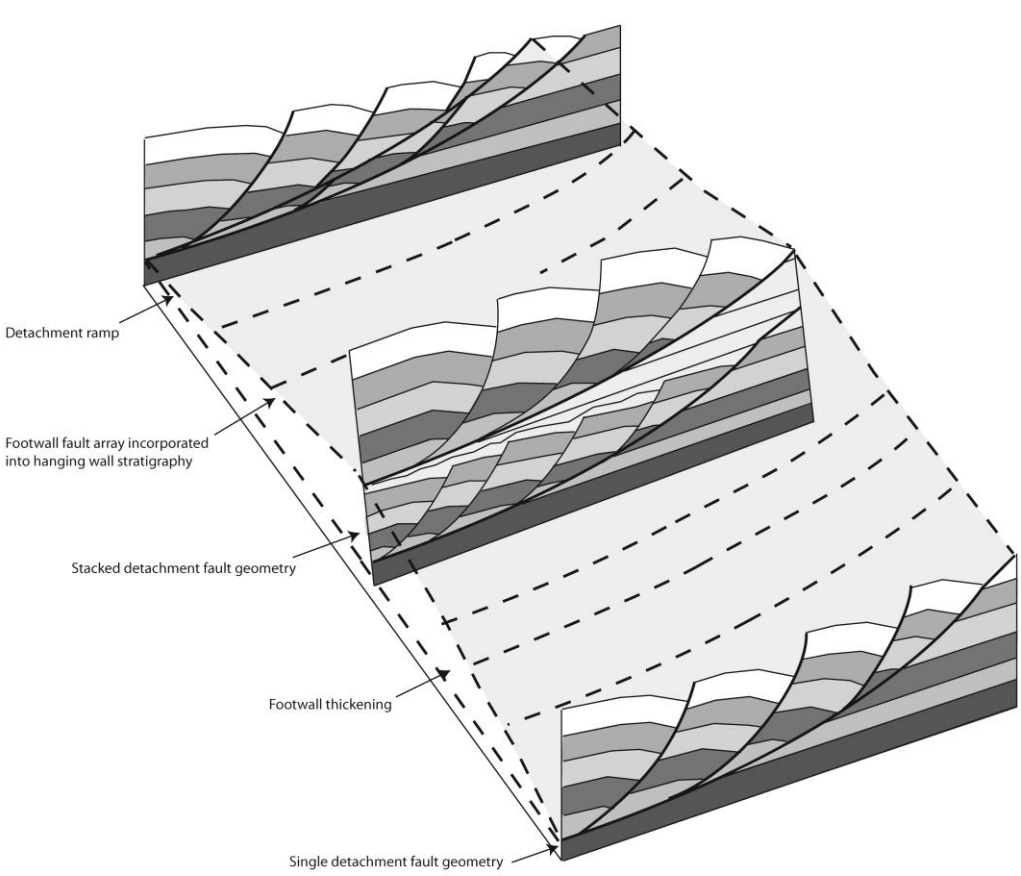

Fig. 3.14. Cross-sectional cartoon depicting the evolution of the footwall region. Approximate lateral geometries of master detachment faults are shown. Footwall evolution is controlled by the propagation of a later master detachment fault. Sedimentary infill between sections is omitted. Not drawn to scale, faults within the footwall are exaggerated to show geometries.

At location B (Fig. 3.13) the generation of new detachments in the basinward (south-western) part of the survey area is observed. The discordant rotated geometries located at the base of the regional hanging wall, overlying reflection J, are interpreted as rotated fault blocks (Fig. 3.13). These fault blocks have rotated antithetically (up-dip) with respect to the underlying dip of reflection J. Sharp terminations in reflection style and angular boundaries mark fault block edges and the location of fault planes, which separate individual fault blocks. There is a clear discordant contact between stratal reflections indicative of the hanging wall deformation style and the rotated fault blocks, marked by disturbed reflections, which drape and overlie the rotated fault blocks. The internal structure of the triangular stratal wedge situated

immediately down-dip from the rotated fault blocks is composed of chaotic and disturbed reflections. Through the centre of the stratal wedge is a shallow dipping detachment (Fig. 3.13 reflection X), which serves to localize strain. Upon this detachment both extensional, and potentially, contractional processes are taking place. Reflection X bounds the base of the stratal wedge and branches off reflection J with the point of separation marked by an inflection point (Fig. 3.13). Overlying reflections terminate against reflection X marking it as a level of detachment. Translation upon reflection X has formed a localized zone of shear, which has served to separate strata lying between reflection J and reflection X. Where reflection J underlies reflection X it is interpreted that reflection J no longer acts as the detachment level for translation of hanging wall strata; hence deformation and shear is preferentially focused along reflection X. Within the upper part of the stratal wedge lie two detachments (Fig. 3.13 reflection Y and Z) upon which reflections within the stratal wedge appear to thicken. The series of stacked rotated reflections at the south-western end contain steep segments that can be mapped up and over reflections Y and Z; thus, reflections within the stratal wedge may be interpreted as small scale imbricate thrust faults.

3.8 Extensional faults within the footwall region

The most significant expression of failure within the footwall region is the presence of an extensional fault array (location A, Figs. 3.3 and 3.8) situated below conventional listric style hanging wall deformation. These reflections are unlikely to be seismic artefacts as they are geometrically compatible with an extensional fault array. Intense zones of deformation are localised at the hanging wall-footwall interface, which may provide insights into how the footwall region evolves. The footwall fault array may have formed through two processes: 1) intra-formation shear through the accommodation of shear stresses acting on the regional detachment fault, which led to up-dip rotation of individual fault blocks and the formation of a domino fault array; 2) gravitationally-driven extension. The two possibilities presented here are addressed below.

Studies have shown that shear can occur above significant layers of weakness within the mechanical stratigraphy, which can lead to the formation of domino style fault arrays (Davis, 1983a; Axen, 1987; Morley and Guerin, 1996; Stewart and Argent, 2000). Accommodation of shear stresses could occur in an intra-formational setting (i.e. the interval that accommodates shear is bound by both an upper and lower detachment). For intra-formational shear to occur the upper detachment also has to stretch to accommodate the extension generated by rotation and slip on individual fault blocks (Stewart and Argent, 2000). For the formation of a domino fault array above a dipping detachment the amount of extension between a pair of fault blocks depends on the dip of the fault plane, the dip of the beds and the dip of the basal detachment (Axen, 1987). The upper detachment extends an amount equal to the total extension generated across the entire domino fault array. This extension would be accommodated by down-dip contraction basinward of the survey area. Rotation of fault blocks has previously been linked as a viable mechanism for generating low angle detachment faults, if significant rotation of pre-existing fault blocks occurs (Davis, 1983b). Considering the size and geometry of these fault blocks it would be difficult to produce a smooth detachment geometry from pre-existing hanging wall structure. In principle, new younger faults should then cross cut older, overly rotated fault blocks and detach on their flank (e.g. Davis, 1983b).

The case of gravitationally driven extension can be separated into three further possibilities. Firstly, part of a slope failure could be being imaged. Mass transport complexes are a common feature of gravitationally driven terrains. The footwall extensional fault array may represent the brittle head domain of a slope failure (e.g. Bull et al., 2009) with the possible translational and contractional domains present down-dip off the south-western margin of the survey area. In this example reflection J would act as the basal shear surface, which would have formed rapidly to facilitate slope failure. Although the internal coherency of the fault blocks makes slope failure an unlikely interpretation it cannot be discounted. Secondly, it could be an early period of growth faulting as a consequence of sediment loading and gravitational processes. Thirdly, it is possible that an extensional duplex is being imaged where deformation on both mater detachment faults occurs coevally. In this scenario both

master detachment faults would have formed at the same time and deformation would have progressed continuously upon both master detachment faults.

Due to the lack of major cross-cutting relationships between the two master detachment faults it is unclear whether an extensional duplex is being imaged or whether an early phase of extension took place, which subsequently ceased. Taking into account evidence for stratal wedging, fault plane geometries and depositional setting our preferred mode of formation is one of an early period of gravity driven extension. This model is reinforced by the listric geometry of fault planes rather than the more planar nature expected in domino fault arrays (Fig. 3.15). This early extensional period subsequently ceased and was buried by a layer of mechanically weak clays. This inherent mechanical weakness in the layered stratigraphy provided the weak layer for the youngest master detachment fault to propagate through with the re-initiation of conventional listric style deformation in the regional hanging wall. However an extensional duplex cannot be ruled out.

3.9 Multiple detachment levels and footwall evolution

Although two examples of footwall deformation at different scales both are described potentially they are related and both essential to footwall architecture and evolution. Stratal wedging within the footwall fault array (Fig. 3.10, reflection package I) indicates that movement upon the regional detachment fault (reflection J) occurred first. As this early extensional period ceased deformation then switched to a shallower master detachment fault with the re-initiation of listric style deformation (Figs. 3.7, 3.9, 3.10, 3.11 and 3.12). Stratal thickening relationships of faults 4–13 (Fig. 3.10) show that movement upon the shallower detachment level is the most recent.

The formation of new detachments also occurs on a smaller scale with the progressive development of local detachments branching off master detachment faults (Fig. 3.13), as seen across location B (Figs. 3.3 and 3.8). Each new

detachment localises deformation by raising the stratigraphic level that detachment and translation occurs while synchronously incorporating strata into the footwall region. The rotational fault blocks situated at the hanging wall-footwall intersection are originally likely to have formed within the hanging wall of fault 10 (Fig. 3.13). Reflection J was the first master detachment fault to move as indicated by the timings of growth faults 10-14 that sole to it (Fig. 3.13). Seismic unit F-G thickens dramatically into growth fault 10 and the south-western part of reflection J may have originally been the down-dip continuation of fault 10. Reflection X (Fig. 3.13) marks a younger detachment, and is currently acting as the primary detachment level for hanging wall translation, as indicated by reflection terminations onto it.

This sequence of progressively upwards younging detachments is essential to the evolution of the footwall region. New detachment faults form in all examples by preferentially shallowing to stratigraphically younger horizons, branching off pre-existing detachments, and cutting-up through stratigraphy to the next mechanical discontinuity. As a function of this process the regional footwall thickens as strata previously situated in the regional hanging wall are transferred into the footwall region of the listric fault system. This implies that the formation of new detachment faults is an important process in controlling footwall and hanging wall architecture (Fig. 3. 15).

3.10 Discussion

3.10.1 Ramping detachment faults

In all examples the dip of younger master detachment faults and detachments is shallower than their older counterparts. This is counterintuitive as faults with shallow dips cease to move (lock-up) as a product of diminishing shear stresses acting upon them and due to an increasing normal stress, which increases the shear stress required for failure (Sibson 1985). Therefore, new younger detachment faults would be expected to have a steeper dip than their older counterparts. If the stress field acting through a normally pressured sedimentary succession in proximal gravitational settings is considered the maximum compressive stress (σ_1) acting on

the active master detachment fault is vertical. With the development of a shallower low angle detachment fault the magnitude of normal stress acting on the detachment fault is reduced with an associated loss of hanging wall strata that is transferred into the footwall. This reduction in normal stress coincides with a synchronous reduction in shear stress acting upon the detachment fault due to the reduction in fault dip. This means that a structural reorganisation of the footwall, and the formation of new detachments, is not induced by progressive locking of detachment faults as intuitively the magnitude of shear stress is still high enough for sliding to take place.

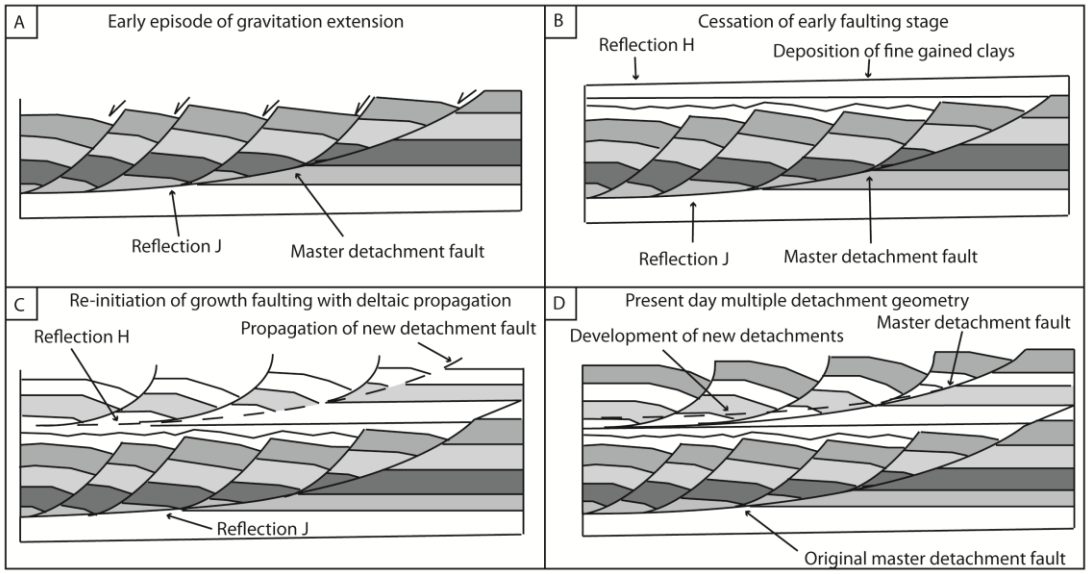

Fig. 3.15. Kinematic model for the development of multiple detachment faults. A) an early period of extensional faulting develops, B) faulting ceases and mechanically weak clays are deposited, C) re-initiation of growth faulting coincides with deltaic progradation and the propagation of a new master detachment fault, D) present day footwall geometry with translation preferentially occurring on the shallowest master detachment fault.

The formation of new detachment faults that have a lower dip can be explained by the location of sediment that is overpressured. Overpressure reduces the shear strength of sediment, which would allow translation of strata to occur at lower magnitudes of shear stress than normally required (e.g. Bilotti and Shaw, 2005). This could account for the low angle of new detachment faults. In order for overpressured horizons to produce a shallow detachment fault the interval within

which overpressure builds up would also have to become shallower. The footwall of the listric system is composed of pro-delta, Cretaceous marine shales and is the main succession that overpressure is generated in a consequence of rapid sediment loading. Evidence for overpressure comes from seismic stacking velocities experienced with the onset of the footwall (the Akata Formation) (Morgan, 2003), fluid escape features including mud volcanoes (Graue, 1999) and a low resistance to basal slip along the Akata-Agbada regional detachment level (Bilotti and Shaw, 2005). A migration of pore-fluids from a deep interval to a shallower fine grained lithology where pore-fluids become trapped, or the generation of new overpressured intervals could influence the location of new detachments.

3.10.2 Deltaic setting

The deformation style imaged here is atypical with respect to the deformation style imaged within the central lobes of the Niger Delta (*cf.* Morley and Guerin, 1996 their figure 4, Ajakaiye and Bally, 2002, cross-sections D1 – D3). Sedimentation and progradation rates have been lower in comparison to the central western and southern progradational lobes of the Niger Delta (Fig. 2). This reduced sediment input has, in part, likely influenced the structural style of the northern margin, which has a different structural style from growth faults within the central deltaic lobes of the Niger Delta. This is highlighted by the following: 1) the close spacing of growth faults; 2) length of continuity along fault strike; 3) the relative displacements of faults, which are significantly lower when compared to the displacement of growth faults within the central Niger Delta. Growth faults in the central delta are widely spaced, strike laterally for tens of kilometres, and synkinematic strata thicken up to 5-8 km in hanging wall growth faults (e.g. Morley and Guerin, 1996; Ajakaiye and Bally, 2002; Back et al., 2006).

The structural styles of deltaic systems can vary greatly depending on the nature of the basal detachment unit (Morley and Guerin, 1996; Morley 2003); however, it is not always clear what factors influence the activation of new detachments. This atypical deltaic setting may have influenced the formation of the stacked detachment fault system as opposed to models with a singular fixed detachment geometry (e.g.

Fig. 3.1). Parallels between the geometry of the stacked master detachment fault system may be drawn with basins that display similar structural architectures. The northern margin of the Niger Delta has likely been subjected to episodic progradational events. Multiple short lived episodes of gravitational failure have been attributed as an important factor in allowing stacked detachment systems to develop in gravitationally driven basins. These include the Orange Basin, offshore West Africa (de Vera et al., 2010) and the Bight Basin, offshore South Australia (Totterdell and Krassay, 2003; Espurt et al., 2009). The structural similarities between the detachment systems imply that the early episode of extension that formed the footwall fault array may be related to an early episode of deltaic progradation that ceased. This was followed by the deposition of a mechanically weak unit that detachment later switched to during the next progradational episode (e.g. Fig. 3.15) (appendix 3, Fig. A5).

The Orange Basin, offshore Namibia, is characterised by stacked gravitational detachment failures that range from tens of kilometres up to 150 km, which are attributed to episodic periods of gravitational sliding (de Vera et al., 2010). Individual gravitational failures are separated by intervals of undeformed strata; an indication of episodic intervals of deltaic progradation and sedimentation. The fact that no undeformed strata is seen separating the master detachment faults may indicate that any intervals of low sediment supply were short lived events. Structural similarities are also seen in the Bight Basin, which is characterised by the two major progradational episodes of the Hammerhead and the White Pointer Deltas (the Ceduna delta system) that detach upon Late Albian shales (Espurt et al., 2009). The White Pointer Delta began to prograde across the Australian margin in the Late Albian-Santonian, which was followed by progradation of the Hammerhead Delta in the Late Santonian-Maastrichtian. In the eastern part of the Bight Basin (in the Ceduna sub basin) the two deltaic systems have formed a massive, vertically stacked detachment fault system (Totterdell and Krassay, 2003; Espurt et al., 2009). Instead of a singular master detachment fault controlling gravity driven deformation two master detachment faults, located at the base of each deltaic system, both exert a control on hanging wall deformation. The stacked detachment nature is also atypical of the dominant structural style of the Ceduna delta system where typically gravity-

driven processes operate above a singular master detachment fault. The formation of a stacked detachment system is related to the progradation of the two deltas. Although the 1st order structural architecture of the detachment fault systems is similar (albeit on a much greater scale) the kinematics are potentially different. The development of the Ceduna detachment fault system is related to strong tectonic controls from continental breakup (Espurt et al., 2009), whereas the development of stacked master detachment faults are speculatively related to changes in sedimentology, the distribution of overpressured horizons and deltaic progradation.

At this stage is not clear whether stacked detachment faults are or are not a common characteristic of classical deltaic systems. Further research into the footwalls of listric systems in basins characterised by consistently high volumes of sedimentation is required to fully understand when a singular fixed master detachment fault controls deformation, and when conditions are favourable for stacked detachment systems to form. The continuing improvement of seismic data will be critical in advancing our knowledge of processes that control footwall architecture.

3.11 Implications

The fact that footwall regions are not necessarily static through time carries implications to methodologies that involve determining the depth to detachment (the base of the listric fault plane) from the geometry of hanging wall strata. These methods assume a fixed footwall; hence a fixed level of detachment (White and Yielding, 1991; White, 1992; Song and Cawood, 2001; Problet and Bulnes, 2005). The depth at which detachment occurs can change temporally, with the development of new master detachment faults, changing the stratigraphic position of the hanging wall-footwall interface. Care must be taken to ensure that the hanging wall geometries used to reconstruct the depth of detachment formed when the most recent detachment level was/is active, or an inaccurate detachment depth will be determined. Analogue models of listric systems where the footwall region is not fixed (e.g. Cloos, 1968; Serra and Nelson, 1988) may be better at duplicating deformation within natural listric systems. Bose and Mitra (2009) performed

analogue modelling of a listric fault system above a fixed and non-fixed footwall and have shown the considerable variability can occur in the hanging wall deformation style as a consequence.

Furthermore as conventional hydrocarbon exploration takes places within the hanging walls of listric systems footwall regions remain relatively underexplored. The recognition of two tier extensional fault system and the transfer of hanging wall strata into the footwall highlights the possibility of effective hydrocarbon traps, which currently are not being exploited. There could be footwall structures that could provide additional prospectivity if similar structures are discovered on a larger scale.

3.12 Conclusions

The footwall architecture of a natural listric growth fault system can be structurally complex as in places regional hanging wall deformation is controlled by more than one master detachment fault. The footwall region includes multiple detachments and master detachment faults upon which are listric growth faults and rotational fault blocks. An extensional fault array was subsequently transferred into the footwall with the formation of a later stage master detachment fault, which splayed off the pre-existing master detachment fault. This incorporated the oldest extensional fault array into the footwall, and a later period of listric fault deformation then followed. Deformation is focussed on detachments at the hanging wall-footwall interface and internally within the footwall region. New detachment faults cut-up through stratigraphy and control the interplay between hanging wall and footwall deformation. The formation of new detachments is likely driven by changes in the distribution of overpressured pore-fluids and the presence of mechanically weak layers. Episodic periods of deltaic progradation, which bring in large influxes of sediment, followed by intervals of reduced deposition may also be influential in the development of a stacked detachment fault system. Formation of a new master detachment fault is coincident with the incorporation of hanging wall strata into the footwall region. Secondary to master detachment faults are discrete localised

detachments, which facilitate basinward translation of material down-dip. Evidence for rotated stratal geometries and earlier fault arrays are critical when considering how detachment fault systems develop, and the possibility of structural traps within the footwall of listric fault systems.

4 New insights into deformation mechanisms in the gravitationally-driven Niger Delta deep-water fold and thrust belt

4.1 Abstract

Interpretation of two- and three-dimensional seismic reflection data from the deep-water Niger Delta fold and thrust belt reveals evidence for two, discrete, post-faulting deformation mechanisms. An early phase of thrust propagation folding is followed by folding caused by thickness changes within the basal detachment unit. The later phase of folding is caused by a lateral redistribution of the strata within the basal detachment unit. This example of late deformation occurred over a 4-5-m.y. period as a result of the displacement of approximately 590 km^3 of the underlying strata. In another deformation event in the basal detachment unit about 16 km^3 moved, laterally creating a synform in the overburden and parallel onlap fill, indicative of the relatively rapid creation of accommodation space. On the basis of seismic reflection data from the delta and a consideration of the volumes and rates of movement of sedimentary rock, it is concluded that the poorly imaged succession commonly referred to as "mobile shale" cannot deform solely by ductile mechanisms as interpretations of shale tectonic provinces have commonly suggested, but instead by brittle processes that involve thickening by thrust faulting and subseismic accommodation structures. Processes such as liquefaction, where a complete loss of shear strength is involved, had a minimal function. Therefore, the term "mobile shale" in this setting is widely exaggerated. An awareness of post-faulting deformation mechanisms will be important for the successful exploration of gravitationally driven fold and thrust belts.

Note the data used for the research detailed in this chapter was acquired at the start of the Ph.D. A published version of this chapter can be found in the digital appendix.

4.2 Introduction

Fault-propagation, fault-bend and detachment folds accommodate thin-skinned shortening within deep-water, gravitationally driven fold and thrust belts. The geometry and kinematics of these structures are well understood (Suppe, 1983, 1985; Jamison, 1987; Mitra, 1990), but the role played by a basal detachment unit, defined as a regionally extensive décollement (shear zone) of finite thickness that underlies the thin-skinned fold and thrust belt, in accommodating strain is still largely unknown. Deformation styles above basal detachment units composed of undercompacted, overpressured "mobile shales" have recently received much attention in the literature (Damuth, 1994; Homza and Wallace, 1995; Morley et al., 1998; Van Rensbergen and Morley, 2000, 2003; Morley, 2003; Corredor et al., 2005; Deville et al., 2006). Previous authors have suggested that the composition, degree of mobility and thickness of a basal detachment unit is fundamental to determining how compressional strain is accommodated by an overlying cover sequence (Erickson, 1996; Stewart, 1996; Waltham, 1997; Costa and Vendeville, 2002; McClay et al., 2003; Bilotti and Shaw, 2005). In brittle end-member thrust kinematic models for fault-propagation folding (Suppe, 1985; Mitra, 1990, Suppe and Medwedeff, 1990) (Fig. 4.1A) and fault-bend folding (Suppe, 1983, Chester and Chester, 1990; Mitra 1990) (Fig. 4.1B), the basal detachment unit serves to decouple fault-accommodated shortening deformation in the overburden from an underlying less deformed substrate. These models contrast with detachment (or décollement) fold geometric-kinematic models, which involve the ductile deformation of an underlying mechanically weak unit (shale or salt) in response to buckling of overlying mechanically competent layers (Jamison, 1987, Dahlstrom, 1990; Epard and Groshong, 1993, 1995; Groshong and Epard, 1994; Hardy and Poblet, 1994; Homza and Wallace, 1995, 1997; Stewart, 1996; Problet et al., 1997; Atkinson and Wallace 2003) (Fig. 4.1C). The growth of these end member types of folding (and variations upon) forms the primary deformation mechanisms in overthrust terranes. Fault kinematic studies have identified that deformation within a basal detachment unit occurs synchronously with deformation mechanisms operating within the overburden (Imber et al., 2003; Owoyemi and Willis, 2006).

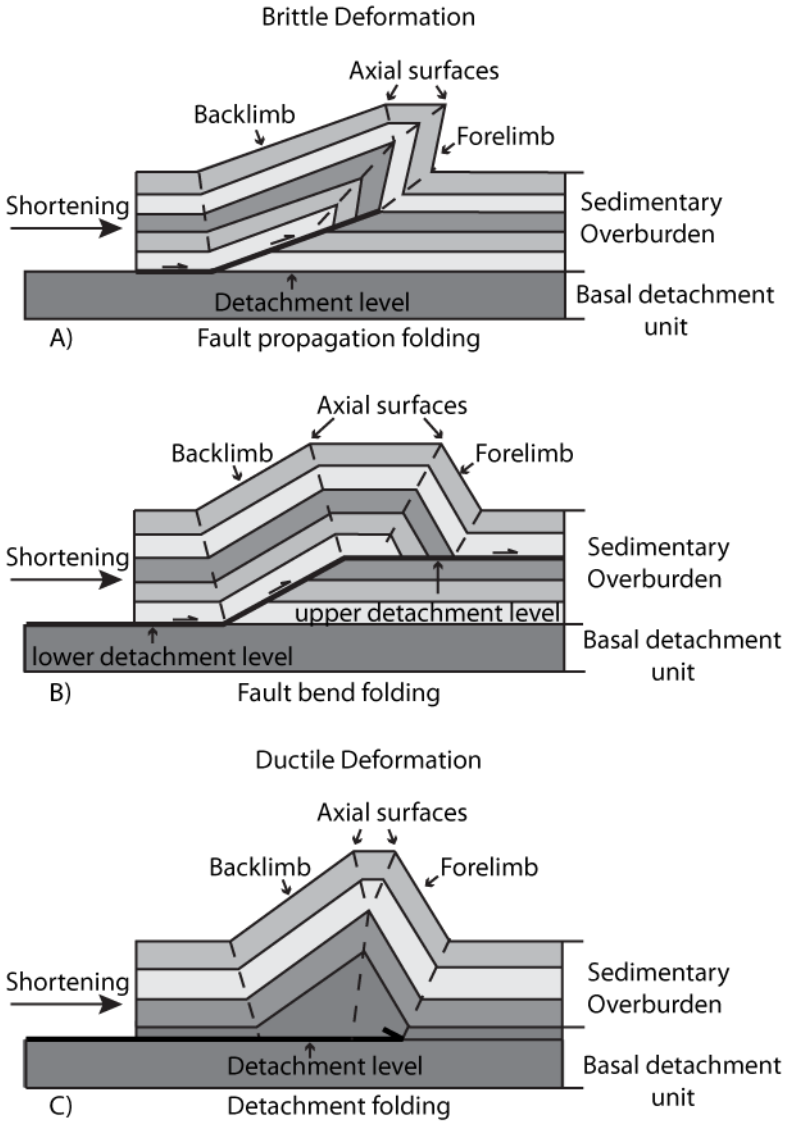

Fig. 4.1. Three types of end member kinematic models which form the primary mechanisms for contractional deformation within a sedimentary overburden a) fault propagation folding (Suppe, 1985), b) fault bend folding (Suppe, 1983) and c) detachment folding (Jamison, 1987).

Some of the deformation observed within an overlying sedimentary overburden is possibly controlled by entirely separate, previously undocumented deformation processes that occur within a basal detachment unit. The processes that occur within an interval that is commonly, loosely referred to as the "mobile shale" are investigated with the aim of providing alternative hypotheses as to the nature of the deformation that occurs in this typically poorly seismically imaged succession. The

problem of determining how deformation is accommodated by a basal detachment unit lies in the difficulty of identifying suitable outcrop analogues for deep-water fold and thrust belts, meaning these features are most commonly studied using seismic reflection data. On seismic reflection data basal detachment units suffer from a lack of acoustic impedance contrasts, which results in poor seismic resolution. This lack of acoustic impedance may be caused by multiple reasons, the primary ones caused by a homogeneous lithology where few acoustic contrasts will be expressed in seismic data and second, the overpressured nature of mud-dominated, basal detachment units. As a consequence of low seismic resolution, relatively little research has been directed at basal detachment units in comparison to overlying, well imaged, sedimentary successions. This has left important, unanswered questions relating to the kinematic nature of mobile shale (how mobile shale actually deforms and subsequently moves), which currently remain poorly constrained.

Investigation of a gravitationally-driven fold and thrust belt, overlying a basal detachment unit, composed of overpressured shales, in the Niger Delta is undertaken to 1) to constrain the relative timing of shale movement to fault movement and fold amplification, 2) to understand the effect of late stage deformation within a basal detachment unit on the geometry and kinematic development of fold and thrust belts and 3) to provide insights on whether deformation (movement) within a basal detachment unit composed of shale occurs by brittle failure or as ductile movement induced by a loss of shear strength. With these aims in mind, two structures from the outer fold and thrust belt from the western and the southern deltaic lobes are compared and contrasted (Fig. 4.2 study areas A and B respectively). Through these analyses, several insights into the role of basal detachment unit deformation in the development of fold and thrust belts are gained. A key point is that detailed mapping and interpretation of stratal packages within a sedimentary overburden can, in some circumstances, provide geological constraints on the timing and spatial distribution of deformation within the underlying basal detachment unit.

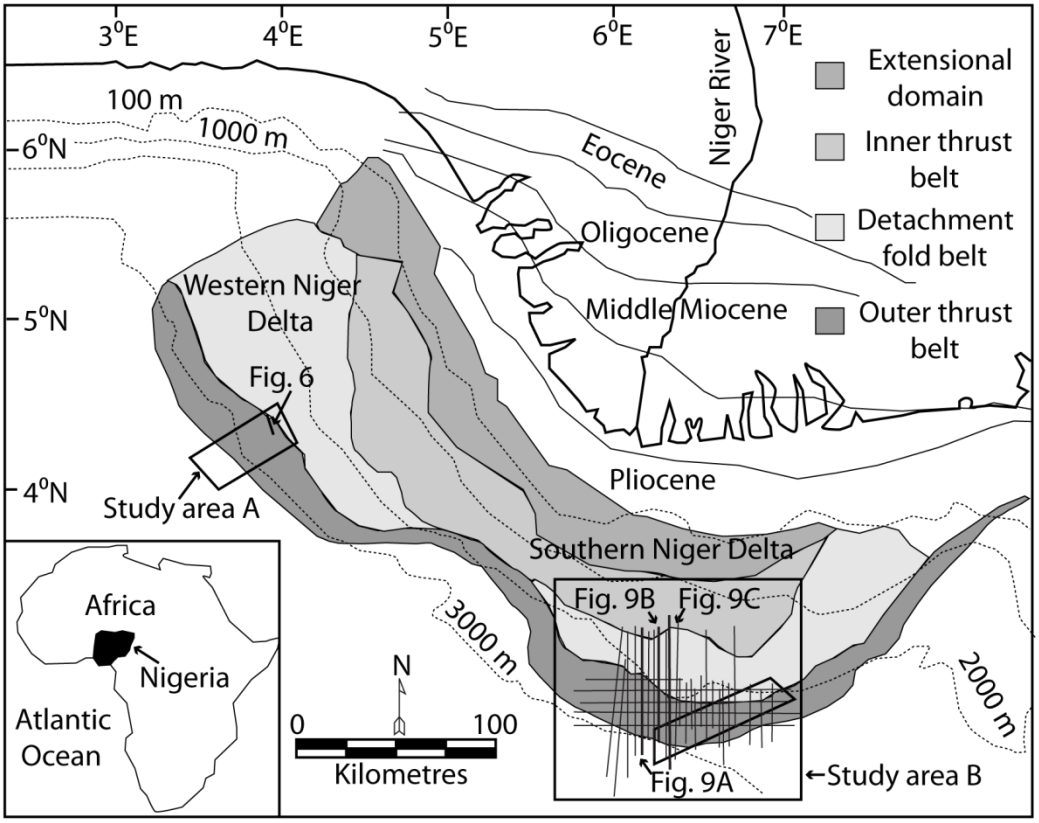

Fig. 4.2. Map of the Niger Delta depicting progressively younging, seaward prograding depolobes (Rouby and Cobbold, 1996) and the main structural domains (Heiniö and Davies, 2006). The locations of the seismic data are shown.

4.3 Geological setting

The Niger Delta has been subdivided into five zones, each of which is characterised by different structural styles. Corredor et al. (2005) identified the following structural zones: 1) a proximal zone of extension dominated by regional and counter regional growth faults; 2) a diapiric zone consisting of passive and active mud diapirs and shale ridges; 3) an inner fold and thrust belt comprising of a series of regional imbricate thrusts; 4) a translational zone between the inner and outer thrust belt where it is thought that sediments are subjected to relatively small quantities of deformation and only detachment folds develop; 5) an outer fold and thrust belt characterised by regional and counter regional verging thrust faults (Fig. 4.2). The outermost parts of the Niger Delta are believed to be underlain by oceanic basement (Briggs et al., 2009).

A unit consisting of marine shale, the Akata Formation, underlies all the structural domains within the western and southern Niger Delta (Fig. 4.3A). The Akata Formation is commonly thought to be mobile in nature (Morely, 2003; Bilotti and Shaw, 2005). In deep-water (distal) regions, the Akata Formation is diachronously overlain by deep-water channel complexes, debris flows and shales of the Agbada Formation, which represents the sedimentary overburden of the deltaic succession (Fig. 4.3B). In landward (proximal) regions the Agbada Formation is in turn diachronously overlain by a series of fluvial, continentally sourced sands known as the Benin Formation (Short and Stäuble, 1967). The Benin Formation is absent in deep-water regions. On 2D and 3D seismic reflection data, what is commonly referred to as the mobile shale is identified by discontinuous, acoustically transparent seismic reflections (Fig. 4.3B). Typically, regional 2D seismic sections that span proximal to distal parts of the delta show that significant vertical thickness variations exist (up to 3 km change in vertical thickness over distances of 100 km) within the Akata Formation) (Corredor et al., 2005; Briggs et al., 2006).

Shale mobility is dependent on a host of factors (mineralogy, pore volume, cementation, degree of overconsolidation and undercompaction; see Osborne and Swarbrick, [1997] for a review on overpressure generation mechanisms in shale basins). Mechanisms that induce plastic mobility of shales involve increasing the intrinsic pore-fluid pressure within a rock volume through either 1) tectonic or sediment loading (pore volume reduction), 2) an increase in fluid volume (water release through diagenetic reactions associated with progressive burial) or 3) fluid migration and buoyancy effects (Osborne and Swarbrick, 1997). All of these mechanisms cause an associated decrease in effective stress and induce subsequent ductile failure. A key causal factor in inducing shale mobility is related to the inability of pore-fluid pressures to remain at hydrostatic during burial (overpressure).

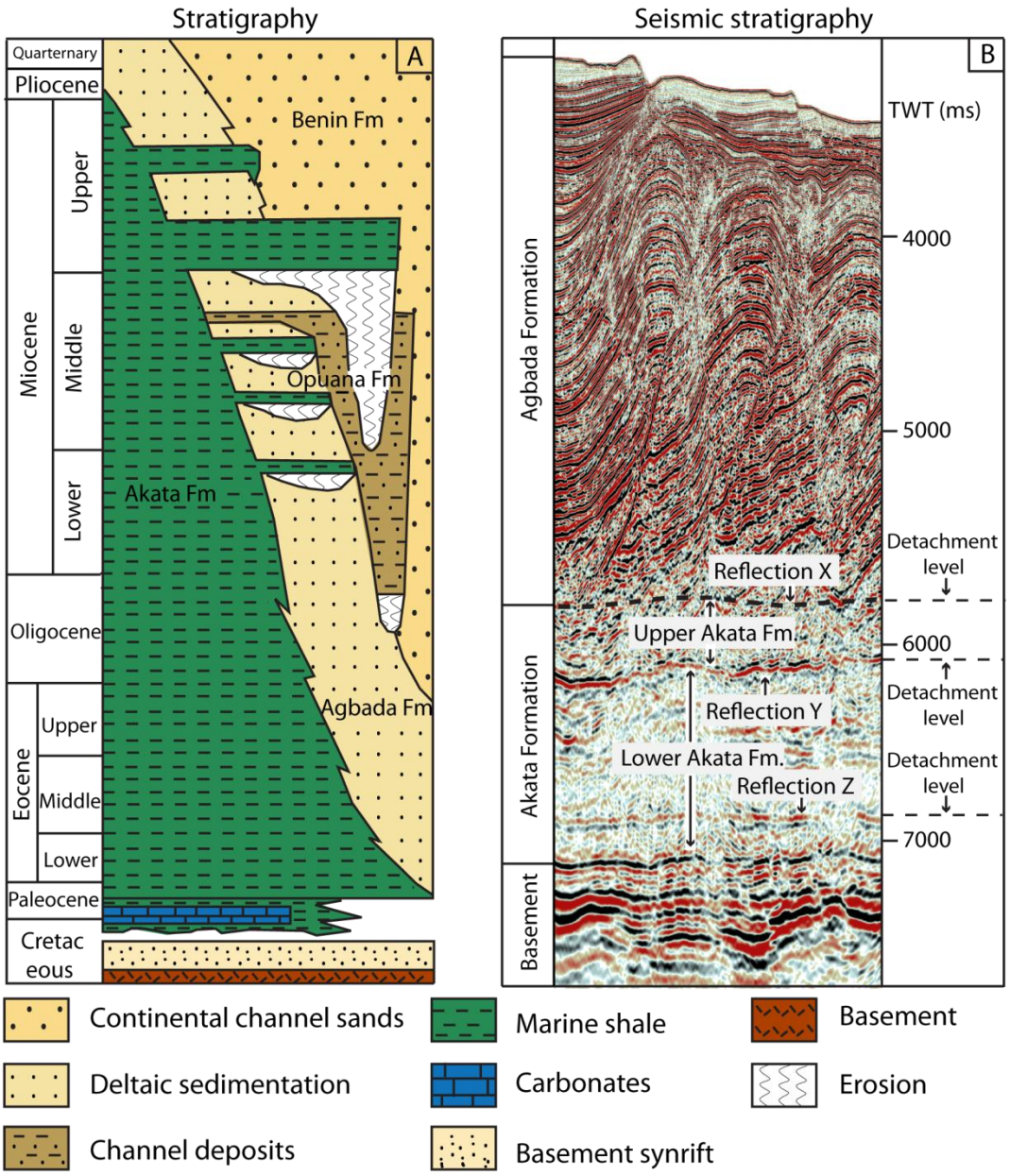

Fig. 4.3 A) Regional stratigraphy of the Niger Delta, depicting the three diachronous lithological units of the Akata, Agbada and Benin Formations (from Corredor et al., 2005) originally modified from Lawrence et al., (2002). B) Seismic stratigraphy of a deep-water section from the southern Niger Delta displaying the prominent acoustic impedance contrast boundary (reflection X) separating the Akata Formation from the overlying Agbada Formation. Further subdivision of the Akata Formation into its upper and lower counterparts is based upon the location of regional detachment levels, reflections X and Y.

Overpressure development provides the conditions to potentially induce plastic mobility of shales (Boltman and Maltman, 1998). In deltaic settings where pore-fluids are likely to be overpressured due to the effects of rapid sedimentation rates and/or tectonic loading the effective stress should include estimates of the pore-fluid pressure ratio (λ). Estimates for λ within the Akata Formation have been placed has high as 0.9 (Bilotti and Shaw, 2005) implying that conditions for overpressure are in place at the present day. In addition, anomalously low seismic stacking velocities were used by Morgan (2003) as evidence for overpressure at the top of the Akata Formation where velocities decrease up to 1000 ms^{-1}.

4.4 Terminology

The terms "mobile shale" and "sediment mobilisation" (see appendix 1, glossary) are commonly used where overpressure is known or inferred to exist in shale-dominated sedimentary basins (Buryakovsky et al., 1995; Wood, 2000; Moscardelli et al., 2006; Stewart and Davies, 2006). These include large prograding deltas that are underlain by a basal detachment unit on passive and active margins (Brown et al., 2004) and regions of tectonic compressional stress (Van Rensbergen et al., 2003) such as accretionary prisms (Deville et al., 2006). However, we refrain from using the terms "mobile shale" (and associated terms for sedimentary successions) or "shale mobilisation" as a process, because both terms have historically been loosely applied to areas of low seismic reflectivity (Bruce, 1973; Evamy et al., 1978) and imply specific deformational processes, where there has been a partial or complete loss of shear strength within a rock volume. Shale mobilisation represents a spectrum of processes ranging from liquefaction, which involves rapid, geologically instantaneous deformation (movement) of sediment, through to slower creep processes (Maltman, 1994). On seismic reflection data, large-scale deformation within a shale dominated basal detachment unit is usually referred to having a ductile deformation style (Van Resenbergen and Morley, 2003). Here, deformation observed within a basal detachment unit is simply referred to as either detachment unit thickening or detachment unit thinning without implying a process.

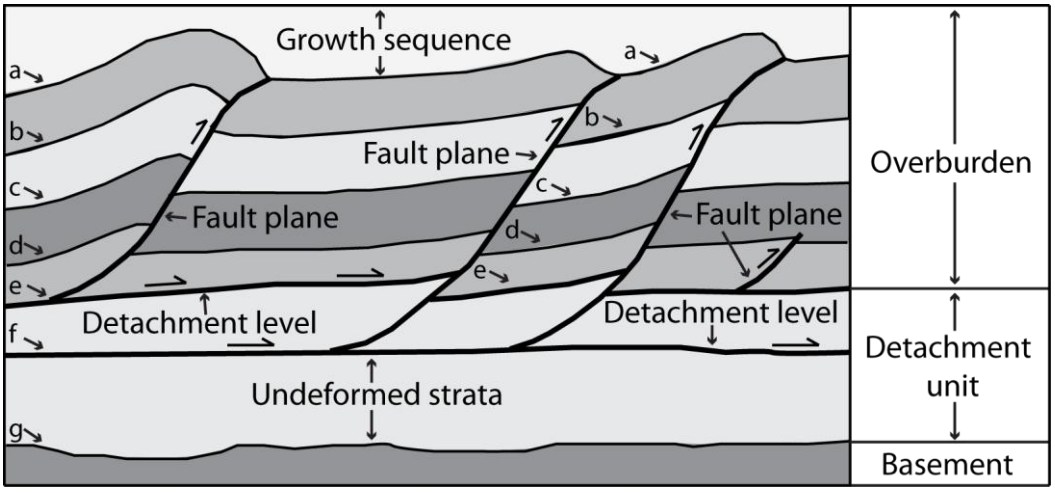

Fig. 4.4. Cartoon illustrating the typical structural style displayed in deep-water fold and thrust belts overlying a shale basal detachment unit. Horizons e and f represent detachment levels, bedding parallel faults to which thrust faults sole to at depth. The basal detachment unit incorporates horizons e-g and includes the two detachment levels and undeformed strata beneath the most basal detachment level (horizon f).

This paper defines a "basal detachment unit" as a zone within the Akata Formation that incorporates multiple detachment levels along which slip may occur through various brittle and ductile deformation processes (Fig. 4.4). The term "detachment level" refers to a basal fault (typically bedding parallel) along which numerous fault planes sole, and separates brittle deformation styles from underlying, undeformed layers (Fig. 4.4). In addition, the types of deformation processes that may occur within a mud-dominated basal detachment unit are discussed.

4.5 Data and methodology

High-quality 3D seismic data sets acquired over the western and southern deltaic lobes were used in conjunction with regional 2D seismic lines covering the contractional toe thrust domain of the Niger Delta (Fig. 4.2). The post-stack time migrated 3D seismic data have an inline and cross line spacing of 12.5 m and are zero phase migrated; however, the data have different polarities. In the southern Niger Delta the seismic data are displayed so that an increase in acoustic impedance is characterised by a red-black-red reflection combination. In the western Niger Delta an increase in acoustic impedance is displayed as a black-red-black reflection

combination. The maximum vertical resolution is approximately 8 m (50 Hz) in shallow sections, which decreases to about 25 m (23 Hz) at the base of the Agbada Formation with the onset of the Akata shale (Fig. 4.3). The seismic stratigraphy was interpreted using regional sequence boundaries, unconformities and reflections, which define important stratigraphic, structural and seismic facies.

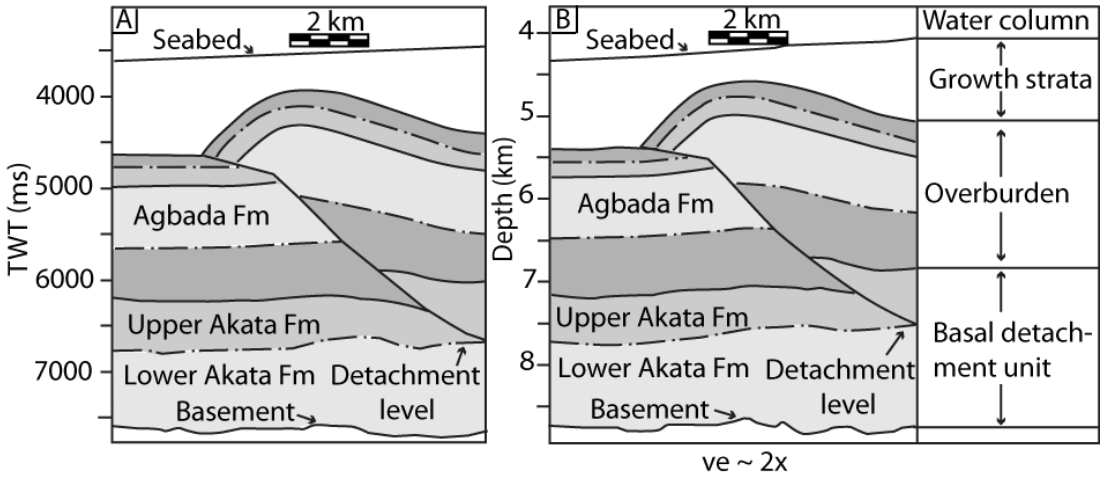

Fig. 4.5. Cross-section of a depth converted time section. A) Cross-section of a fault bend fold in TWT and B) depth converted section of the fault bend fold shown in (A). In panel B) the amplitude of the anticline has slightly increased and the basement architecture has become irregular. VE = vertical exaggeration.

Velocity generally increases with depth; hence structures imaged in the subsurface may undergo geometric changes when depth converted (Fig. 4.5). To depth convert from two-way travel-time (TWT) into metres, a velocity of 1480 ms^{-1} was used for water and interval velocities were extrapolated for underlying sedimentary packages from the closest available well (note that the well data are confidential hence the values used are not listed here). Figure 4.5 shows that the geometric impact of depth conversion here is minimal, as the depth converted geometry of the fault-bend fold is relatively unchanged from its equivalent time section. The only notable change occurs at the base of the section where the basement architecture becomes irregular. This mostly negligible geometric effect is consistent with all depth-converted sections, and so herein, data sets are typically displayed in milliseconds (ms) TWT.

4.6 Western Niger Delta

4.6.1 Seismic observations

Within the western Delta (Fig. 4.2, study area A), three distinct seismic facies have been identified. Figure 4.6 depicts a prominent, high-amplitude seabed reflection, which is underlain by a package of dominantly continuous reflections (appendix 2, Figs. A2B and A2C). These are of variable amplitudes, locally cut and offset by well-imaged fault planes, and are deformed by seaward verging (regional) and landward verging (counter regional) fault propagation-folds. Fault plane reflections are planar in the shallower parts of the seismic sections, with fault plane curvature increasing with depth. Fault plane reflections either become sub-parallel to stratal reflections at their base or appear to terminate downwards abruptly at two reflections (Fig. 4.6, reflections X and Y). The termination of fault plane reflections at these two seismic intervals marks reflections X and Y as detachment levels (Briggs et al., 2006) (appendixes 2 and 4, Figs. A2D, A2E and A6A and A6B). The increase in fault plane curvature with depth has been cited as evidence for an increase in pore-fluid pressure, which occurs within sediments at deeper levels within deltaic stratigraphy (Cobbold et al., 2009). The base of the folded and faulted overburden is marked by a series of discontinuous reflections collectively labelled reflection X (Fig. 4.6, dashed black line). This reflection marks a distinct change in seismic character and represents the base of the Agbada Formation (sedimentary overburden) and the top of the Akata Formation (basal detachment unit). Reflection X defines the top of an underlying seismic package whose base is defined by reflection Y (Figs. 4.3B and 4.6). The seismic character between reflection X and reflection Y is dominated by discontinuous, low-amplitude reflections. A lack of acoustic impedance within this interval is common but is not laterally persistent, as in places coherent reflectivity can be identified (Figs. 4.3B and 4.6). This interval will herein be referred to as the upper Akata Formation (Fig. 4.3B). Reflection Y typically lies at approximately 7000 ms (TWT) and is regionally correlative throughout the deep-water Niger Delta. Reflection Y has been identified as a detachment level in previous deep-water studies in the Niger Delta (Corredor et al., 2005; Briggs et al., 2006; Higgins et al., 2007).

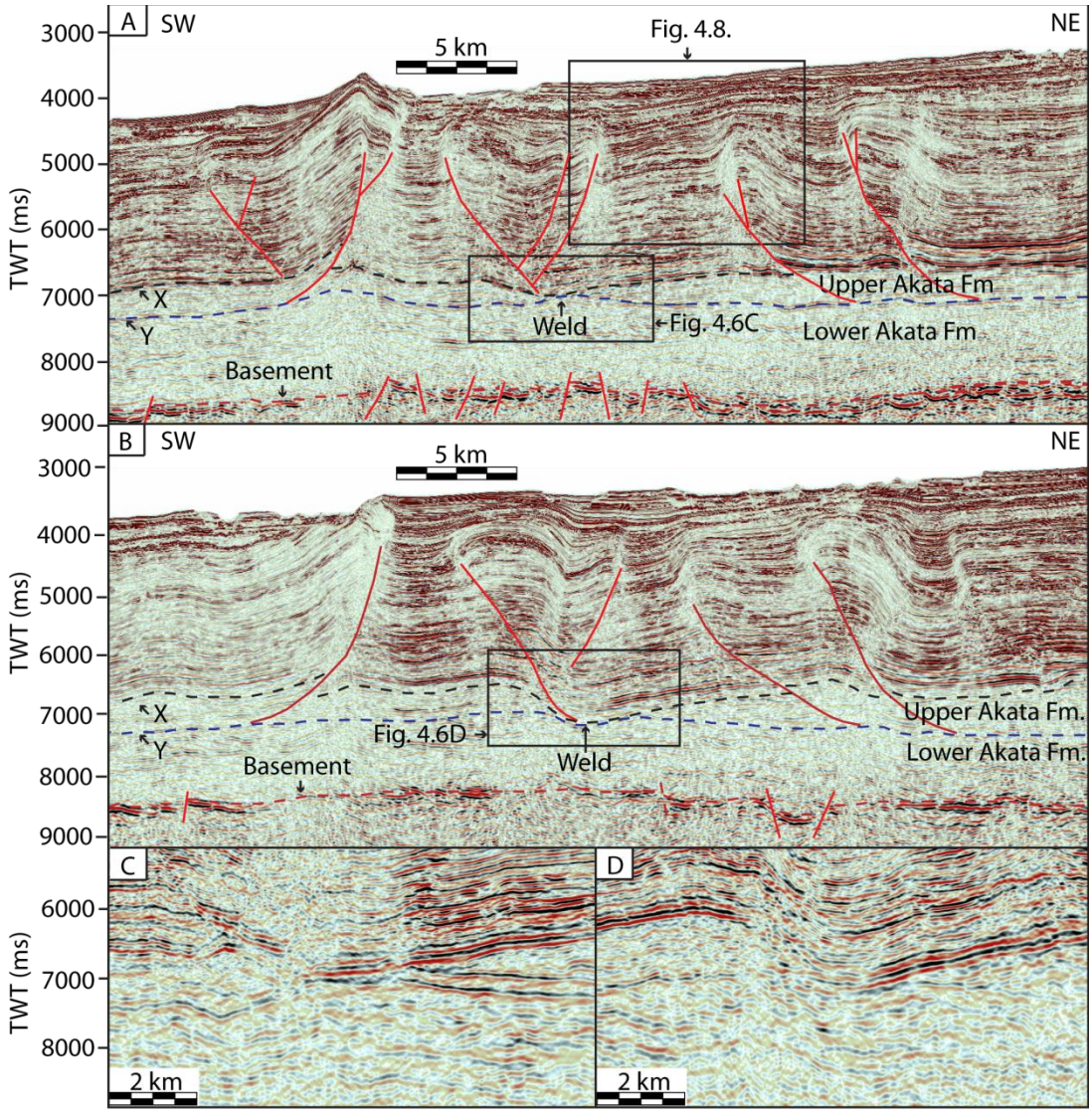

Fig. 4.6. Seismic lines from a 3D survey showing deformation within the upper Akata Formation expressed as detachment unit thinning. This has resulted in juxtaposition of the overlying Agbada Formation (reflection X) with the mid-Akata detachment level (reflection Y) and the formation of a shale weld (grounding). Vertical scale is approximately 2x the horizontal scale.

From herein, reflection Y is referred to as the mid-Akata detachment level based upon its location within the Akata Formation. The amplitude of the mid-Akata detachment level varies regionally but within the survey area typically has a low seismic amplitude (Fig. 4.2, study area A and Fig. 4.6). The interval between

reflections X and Y represents the upper Akata shale through which numerous lateral and vertical variations in thickness occur (appendix 4, Fig. A7).

The lowermost seismic package lies between the mid-Akata detachment level (Fig. 4.6, reflection Y) and is bound by a high-amplitude reflection at its base at approximately 8800 ms (TWT) that overlies reflections displaying hummocky characteristics (Fig. 4.6, red dashed line). This interval is referred to as the lower Akata Formation (Fig. 4.3B). The high-amplitude reflection situated at the base of this sequence is locally vertically offset. This reflection is interpreted to mark the top of the likely oceanic crust, which displays numerous geometries reflecting horst and graben features (Fig. 4.6, dashed red line) (appendices 2 and 4, Figs. A2F and A6C). Seismic resolution within the lower Akata Formation is poor, but in places, it is characterised by discontinuous, low-amplitude reflections, hence has similar seismic characteristics to the upper Akata Formation. Seismic resolution immediately below the top basement reflection rapidly deteriorates. No structures are seismically resolvable approximately 0.5 ms (TWT) below the top basement reflection. By separating the Akata Formation into its lower and upper counterparts the level at which detachment occurs can be differentiated enabling rheological insights to be made within the basal detachment unit.

In the central part of figure 4.6A and B, the vertical thickness of the upper Akata Formation decreases from about 500 ms to 50 ms (TWT) (see Figs. 4.6C and 4.6D for zoomed uninterrupted sections of the weld). The thinnest section of the upper Akata Formation is located beneath and adjacent to the hanging walls of landward- and seaward- verging thrust faults. Vertical thinning of the upper Akata Formation has led to juxtaposition of reflection X with refection Y directly beneath landward- and seaward- verging thrust faults (Figs. 4.6 and 4.7). This structure is interpreted to be a weld or touchdown (Morley and Guerin, 1996) where shale originating from the upper Akata Formation has moved out the intervening section, and as a consequence, reflections X and Y have become coincident (Figs. 4.6C and 4.6D). Coupled with a decrease in vertical thickness of the upper Akata Formation is an increase in depth of reflections in the overlying Agbada Formation. Figure 4.7A, a TWT map of the boundary between the Agbada and upper Akata Formation (reflection X, Figs. 4.3

and 4.6) displays an increase in TWT (depth), which correlates with the geometry of the underlying weld (indicated by the dashed line) (Fig. 4.6A). Minor changes in weld geometry occur along strike as the vertical thickness of the upper Akata Formation varies laterally and reflections X and Y are not always coincident. This led to the development of a welded region within which juxtaposition and minor separations of reflection X and Y occur (Fig. 4.7). Changes in weld geometry are primarily expressed by the degree of rotation exhibited in the overlying overburden and the lateral extent to which reflections X and Y are coincident. Changes in weld geometry also are dependent on the variable thrust geometries that occur along weld strike (Figs. 4.6 and 4.7B). This lateral variation in the vertical thickness of the upper Akata Formation is attributed to growth of thrust faults along weld trend that detach at the mid-Akata detachment level. This has allowed the upper Akata Formation to thicken locally up the base of fault ramps (Fig. 4.6). Figure 4.7 B shows the zone of welding to be approximately 3.3 km wide and laterally persistent for 23 km trending in a north-north-east–south-south-west orientation. The main weld trace within the welded regions where the base of the overburden (Fig. 4.6, reflection X) has ground against the mid-Akata detachment level is laterally persistent for 20 km along trend.

4.6.2 Growth strata

Stratal relationships and thickness changes within the Agbada Formation can be used to constrain the nature and timing of weld formation. There are three seismically distinct stratigraphic units above the weld (Fig. 4.8). A basal package (Fig. 4.8 package C) consisting of continuous layer-parallel reflections that identify this package as subkinematic and therefore deposited before the growth of adjacent thrust faults initiated. This basal subkinematic package is overlain by reflections that display stratal thickening (wedging) and multiple onlaps onto forelimbs and backlimbs of thrust-propagation folds (Fig. 4.8 package B). Here, growth strata display both parallel and upward-shallowing of dips above the forelimbs of seaward and landward verging thrust faults. Hence, this package is synkinematic and records the growth of thrust-related folds. Overlying this synkinematic growth package is a prominent angular discordance, which marks the base of a younger stratal package (Fig. 4.8 package A). This uppermost package displays a succession of reflections

that onlap onto the angular discordance. This package is laterally persistent for 15 km in parallel with the strike of the underlying weld. Erosion by deep-water channel systems obscure and terminate onlapping patterns to the west (Figs. 4.6 and 4.8).

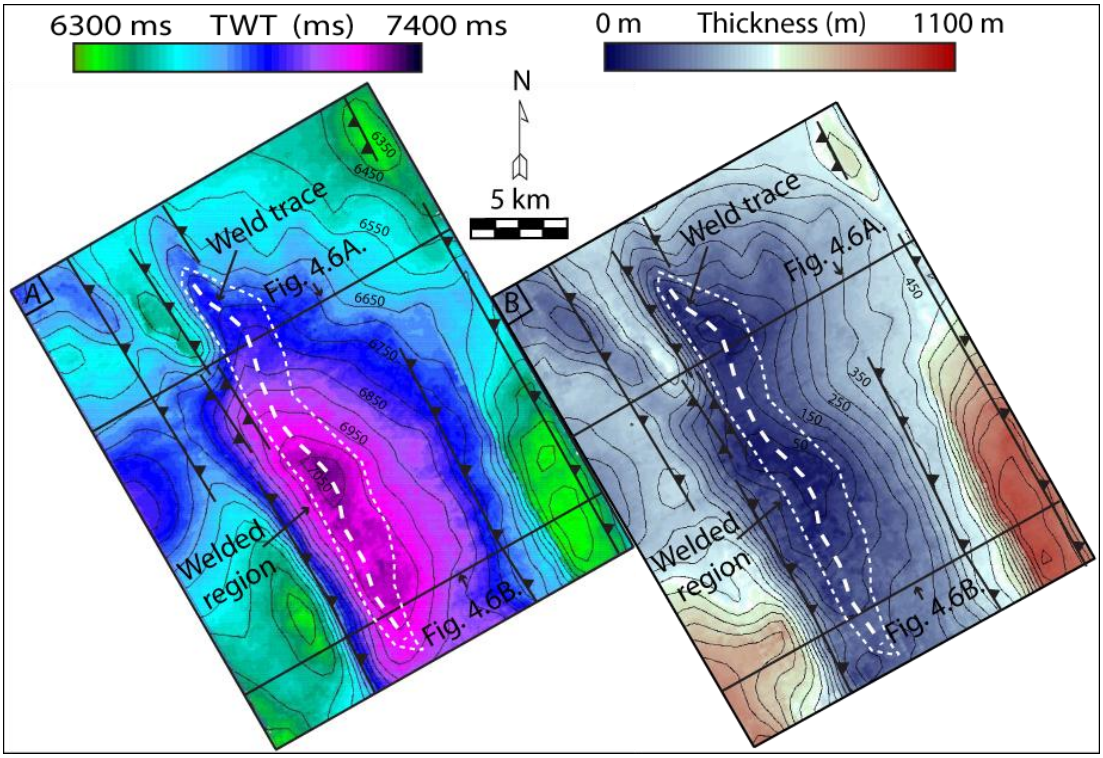

Fig. 4.7. A) TWT map of upper-Akata reflection (reflection X Figs. 4.3B and 4.6) displaying the inclination of the overburden into the upper Akata Formation. The lateral extent of the welded region and the main weld trace is shown. B) Isopach map between the upper-Akata reflection (X) and the mid-Akata detachment level (Y) depicting the location and geometry of the welded region and the trend of the main shale weld which is marked by zero thickness in the isopach data.

4.6.3 Interpretation

Two separate stratal packages are present (marked packages A and B in Fig. 4.8), which can be related to two separate stages of deformation. The prominent angular discordance serves to differentiate earlier synkinematic strata associated with tectonic uplift from a later phase of post-faulting deformation. The thrust-related growth package (package B in Fig. 4.8) is related to the development of the prominent thrust-propagation folds. The upper limit of this growth package is

marked by the cessation of stratal thickening caused by uplift of thrust related anticlines (Fig. 4.8B). Within the overlying stratal package (package A Fig. 4.8), little evidence of growth (stratal wedging) is recorded, suggesting onlaps formed through a passive infilling of sediment. This package is interpreted to record the postfaulting, tilting of the fold and thrust belt into the underlying upper Akata Formation (basal detachment unit) (see appendix 4, Fig. A8).

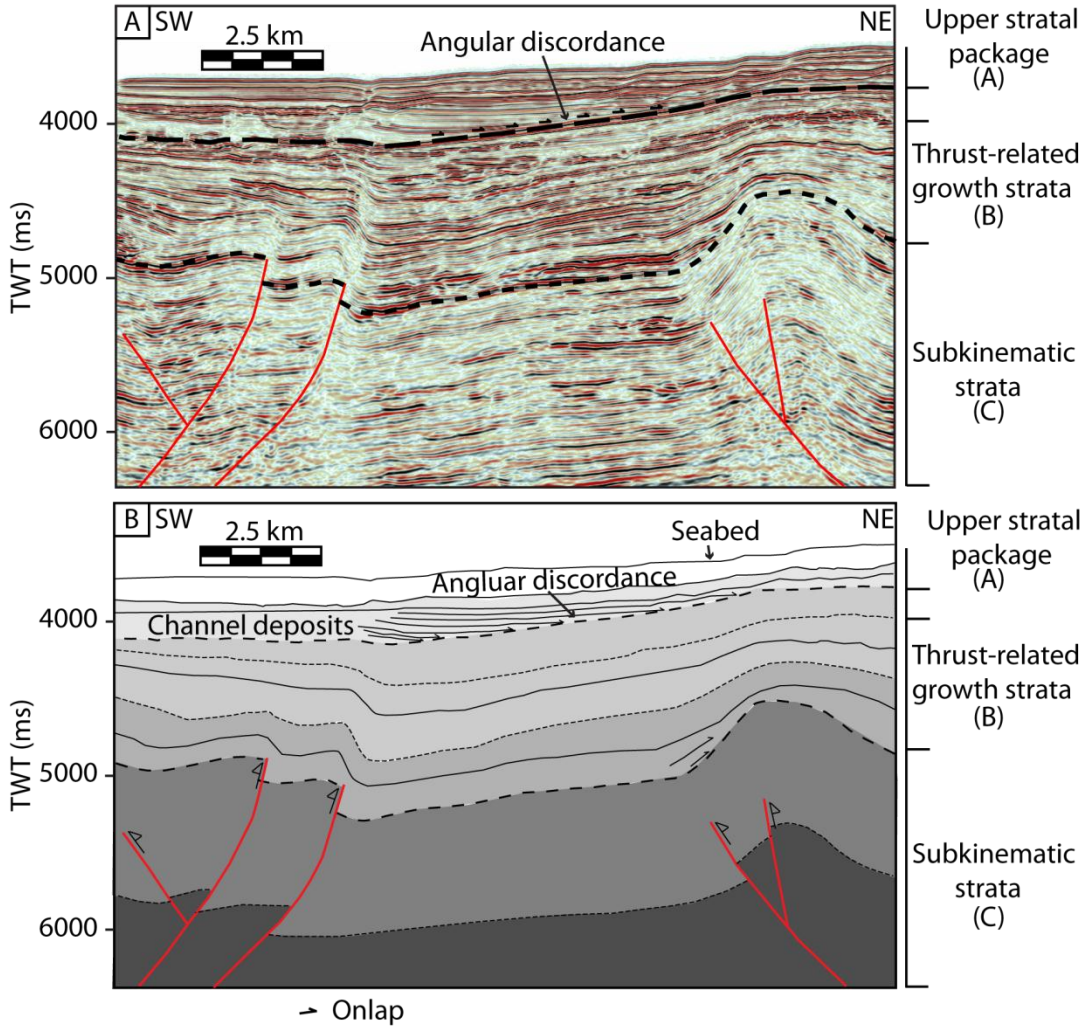

Fig. 4.8. A) Architecture of growth and stratal packages lying above the shale weld identify two separate phases of deformation. An underlying growth package (B) related to the kinematics of uplifting of thrust related folds. Package (A) is separated from the underlying counterpart by an angular discordance and displays numerous onlaps onto this discordance. This records the underlying thinning of the detachment unit. B) A line drawing of A) depicting the main stratigraphic architectural elements. Vertical scale is approximately 2x the horizontal scale.

This separate phase of deformation recorded within this stratal package does not coincide with deformation associated with the formation of the fold and thrust belt and is unseen elsewhere within the survey area. The passive nature of the onlaps and lack of erosional truncations suggests that tilting of the fold and thrust belt was a geologically instantaneous event. Tilting of the fold and thrust belt and the formation of a weld is interpreted to have been caused by deformation and consequent movement of shale in the upper Akata Formation (basal detachment unit) (see appendix 4, Fig. A8). This shale previously occupied the stratigraphic interval between the upper- and lower-Akata detachments (Figs. 4.6 and 4.7 reflections X and Y). The primary locus of shale deformation occurred beneath a structurally thickened area of the overburden. Thinning of the upper Akata Formation occurred beneath hanging walls of landward and seaward verging thrust faults (Fig. 4.6). Weld formation (grounding) is interpreted to be coincident with the cessation of shale movement in this region. As the youngest stratal package (Package A) only directly overlies the location of the shale weld, note that deformation of shale, and hence movement, has only occurred directly beneath the tilted section of the fold and thrust belt. Complete removal of shale has not occurred within the upper Akata Formation and this stratigraphic interval returns to an average thickness in areas directly adjacent to the tilted section (Fig. 4.6). The key conclusion is that analysis of stratal relationships demonstrates that shale movement and thinning within the basal detachment unit occurred after the main faulting episode ceased. In the following section, evidence is found for late stage of folding driven by deformation within the basal detachment unit within the southern Niger Delta.

4.7 Southern Niger Delta

4.7.1 Seismic observations

Representative 2D seismic lines spanning the contractional domain from the southern part of the deep-water delta used in conjunction with a 3D seismic survey (Fig. 4.2 survey area B) image a large west-east-trending anticline measuring approximately 40 km along strike (Fig. 4.9). The dip of the northern fold limb is 6° and the southern limb is 9°. The steeper dip of the southern limb is attributed to erosional activity caused by deep-water channel complexes, which undercut the fold limb (Fig. 4.9).

On 2D and 3D seismic data the fold is cored by low-amplitude, discontinuous reflections, which are seismically transparent. Zones of seismic noise and low reflectivity also constitute the seismic characteristics within the fold core. Continuous low-amplitude reflections are present in areas adjacent to the fold core and some of these reflections can be traced through the fold interior. In addition, some high-amplitude events are present within the fold core (Fig. 4.9), and the nature of these reflections is discussed below. In both data sets the seismic resolution within the fold core is poor, but the seismic characteristics on both 2D and 3D seismic data are consistent with the fold being cored by the Akata Formation (basal detachment unit). A TWT to depth conversion through a cross-section of the anticline shows that the fold has an amplitude and wavelength of 4 km and 35 km respectively (Fig. 4.10).

Thrust faults in the toe-of-slope are approximately 2.3–2.5 km in height, predominantly north-west striking and are mainly seaward verging in the survey area (appendix 2, Fig. A2D). This observation places the shale cored anticline slightly oblique to the main structural trend (thrust faults). Fault-propagation folds and fault-bend folds occur throughout the area, and fault planes dip between 27° and 33°. Fault plane reflections are typically planar in shallow sections as seen in the western Niger Delta with fault plane curvature increasing with depth, coming close to paralleling three reflections (Figs. 4.9 and 4.10, reflections X, Y and Z). This relationship indicates the presence of three detachments at multiple levels within the Akata Formation in the deep-water southern Niger Delta, an interpretation that is in agreement with previous studies of the area, which identify thrust faults soling to multiple detachment levels (Briggs et al., 2006; Corredor et al., 2005). Reflection X consists of a series of discontinuous reflections that separate an overlying package of high-amplitude reflections (which constitute the Agbada Formation) from the underlying Akata Formation. Reflection Y lies at approximately 6500 ms (TWT) and is characterised by a strong acoustic amplitude in the southern delta. This reflection has been previously identified as the mid-Akata detachment level in the western Niger Delta (section 4.6.1). Reflection Z lies at approximately 6900 ms (TWT) and close to the top of the oceanic basement.

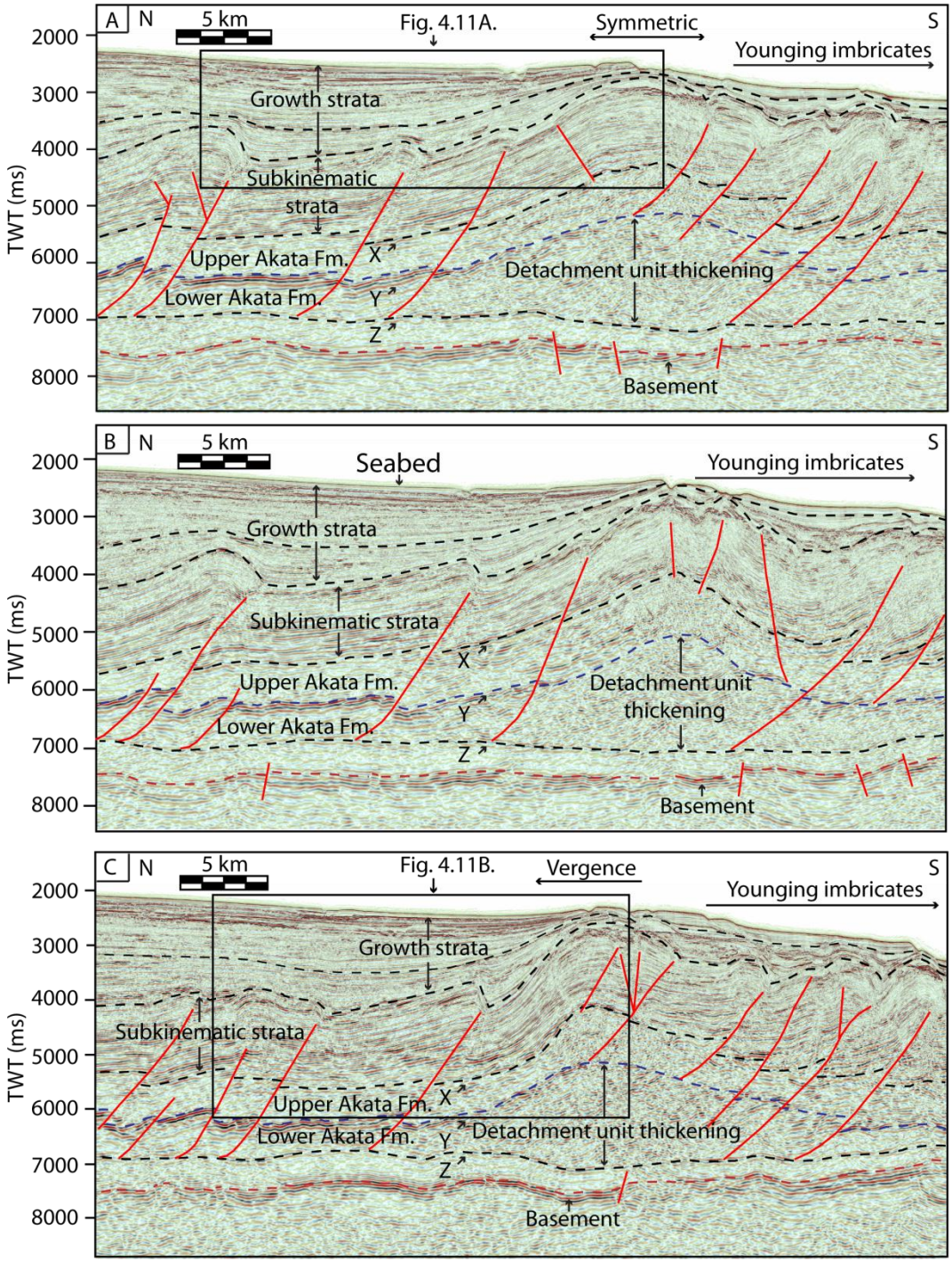

Fig. 4.9. Interpreted cross sections through a shale cored anticline from regional 2D seismic lines (location shown in Fig. 4.2). Thickening and hence deformation within the basal detachment unit is restricted to the lower Akata Formation beneath the mid-Akata detachment level (reflection Y) and bound by a deep detachment level lying above the basement (reflection Z). Note the change in fold geometry and vergence moving progressively westward along strike. Vertical scale is approximately 2x the horizontal scale.

Landward-verging thrust imbricates are incorporated onto both the southern and northern limbs of the large shale-cored fold, whereas steeply-dipping forethrusts and a backthrust occurs within the crestal region of the anticline (Fig. 4.9Fig. 4.9) (appendix 4, Fig. A9). Thrust faults on the northern fold limb are interpreted to detach deep within the lower Akata Formation at a detachment level, which lies close to the top of the oceanic basement (Figs. 4.9 and 4.10 reflection Z) because the high-amplitude mid-Akata detachment level is offset (Figs. 4.9 and 4.10, reflection Y). Thrust faults on the southern limb of the fold detach on either the upper-Akata (reflection X) or the mid-Akata detachment level (reflection Y). The level that thrust faults incorporated within the crestal region of the detachment fold detach at is difficult to distinguish, due to sudden loss of coherent reflectivity within the detachment fold interior. Thrusts are interpreted to either detach on the mid-Akata detachment level (Y) or within the fold core itself, based on whether the mid-Akata detachment is offset. The gross architecture of the shale-cored fold changes along strike from symmetrical fold limbs in the north-west (Figs. 4.9 and 4.10) to having well-developed landward vergence in south-eastward cross-sections (Fig. 4.9C).

The acoustic amplitude of the distinctive mid-Akata detachment reflection level (Y) decreases towards the centre of the shale-cored anticline and is interpreted to shorten by a combination of folding and faulting within the anticlinal core (Figs. 4.9 and 4.10). Reflection Z can be mapped through the fold core and remains at a constant depth, about 6800 ms TWT (Fig. 4.9). The lower Akata Formation undergoes a dramatic vertical thickness change within the fold core. The concordant, tramline nature of reflectors X (upper-Akata) and Y (mid-Akata detachment level) in regions adjacent to and away from the thickened section beneath the fold indicate that the average vertical thickness of the entire Akata Formation is approximately 2.3 km (~2000 ms TWT), with 1.5 km and 0.8 km composed from the lower and upper Akata Formation, respectively. The total thickening of the lower Akata Formation within the fold core varies laterally, but the basal detachment unit undergoes approximately 2 km of thickening to a total thickness of 4.3 km (~3000 ms TWT, Figs. 4.9 and 4.10). In directions both along and across strike of the detachment fold the thickness of the Akata Formation returns to regional thickness, and no evidence

of excessive detachment unit thinning exists within the survey area. Insights into the source of the thickened shale are discussed later in this paper.

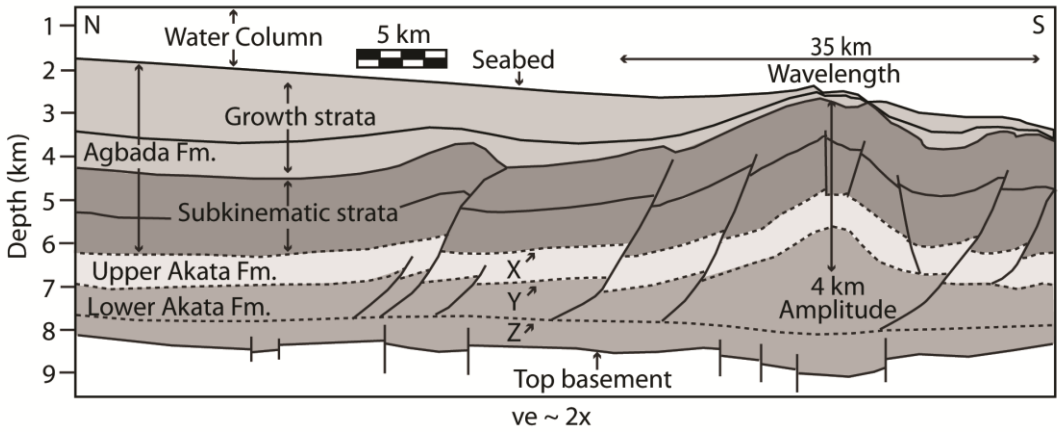

Fig. 4.10. Depth converted cross-section through the large-scale shale-cored anticline. The time related section is shown in figure 4.9B. Detachment levels (relections X, Y and Z) are represented by dashed lines. VE = vertical exaggeration.

4.7.2 Structural interpretation

The first-order geometry of the shale-cored anticline is similar to that of a detachment fold (Jamison, 1987) with the additions of numerous thrust imbricates situated on both fold flanks (see appendix 4, Fig. A9). The folded, more competent overburden is cored by the underlying Akata shales (basal detachment unit). Potential insights into the nature of the fold interior can be derived from a combination of fold geometry and adjacent thrust imbricates, and the presence of coherent reflectivity at depth (Fig. 4.9, at 6600 TWT) within the Akata shale directly adjacent to the fold core. The detachment fold is not bound by synclines, which would normally be expressed in the overburden as a consequence of mobility within an underlying basal detachment unit. In such a case, the overburden 'subsides' beneath the regional for the competent unit, as is depicted for detachment fold models, which capture the movement of ductile material into the fold core (Mitra, 2002; 2003). The absence of synclines bounding the detachment fold may imply that a ductile redistribution of the Akata shale has not taken place within the fold core. Within the fold core, the two underlying, uppermost detachment levels (Fig. 4.9,

reflections X and Y) have shortened within the fold core. The mid-Akata detachment level (reflection Y) has likely shortened through a combination of thrust faults detaching within the lower Akata Formation (reflection Z), and by layer-parallel shortening in a manner that is directly analogous to the shortening style displayed in the overburden. The source of the redistributed shale is from the lower Akata Formation. This locally restricts the plastic unit as depicted in detachment fold models (e.g. Fig. 4.1C), which redistributes and thickens within the fold core to the area between the mid-Akata detachment level (Fig. 4.9, reflection Y) and the lower-Akata detachment (Fig. 4.9, reflection Z). Mechanical competency contrasts are inferred between the lower Akata Formation and the upper Akata Formation along with the Agbada Formation in this part of the delta. A few high-amplitude events are visible within the thickened basal detachment unit, but the structural style depicting how the lower Akata shale actually thickens within the fold core cannot be seismically resolved and remains ambiguous.

The style of vertical and lateral basal detachment unit thickness variations within the fold core varies with the overall geometry of the detachment fold. Figure 4.9 displays a relationship between variations in the redistribution of Akata shale and competent components of the detachment fold geometry. Where fold limbs are symmetrical, the main thickness increase in the Akata shale has occurred directly beneath the axial trace, and a uniform decrease in thickness occurs within the Akata shale either side of the axial trace as it returns to regional (Figs. 4.9A and 4.9B). In contrast, Figure 4.9C shows that asymmetrical growth of the competent fold limbs has led to a similar asymmetrical redistributional thickening of the Akata shale. It is interpreted that this asymmetric basal detachment unit thickening is controlled by the degree of asymmetry displayed by the first-order detachment fold geometry in the overburden.

4.7.3 Growth strata

Seismic data show that two distinct packages of growth strata can be recognised flanking the detachment fold (Packages V and W in Figs. 4.9, 4.10 and 4.11), which

reflect two episodes of fold growth. The oldest growth package (growth package W in Figs. 4.9 and 4.11) records the growth of adjacent thrust imbricates and the detachment fold. Within this growth package, strata thin dramatically towards the fold limbs and onto the crest of the detachment fold. The architecture of growth package W consists of multiple wedge-shaped, fanning geometries and numerous unconformities that onlap onto both fore- and backlimbs of thrust-related anticlines and the detachment fold. The basal part of growth package W also displays sections where growth stratal geometries lie parallel to underlying pre-growth strata in both thrust-related and the detachment fold forelimbs. These limb-parallel sections display structures resembling growth triangles in the synkinematic strata where active axial surfaces and growth axial surfaces converge (Suppe et al., 1992) (Fig. 4.11). The internal structure of growth geometries within package W varies laterally along strike of the detachment fold. The change in growth architectural elements coincides with the degree of asymmetry displayed by the competent units (overburden) of the detachment fold. Where detachment fold limbs are symmetrical, growth strata typically display wedge-shaped geometries and minor sections that lie parallel to the underlying pre-growth component of the detachment fold limb (Fig. 4.11). Convergence of axial surfaces in the growth strata have not always led to the formation of a complete growth triangle as the apex has been truncated by the deposition of younger unconformable beds (Fig. 4.11). In contrast, where northward vergence is present, growth strata display a shallowing of dips, wedge-shaped geometries which thin towards, and onlap the fold crest, younging up through growth package W (Fig. 4.11).

An 800 m thick onlapping growth package (Fig. 4.11, growth package V) overlies growth package W. The internal architecture of growth package V depicts a series of wedge-shaped fanning geometries and numerous onlaps, and toplaps moving progressively up-section towards the fold crest. Growth strata onlap the fold limb at the base of package V, and progressively younger syntectonic strata decrease in dip up-section and thin towards the anticline crest. Growth strata at the base of package V dip 12° and shallow to 2° in the upper part of the growth package. The youngest strata overlap and thin onto the anticline crest. Limb-parallel growth geometries are absent within package V. This distinct change in growth architecture coincides with

the cessation of thrust-related growth. Onlapping reflections on the southern limb of the detachment fold are absent. This is likely due to notable erosional activity by deep-water channels and by uplift of thrust imbricates.

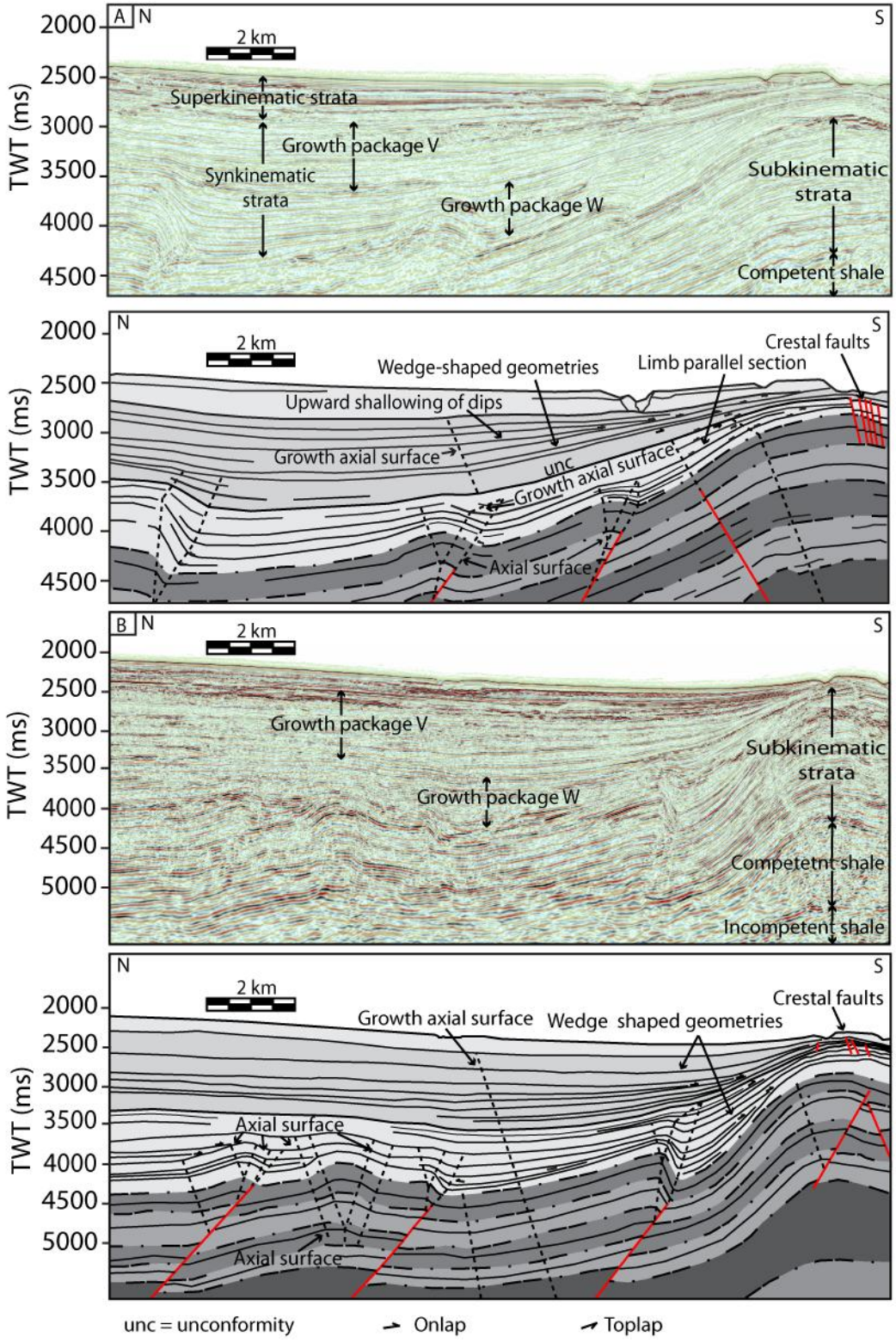

Fig. 4.11. Architecture of growth strata packages flanking the shale cored anticline. The earliest growth package (W) records the coeval uplift associated with thrust-related anticlines and the shale core anticline. Growth package (V) was deposited after thrust uplift had ceased and displays numerous thinning wedge shaped geometries that onlap and overlap the fold crest recording the movement of shale into the fold core. Vertical scale is 2x the horizontal scale.

4.7.4 Interpretation of growth strata

The presence of numerous onlaps onto fold limbs of thrust-related anticlines and the detachment fold within both growth packages (Figs. 4.9 and 4.11, growth packages W and V) indicate that the rate of structural uplift periodically outpaced the rate of sedimentation. Growth package W (Figs. 4.9, 4.10 and 4.11) demonstrates coeval uplift between adjacent thrust imbricates and the shale-cored detachment fold. As the symmetry of the detachment fold changes along strike, so too does the architecture of growth packages flanking the fold limbs. This is represented by thickness variations and varying stratal geometries implying two kinematic mechanisms for fold growth. Within growth package W, flanking symmetric limbs of the detachment fold, limb-parallel reflections with associated growth triangles indicate that detachment fold growth may have included a minor element of hinge migration (self similar fold growth, Suppe, 1983). Wedge-shaped refection geometries within growth package W are a characteristic of limb rotation, where fold limbs progressively rotate, and become steeper during fold amplification (Hardy and Problet, 1994) (Fig. 4.11). Growth package W flanking asymmetric crestal regions of the detachment fold indicate that limb rotation was the only mechanism for fold amplification in the early stages of fold growth, with growth stratal characteristics indicative of hinge migration absent within this synkinematic package (Fig. 4.11B).

Growth package V (Figs. 4.9, 4.10 and 4.11) documents the continued growth of the detachment fold after faulting on adjacent thrusts had ceased. Deformation caused by the uplift of adjacent thrust imbricates had ceased by when growth package V was deposited (Figs. 4.9 and 4.11). A key observation is that a change in kinematic

mechanism of detachment fold growth coincides with the cessation of faulting. Stratal wedging coupled within an upward shallowing of dips within growth package V is consistent along the strike of the fold. This indicates that in the later stages of fold growth (post-faulting stage) the amplification mechanism was solely by limb rotation. Growth package V extends close to the seabed, which suggests that growth of the detachment fold has recently ceased or is still ongoing. It is interpreted that fold growth initiated as a series of thrust-related folds as a product of gravitationally driven extension in proximal regions. Overall fold geometry subsequently became modified into a detachment fold and the Akata shale thickened within the fold core. Detachment fold growth continued as adjacent thrust-related uplift ceased. This change in the kinematic amplification mechanism is not reflected in any of the end-member kinematic models for fault-propagation, fault-bend or detachment folding. Therefore, in the southern Niger Delta, evidence for an episode of unusual phase of late-stage folding is observed. The possible nature of the processes taking place within the basal detachment unit is discussed further below

4.8 Implications

These examples show that deformation within a basal detachment unit occurred, or continued after the main episodes of thrust faulting on adjacent structures had ceased. Detachment occurred at different depths within the Akata Formation, with detachment occurring at a shallower stratigraphic level in the western Niger Delta than in the southern Niger Delta. This implies that the strength of the basal detachment unit fluctuates throughout the delta. Basal detachment unit deformation in the western Niger Delta only involved deformation of the upper Akata Formation (expressed as detachment unit thinning), and the lower Akata Formation did not undergo deformation (Figs. 4.6); however, in the southern Niger Delta, the lower Akata Formation deformed (expressed as detachment unit thickening, Fig. 4.9 and 4.10). The presence of detachments at different stratigraphic levels is interpreted to coincide with overpressure development within the Akata shale, with overpressure generation occurring at a deeper level in the southern Niger delta than the western Niger delta.

A correlation between deformation within a basal detachment unit and the deformational style manifest in an overlying sedimentary overburden has been observed. In the Niger delta, two contrasting deformation styles expressed at the level of the basal detachment unit exist: 1) detachment unit thinning and overburden collapse, coupled with weld development (touchdown) (e.g. section 1.11.3); 2) amplification of a kilometre-scale, late-stage detachment fold. These two examples imply that multiple, and contrasting deformation processes are occurring within a basal detachment unit at a subseismic scale, which leads to either an expression of thickening or thinning. In the western Niger Delta, evolution of the shale weld is likely linked to loading by the overlying fold and thrust belt as deformation within the basal detachment unit is concentrated beneath overlying thrust faults (Fig. 4.6). A possibility is that structural thickening may have caused deformation within the upper Akata Formation by generating overpressure. This differential loading from the weight of structurally thickened areas of the overlying fold and thrust belt has caused the Akata shale to deform. Differential loading is defined as an applied load with a great enough density or thickness to cause the underlying substratum to become overpressured and subsequently deform (Van Rensbergen et al., 1999) and has long been invoked by authors as a causal factor to induce large-scale deformation within shale detachment systems (Bruce, 1973). The redistributed volume of shale is relatively small, so significant thickening of adjacent areas within the Akata Formation is not seen in the survey area or is likely to be seismically notable elsewhere in the basal detachment unit. As accommodation space (tilting of the fold and thrust belt) was generated rapidly, this implies that the deformation mechanism within the basal detachment unit is consistent with previous interpretations of sediment mobilisation (mobile shale). Deformation may have involved liquefaction where the pore-fluid sustains the stresses and the rock volume experiences a complete loss of shear strength and undergoes instantaneous deformation (Maltman, 1994).

4.9 Reinterpretation of mobile shale in the south Niger Delta

In the two examples studied the detail of the seismic resolution within the basal detachment unit is lacking. An important question with respect to the detachment fold is, What deformation processes take place within a detachment unit that can cause the observed thickening? With the improvement of seismic reflection data and reviews on shale tectonics, there has been a change from the traditional view that shale detachment units are mobile and flow, to a view that deformation occurs through brittle failure without complete loss of shear strength on a subseismic scale (e.g. Van Rensbergen and Morley, 2003). Structures typically involving a mobile shale interpretation have been termed ductile in the sense that individual structures that contribute to the overall thickening or thinning cannot be seismically resolved. In the southern Niger Delta in areas adjacent to the detachment fold, no evidence for evacuation (detachment unit thinning) of large volumes of shale from beneath synclinal regions exists; in fact, the thickness of the Akata Formation returns to its regional average thickness in areas adjacent to the detachment fold in both along- and across-strike orientations. In addition, the presence of continuous reflections within the both lower and upper Akata Formations indicates that the Akata shale is not behaving as a mobile mass, but has a coherent, organised structure (Fig. 4.9) and hence is not behaving in a ductile manner.

Geometric-kinematic models of detachment folding incorporate a mechanically weak, mobile unit of salt or shale in which the ductile layer flows into the fold core due to the geometric constraints imposed by fold growth (Jamison, 1987; Dahlstrom, 1990; Epard and Groshong, 1993, 1995; Hardy and Problet, 1994 Homza and Wallace, 1997; Atkinson and Wallace, 2003; Latta and Anastasio, 2007). These models indicate that the mechanically incompetent layer does not undergo layer parallel folding by flexural slip (as do the competent overburden units), but instead deforms internally either ductilely or brittely through folding, faulting, penetrative vertical thickening or combinations of the above (Fig. 4.12). The internal architecture of weak incompetent units that have been imaged within detachment folds have revealed that the incompetent unit often accommodates strain by forming compressional structures in a style analogous to the deformation style exhibited in

overlying, competent units (Noack, 1995; Martinez et al., 1997, Couzens-Schultz et al., 2003; Plesch et al., 2007).

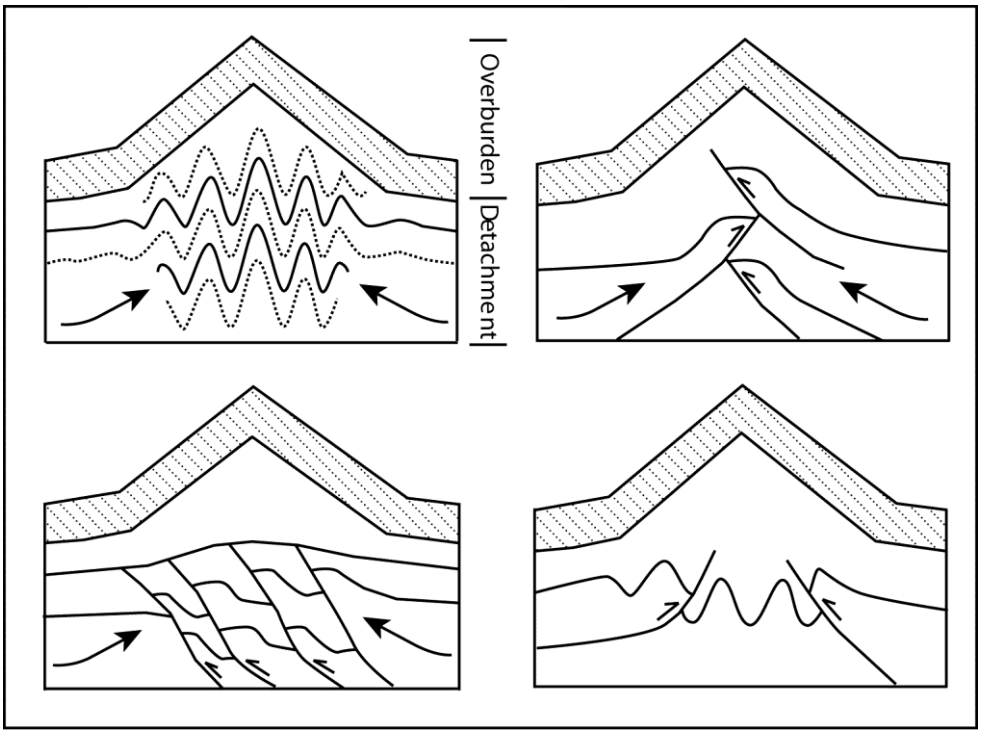

Fig. 4.12. Schematic diagram showing how incompetent units are thought to accommodate strain within detachment fold cores (modified from Epard and Groshong 1995).

Insights into the internal mechanism for detachment unit thickening can be derived from the rate that shale thickened (flowed) into the detachment fold core. Through biostratigraphic correlation, the average sedimentation rate within the survey area is calculated to be about 195 m/m.y. This rate is rapid, in agreement with high sedimentation rates for deltaic environments, but is significantly higher than other cited sedimentation rates from the Niger Delta (Davies, 2003, cited a sedimentation rate of 100 $m/m.y^{-1}$ in the western Niger Delta). The thickness of the adjacent growth package onlapping the detachment fold is 800 m thick. Assuming no hiatial periods and constant sedimentation rate, fold amplification is estimated to have begun approximately 4.1 Ma, in the mid-Pliocene. Through detailed seismic interpretation of key stratigraphic levels and intervals from both the 2D and 3D

seismic data sets covering the southern Niger Delta (Fig. 4.2), the volume of Akata shale can be calculated (see appendix 4, Fig. A10). By mapping the key reflections that define the geometry of the detachment fold the average volume of Akata shale between the basement and the upper-Akata boundary is found to be approximately 415 km^3. This volume was calculated between the synclinal hinges and the immediate adjacent area where it is assumed that the Akata Formation is representative of normal thickness (approximately an area of 1600 km^2). The average volume of the Akata shale increases to approximately 1004 km^3 within the detachment fold core, a volumetric increase in shale of approximately 590 km^3. The rate of thickening can now be calculated and equates to an average flow rate of 144 km^3 per Ma. However, with the imaging of coherent reflectivity within the Akata Formation it is questioned whether it is reasonable for this volume of shale to be deforming and thickening as a ductile flow. This calculated flow rate does fall within the range of projected estimates of shale ejected from mud volcanoes over the same timescale (e.g. Davies et al., 2007 their table 1) (see appendix 4, Table. A1). However, it is cautioned that these estimates are based upon continuous flow rates and in some examples are based upon very short averaged timescales (see appendix 4, Table. A1), and in addition eruptions from mud volcanoes do not occur continuously on a million year time span. Due to the duration of this flow rate and the volume of shale that has moved it is proposed that this flow rate suggests internal structural thickening of the basal detachment unit, rather than as a flow with a plastic behaviour into the anticlinal core.

The authors note that shale tectonic provinces do deform by ductile mechanisms, but the regional scale to which this interpretation has been commonly applied is questioned. In the example of weld formation, approximately 16 km^3 of shale was estimated to have moved. This volume was calculated over an area of about 53 km^2, which defined the weld geometry (e.g. the welded region in Fig. 4.7). This movement was rapid, implying that, in this example, the basal detachment unit did likely deform by a ductile mechanism. Taking into consideration the volume of shale that has moved by calculating ‘flow rates’ can be a useful and important tool

when drawing conclusions into the type of deformation that occurs within basal detachment units.

This work complements recent work on the reinterpretation of mobile shale where vast areas of ductile mobile shales had been previously assigned to seismic reflection data that were characterised by poor reflectivity (Van Rensbergen and Morley, 2003). As the quality of seismic reflection data has improved, regions of what were previously thought to be mobile shale have been imaged as regions of coherent reflectivity. The examples detailed here show that shale does not purely deform by plastic flows, which involve a complete or partial loss of effective stress and shear strength (fluidized flows, grain flows or liquefaction), but involves brittle processes, which may play an important role in accommodating strain within a basal detachment unit. With the improvement of seismic reflection data the type and scale of processes occurring within basal detachment units may need to be re-evaluated to identify whether coherent structures that are mobile, but are undergoing brittle deformation are taking place.

With the traditional interpretation involving detachment folding and ductile mobile shale, shale was simply able to flow into the available space created by fold amplification. The concept of mobile shale originated in the 1960s (Musgrave and Hicks, 1966) and has been cited as a common interpretation where thick sequences of mudrocks exist through to recent times (Morley 2003). If shale is unable to flow, i.e., deforming by brittle failure rather than a plastic flow, it is unable to effectively fill the shape of the void created, strain compatibility problems may occur within the core of detachment folds where the redistribution of relatively incompetent material occurs. Problems may arise as brittle mechanisms of thickening are unable to effectively fill all the space created by fold amplification, which a ductile detachment unit (such as salt) would effectively be able to fill. This problem may be solved by detachment unit thickening occurring completely by brittle deformation at a variety of scales from seismically resolvable kilometre scale through to subseismic structures.

Our preferred method of accommodating strain within the detachment unit by brittle deformation is through second-order thrusting and/or folding (Fig. 4.13). The observation that the basal detachment unit returns to its regional thickness adjacent to the detachment fold supports the idea that structural thickening through the development of a thrusted duplex (e.g. Plesch et al., 2007) or an anticlinal stack (e.g. Noack, 1995), as opposed to a plastic flow, which accommodates regional strain in a manner directly comparable to shortening mechanisms in the overburden (Martinez et al., 1997; Feinstein et al., 1999; Couzens-Schultz et al., 2003). Figure 4.13 displays a shortening mechanism by which the Akata shale in the fold core thickens as an anticlinal stack. These thrust sheets would provide the source of the thickened shale and help explain our observations of coherent reflectivity and lack of thinned regions of Akata shale in adjacent regions. As thrusting as an anticlinal stack within the Akata shale initiates, displacement is progressively accommodated on upper detachment levels as each thrust forms. The total missing displacement is the sum of displacements taken up by all the upper detachment levels and is accommodated within the interior of the detachment fold. This causes the detachment fold to grow upward rapidly with relatively little displacement. Additionally the validity of this model is reinforced by the lack of shortening structures present within the adjacent Akata shale. Displacement has to be accommodated on discrete detachment levels within the fold interior or additional shortening structures would develop. The interpretation that shortening takes places within the detachment unit means that the detachment unit does not act as a passive decollement layer but rather plays an active role in deformation. Note that this interpretation of structural thickening is by no means the only valid one. Thickening may also occur through brittle movement of more coherent blocks combined with more ductile elements that are able to occupy the void fulfilling any strain compatibility problems that may arise through purely brittle mechanisms.

4.10 Implications of basal detachment deformation in shale tectonic provinces

This article has demonstrated that a deforming basal detachment unit can significantly affect the tectonostratigraphic evolution of gravitationally driven fold and thrust belts. Basal detachment units are structurally complex zones that incorporate multiple detachment levels, and detachment occurs at different stratigraphic levels. The types of deformational processes that occur within a basal detachment unit exert a fundamental control on the final geometries of thrust-related and detachment anticlines, which have important implications for fluid migration pathways and hydrocarbon trap formation. Understanding whether brittle or ductile mechanisms are operating within a basal detachment unit has significant implications on trap geometries. This is of fundamental importance to the petroleum industry, especially with regards to the timing of basal detachment unit deformation with respect to shortening mechanisms in the overburden. A separate, post faulting episode of deformation in a basal detachment unit has the potential to create new preferred migration pathways for fluid flow, to either create or destroy traps and can potentially alter pre-existing trapping geometries possibly rendering them ineffective. This also applies to deformation that starts and continues after the faulting episode has ceased. The implications of this paper extend beyond gravitationally driven deep-water fold and thrust belts but rather to all thrust belts that are classified in a shale tectonic provenance involving previous records of ductile deformation styles.

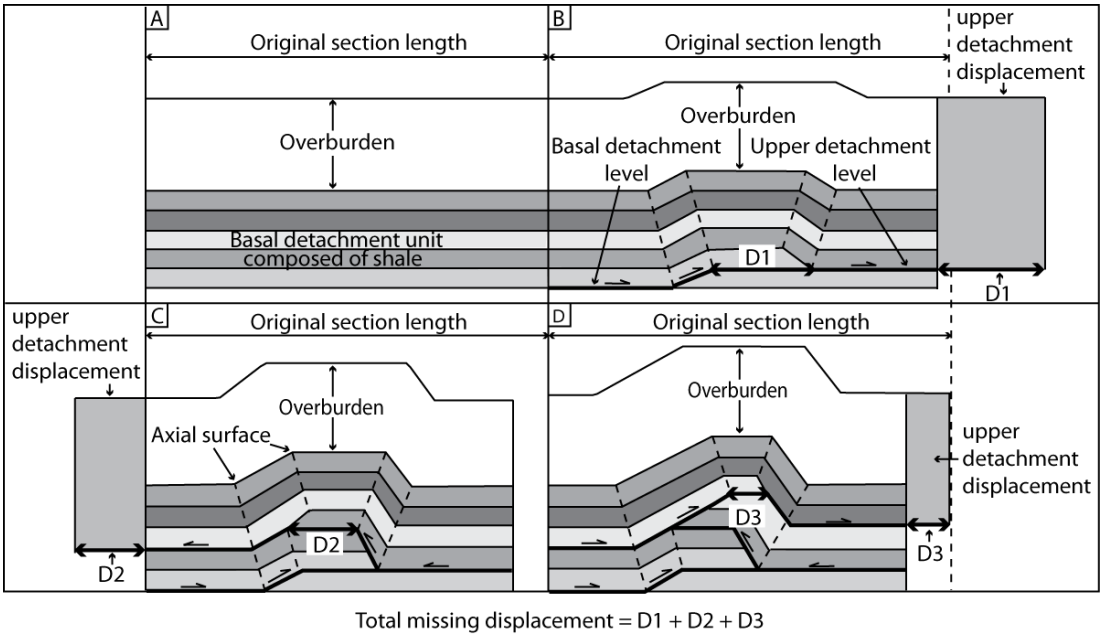

Fig. 4.13. Model showing how thickening of the incompetent unit may occur within the detachment fold core. Thickening in the detachment unit occurs via a series of stacked imbricates thrusts causing fold amplification within the overburden.

4.11 Summary and conclusions

Through the interpretation of growth and stratal packages in gravitationally-driven fold and thrust belts, deformation that is driven by lateral redistributions of strata in the basal detachment unit can be identified. Interpretation of growth and stratal packages can differentiate between deformation caused by shortening mechanisms in the overburden and deformation driven by separate post-faulting phases within a basal detachment unit. A discrete folding mechanism continued after the earlier, classical mechanism of fault bend faulting and fault propagation faulting, where folding was driven by changes in the thickness of the basal detachment unit. It is proposed that thickness variations within the basal detachment unit are not the result of the lateral movement of a ductile mass of shale (mobile shale), but instead are caused by structural thickening through brittle mechanisms within the basal detachment unit. In contrast, formation of a shale weld occurred rapidly as a product of deformation in the underlying basal detachment unit indicating that ductile deformational processes do also occur. Calculated volumes of shale used in

conjunction with rates and duration of shale movement indicate that basal detachment units cannot deform purely by ductile mechanisms alone. A reinterpretation of shale tectonic provinces is necessary to assess the regional importance and extent at which both these mechanisms occur.

5 Imbricate thrusts and duplexes within detachment fold cores in the Niger Delta

5.1 Abstract

High-resolution 3D seismic data is used to reveal the structural style within the cores of kilometre-scale detachment folds in the deep-water Niger Delta. Existing models for detachment folds propose that fold cores consist of a mechanically weak (detachment) succession that is significantly thickened relative to equivalent strata outside the extent of the fold. Here, it is shown that thickening within the detachment succession occurs via a series of imbricated thrust faults, which form duplexes and stacked imbricates within the cores of detachment folds. On a first-order scale the detachment succession is mechanically weak in comparison to overlying sediments. However, internally the detachment succession can be separated into relatively competent and incompetent layers and zones, which together determine and characterise the deformation style. The detachment succession is best represented as an anisotropic multilayer. Individual beds exhibit a combination of brittle and ductile deformation styles that are likely related to the rheology and shear strength of individual beds, which are probably caused by subtle changes in lithological makeup. Shortening estimates within fold cores display modest amounts of shortening (6% to 8%) whereas only 4% of shortening is accommodated in the overlying overburden, giving rise to a shortening differential across a folded profile. The recognition of imbricate duplexes and thrust stacks within fold cores shows the level of detail that can be missing from current detachment fold models when applied to shale tectonic settings. Furthermore, the presence of imbricate thrusts in a relatively mechanically weak succession offers an alternative explanation for regional structural restorations, where estimates of extension and contraction do not balance, rather than needing to invoke layer parallel strain or out of plane (re)mobilisation of sediments.

Note the data used in this chapter was acquired in the final year of the Ph.D. two years after the research detailed in chapter 4 had been completed.

5.2 Introduction

Detachment folds are a common deformational mechanism in thin-skinned fold and thrust belts and form at the tips of propagating bedding parallel thrust faults (Jamison, 1987; Problet and McClay, 1996; Atkinson and Wallace, 2003) (Fig. 5.1). Displacement is transferred from a propagating thrust tip into an overlying mechanically weak detachment layer, which accommodates most of the shortening during folding, and induces buckling within an overriding mechanically competent layer (Jamison, 1987; Homza and Wallace, 1997; Mitra, 2003). A geometric requirement of detachment folds is that buckling occurs within competent strata (e.g. sandstone or limestone), which overlies a mechanically weak incompetent strata (composed of salt or overpressured, fine-grained argillaceous sediments). The kinematics of competent (mechanically strong) fold limbs is well understood. Previous studies have demonstrated that competent strata within detachment fold limbs can amplify by the following mechanisms: 1) hinge migration; 2) limb rotation; 3) combinations of both (Hardy and Problet, 1994; Epard and Groshong, 1995; Homza and Wallace, 1995; Problet and McClay, 1996; Mitra, 2003) (section1.12.4).

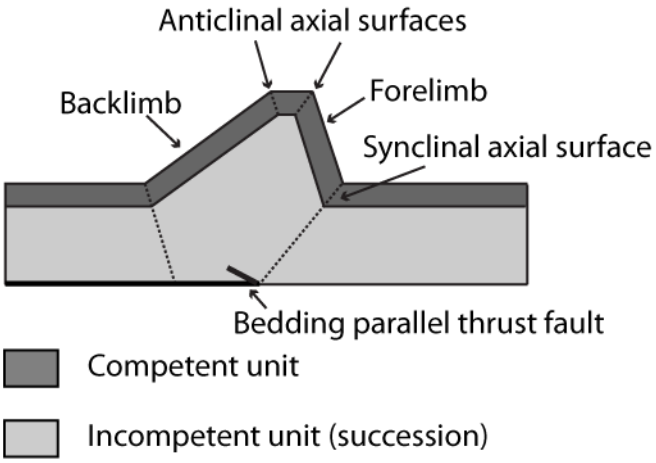

Fig. 5.1. Model of a detachment fold. The upper unit is composed of mechanically competent strata whilst the underlying unit, which thickens in the fold core, is composed of mechanically weak strata.

A basal detachment succession, defined as a regionally extensive shear zone of finite thickness that underlies deep-water fold and thrust belts, commonly constitute the incompetent succession (e.g. Fig. 5.1). Basal detachment successions strongly influence the overlying structural style of overthrust terranes (Davis and Engelder, 1985; Cotton and Koyi, 2000; Costa and Vendeville, 2002; Maloney et al., 2010), and have been separated into frictional and viscous end-members (Cotton and Koyi, 2000; Bahroudi, 2003; Bonini, 2007). When both frictional and ductile basal detachment successions operate within a tectonic setting (e.g. brittle-ductile wedges) the resulting deformation style can be highly complex with structural style, vergence and progradation rates of overlying sediments all affected by the composition and nature of the basal detachment succession (Bahroudi and Koy, 2003; Bonini, 2007). During detachment fold amplification deformation within the fold core is considered to be characterised by a ductile thickening that is synchronous with the folding of the overlying competent fold limbs. Basal detachment successions composed of salt, which has a shear strength approaching zero (Jackson and Vendeville, 1994), behave in a ductile manner and are able to flow into the fold core to accommodate fold amplification. A basal detachment succession composed of argillaceous, fine-grained sediments, however, is unlikely to be mechanically and therefore rheologically homogeneous, as for example in the Niger Delta the basal detachment succession is composed of clays, silts, sands and carbonate interbeds (Avbovbo, 1978; Cohen and McClay, 1996). This can lead to a variable deformation style with coarser-grained (harder) lithologies preferring to fracture rather than deform in a ductile manner (Maltman, 1994).

Field studies of detachment folds, for example, indicate that a variety of complex deformational styles occur at multiple scales within the basal detachment successions, especially within the hinge regions where they are intensely deformed, characterised by zones of high strain (e.g. Homaza and Wallace, 1997; Mitra, 2003). Although mechanical anisotropies within a layered succession are known to have a dominant influence on strain (e.g. Curie et al., 1962; Butler and McCaffrey, 2004; Latta and Anastasio, 2007; Iacopini and Butler, 2011) this is rarely applied to basal detachment successions composed of argillaceous sediments. This is likely due to the development of overpressure in such successions that has lead to a common

interpretation that deformation occurs in some form of ductile flow (e.g. "mobile shale"). However, the magnitude of overpressure needs to be approaching lithostatic pressure to induce a complete loss of strength and liquefaction of sediments (Maltman and Bolton, 2003). In addition, the magnitude of overpressure will likely vary vertically and laterally throughout the basal detachment succession implying that the strength of sediments will also fluctuate. Differing mechanical properties within a multilayered interval can result in a variety of deformational responses as a function of the pre-shortening rheology and shear strength of individual beds (e.g. Curie et al., 1962; Fisher and Jackson, 1999; Butler and McCaffrey, 2004; Bonini, 2007; Latta and Anastasio, 2007). Some studies have concentrated on the mesoscopic and macroscopic structures that form within the mechanically competent unit during deformation (e.g. Homza and Wallace, 1997; Hayes and Hanks, 2008), but aside from modelling studies (e.g. Cotton and Koyi, 2000; Costa and Vendeville, 2002; Bahroudi and Koy, 2003; Bonini, 2007) few studies have been directed at deformation focussed within the underlying incompetent unit.

Within regions undergoing thin-skinned shale tectonics a thick succession of overpressured, argillaceous sediments constitutes the basal detachment succession (the incompetent unit) (e.g. Fig. 5.1). The term "mobile shale" is commonly adopted for this succession in the literature (Morley and Guerin, 1996; Morley, 2003), but the term has recently been challenged as it implies processes that involve a complete loss of shear strength, which may portray unrealistic representations regarding the types and styles of deformation that occurs within this succession (e.g. Deville et al., 2010; Maloney et al., 2010). In addition, improved seismic imaging is revealing highly organised coherent structures within what was previously thought to be a ductile mass casting doubt on the widespread occurrence of "mobile shale" (Van Resenbergen and Morley, 2003; Deville et al., 2010). Here we use high-quality 3D seismic reflection data that provide some of the first imaging within the cores of 10 km wavelength-scale detachment folds. This has allowed an analysis of the structural style within a mechanically weak basal detachment succession, and for deformational mechanisms within the type of seismic facies that is commonly labelled "mobile shale" to be revealed.

5.3 Geological setting

The Niger Delta is located in the Gulf of Guinea at the southern end of the Benue Trough, which formed during the opening of the Equatorial Atlantic in the Late Jurassic-Cretaceous with the breakup of African and South American plates (Lehner and De Ruiter, 1977; Doust and Omatsola, 1990). Deltaic progradation began over the African passive margin in the Eocene with the onset of wave dominated sedimentation and deposition of paralic siliciclastics (Burke, 1972). The regressive Tertiary stratigraphy of the Niger Delta is represented by diachronous clastic successions of the Akata, Agbada and Benin Formations (Short and Stäuble, 1967) (section 2.2). The Akata Formation is the basal unit of the delta and is mostly composed of fine-grained, pro-delta marine shales with interbedded silts, sands and carbonates (Cohen and McClay, 1996). The Akata Formation ranges from 7 km thick in shelfal regions down to 2 km thick in deep-water settings (Doust and Omatsola, 1990) and is the succession that is overpressured and referred to as the mobile shale (Cohen and McClay, 1996; Morely, 2003; Bilotti and Shaw, 2005). Major detachment faults are present at multiple depths within the Akata Formation, which decouple predominantly brittle from ductile deformation or undeformation (passive) strata (Corredor et al., 2005; Briggs et al., 2006). The Agbada Formation is up to 5 km thick and is composed of altnerating successions of sands and shales deposited by turbidites, debris flows and hemipelagic sedimentation. The Agbada Formation is deformed by large-scale listric faults in up-dip extensional settings and fault-related folds in down-dip contractional settings with a relatively undeformed translational domain in-between (Fig. 5.2B).

5.4 Seismic data and interpretative methods

The 3D seismic survey is situated on the north-western margin of the Niger Delta and covers an area of 1878 km^2 (Fig. 5.2). The survey area is a pre-stack, time-migrated volume with a line spacing of 12.5 m in crossline and 18.75 m in inline directions. The vertical resolution is 12 m (frequency 42 Hz), a quarter of the dominant wavelength in the initial 0.5 s TWT below the seabed, which deteriorates to approximately 17 m (frequency 28 Hz) at the level that structural detachment

occurs. The data are zero phase migrated and an increase in acoustic impedance is characterised by a black-red-black reflection combination. The data have a vertical scale in seconds (s) two-way travel time (TWT).

The 3D seismic volume images high angle vertical discontinuities in seismic profiles across which seismic reflections are vertically and horizontally offset; an indicator for the presence of fault planes. Root mean square (RMS) amplitudes (see Brown, 2004) were extracted from interpreted horizons and from TWT windows used either side of key reflections. RMS amplitude maps were used in conjunction with seismic mapping to identify faults and structural features throughout the survey area. Selected seismic TWT profiles were depth converted to determine geometric data for the structural features analysed within the survey area.

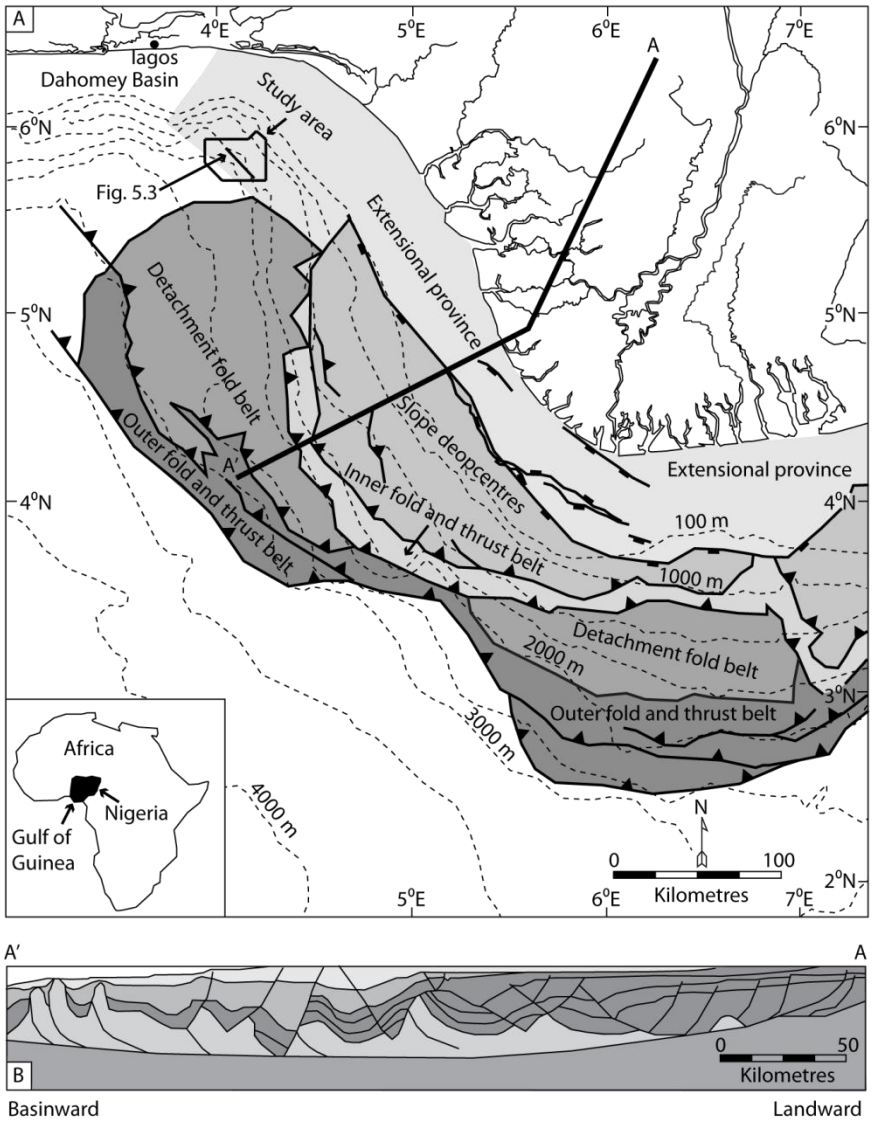

Fig. 5.2. A) Geological setting of the Niger Delta showing the gravitational deformation style and the location of the 3D survey area. B) Cross-section through the deformational domains showing extension in proximal settings and translation al domain of shale cored anticlines and thrust-related folding in the deltaic toe.

5.5 Seismic stratigraphy and structural styles

The Agbada and Akata Formations can be subdivided into four seismic packages on the basis of different seismic facies, structural and stratigraphic styles (Fig. 5.3). The shallowest seismic package (the initial 0.5 s [TWT] imaged beneath the seabed) is dominated by a series of semi-continuous, sub parallel reflections with high seismic amplitudes (seismic package 1, Fig. 5.3). The continuity of seismic reflections is punctuated by numerous sinuous erosional incisions that are occasionally flanked by

wedge shaped geometries, which thin and taper away from the central incision. These erosional features, on occasion, stack vertically and are interpreted to be deep-water channel complexes and the adjacent tapering wedge shaped geometries channel levees (Deptuck et al., 2003). This shallowest seismic facies identifies part of a large kilometre-scale deep-water channel complex in the survey area. Beneath the deep-water channel facies lays the second seismic package, which is identified by a change in seismic facies and structural style (Fig. 5.3, seismic package 2). Reflections within seismic package 2 are laterally continuous and have lower seismic amplitudes. Some reflections have been incorporated into the limbs of large-scale folds, and reflections that represent strata deposited on the limbs of these large-scale folds display changes in thickness, often displaying wedge shaped geometries. Strata within seismic package 2 (Fig. 5.3) and strata within the lowermost part of overlying channel facies onlap and overlap fold limbs.

The presence of onlap and overstep unconformities, together with the thickness changes within strata flanking fold limbs identifies these strata as synkinematic strata; hence they were deposited coevally with fold amplification. The presence of onlaps indicates that structural uplift periodically outpaced the rate of sedimentation. The architecture of synkinematic strata have largely been reworked and removed due to erosion by deep-water channels. In places strata display wedge shaped, fanning geometries and an upward shallowing of dips, which may suggest that fold growth involved a component of limb rotation (Hardy and Problet, 1994; Suppe et al., 2004). Kilometre-scale folds have amplitudes that range between 4 km to 6 km, wavelengths in the range of 3 km to 9 km and strike for tens of kilometres. In addition, the lateral continuity of reflections is punctuated by high angle vertical discontinuities, which indicate the presence of faults. Reflections are offset in both a normal and reverse sense indicative of both thrust and normal faults. The base of this seismic package is defined by a positive acoustic impedance reflection combination with a high seismic amplitude (marked reflection A in Fig. 5.3). A high-resolution RMS amplitude map (Fig. 5.4A) coupled with a TWT map of reflection A with the structural interpretation overlain (Fig. 5.4B) highlights the dominant structural trends through the survey area. Dark and light shaded discontinuities on the RMS amplitude map (Fig. 5.4A) indicate the strike of faults

and folds. Two main structural trends are identified: 1) fault related folds that trend approximately north-east-south-west; 2) north-west-south-east trending normal faults.

Deformation in the south-eastern section of the survey area is largely characterised by a large north-east-south-west trending fault trace (Figs. 5.3 and 5.4). In seismic cross-section (Fig. 5.3) this fault is represented as a vertical, discontinuous narrow zone of low reflectivity (Fig. 5.3). Adjacent reflections appear to be displaced vertically and "curve upwards" across and into this vertical zone of low reflectivity. In plan view north-south trending folds curve into and terminate against this north-east-south-west trending fault, as do east striking normal faults (Fig. 5.4). This large-scale structure is a prominent strike-slip fault, which serves to compartmentalise the north-western margin of the Niger Delta (e.g. Morgan, 2001, 2003). Studies have indicated that this fault is a dextral strike-slip fault that has accommodated up to 6 km of slip (Leduc et al., in review).

Fig 5.3. A) Uninterpretated seismic line and B) detailed line drawing showing the interpreted structural styles within the area. Four main seismic packages are identified. An upper package composed of high seismic amplitude channel deposits, which is underlain by strata that form the incompetent succession within the cores detachment folds (e.g. Fig. 1). Seismic package 3 displays significant thickness changes and thrust-related folds within the detachment fold cores. Large black arrows within the key represent major detachment levels and grey arrows represent minor detachment levels. Vertical scale is approximately 2.5x the horizontal scale.

.

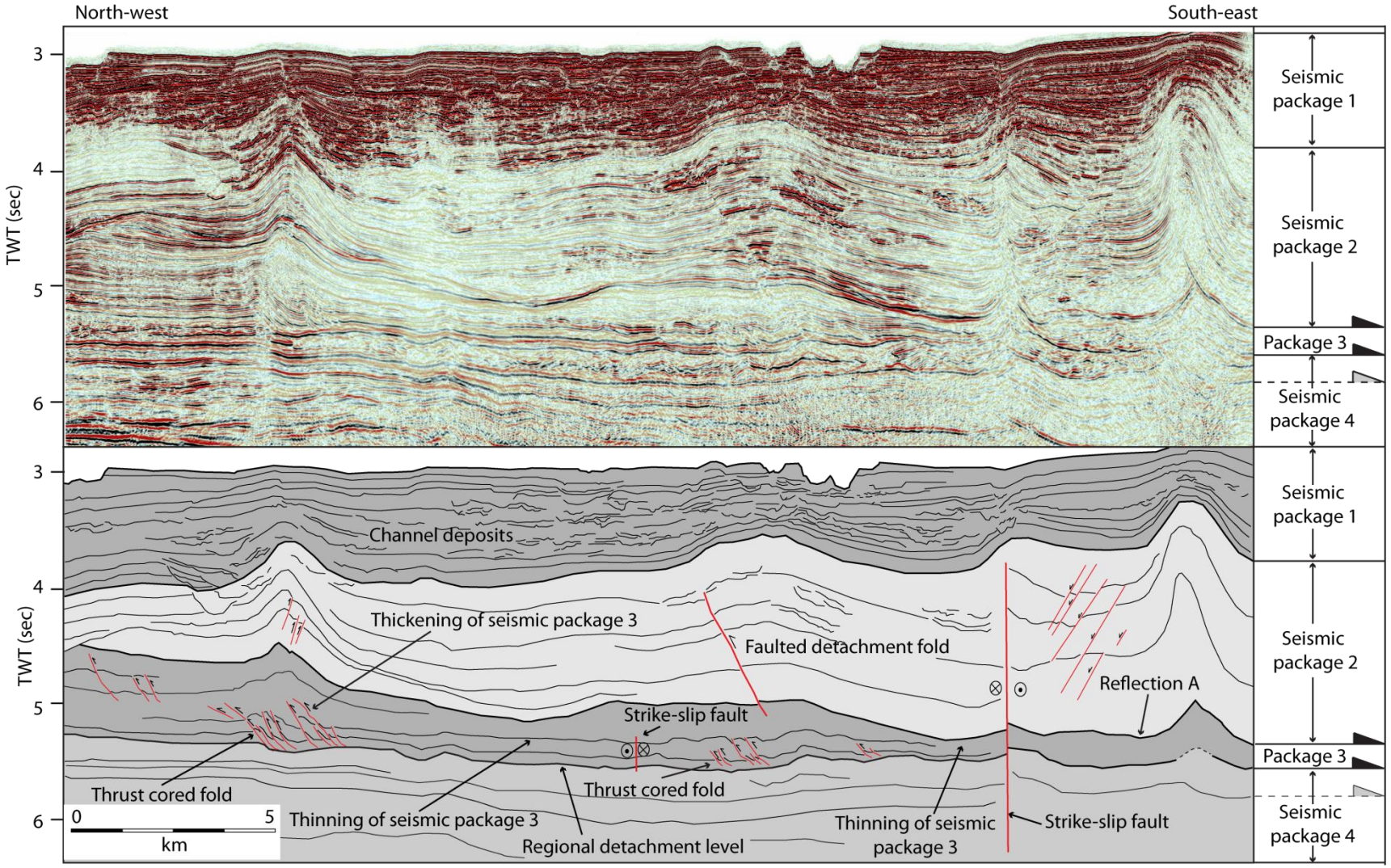
North-west
South-east
TWT (sec)
3
4
5
6
Seismic package 1
Seismic package 2
Package 3
Seismic package 4
Channel deposits
Thickening of seismic package 3
Faulted detachment fold
Reflection A
Strike-slip fault
Thrust cored fold
Thrust cored fold
Thinning of seismic package 3
Regional detachment level
Thinning of seismic package 3
Strike-slip fault
0
5
km

1

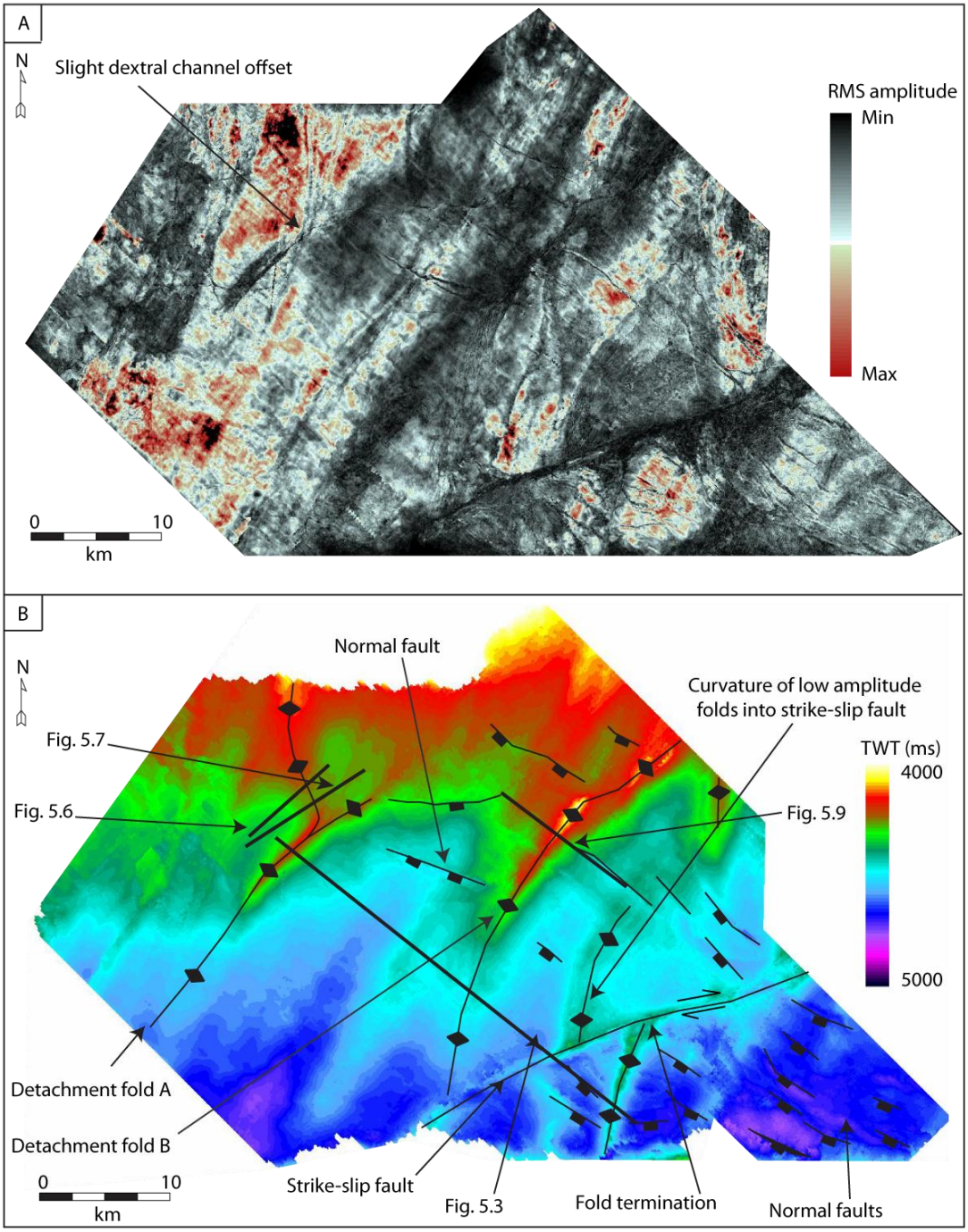

Fig. 5.4. A) RMS amplitude map of a 20 ms window extracted from the top of reflection A, and B) a TWT map with the structural interpretation overlain. The amplitude map highlights three dominant structural trends within the survey area: south-east striking normal faults, predominantly north-east-south-west trending compressional folds and a north-east-south-west trending strike-slip fault.

On the basis of seismic facies the folded stratigraphy can be separated into two major seismic facies. Well imaged, laterally continuous reflections (seismic package 2, Fig. 5.3) are underlain by a seismic interval that contains zones of seismic transparency and cores the overlying folds (seismic package 3, Fig. 5.3). Seismic package 3 displays significant lateral changes in vertical thickness, thickening up to 1.5 s (TWT) within the interior of fold anticlines and thinning to a minimum of 0.2 s (TWT) in synclinal regions and areas adjacent to the folds (Fig. 5.5). Downward bulges in the apparent geometry of reflections occur in places beneath kilometre-scale folds. This is interpreted as seismic pushdown (a seismic artefact caused by overlying low velocity sediment) (see Brown, 2004) and can be seen in some areas directly beneath large-scale fault related folds. This has the affect of causing a distortion in the apparent geometry of underlying seismic reflections. Based upon this observation this interval is interpreted to contain, in places, overpressured sediments, which have low seismic velocities (Morgan, 2003). This change in seismic facies and associated lithological contrast is a characteristic feature of detachment folds (e.g. Fig. 5.1). The well imaged reflections incorporated into fold limbs are associated with the competent unit and the underlying interval that thickens and thins is associated with the incompetent unit, which is from herein referred to as the incompetent succession with respect to the overlying detachment folds (e.g. Fig. 5.1). An isochron map of the incompetent succession records differences in the vertical thickness in TWT across the survey area (Fig. 5.5). In particular, how the degree of thickening and/or thinning within the incompetent succession is related to structural style. Places where the incompetent succession is at its thickest are beneath the anticlinal hinges of major detachment folds. The vertical TWT thickness of the incompetent succession beneath the keels of normal faults (represented by north-west-south-east trending discontinuities on the isochron map) is close to zero. This implies that significant volumes of sediment have withdrawn from beneath these normal faults possibly as a consequence of sediment loading by the prograding deltaic overburden as is advocated in many thin-skinned gravitationally-driven detachment systems (e.g. Morley, 2003, 2009; Rown et al., 2004;). The nature of reflections imaged within the incompetent succession is discussed in detail in the following sections (sections 5.5.1 and 5.5.2).

Differences in structural style are also highlighted by variability in fold tightness (Fig. 5.3). Tight folds are related to strike-slip deformation and longer wavelength folds to fault-related folding. The majority of normal and thrust faults within the survey area sole to a high-amplitude reflection situated at approximately 5.1 s (TWT) (Figs. 5.3 and 5.4). The major strike-slip fault is a notable exception, which appears to offset deep-seated basement reflections (see appendix 5, Fig. A11). This high-amplitude reflection is a major detachment level and decouples overlying deformed strata from predominately undeformed, underlying strata. The basal seismic package constitutes stratal reflections beneath the regional detachment level (seismic package 4, Fig. 5.3). Some reflections still display breaks in lateral continuity and are regularly offset by small-scale thrust faults that also detach on a high-amplitude reflection (Fig. 5.3) (see appendix 5, Fig. A12). Deeper reflections are generally sub parallel, display changes in vertical thickness and local onlap relationships (see appendix 5, Fig. A13). This basal seismic package is tentatively interpreted as the interval that is predominately occupied by the Akata Formation. It is the basal detachment succession, serving to decouple brittle deformation styles involved in thin-skinned gravitational tectonics and overlies the acoustic basement (Briggs et al., 2006) (appendix 2, Fig. A1F).

5.5.1 Internal architecture of detachment fold A

Within the core of detachment fold A stratal reflections are offset, in a reverse sense, by closely spaced high-angle discontinuities (Figs. 5.3, 5.6 and 5.7). These are interpreted as thrust faults that predominantly verge towards the south-west in the north-western section of the survey area, otherwise thrust faults display an approximate north-westward vergence. Fault-related folds above and adjacent to fault planes are characterised by short, steeply dipping forelimbs and longer more shallowly dipping backlimbs. Reflections incorporated into fold backlimbs dip substantially less than underlying fault planes; however, some backlimbs display fault plane parallel profiles. All thrust faults within the detachment fold core sole to a high seismic amplitude reflection, which has been earlier been identified as the regional detachment level (e.g. Fig. 5.3). The steepest forelimbs are typically underlain by the upper tip points of fault planes that terminate at the front of forelimbs or the steepest segments of fault planes. However, steep forelimb folds are

also situated adjacent to the centre of fault planes (Figs. 5.6 and 5.7). Shallower dipping forelimbs sole to an upper bedding parallel detachment where the fault plane has formed a through-going structure forming a flat-ramp-flat geometry, and such faults are interpreted as fault-bend folds (Suppe, 1983). The majority of upper tip points, of fault planes, sole to or terminate within the reflection interval that marks the top of the incompetent succession, underlying reflection A (Fig. 5.3). Fault tip points also terminate internally within the incompetent succession (Figs. 5.6 and 5.7). Fault planes are, typically, not planar, but display subtle changes in dip across some reflections. This is likely to represent fault plane refraction with the change in fault dip induced by changes in the mechanical properties of the strata through which the fault plane is propagating (Schöpfer et al., 2006).

Axial surfaces mark changes in fold limb dip (where strata rotate as they are incorporated into fold limbs during a widening of axial surfaces during fold amplification) (Suppe et al., 1992), which form contemporaneously with the onset of fold amplification (Suppe, 1983, 1992) (marked by dashed lines on Figs. 5.6C and 5.7C). Axial surfaces highlight the multiple dip domain segments present on both fold forelimbs and backlimbs. The synclinal axial surfaces on thrust-related backlimbs have both planar and non planar geometries in order to intersect the base of underlying fault ramps. The general absence of any fault plane parallel segments, on fold backlimbs, implies that shear has been an important process during their amplification (e.g. Suppe et al., 2004). As no synkniematic strata are present (or can be seismically resolved) neither the exact amplification kinematics nor the sequence of thrusting can be determined. However, the majority of thrust faults are interpreted as shear fault-bend folds due to their relatively long, shallowly dipping backlimbs that dip at a shallower angle to an underlying fault plane, (Suppe et al., 2004; Corredor et al., 2005; Morley, 2009), and for them to have formed in an intra-formational setting, i.e. fault tips did not reach the paleo-seabed. Shear fault-bend folds can be separated into simple-shear and pure-shear variations (Suppe et al., 2004; Morley, 2009). Where the synclinal axial surface forms a planar surface and intersects the base of the fault ramp and the backlimb dips shallower than the to the underlying fault ramp, thrust faults are interpreted to be simple shear fault-bend folds (Suppe et al., 2004). Simple-shear fault-bend folds do not require slip upon a basal

detachment fault, rather the incompetent succession at the base of the fault ramp undergoes an externally imposed layer-parallel simple shear (Suppe et al., 2004; Corredor et al., 2005). Where synclinal axial surfaces do not do not linearly bisect the base of the fault ramp an element of thickening at the base of the fault planes is implied, identifying this type of thrust-related fold as a pure-shear fault-bend fold (Suppe et al., 2004). Pure-shear fault-bend folds require some slip to occur along a basal bedding-parallel detachment fault and the weak incompetent succession (incompetent succession) shortens and thickens up the base of the fault ramp (Suppe et al., 2004; Corredor et al., 2005; Morley, 2009).

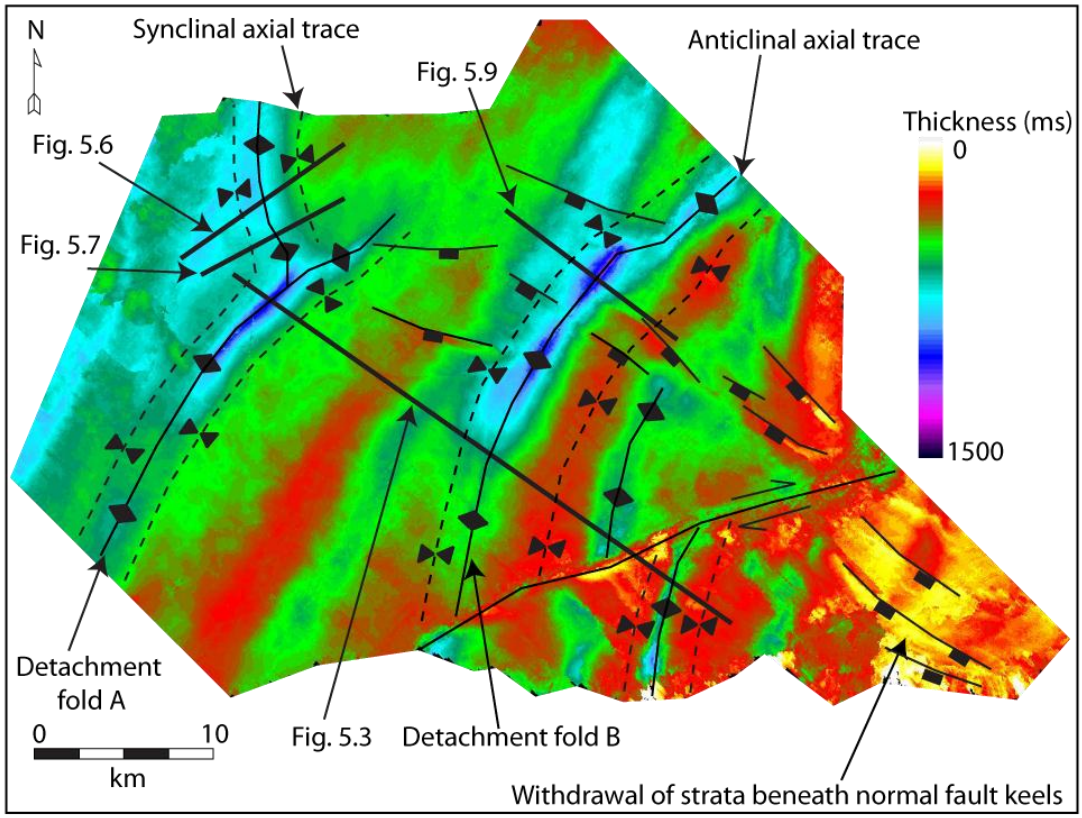

Fig. 5.5. Isochron map between reflection A and the regional detachment level (the base of seismic package 3 on Fig. 5.3) with the structural interpretation overlain. The seismic package is at its thickest beneath the anticlinal hinges of large-scale detachment folds and is relatively thin in adjacent synclinal regions. Withdrawal of strata beneath the keels of normal faults has led to complete removal of strata and juxtaposition of strata.

An RMS amplitude map of a 30 millisecond (ms) window extending above the regional detachment level (Fig. 5.8A) together with a structural TWT map of the regional detachment level (Fig. 5.8B) highlights the strike of thrust faults within the detachment fold core. Thrust faults strike in parallel with the overlying fold crest in the sedimentary overburden (*cf*. Figs. 5.4 and 5.8). The cross-sectional height of thrust faults increases, or decreases, with a corresponding change in the first-order amplitude of the overall detachment fold (*cf*. Figs. 5.4, 5.5 and 5.8). The left-hand bend in the trend of detachment fold A in the north-western part of the survey area represents an accommodation zone. An oblique liniment of north-south trending thrust faults links with north-west-south-east trending thrust-related folds within the core of detachment fold A.

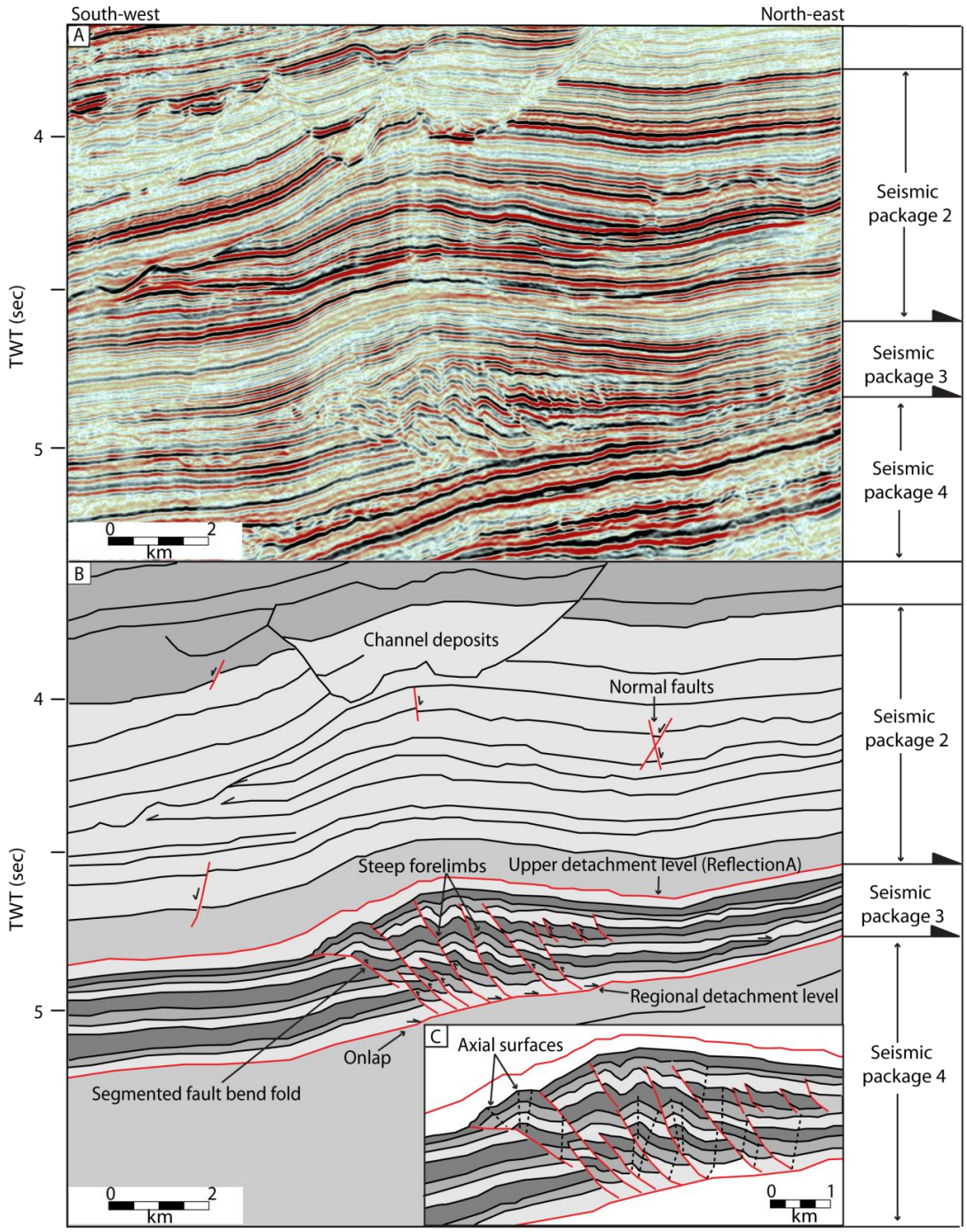

Fig. 5.6. A) Uninterpreted seismic line B) detailed line drawing showing the presence of closely spaced south-west verging thrust faults within the core of detachment fold A. C) Zoomed in detail of the thrust faults in B) showing the position of axial surfaces together with fold and fault geometries. Vertical scale is approximately 3x the horizontal scale.

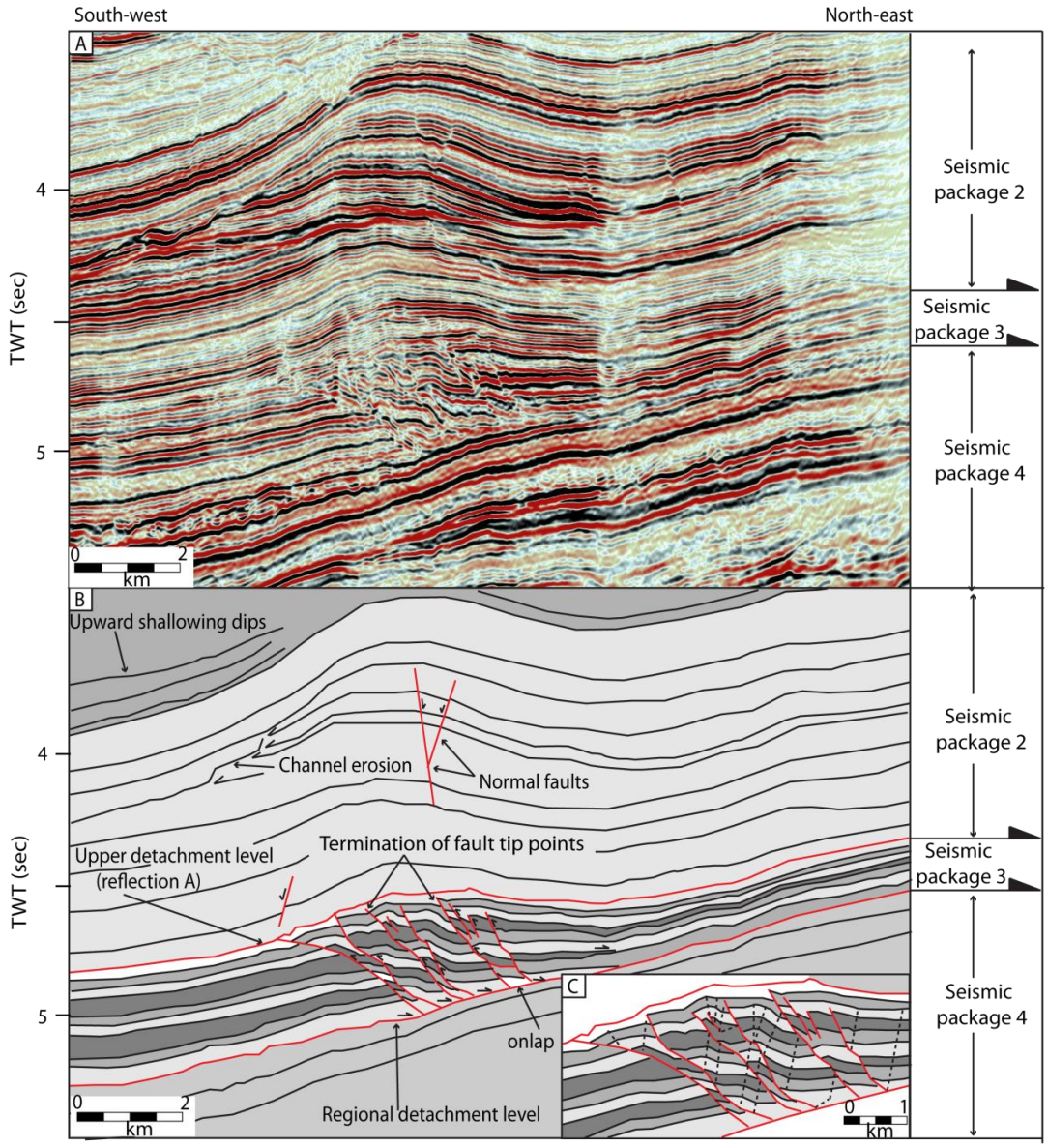

Fig. 5.7. A) Uninterpreted seismic line and, B) line drawing showing the presence of closely spaced south-west verging thrust faults within the core of detachment fold A. C) Zoomed in detail of the thrust faults in B) showing the position of fold and fault geometries with axial surfaces. Vertical scale is approximately 3x the horizontal scale.

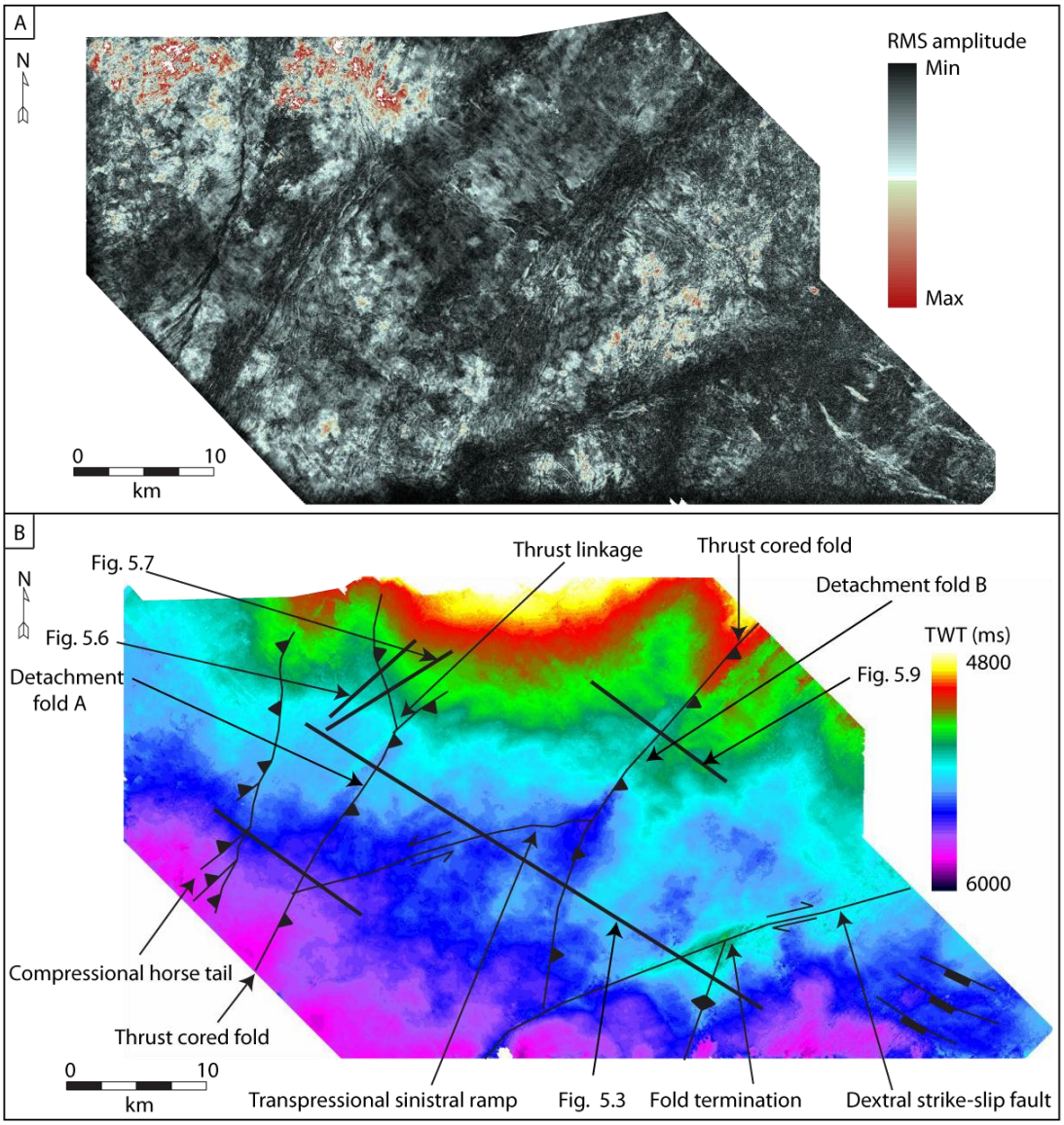

Fig. 5.8. A) RMS amplitude map extracted from the regional detachment level and B) a structural TWT map showing the structural interpretation. A series of closely spaced westward verging thrust faults trend in parallel with the anticlinal hinges of the overlying detachment folds. Compressional thrust-related folds and strike-slip features are evident.

5.5.2 Internal architecture of detachment fold B

The structural style within the core of detachment fold B is similar to the style described within the core of detachment fold A. Reflection offsets, in a reverse sense, and the presence of high-angle discontinuities again indicate the presence of thrust faults (Fig. 5.9). Dark shaded discontinuities on the RMS amplitude map, of a 30 ms window above the regional detachment level (Fig. 5.8A), show that thrust

faults strike in parallel with the strike of the overlying first-order geometry of the overall detachment fold (*cf*. Figs. 5.4 and 5.8). Generally, the upper tip points of fault planes are immediately overlain by steeply dipping forelimbs (Fig. 5.9). Backlimbs are short and either dip parallel to their underlying fault planes, or have significantly shallower dips than underlying fault planes. Numerous dip domain segments are seen on fold backlimbs. Where backlimbs are aligned parallel to underlying fault planes the synclinal axial surfaces is able to bisect the base of fault plane with a planar geometry. Shallowly dipping backlimbs are characterised by planar and non-planar synclinal axial surfaces in order for them to bisect the base of the fault ramp. No synkinematic strata are present, or are seismically resolvable, flanking the limbs of the fault-related folds. Fault-propagation, fault-bend, and pure and simple shear fault-bend folds are interpreted to have collectively formed the architecture of the detachment fold core. Similarly, fault planes also display multiple subtle changes in dip across individual reflections, which again is likely to be indicative of fault plane refraction. In contrast to the previous example (detachment fold A), reflections within the upper parts of the detachment fold core are not resolved on the seismic data. The upper tip points of fault planes are not clearly resolved; consequently it is not clear where the upper tip points of fault planes terminate within the detachment fold core. The upper tip points of the majority of fault planes appear to terminate within the uppermost reflection interval within the incompetent succession (Fig. 5.9). Reflections within the interior of detachment fold B display numerous variations in vertical and lateral thickness, including reflections that have been faulted. The incompetent succession thins significantly towards the synclinal hinges and is at its thickest within the anticlinal hinge region with respect to the geometry of the detachment fold (Figs. 5.3, 5.5 and 5.9).

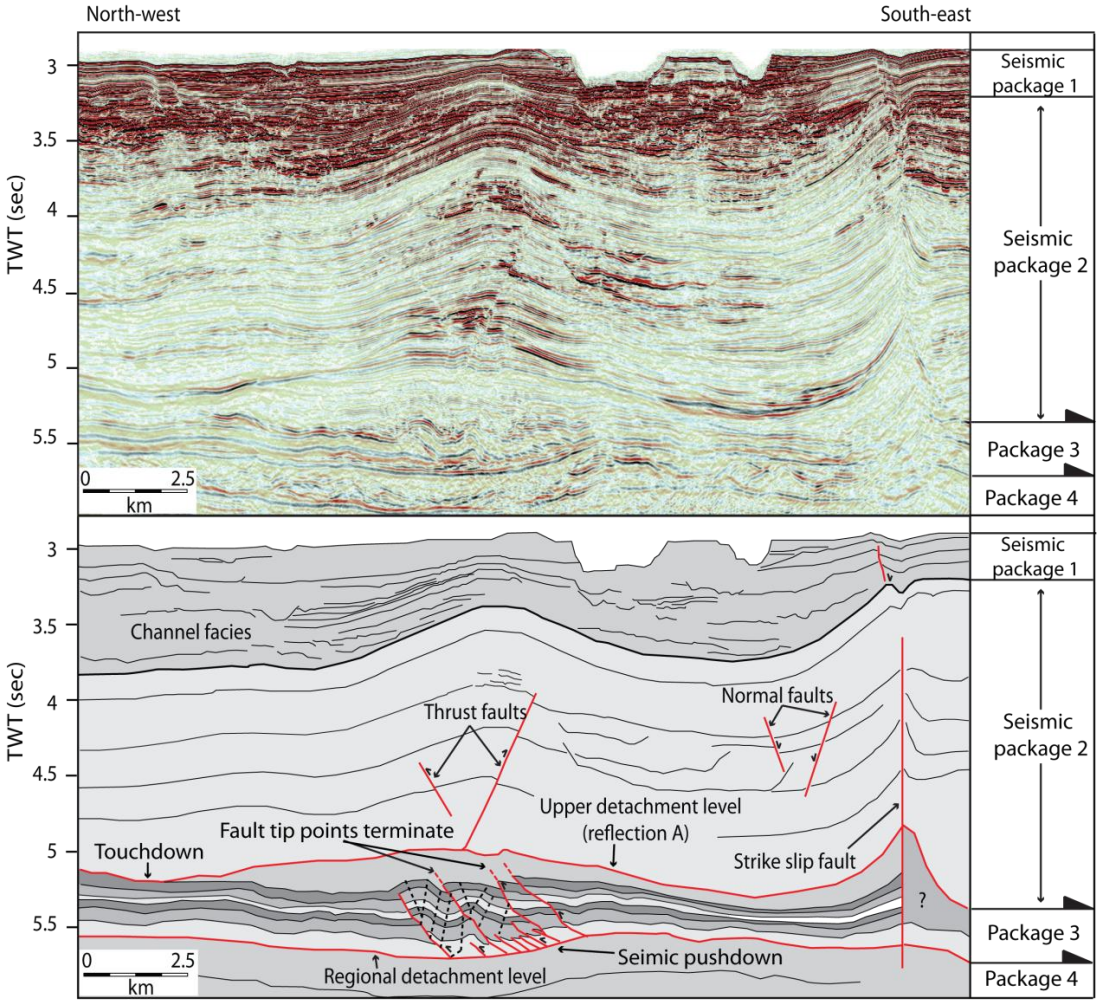

Fig. 5.9. A) Uninterpreted seismic line and B) line drawing showing the presence of closely spaced north-west verging thrust faults within the core of detachment fold B with the positions of axial surfaces and fold and fault geometries. Reflections that constitute the incompetent succession within the fold core display numerous changes in vertical and lateral thickness. Reflections have preferentially thinned beneath the synclinal hinges and thickened within the fold core. Thickening appears to have occurred through an amalgamation of brittle and ductile processes. Vertical scale is approximately 3x the horizontal scale.

5.6 Structural styles of detachment fold cores

The incompetent succession that thickens within the cores of detachment folds is interpreted to have onlapped onto the regional detachment level, before it subsequently faulted. The incompetent succession, displaying significant lateral changes in thickness (e.g. Fig. 5.5), is precisely the type of interval that would have

previously been interpreted to be entirely occupied by overpressured, mobile shale. The significant thickness changes implies that the seismic interval is occupied by mechanically weak material, which is the case in comparison to the overlying seismic packages; however strata within the incompetent succession can be separated into coherent, relatively ridgid beds, which appear to be bound by ductile layers. This enables the presence of imbricate thrust faults and apparent ductile deformation to be explained. Thrust faults within the cores of the detachment folds geometrically resemble contractional duplex structures (e.g. Dahlstrom, 1970; Boyer and Elliot, 1982), which are bound by lower and upper detachment levels and connected by propagating footwall fault ramps (floor and roof thrusts). The structural style is analogous to passive-roof duplexes (also referred to as tectonic wedge structures) (e.g. Banks and Warburton, 1986; Harrison, 1995; Homza and Wallace, 1997; Bonini, 2007) that display complex architectural changes along strike. The overlying roof sequence incorporates the mechanically competent succession of the kilometre-scale detachment folds (e.g. Fig. 5.1), which is detached and decoupled from the underlying predominantly westward verging imbricate duplexes within the mechanically weak incompetent succession. The upper detachment level (roof thrust) is interpreted to be within mechanically weak shale, which is interpreted to be represented by the uppermost stratal reflection within the incompetent succession (i.e. reflection A on Figs. 5.3 and by black arrows on subsequent seismic profiles). The uppermost reflection interval directly beneath the upper detachment level appears to have deformed in a ductile manner, as it is absent, or infinitesimally small, in synclinal hinge regions and has preferentially thickened with fold cores (Figs. 5.3 and 5.9). Where this reflection is absent the resulting geometry is referred to as a touchdown (also known as a weld) in basins where gravitational detachment occurs upon basal successions of overpressured argillaceous sediments (e.g. Morley, 2003). Touchdowns are the resultant geometry that forms due to the withdrawal of a ductile material, which originally separated two reflection intervals. Ductile deformation of this mechanical weak interval has the result of leaving two lithologies that were not deposited adjacent to each other now juxtaposed (e.g. western section of Fig. 5.9). The formation of a touchdown is interpreted to mark the cessation of ductile movement (Morley, 2003).

5.7 Structural restoration

Based on structural interpretations, contrasting structural styles and the presence of detachment levels we have restored structural cross-sections, which validate our interpretations and reveal the evolution of the structurally complex detachment folds. As borehole data were unavailable for this study, TWT sections were depth converted using stacking velocities published in Morgan (2003). However, unstable geometries were attained for the regional detachment level, as a consequence of the thickened succession of low velocity sediments within the fold cores, and due to an uncertainty in what velocity to assign to the incompetent succession, which caused a significant artificial pushdown of the regional detachment level during depth conversion. Instead, a uniform velocity of 2000 ms^{-1} was used for sediments and 1480 ms^{-1} for the velocity of water, which gave the most stable regional detachment level geometry. A stable geometry for a detachment level was considered to be one with a gently dipping slope with no significant obstacles to slip. The TWT profiles in figures 5.7 and 5.9 were depth converted, and the water column and growth strata were decompacted, which allowed the underlying sections to expand. Beds that had been removed by angular unconformities and erosion through channel activity were reconstructed using the orthogonal bed thicknesses and geometries of un-eroded, underlying beds as a template.

Structural restoration was done using the 2DMOVE software. Balancing necessitates a decoupling of the uppermost ductile layer within the incompetent succession, which in this case is represented by the upper detachment level. Based upon the differences in shortening mechanisms and the presence of an upper detachment level, the competent strata (overburden) was decoupled and restored separately from the underlying thrust-related folding within the detachment fold cores. The competent strata were restored with the assumption that line-length and orthogonal bed thickness stayed constant during folding and variations in bed thickness were maintained. The competent strata were restored using flexural slip and small thrust faults were restored using fault parallel flow (see appendix 5, Figs A14 and A15). Deformation within the incompetent succession was restored by flexural slip to deal with the complex fault-related fold geometries. Individual fault blocks were

unfolded using local pins, which were then translated and rotated back into their undeformed state. Line-lengths within the incompetent succession were assumed to have remained constant during fault-related folding. Where significant thickness changes have occurred (i.e. where balancing cannot be done using line-length methods) the incompetent succession was area balanced (e.g. Chamberlin, 1910; Mitra and Namson, 1989; Mitra, 2003). The sections were balanced using a regional pin (the (south)western section boundary), which was inserted through areas that are considered to be representative of an undeformed area of the incompetent succession or parallel to a synclinal axial surface (e.g. Suppe, 1985; Mitra and Namson, 1989). Within the competent unit local pins were also inserted parallel to anticlinal fold hinge lines for the purposes of flexural slip unfolding (see appendix 5, Figs. A14 and A15).

The restoration shows that while removing slip on fault-related folds within the incompetent succession some slip on the regional detachment level is required (Fig. 5.10) (see appendix 5, Fig. A14). Restoration reveals a differential in the estimates of shortening that has taken place between contractional structures the incompetent succession and the overlying mechanically competent succession (the sedimentary overburden) (Fig. 5.10). Estimates of shortening reveal that 720 m has been accommodated within the incompetent succession; in contrast only 260 m of shortening is estimated within the sedimentary overburden. Once restored overburden geometries take on the appearance of a wedge that tapers (thins) up-dip, revealing that strata were deposited as a large-scale onlapping package before they were deformed.

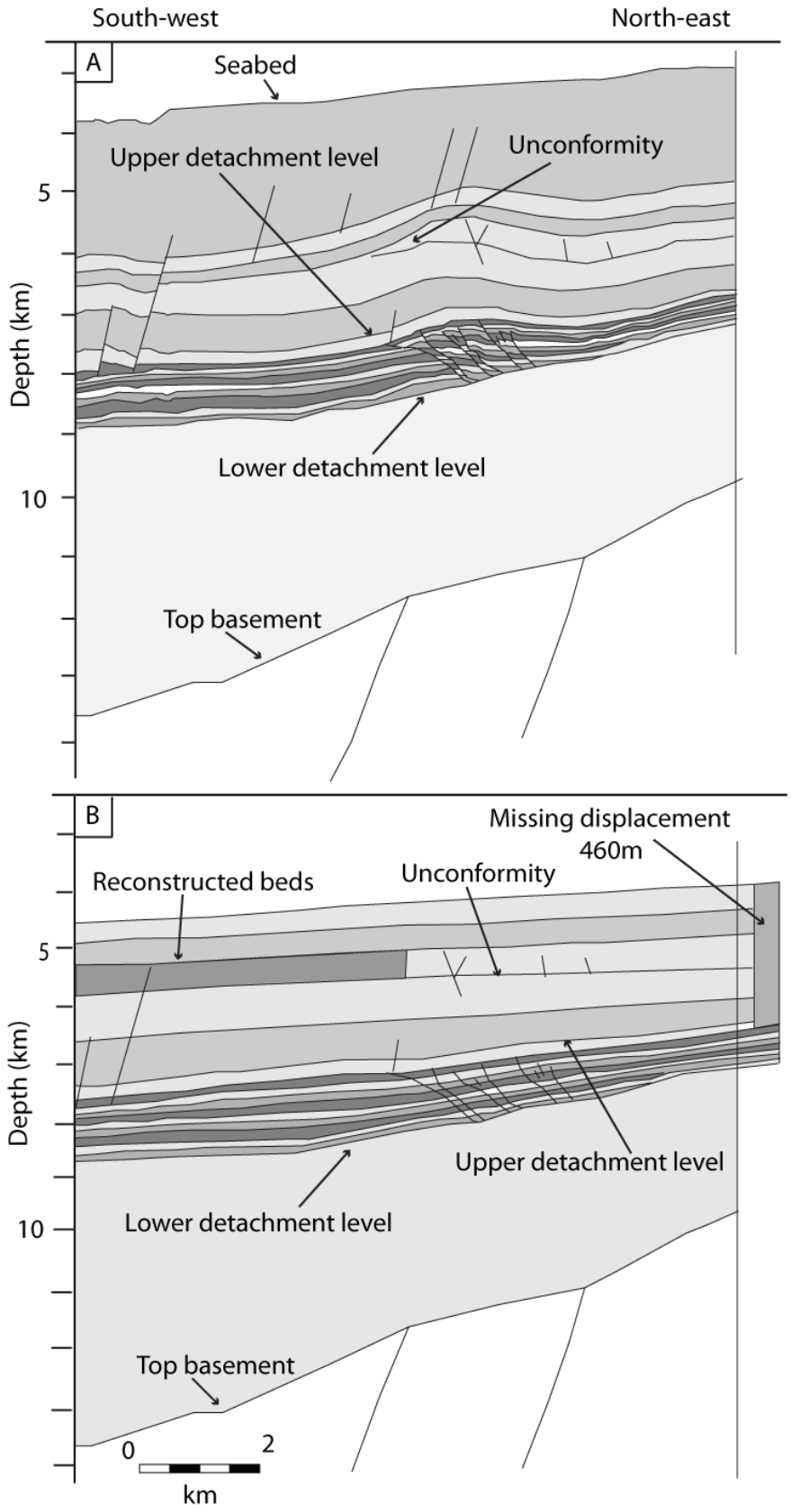
South-west
North-east
A
Seabed
Upper detachment level
Unconformity
5
Depth (km)
Lower detachment level
10
Top basement
B
Missing displacement
460m
Reconstructed beds
Unconformity
5
Depth (km)
Upper detachment level
Lower detachment level
10
Top basement
0
2
km

Fig. 5.10. Restoration of the structural styles and geometries in detachment fold A. The TWT profile shown in figure 5.7 was depth converted, water column and growth strata were decompacted and the structure was subsequently restored. The steep dip of the top basement reflection is an artifact of the depth conversion process. Vertical scale is equal to the horizontal scale.

In the second restored cross-section (Fig. 5.11, the TWT profile in shown in Fig. 5.9) the uppermost bed within the incompetent succession is not represented beneath the western synclinal region (Fig. 5.9) (see appendix, Fig. A15). Reflections within the fold cores can be clearly seen to thin and terminate towards synclinal regions implying that there has been some ductile deformation and potentially some out of plane movement (Fig. 5.9). In addition, the uppermost reflection interval within the incompetent succession terminates against the flanks of overlying fold limb and so some material may have migrated into the detachment fold core (e.g. Mitra, 2003). As all beds within this section of the incompetent succession display significant thickness changes the incompetent succession was area-balanced (e.g. Mitra and Namson, 1989). Area-balancing necessitated calculating the area of the incompetent succession beneath the fold and constructing stratal reflections to approximate their initial depositional thicknesses, and geometries, based on the orthogonal bed thicknesses of an undeformed section of the incompetent succession (e.g. Mitra and Namson, 1989). Identifying a representative undeformed section of the incompetnt succession was based on the presence of undeformed layer parallel reflections. Undeformed areas of the incompetent succession are present within parts of the western section of the survey area (as seen in the north-western part of Fig. 5.3) and were used as a template for area balancing. During restoration plane strain was assumed. Restoration estimates that 350 m of shortening has been accommodated within the competent strata and 708 m within underlying fault-related folds in the incompetent succession. The incompetent succession has accommodated a further 3% of shortening than the overlying overburden layer. Reasons for this shortening differential are discussed below.

In both of these examples shortening estimates are greater within the incompetent succession than within the overlying faulted and folded overburden stratigraphy, showing that the sections do not completely balance as an overall structure. This shortening discrepancy is also apparent in the seismic cross-sections based on the assumption of constant line-lengths within the sedimentary overburden and incompetent succession, as a discrepancy in the amount of shortening is still be apparent between the two packages (*cf.* Figs. 5.9 and 5.11 and 5.7 and 5.10).

There are a few additional, possible, explanations for the missing displacement within overlying sedimentary overburden: 1) the missing displacement could be accommodated by adjacent contractional structures, 2) slip could have been transferred on the upper detachment level and/or within the incompetent succession if it was active during amplification of overlying folds, 3) displacement could be accommodated by layer parallel shortening within the competent folded strata, 4) the missing shortening could be accommodated on sub seismic contractional structures, 5) volume loss could have occurred during fold amplification, 6) the structures are not kinematically linked and amplified independently of each other.

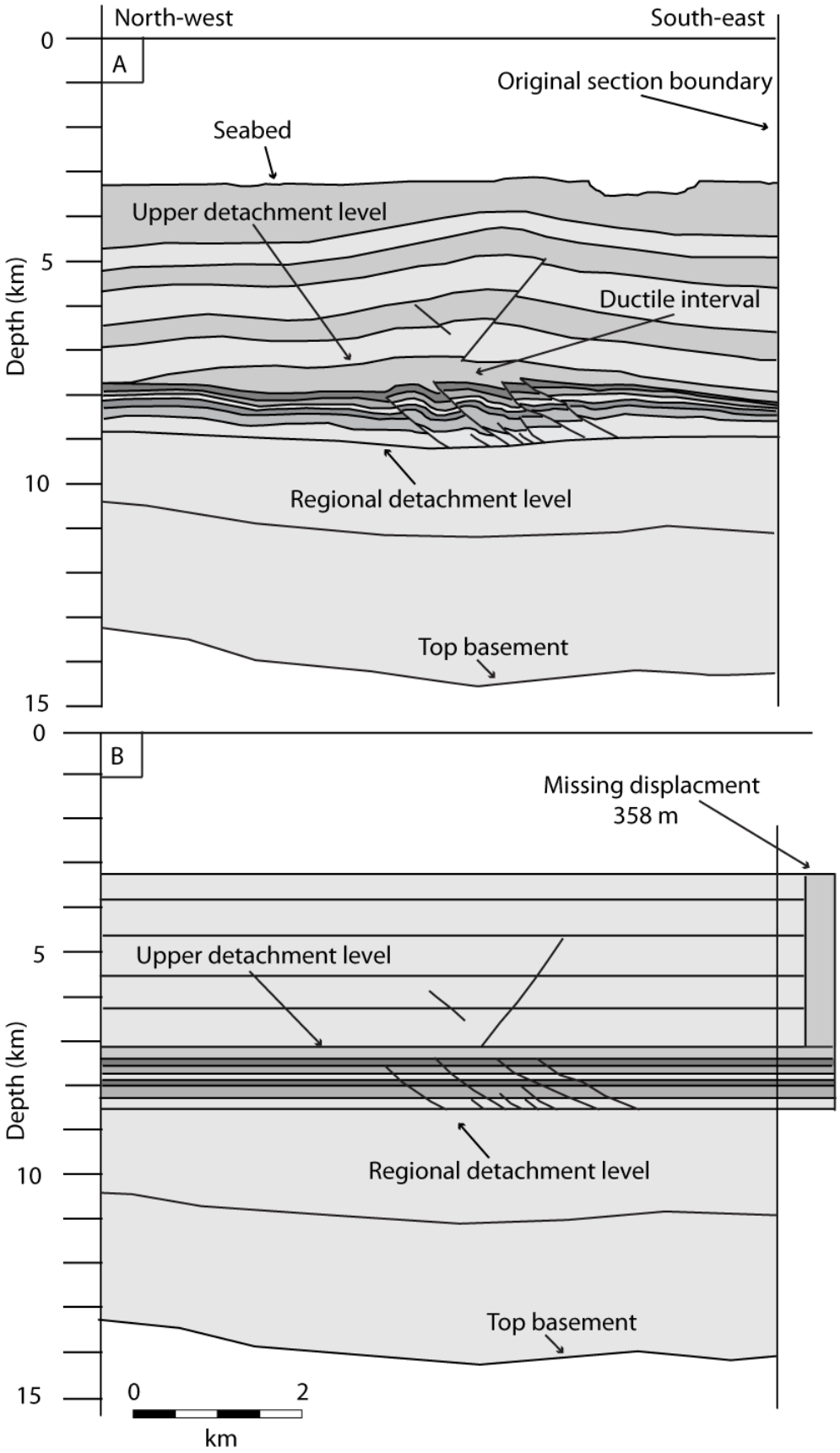
North-west
South-east
A
Original section boundary
Seabed
Upper detachment level
Ductile interval
Regional detachment level
Top basement
Depth (km)
0
5
10
15
B
Missing displacment
358 m
Upper detachment level
Regional detachment level
Top basement
0
2
km

Fig. 5.11. Restoration of the structural styles and geometries in detachment fold B. The TWT profile shown in figure 5.9 was depth converted, water column and growth strata were decompacted and the structure was subsequently restored. Vertical scale is approximately 2x the horizontal scale.

5.8 Discussion

5.8.1 Detachment fold formation

The nature of brittle-ductile coupling relationships (heterogeneous rheological layering) within the incompetent succession of detachment folds (and basal detachment successions) is critical to understanding how fold and thrust belts deform and for revealing how thickening occurs within detachment fold cores (Problet and McClay, 1996; Cotton and Koyi, 2000; Costa and Vendeville, 2002; Bonini, 2003, 2007; Mitra, 2003; Morley, 2009). Deformation here, within the interior of detachment folds, cannot be adequately represented by the detachment fold model. Furthermore, deformation is not likely to solely obey plane strain as out of plane migration of material is likely to have occurred within the synclinal hinges where thinning of the incompetent succession occurs. However, neither is deformation characteristic of the end-member modes of fault-related folding where prekinematic, layer parallel strata are deformed as a consequence of a ramp in a propagating fault plane. This leads to difficulties in balancing in the current restoration tools that rely on end-member interpretations for fault-related fold growth unless the entire incompetent succession is treated as purely ductile, which is not the case in these examples, or is area balanced. Possible interpretations for the presence of significantly thinned reflections beneath the synclinal hinges of detachment folds involve 1) differential loading by sediments that were deposited within the synclinal regions coeval with, or after fold amplification, which could of caused high levels of overpressure within underlying sediments and induced ductile deformation, 2) a ductile migration of material into the detachment fold core, which can be potentially related to distribution of overpressured pore-fluids, 3) it could be due to different rates of slip between weaker, overpressured material and frictional material that are sliding basinwards, 4) the thinned incompetent succession is actually a function of

depositional variation across pre-existing palaeo-topography 5) alternatively, thrusting within the incompetent succession could of occurred before folding occurred within the sedimentary overburden, and 6) the opposite scenario could also occur. These possibilities are expanded below.

Differential loading has long been advocated as the primary mechanism for generating high levels of overpressure and subsequent ductile movement of overpressured shales (Bruce, 1973; Morley and Guerin, 1996; Swarbrick and Osborne, 1998; Maltman and Bolton, 2003; Morley 2003). Preferential, rapid deposition of overlying sediments into the synclinal depocentres could have occurred, as accommodation space was created synchronously with fold amplification. As the accommodation space is progressively filled by deltaic sedimentation the magnitude of the vertical stress acting upon the incompetent succession would increase (as a consequence of the additional sedimentary load). If pore-fluids are unable to escape with increased burial the lithostatic load becomes imposed onto the pore-fluids causing them to become overpressured. If the lithostatic load is sustained entirely by the pore-fluids then the sediments loses all strength and becomes liquidized (Maltman and Bolton, 2003). Alternatively, if pore-fluids are able to remain at hydrostatic pressure with the increase in burial load, the increase in effective stress would serve to preferentially compact sediments beneath the synclines, which alternatively lead to a thinning of strata.

For differential loading to be an effective mechanism in causing sediments within the incompetent succession to become liquidized, it seems that a significant volume of sediment would have to be deposited in the synclinal regions of the detachment folds. The vertical distance between the anticlinal and synclinal regions of detachment fold B is approximately 0.7 km (Fig. 5.11). The differential load, the difference in the magnitude of the lithostatic stress, acting upon the incompetent succession in anticlinal and synclinal regions of detachment fold B is estimated to be 11 MPa, with the lithostatic pressure 44 MPa and 55 MPa in anticlinal and synclinal regions respectively. This is based on the density of seawater being 1030 $kg \cdot m^{-3}$ with an average mud density of 1500 $kg \cdot m^{-3}$ for the first 500 m of burial, which

increases to an average density of 1550 $kg \cdot m^{-3}$ after depths of 500 m (Janik et al., 1998; Davies, 2003). It seems that the excess load within in the synclines would be ineffective in liquidizing sediments enabling movement in the form of a sediment-water mixture, unless the magnitude of overpressure was already close to lithostatic pressure prior to the additional sediment loading.

The uppermost reflection interval within the incompetent succession, directly beneath the upper detachment level (Figs. 5.3 and 5.9) within detachment fold B may have been under conditions where a large proportion of the lithostatic stress was being supported by the pore-fluids so that when additional sediment was deposited a further increase in overpressure caused the lithostatic load to become fully sustained by the pore-fluids. Once in a liquidized form the sediment is subject to pressure differentials and so would flow into the amplifying detachment fold core as it would be a low pressure region. The distribution and magnitude of overpressured beds could explain the ductile deformation of individual beds within the incompetent succession, which thinned beneath the synclines and thickened within the anticlines.

The distribution of overpressured pore-fluids is critical to the ductile deformation of argillaceous sediments (Maltman, 1994; Morley and Guerin, 1996; Deville et al., 2010). The development of overpressure has the effect of reducing sediment's ability to transmit a shear stress, as a function of decreasing the effective stress, which results in a separation of grain to grain contacts, promoting ductile failure. During shortening overpressured strata could potentially migrate into the fold core and out of plane via ductile processes to accommodate fold growth (e.g. Mitra, 2003). This may include sediment-water mixtures where there is a partial or complete loss of shear strength.

The distribution of overpressured and the magnitude of overpressure, or spatial variability in mechanically weaker material, i.e. shales with high clay contents or high proportions of organic material, within the incompetent succession may cause differences in the rate of basinward slip. If overpressure is distributed in pockets

creating a brittle-ductile wedge then the relatively weaker, overpressured sediments could potentially translate basinward at a faster rate in comparison to hydrostatically pressured sediments that would have a greater resistance to an applied shear stress and therefore to basal slip. Consequently the incompetent succession would take on the appearance of thickening and thinning succession due to the different rates in slip.

For thickness changes in the incompetent succession to be related to pre-existing depositional variability thinned areas would likely have to be deposited over paleo structural highs and thicker successions deposited in adjacent mini basins. Although plausible there is no evidence for any pre-existing highs as all underlying reflections are relatively undeformed (apart from slump deposits) and laterally continuous. In addition, the deposition of incompetent succession likely occurred in the pro-delta synchronous with the deposition of the Akata Formation (Doust and Omatsola, 1990); hence such beds would have likely been deposited flat and layer parallel rather than as a thickening and thinning succession.

The thrust-related folds in the incompetent succession could be kinematically unrelated to the folding that has occurred above it in the sedimentary overburden. Thrust faulting within the incompetent succession could have occurred prior to the amplification of overlying folds. If this was the case then of overlying folds could have developed as a function of the pre-existing topography. An early stage of thrust faulting within the incompetent succession may cause the succession to have the appearance of ductility with lateral thickness changes. The incompetent succession would be preferentially thickened where thrust faulting had occurred, which would leave the impression of a thinned succession in comparison to adjacent areas. However, as thickness changes within individual reflection intervals can be resolved, coupled with the termination of reflections, implies that ductile deformation has taken place and so the thickening the thinning cannot be purely explained by brittle structural thickening.

Kinematic models for detachment fold amplification initially solve balancing problems by requiring the structural thickness of the incompetent succession to vary during fold amplification (e.g. Homza and Wallace, 1997; Mitra, 2003). We hesitate to apply restoration techniques applied to detachment folds as the underlying, mechanically weak incompetent succession would be required to solely deform by ductile mechanisms, which is clearly not the case in the examples shown here. The incompetent succession is likely predominantly composed of fine-grained argillaceous sediments within which are coarser lenses of sandstone (Cohen and McClay, 1996). In order to deform via ductile processes elevated pore-fluid pressures are a necessity. For ductile deformation to be subsequently followed by faulting the excess pore-fluid pressure would have to rapidly dissipate (possibly by hydraulic fracturing) in order to restore sediment strength, to then allow strata to fault. If hydraulic fracturing occurred as the overpressured pore-fluids were able to escape the seismic resolution within the incompetent succession would likely be heavily compromised, as is observed by seismic studies on mud-volcanoes (Stewart and Davies, 2006; Deville et al., 2010).

A heterogeneous, lateral and vertical multilayered rheology is invoked to explain deformation within the incompetent succession. Although, in comparison to the sedimentary overburden, the entire seismic package that thickens and thins is relatively incompetent (at the largest scale), however, internally it is highly likely to be anisotropicly layered rather than a purely mechanically homogeneous succession. The presence of mechanical layering is alluded to by individual beds exhibiting a control on the dip of the fault planes. Steeper fault segments are associated with relatively competent beds while weaker beds are associated with shallower fault plane dips (e.g. Schöpfer et al., 2006). Internally, relatively brittle-ductile coupling between beds provide the necessary mechanical properties for thrust flats to develop, while competent beds will be characterised by the presence of thrust ramps.

A differing rheological response to an applied shear stress can be explained by potential brittle-ductile coupling relationships within the multilayer and variations in the distribution of pore-fluid pressures, which would create mechanical anisotropies

throughout the incompetent succession (Fig. 5.12). In addition to the pore-fluid explanation, the presence of lithologies that have a tendency to deform plastically interbedded with those that have a greater tendency of fracture would also control the individual and overall rheological response of the incompetent succession. Lithologies that have a natural tendency to deform plastically are related to having a large percentage of clay minerals and or organic content, while the relatively competent layers may are likely to be coarser grained or contain non-clay minerals (Booth, 1986; Maltman, 1994). The deformational response of the incompetent succession is likely controlled by a combination of factors, such as: 1) the strength of the incompetent succession as a whole, including the relative shear strengths of individual beds; 2) the presence or absence of ductile beds; 3) brittle-ductile coupling (mechanical strength contrasts) (e.g. Costa and Vendeville, 2002; Bonini, 2003, 2007; Cotton and Koyi, 2000). The weakest, ductile, beds are characterised by low shear strengths and either act as detachment levels or deform in a ductile manner, which in these examples are used to explain how any potential void space created during fold amplification would be filled.

Similar styles of thickening have been described from detachment folds that have formed above basal detachment successions (incompetent successions) composed of evaporates. The style of thickening depicted in the detachment folds in these examples is analogous to what have been termed “salt welts,” which have been described in large-scale salt detachment systems (e.g. Harrison, 1995) (Fig. 5.13). Salt welts are an amalgamation of ductile and brittle thickening structures that have formed as a function of lithological contrasts with different rheologies. The salt thickens in a ductile manner migrating from synclinal to anticlinal regions to accommodate the growth of overlying folds. However, the competent beds deform through complex interactions that involve volume loss through compaction, thrust faulting and folding. Intriguingly, the competent beds are also shown to thin beneath the synclinal hinges of anticlines in a similar fashion to what is observed here (Fig. 5.13). In addition, fault studies through complex multilayers have also demonstrated that as deformation commences strata can experience significant volume loss through compaction and penetrative strain. Therefore the natural complexity demonstrate

within outcrop studies are not captured by the end-member fault models (Butler and McCaffrey, 2004; Iacopini and Butler, 2011).

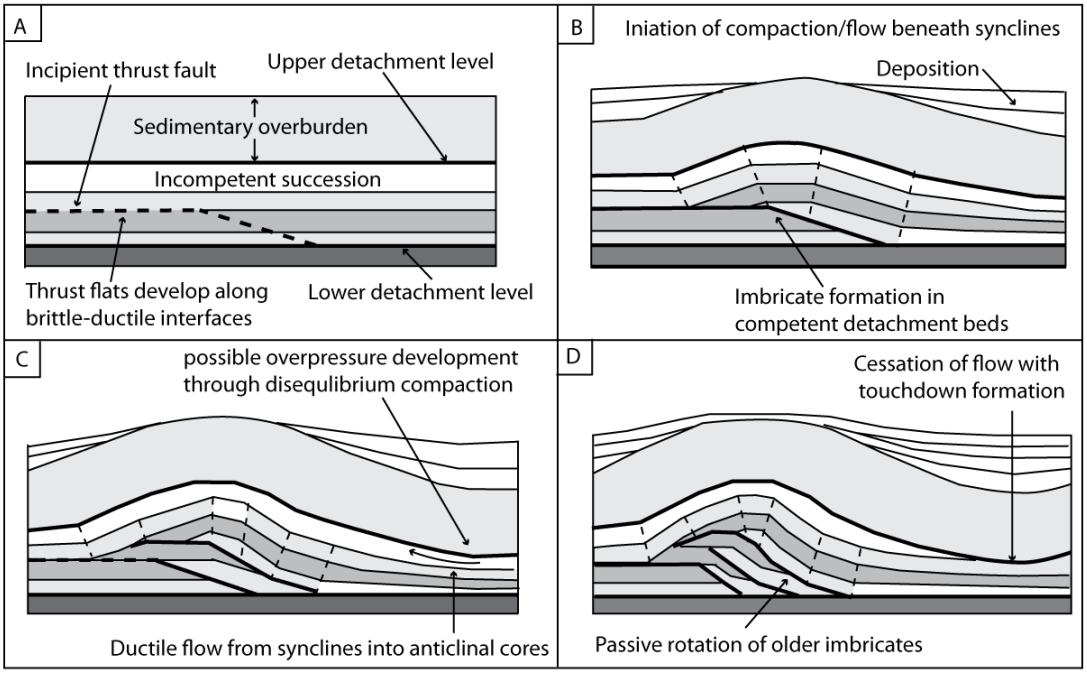

Fig. 5.12. Preferred model for the amplification and evolution of detachment folds in the study area. A) Initiation of thrust faulting within the incompetent succession is coupled with folding in the sedimentary overburden. B) Continued amplification and deposition of sediments in the fold synclines creates a differential load, which may overpressure pore-fluids and induce ductile deformation of underlying shales C). D) Cessation of ductile withdrawal occurs with the juxtaposition of competent beds.

5.9 Implications

The presence of a series of imbricate thrust faults within what is typically thought to be a seismic interval dominated by ductile deformation processes causes a rethink of how strain is accommodated within the cores of large-scale, detachment-style folds in shale tectonic settings. Instead of the purely ductile thickening approach thickening has occurred by a combination of faulting and ductile thickening showing that mechanically weak successions composed of overpressured shales do not necessarily conform to the deformation style implied in current conceptual models. Furthermore, the presence of imbricate thrust sheets within detachment fold cores

may provide alternative insights as to why certain regional cross-sections do not balance without invoking non plane strain reasons. Often, the estimates of extension and contraction from balancing regional cross-sections provide greater estimates of extension than contraction, for example a discrepancy of 8 km was estimated from the Orange Basin, offshore West Africa (de Vera et al., 2010). Shortening structures within incompetent successions, which are just now coming to the fore of seismic resolution in high-quality data, would have been sub-seismic within older seismic data sets and so not included in the restoration of large-scale structures on regional seismic lines. Although the shortening estimates here do not completely solve a discrepancy of that magnitude the incorporation structures that were sub-seismic into regional restorations may improve the compatibility between estimates of extension and contraction.

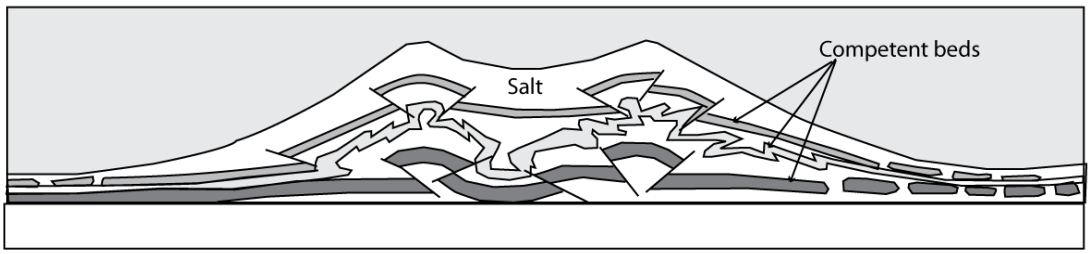

Fig. 5.13. Line drawing of a "salt welt" (from Harrison, 1995) showing an analogous structural style of thickening within the cores of detachment folds that is depicted within the north-western Niger Delta. The weak salt has thickened within anticlinal cores in a ductile manner where as the relatively more competent beds have thickened through combinations of folding and fault-related folding.

5.10 Conclusions

The recognition of imbricate duplexes within the cores of kilometre-scale detachment folds shows the level of detail that, in some cases, is missing from current detachment fold models in shale tectonic settings. In contrast to what are depicted in typical conceptual models, which attempt to capture the deformation style within an incompetent succession by a ductile thickening, the structural style is characterised by a series of complex contractional duplexes interbeded with layers that display ductility with significant lateral variations in thickness. The incompetent succession is mechanically weak in comparison to sediments within the overlying

sedimentary overburden whose strength and rheology is ultimately controlled by the mechanical stratigraphy. It is speculated that the mechanical properties of the detachment succession together with the magnitude of any overpressure play a dominant role is controlling the deformational response within the detachment succession. The variability in deformational response within the incompetent succession is likely controlled by a variety of factors, which include 1) the distribution of overpressured pore-fluids, 2) the magnitude of overpressure, 3) variations in lithology, which can govern the tendency for material to fracture or deform plastically. Thick successions of weak, homogeneous shale could allow ductile flow during fold growth whereas beds with variable lithologies and differing shear strengths may prefer to thicken in a brittle manner. All of these factors influence the relative shear strength of individual beds, which cumulatively contribute to the strength of the incompetent succession as a whole. Evidence for both ductility and fault-related folding within the detachment succession implies a spectrum of processes that encompass deformation styles ranging from a ductile flow through to more complex brittle styles.

6 Discussion

Chapters 3, 4, and 5 where research results are detailed include discussion sections. This chapter provides a broader discussion on basal detachment successions within shale tectonic provinces. The results of the analysis in chapters 3, 4 and 5 are summarised. In addition, comparisons and analogues are made with field and modelling studies and the mechanisms of how shale can move from one area to another are discussed.

6.1 Deformational processes that operate within a basal detachment succession composed of argillaceous sediments

Chapters 3, 4 and 5 have demonstrated that a basal detachment succession composed of overpressured, argillaceous sediments is in places characterised by brittle deformation styles. This is in direct contrast to early and more recent works on shale tectonics that consider that overpressured, fine-grained sediments solely deform as a form of sediment-water mixture (mobile shale) in response to differential loading by overlying sediments (e.g. Bruce, 1973; Barber et al., 1986; Morley and Guerin, 1996, Morley, 2003; Deville et al., 2006). Together, chapters 3, 4 and 5 have provided alternative, or interpretations that are considered atypical, interpretations to structural models that have been developed over large deltas that are undergoing gravitational collapse upon basal detachment successions of overpressured, argillaceous sediments (e.g. section 1.11). Initially structural models relied on the presence of a ductile succession at the base of the sedimentary overburden; however, the interpretation of ductile deformation is proving to be, in some examples, oversimplified, as it is suspected that style of deformation is likely to be dependent on the mechanical properties of the stratigraphy that constitute the basal detachment succession. Studies based on older seismic data (e.g. pre-1998) found it difficult to determine whether a seismic interval containing overpressured, argillaceous sediments that appeared to deform in a ductile manner deformed in a solid state or as a sediment-water mixture; however, chapters 3 and 5 have been able to differentiate between the two. Chapter 3 documented the presence of extensional faults (in up-dip regions)

within the basal detachment succession showing that, potentially, pre-existing structures can become incorporated into the basal detachment succession. Chapter 5 detailed the presence of imbricate thrust faults within the cores of kilometre-scale detachment folds implying that the mechanical stratigraphy, together with the magnitude of the pore-fluid pressure, plays a key role in determining the type and style of deformation that occurs within the basal detachment succession. Chapter 4 demonstrated that both brittle and ductile process operate within a basal detachment succession and implies that ductile deformation occurs on a smaller scale than brittle styles. Significantly, the presence of brittle deformation styles within a basal detachment succession has important ramifications on the end-member models currently used to assist the interpretation of gravitational-driven detachment systems (e.g. section 1.11). As a broad spectrum of deformational processes can operate within the basal detachment succession, incorporating varying degrees of ductile and brittle deformation, the typical view of solely ductile deformation needs to be reviewed. Models that depict thrust-related folding in detachment fold cores which are considered atypical in gravitational detachment systems that prograde over basal detachment successions composed of overpressured, argillaceous sediments maybe more applicable (e.g. Fig, 4.12). The importance of this is discussed within the remainder of this chapter.

6.2 The issue of scale and seismic resolution

This thesis has analysed deformation styles within a basal detachment succession composed of overpressured, fine-grained sediments exclusively using seismic reflection data. As a consequence, research into the concept of mobile shale has been limited by the vertical resolution of the 2D and 3D seismic data sets. The vertical resolution of 3D seismic data at the depth of the basal detachment succession ranges between 17 m and 25 m, a quarter of the dominant wavelength calculated at the depth of the basal detachment succession. With this in mind it is worth considering whether deformation interpreted as deforming in a ductile manner is related to the vertical resolution of the seismic data at this depth. On seismic reflection data what is described as ductile deformation could be characterised by faults with offsets of less than 25 m and folds with amplitudes of less than 25 m, and

so a deformational architecture would not be resolved leaving the impression of seismic transparency. With the continuing improvement in the quality of seismic reflection data structures that were previously beyond the vertical resolution are now becoming imaged. This has been highlighted by studies whose structural interpretations initially followed models developed for where thin-skinned detachment occurs upon a basal succession of overpressured shales (e.g. section 1.11), which were then reinterpreted at a later stage with higher-quality 3D coverage (Fig 6.1). This is demonstrated by two publications by Van Rensbergen and Morley in 2000 and 2003. Van Rensbergen and Morley (2000) initially interpreted a series of shale diapirs and shale rollovers at the base of listric faults (e.g. sections 1.11.1 and 1.11.2) from 2D seismic data from offshore Brunei. However, following a reinterpretation on 3D seismic data the initial structures that appeared to have deformed by ductile processes (i.e. a seismic facies that displayed lateral thickness changes and was characterised by zones of low reflectivity) were later found to contain laterally continuous, coherent reflections (Van Rensbergen and Morley 2003). As a consequence Van Rensbergen and Morley's (2000) original interpretation of active and reactive diapirs were found to be vertical chimneys and footwall horst blocks respectively (Fig. 6.1). The widespread occurrence of large-scale counter regional growth faults separating chaotic, discontinuous seismic reflections facies from coherent reflections was also cast into doubt as reflectivity was found to continue into what was previously identified as a mobile shale seismic facies (Fig. 6.1).

Chapters 3, 4 and 5 provide alternatives and additions to structural models originally developed to explain evolution of gravitational-detachment systems and widespread applicability of these models (e.g. Musgrave and Hicks, 1966; Morgan et al., 1968; Pennebaker, 1968; Bally et al., 1981; Van Rensbergen and Morley, 2000). In particular, this study has alluded to the detachment fold model when underlain by an argillaceous basal detachment succession. Conventional models for the amplification of detachment folds involve the basal detachment succession (or the incompetent succession) flowing into the detachment fold core during fold amplification (section 1.12.4). Ultimately this may be dependent on the properties of the mechanical stratigraphy that constitute the basal detachment succession. Where

thick successions of overpressured, homogeneous shale have been deposited, deformation may occur in a ductile manner. However, chapter 4 suggests that an anticlinal stack may be a preferable interpretation whereas chapter 5 depicts large-scale passive duplex structures causing the thickening within the basal detachment succession. These complex deformational styles within detachment fold cores have been previously identified from outcrop studies in the cores of detachment folds (e.g. Fig. 4.12), but are not applied to shale tectonic settings. The identification of contractional duplexes within fold cores also has implications into the interpretation of shale diapirs (shale cored thrust faults) and associated domal structures, which also rely on the presence of a ductile mass of overpressured shale within their cores

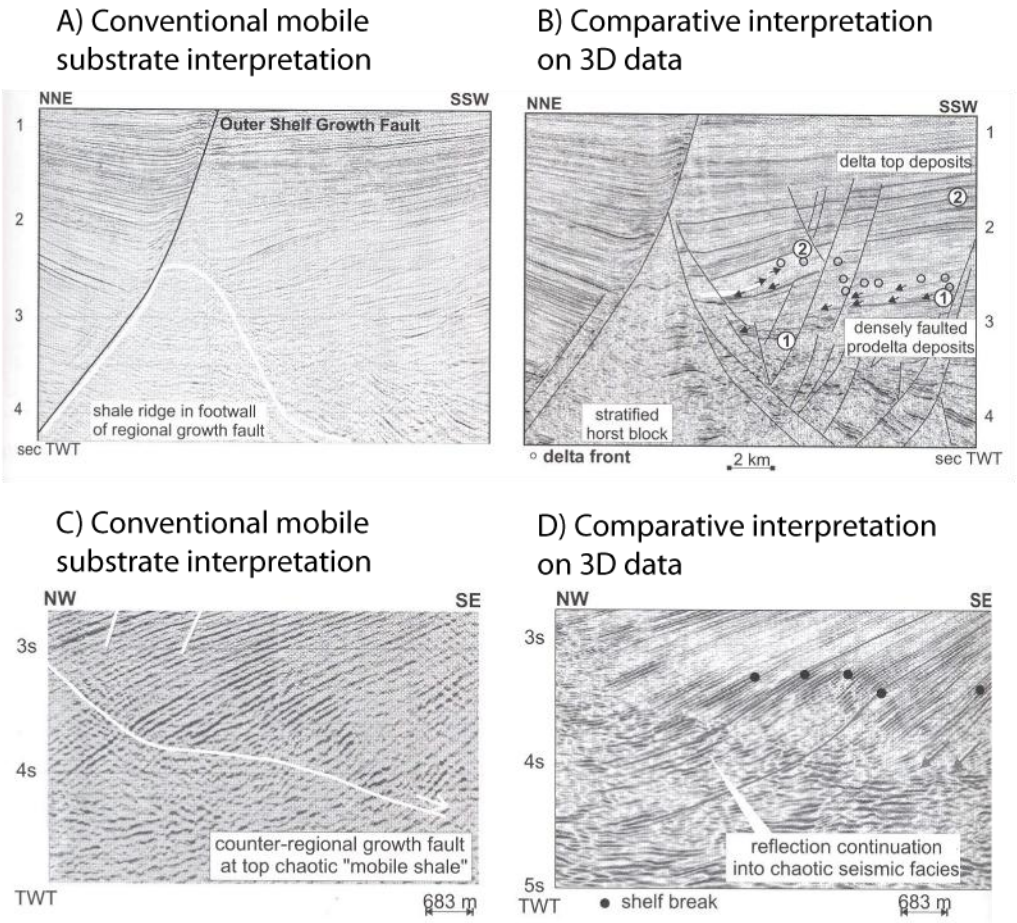

Fig. 6.1. Interpretation of structural features that involved the presence of mobile shale using 2D seismic data (panels A and C), and their re-interpretation using 3D data (panels B and D) (from Van Rensbergen and Morley, 2003).

6.3 Outcrop studies

Due to the limited vertical resolution of seismic reflection data at the depth that basal detachment successions reside field studies are important, as they reveal structures that are beyond the seismic resolution. However, few field studies have successfully demonstrated how detachment successions composed of overpressured, argillaceous sediments accommodate strain and internally deform. This is most likely because such successions are generally inaccessible, poorly exposed, not exhumed or not recognised in the field (e.g. Morley, 2003B; Huuse et al., 2010). Relatively little is known about the deformational processes and resultant structures that characterise subseismic deformation, especially the architecture associated with shale diapirism and how bodies of mobile shale migrate into an overlying succession or laterally within the same succession. There are no field studies that can convincingly demonstrate the rise of an argillaceous diapiric body. Indeed, Deville et al. (2010) go as far to state: "no intrusive mobile shale bodies have been identified that resemble salt tectonic structures." This is reinforced in the literature for mud volcano systems where 90-95% of the remobilized mud is contained in extrusive edifices whereas the intrusive components are rarely preserved (Huuse et al., 2010). Despite the lack of field evidence for thick accumulations of mobile shale the search for applicable analogues is explored in an attempt to assign deformational processes, lithological types and deformation styles to this low-resolution seismic facies.

6.3.1 Mudstone intrusions

Analysing the mechanisms of how mud intrusions are emplaced is critical to furthering our understanding of how overpressured sediments are able to move. It is of particular importance to understanding how overpressured shale may rise and intrude into overlying country rock. The process of how sediment-water mixtures can potentially move vertically, laterally and downwards involves injection and intrusion allowing the formation of mud filled fractures, dykes, sills and laccoliths. These processes could provide explanations for the thickness changes seen within seismic facies interpreted to be occupied by mobile shale (e.g. the apparent ductility). How mud intrusions are linked to a fluid source of mobile mud and intrude into surrounding country rock could shed light on the kinematics of mobile shale

successions. The geophysical signature associated with overpressured, argillaceous sediments has made the gross structural style within such successions difficult to interpret on seismic reflection data (e.g. section 1.8). Field studies on mud filled intrusions can reveal the architecture and scale of potential features that may constitute a mobile shale seismic facies on a subseismic scale. Morley (2003B) documented in excess of 50 mudstone intrusions over an area of 1 km^2 from the Jerudong Anticline, onshore Brunei, which he relates to the rise of a diapirc argillaceous body. The smallest intrusions are a series of lithologically homogeneous, soft mudstone dykes. Dyke geometry is varied as some have formed en-echelon mud filled fractures and splays as well as lateral jogs influenced by pre-existing fault planes. The largest mud filled intrusion documented was a laccolith with dimensions of 10 m thick and 25 m wide, which internally contained fissile blocks of shale. The dimensions of these intrusions are significantly smaller than the dimensions of features typically interpreted as shale diapirs (e.g. Fig. 1.2 and 1.13), and may suggest that the low-reflectivity bulbous masses interpreted as diapiric bodies are actually intensely fractured masses of country rock.

6.3.2 Vertical emplacement of overpressured sediments

High levels of overpressure are necessary for mud-water mixtures to intrude into surrounding country rock (Jolley and Lonergan, 2002). Injection of a high-pressure fluid within a propagating fracture or intrusion requires a large pressure differential between the pore-fluid pressure within the propagating crack and the pore-fluid pressure within the surrounding country rock (Jolley and Lonergan, 2002). This causes the fracture to dilate and allows the sediment-water mixture to flow through the propagating fracture (Lorenz et al., 1991). At the time of intrusion abundant amounts of pore-fluids have to be present within the source rock. The fluid content within overpressured successions whose pore-fluids are high enough to initiate hydraulic fracture is estimated to be around 70% (Morley, 2003B). The loss of pore-fluids associated with fracture propagation (as with diapiric rise and dyke formation) is the critical factor in controlling the final dimensions of the intrusion, as once the excess pore-fluid pressure dissipates fracture propagation ceases. After hydraulic failure fluid content is estimated to be around 20-30% (Morley, 2003B). Conventionally, the propagation of hydraulic fractures, as with diapiric rise, is

considered to be controlled by the tensile strength of overlying sediments and the *in situ* stress state (Vendeville and Jackson, 1992; Jolly and Lonergan, 2002). Vertical emplacement of fractures is driven by the difference in pore-fluid pressure between deeply buried sediments, in comparison to shallower buried sediments, in the presence of a vertical or subvertical maximum effective stress. This is a common situation in the proximal settings of deltas on passive margins as there is no externally imposed tectonic stress state and the maximum principal stress is vertical, due to gravitationally-driven sediment loading (Jolly and Lonergan, 2002).

Mud filled intrusions are an example of hydraulic fracturing. Conditions for hydraulic fracturing are favourable when the pore-fluid pressure in the overpressured succession overcomes the minimum effective stress and the tensile strength of the rock. This is demonstrated in Equation 6.1 (Jolly and Lonergan, 2002; Yassir, 2003).

$$Pp > \sigma'min_{ob} + T_{ob} \qquad \text{Equation 6.1}$$

$\sigma'min_{ob}$ is the minimum effective stress of the sedimentary overburden and T_{ob} the tensile strength. Fractures open parallel to the maximum effective stress and normal to the minimum effective stress. Within an anisotropic multilayer the tensile strength of sediments can be different in directions parallel and normal to bedding (Jolly and Lonergan, 2002). For emplacement of a dyke (vertical intrusion) the pore-fluid pressure must exceed minimum effective horizontal stress (σ'_h) and the tensile strength (T_h) of sediments that acts parallel to bedding (Equation 6.2).

$$Pp > \sigma'_h + T_h \qquad \text{Equation 6.2}$$

Hydraulic fracturing weakens the country rock. If hydraulic fracturing were to act as a precursor to diapiric rise, resistance to the rise of a diapir would now be controlled by the lower or negligible tensile strength of pre-existing fault zones (Morley,

2003B). The same would be true if the sedimentary overburden has already been faulted. Where there are pre-existing faults or fractures within the sedimentary overburden the pore-fluid pressure has to only exceed the normal stress (σ_n) across faults or fractures for dilation to reoccur (Equation 6.3) (Jolly and Lonergan, 2002).

$$Pp > \sigma_n \qquad \text{Equation 6.3}$$

Initiation of hydraulic fracturing and subsequent fracture propagation could provide an alternative explanation for the formation of new shallower detachment levels, as seen in chapter 3. Open fractures can act as migration pathways for pore-fluids from the overpressured succession to a lower pressured succession, typically at a shallower depth, within the subsurface (e.g. Moore et al., 1998, Deville et al., 2010). If the excess pore-fluid within the propagating fracture is able to dissipate fracture propagation would cease. The fracture would then close and fluid migration would no longer be possible.

6.3.3 Lateral emplacement of overpressured sediments

The lateral movement of sediment-water mixtures is more problematic than vertical emplacement as it is harder to create a favourable pressure differential within successions at equivalent depths. For sill emplacement the pore-fluid pressure must exceed the effective vertical stress (σ'_v), and the tensile strength of sediments normal to bedding (T_v) (Price and Cosgrove, 1990; Jolly and Lonergan, 2002) (Equation 6.4).

$$Pp > \sigma'_v + T_v \qquad \text{Equation 6.4}$$

In compressive settings (deltaic toes) the orientation of the stress field favours the emplacement of horizontal or subhorizontal hydraulic fractures as the minimum compressive stress is vertical. This allows pore-fluid pressures to be attained near

lithostatic pressure and so high levels of overpressure can be supported by the pore-fluids before hydraulic fracture occurs (Deville et al., 2010). If overpressure development within a fine-grained succession deep within the subsurface reaches a magnitude great enough to induce hydraulic fracture, a series of subhorizontal fractures would propagate from the overpressured interval. Again, these fractures could act as conduits for sediment-water mixtures that utilise the pressure gradient (Deville et al., 2010; Huuse et al., 2010). This process has been used to explain the formation of décollement surfaces within the fore of accretionary prisms and wedges (Moore et al., 1998; Deville et al., 2010). Emplacement of subhorizontal fractures has the effect of reducing the strength of the rock volume within which the fracture network is emplaced. Continued fracturing and the development of fluid pathways could allow the development of an effective décollement surface. A ponding of pore-fluids at the fore of these fractures could allow an effective décollement surface to form.

6.4 Possible field analogues

6.4.1 Mud volcanoes

Mud volcano systems have been relatively well studied in both seismic reflection data (e.g. Graue, 2000; Stewart and Davies, 2006; Gamberi and Rovere, 2010) and from outcrop (e.g. Roberts et al., 2010). The extrusive mud brought to the surface is a fine-grained mud-water gas mixture that entrains sand blocks, rock fragments and breccia fragments on its way to the surface (Huuse et al., 2010). Importantly, mud volcanoes provide evidence which proves that under certain conditions large volumes of fine-grained sediments can behave as a fluid. However, the intrusive parts of mud volcanoes, the components that may be analogous to mobile shale facies, still remain relatively unknown in comparison to their extrusive counterparts. This is a combination of few intrusive components being exhumed and due to the fact that they are rarely preserved (Huuse et al., 2010). On seismic reflection data the intrusive components are often obscured by zones of low reflectivity thought to be related to gas associated with volcanism (Graue, 2000; Morley, 2003; Stewart and Davies, 2006). Outcrop studies, and studies on seismic reflection data, have revealed

that mud volcano feeder systems are highly fractured regions of country rock which contain numerous mudstone intrusions (Roberts et al., 2010).

6.4.2 Thrust-related folding

In detachment fold models the behaviour of the incompetent succession that thickens within fold cores is still relatively unconstrained (Homza and Wallace, 1997). Detailed studies on field examples of detachment folds could provide useful insights into how overpressured, argillaceous sediments accommodate strain within the cores of detachment folds, thrust-cored diapirs and similarly described diapiric structures (e.g. Fig. 1.10). Strain indicators in the incompetent successions of detachment folds yield insights into deformation styles, mechanisms and kinematics within these mechanically weak successions. Studies have shown that the incompetent successions are intensely deformed and unlike their competent unit counterparts, which form the outer arcs (e.g. Fig, 1.10), they show considerable variability deforming by disharmonic folding, solution cleavage, cataclasis, pressure dissolution and closely spaced small-scale contractional thrust faults (Figs. 6.2 and 6.3). Deformation within the hinge regions of detachment folds are especially complex (e.g. Homza and Wallace, 1997; Mitra, 2003). Mitra (2003) showed that within synclinal hinge regions the incompetent succession can display a variety of fold wavelengths and styles (Fig. 6.2). Parasitic folds and isoclinals folds that display a considerable disharmonic component are not uncommon (e.g. Homza and Wallace, 1997; Mitra, 2003). Second-order structures involve small-scale thrust faults and faulted disharmonic folds (Fig. 6.2).

Homza and Wallace (1997) studied a series of detachment folds from the north-eastern Brooks Range, Alaska. They also analysed strain indictors within the incompetent succession by analysing rock samples from the synclinal and anticlinal hinge regions. On a first-order scale the incompetent succession displays disharmonic geometries with a variety of fold wavelengths present within the anticlinal core. Anticlinal hinge regions are characterised by zones of high strain, as indicated by solution cleavage and cataclasis (Fig. 6.3).

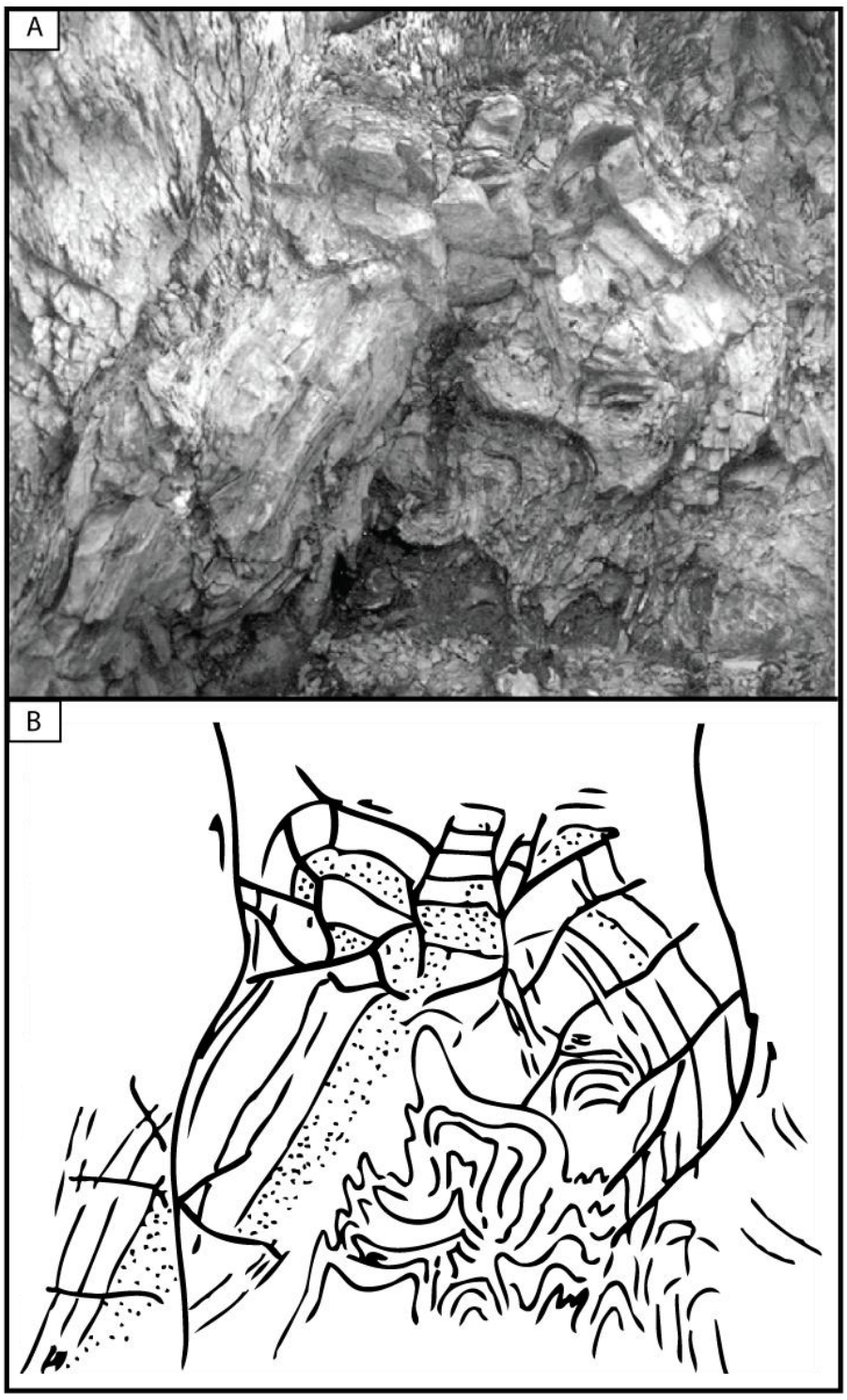

Fig. 6.2. A) Photograph and B) line drawing of the intense deformation style within the synclinal hinge region of a detachment fold. The strata within the core show tight isoclinal folding and small-scale discrete contractional fault surfaces (from Mitra, 2003). Scale was not indicated.

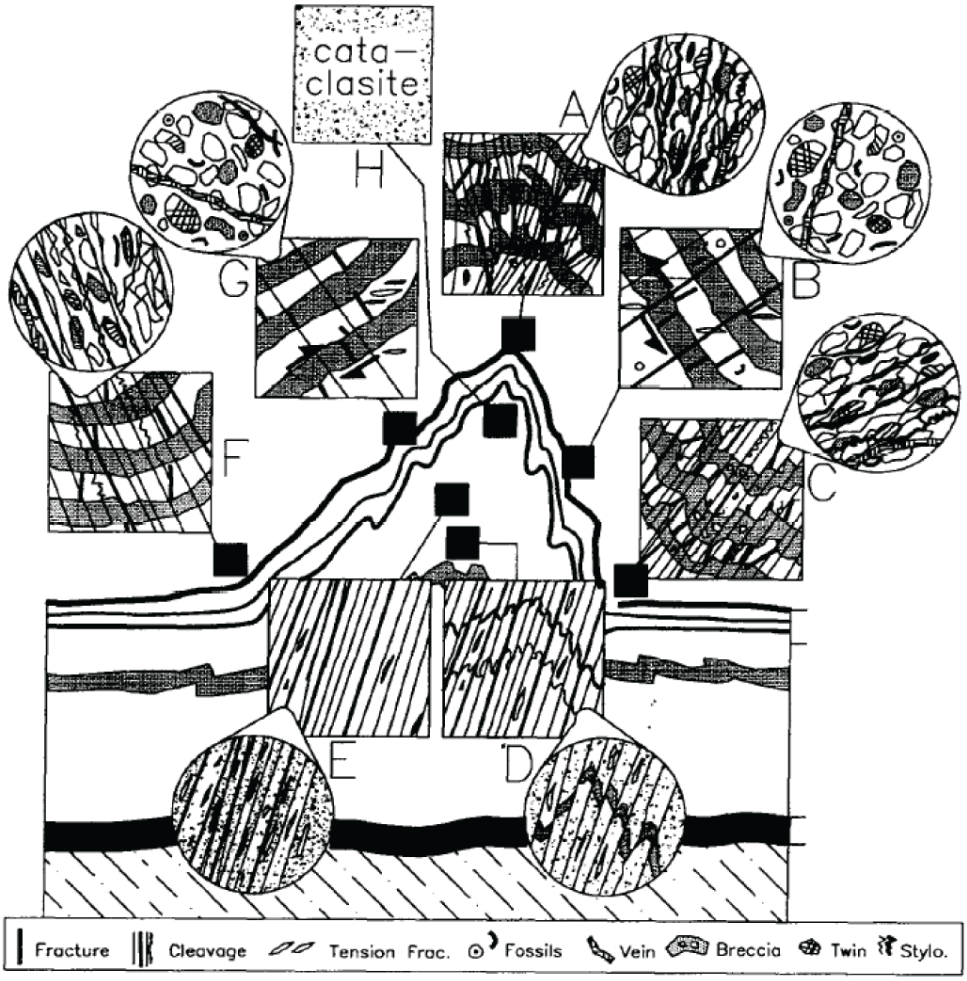

Fig. 6.3. Schematic diagram of a detachment fold illustrating the range of deformation styles that can occur within the competent and incompetent units of detachment folds. Boxes represent one metre of squared rock and the circles represent thin sections. The incompetent succession deforms though solution cleavage and cataclasis (panels D, E and H) within the fold core (from Homza and Wallace, 1997).

As the above examples show, seismic reflection data does not reflect the structural complexity associated with structural features below the scale of the seismic data. For example, on seismic reflection data the architecture of a fault plane is portrayed as a singular discontinuity, a significant oversimplification of the associated architecture recorded in outcrop. Outcrop examples reveal the structural complexity involved in the fault cores and adjacent damage zone of thrust faults (Fig. 6.4). These complex styles of thickening, as shown by outcrop studies, may provide a more realistic representation of how basal detachment successions composed of

argillaceous sediments thicken within cores of detachment folds and associated domal (diapiric) structures that appear to be cored by a mass of shale.

6.4.3 Salt detachment systems

Gravitational detachment systems that detach upon a basal detachment succession composed of salt have long been used as a comparison for mobile shale due to the similar deformation styles observed on seismic reflection data (e.g. Morley and Guerin, 1996). Rather than focussing on the rheological similarities and differences between salt and shale the gross architecture of brittle-ductile wedges could provide important insights into how basal detachment successions accommodate shortening. Detachment folds in the Canadian Rockies are cored by a basal detachment succession composed of salt, which reveals a similar deformation style to that imaged within the anticlinal cores in chapter 5 (e.g. Harrison, 1995). The basal detachment succession is weak in a relative sense as the overlying sedimentary succession is mechanically stronger. However, internally within the basal detachment succession is interbedded successions of dolostone and anhydrite, which are mechanically competent relative to salt with higher shear strengths (e.g. Fig. 1.3). Thickening of the basal detachment succession within the detachment fold cores has occurred though a combination of brittle and ductile deformation styles: thrust faulting, folding and a ductile thickening of the salt (Figs 5.13 and 6.5). The resultant deformation is controlled primarily by the rheology and the differing shear strengths of the individual lithologies (Harrison, 1995). Salt is an inherently plastic material with a shear strength close to zero (Fig. 1.3) and thickens in a ductile manner into fold cores to accommodate detachment fold amplification (Figs. 5.13 and 6.5). In contrast, the competent beds are those that have thickened by combinations of thrust faulting and thrust-related folding. The overall gross architecture resembles a series of passive duplexes (Figs. 5.13 and 6.4) (Banks and Warburton, 1986; Bonini, 2007).

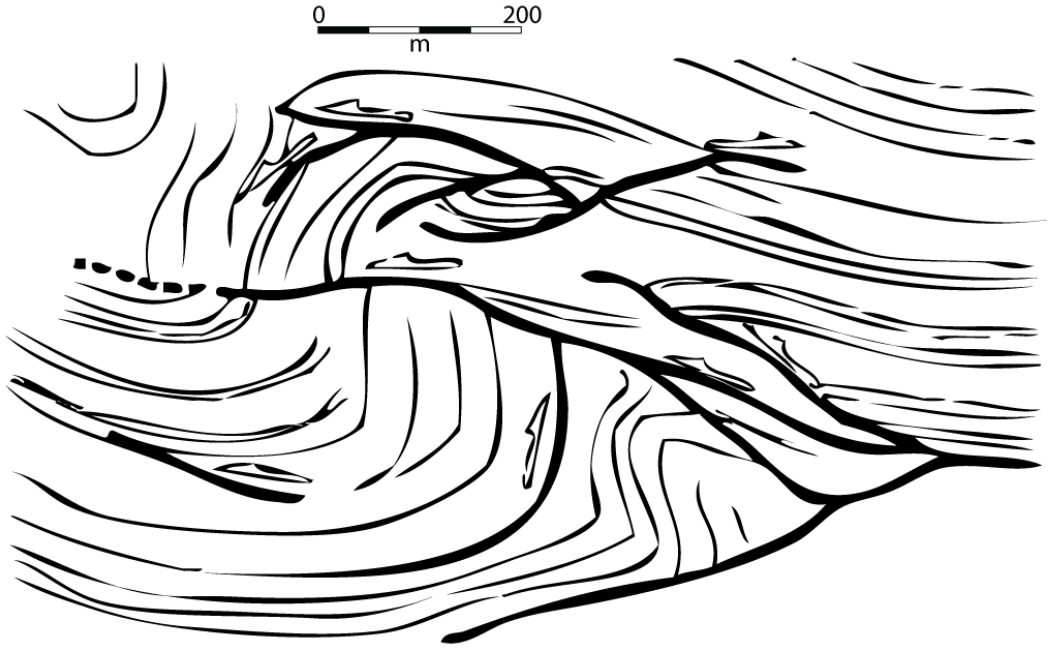

Fig. 6.4. Outcrop example of a thrust fault showing a complex damage zone defined by several fault strands, compacted and strained zones (from Iacopini and Butler, 2011).

Fig. 6.5. Structural cross-sections through a detachment fold and thrust belt from the Parry Islands from the Melville Island. The basal detachment succession is dominantly composed of mechanically weak salt and more competent interbeds. The contrasting strengths of the differing lithologies have caused a combination of brittle fault-related folding and a ductile thickening within the cores of detachment folds (from Harrison, 1995).

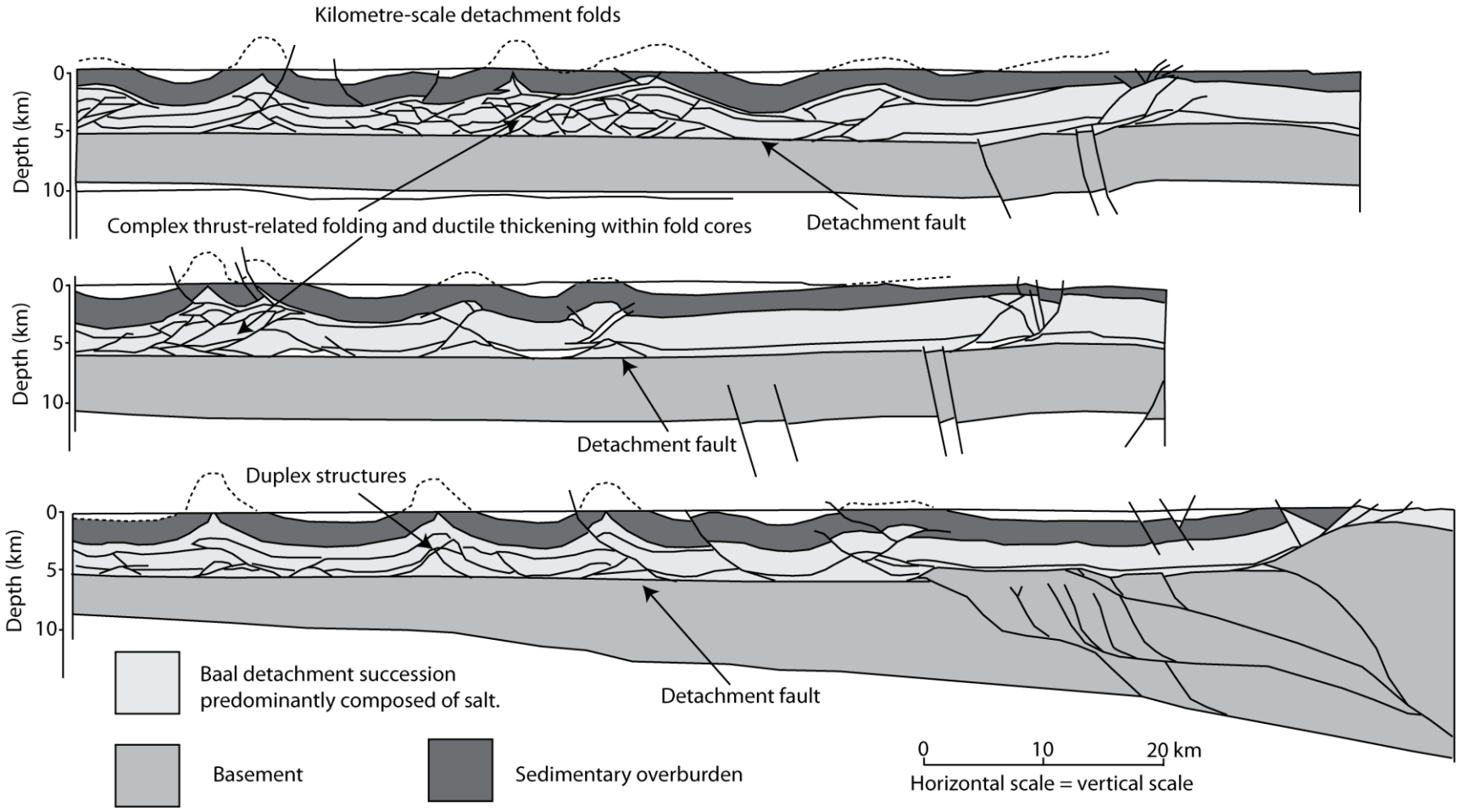
Kilometre-scale detachment folds
Depth (km)
0
5
10
Complex thrust-related folding and ductile thickening within fold cores
Detachment fault
Detachment fault
Duplex structures
Detachment fault
Baal detachment succession predominantly composed of salt.
Basement
Sedimentary overburden
0
10
20 km
Horizontal scale = vertical scale

6.5 Modelling studies

Analogue modelling is an important tool for furthering our understanding of how basal detachment successions evolve. Deformation styles that occur within the sedimentary overburden are generally well understood; however, as with studies based on seismic reflection data, the basal detachment succession is often overlooked in modelling studies. Previous modelling studies have focussed on analysing 1) deformation styles that occur within a sedimentary overburden, 2) the strength of a basal detachment succession (Costa and Vendeville, 2002; Bonini, 2007) 3) overpressure generation and fluid flow (e.g. Guerlais, 2000). Analogue models of frictional (strong) and ductile (weak) basal detachment successions show that the resulting deformation style in the sedimentary overburden can differ significantly as a function of strength of the basal detachment succession (Cotton and Koyi, 2001; Bahroudi, 2003; Bonini, 2007). Studies have shown that basal friction significantly influences structural vergence and progradation rates of overlying structures and sediments in the sedimentary overburden (Cotton and Koyi, 2000; Costa and Vendeville, 2002). Basal detachment successions that are ductile allow overlying sediments to prograde further oceanward and favour the development of both fore- and backthrusts in compressional settings as a horizontal σ_1 is favoured (e.g. Davis and Engelder, 1985; Bonini, 2007). The presence of a horizontal σ_1 favours the formation of fore- and backthrusts equally as both thrust sets would have similar fault dips, and so an equal amount of shortening can be accommodated for a corresponding increase in gravitational energy (Davis and Engelder, 1985; Bonini, 2007). A frictional basal detachment succession favours an inclined σ_1 and the development of forethrusts is favoured (Bilotti and Shaw, 2005, Higgins et al., 2007).

Instead of having a purely ductile or frictional basal detachment succession at the base of the modelling setup it would be intriguing to see if interlayered brittle-ductile materials can replicate the combination of brittle and ductile deformation styles that have been observed in chapters 4 and 5. In particular it would be of interest to analyse the effect that a brittle-ductile multilayer has on the deformation styles within a prograding overburden.

Modelling studies that attempt to capture the magnitude of overpressure generation and fluid migration pathways in the subsurface can potentially reveal insights into mobile shale mechanics. Integrating borehole data into models to predict the magnitude of overpressure within a shale tectonic province could reveal when sediments become liquidized and/or hydraulic fracturing is likely to occur. Modelling of overpressure and fluid migration pathways in the Barbados accretionary prism has been performed by Guerlais (2000) who shows that the highest levels of overpressure develop close to the depth at which the basal detachment succession is present (Figs. 6.6 and 6.7). Sediments within the basal detachment succession develop the highest levels of overpressure, which is in agreement with other studies where gravitational detachment occurs on basal detachment successions composed of overpressured, argillaceous sediments (e.g. Badri et al., 2000; Corredor et al., 2005; Moscardelli et al., 2006; Morley, 2009), and is in agreement with sparse borehole data from these settings (e.g. Fig. 1.3).

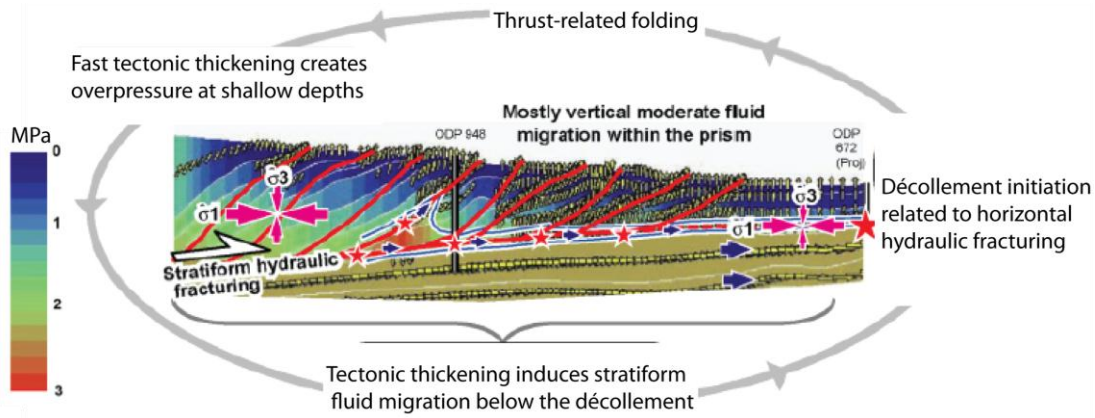

Fig. 6.6. Model of overpressure generation and fluid migration pathways within the Barbados accretionary prism. Small yellow arrows within the sedimentary overburden and larger blue arrows within the basal detachment succession represent fluid migration pathways. The highest levels of overpressure are generated close to the master detachment fault. Sedimentary loading induces a lateral migration of fluids within the basal detachment succession whereas fluid migration within the sedimentary overburden is restricted to individual fault blocks (from Deville et al., 2010, originally from Guerlais, 2000).

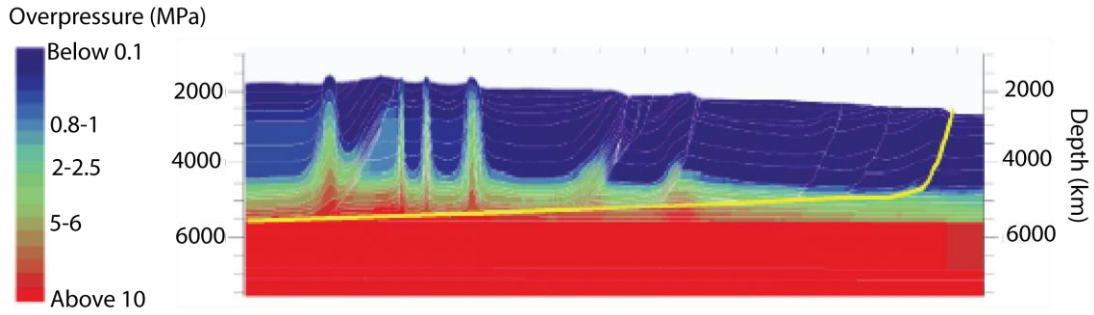

Fig. 6.7. Simulation of fluid migration in the south Barbados accretionary prism (from Deville et al., 2010, originally from Guerlais, 2000). The highest levels of overpressure are generated just above the master detachment fault (marked in yellow) and within the basal detachment succession as a consequence of sediment loading.

6.6 Further data

This study would have greatly benefitted from well log data and sediment cores through the basal detachment succession of the Niger Delta. This could have enabled the lithological types, facies and deformation styles to be determined more accurately. Throughout this study there was only limited access to well data with seismic velocities and some biostratigraphic data, which had to remain confidential and could not be included. Wireline data would have also been a useful addition to analyse at what depth overpressure develops within the sedimentary column, the magnitude of overpressure within the basal detachment succession and how the magnitude of overpressure varies throughout the basal detachment succession. Porosity data would have improved the estimates of vertical expansion undergone by the section during the decompaction process and provide estimates on the degree of undercompaction within the basal detachment succession. Unfortunately obtaining sediment cores from a basal detachment successions composed of overpressured sediments is a major drilling hazard and so no cores are likely to be obtained from these types of successions in the near future.

In addition, this study would have also benefitted from having the ability to depth convert 3D seismic volumes from an accurate 3D velocity model developed from

stacking velocities that are acquired with acquisition of the 3D seismic data. The boreholes utilised from which interval velocities were obtained do not penetrate the basal detachment succession because of the drilling hazards that they pose. A 3D velocity model would significantly reduce the uncertainty and therefore the error that was introduced when assigning interval velocities to overpressured seismic intervals when depth converting. This would have removed the need to extrapolate interval velocities from the nearest available boreholes or using 2D velocity models developed from stacking velocities for other regions of the Niger Delta (e.g. Morgan, 2003). This is of particular relevance to chapter 5 where depth conversions were performed using a uniform seismic velocity for the whole cross section as a consequence of the errors being introduced during the depth conversion process (section 2.9). A depth converted seismic volume would give a true realistic, representation of the structural geometries and would provide accurate comparisons to their time equivalent sections.

Access to 3D seismic coverage through the central sections of the western and southern lobes of the Niger Delta where the basal detachment succession is at its thickest would have been beneficial to the analysis of the mobile shale concept. The concept of mobile shale was developed where basal detachment successions were at their thickest and sedimentation rates were that their highest (e.g. Bruce, 1973). It would have been useful to analyse whether the thickness of the basal detachment succession itself influences the deformation style that occurs within the succession.

6.7 Redefinition of mobile shale

One of the resounding questions related to the concept of mobile shale is whether sediments within basal detachment successions are behaving as fluids (e.g. as a type of sediment-water mixture) or whether movement within this type of seismic facies occurs through brittle processes. Firstly, the possibility of widespread liquefaction will be considered. To induce liquefaction the pore-fluid pressure must be approaching lithostatic pressure (Maltman and Bolton, 2003). However, hydraulic failure should occur before pressures reach this level. A common criterion for

hydraulic failure is that failure occurs at 80% of the total lithostatic stress (Nygard et al., 2006). This consideration is of particular importance within the proximal (extensional) settings of deltas where the minimum effective stress is not vertical and so pore-fluids cannot sustain lithostatic pressures. This opposes mobile shale mechanics where the withdrawal of ductile shale as hydraulic failure should occur prior to liquefaction, which would allow the excess pore-fluid pressure to dissipate and mobility would cease. For thick accumulations of shale to liquefy and behave as a fluid it implies that the minimum effective stress within the sedimentary overburden is unusually high (near lithostatic pressure) and that pore-fluid pressures lie just beneath the fracture gradient. Both of these possibilities could explain why hydraulic failure would not occur within a seismic facies occupied by mobile shale; however, both possibilities seem unlikely. This leads one to consider if basal detachment successions that are composed of mobile shale at the base of deltas, which are unable to dewater as plausible interpretations.

Secondly, critical state deformation (section 1.5.2.1) is only applicable to perfectly plastic homogeneous accumulations of shales (Maltman, 1994; Maltman and Bolton, 2003). The tendency for shale to deform in a plastic manner is dependent on the organic carbon content and the amount of clay minerals within its matrix (Booth and Dahl, 1986; Maltman, 1994). For basal detachment successions composed of fine-grained, argillaceous sediments to be able to behave in a perfectly plastic manner they will need to contain over 50% clay minerals and a large amount of organic content (Maltman, 1994). Studies on the influence of organic carbon content on the deformation style of shale have shown that a 1% increase in organic carbon content can lead to a 14% increase in plastic limit (Booth and Dahl, 1986; Maltman, 1994). As highlighted in section 1.3, although the term mobile shale is widely used in the literature basal detachment successions are actually composed of interbedded successions of clays, silts, sands and carbonates. The lithological variability within basal detachment successions implies that they are highly unlikely to be rheologically homogeneous with coarser grained sediments displaying less of a tendency to deform in a plastic manner, instead preferring to fracture (e.g. Nygard et al., 2006). The imaging of closely spaced thrust faults together with an apparent ductile thickening and thinning of beds in detachment fold cores (i.e. chapter 5),

shows that the basal detachment succession does not behave in a rheologically homogeneous manner. Interestingly, authors working on shale tectonic provinces do not invoke critical state deformation instead preferring the interpretation of liquefaction or movement in some form of sediment-water mixture (e.g. Morley, 2003). For the reasons outlined above large-scale plastic shearing at the critical state also seems an unlikely scenario.

This thesis has demonstrated that the style of deformation that occurs within the basal detachment successions is ultimately dependent on the pore-fluid pressure and lithological makeup. Although the basal detachment succession is mechanically weak the rheology and shear strength of individual beds that constitute basal detachment successions will exert a strong control on the resultant deformation style. A likely scenario is that the occurrence of ductile deformation (mobile shale) is likely to be restricted where areas of thick, homogenous, weak shales have been deposited and where high levels of overpressure have been able to develop, and may occur on a smaller scale as chapter 4 has suggested. Where alternating successions of sands and shales have been deposited each with differing mechanical properties the basal detachment succession will prefer to deform with a complex amalgamation of brittle and ductile deformation styles.

6.8 Future research

Numerous proposals have been made for the manner in which seismic intervals interpreted to be occupied by overpressured, mobile shales behave, but uncertainties regarding the exact nature by which overpressured sediments deform (move) remain. In particular, outstanding questions regarding the mobilization and associated transportation processes that occur within basal detachment successions composed of overpressured, argillaceous sediments are still unanswered. It is likely that the continuing improvement in the quality of 3D seismic reflection data will be critical in furthering our understanding into how basal detachment successions composed of overpressured argillaceous sediment deform. A reappraisal of many shale tectonic provinces with high-quality 3D seismic data in conjunction with well data would be

advantageous to reassess the dependency of deformation style on the mechanical properties of the basal detachment succession. In addition it would be useful to see whether mobile shale seismic facies show coherent reflectivity, and, critically, whether any further evidence for large-scale brittle deformation styles is uncovered.

7 Conclusions

- In the up-dip extensional domain within a deltaic sequence, the architecture of a basal detachment succession of a listric growth fault system can be structurally complex. In places, deformation is controlled by more than one master detachment fault leading to the formation of vertically stacked master detachment faults.
- The basal detachment succession includes multiple detachments and master detachment faults upon which in extensional settings are listric growth faults and rotational fault blocks. Structures developed during early stages of extensional deformation can later become incorporated into the basal detachment succession with the formation of a new master detachment fault, which cuts-up through stratigraphy, splaying upwards from the pre-existing master detachment fault.
- The formation of new detachments is probably driven by changes in the distribution of overpressured pore-fluids and the presence of mechanically weak layers.
- In down-dip compressional settings the relative timing between deformation that occurs in the sedimentary overburden and within the basal detachment succession in some cases can be constrained though the interpretation of growth and stratal packages. Deformation within the basal detachment succession was found not to be always coeval with the amplification of fault-related folds within the overlying sedimentary overburden.
- Lateral redistributions of strata within the basal detachment succession that occurred after the amplification of fault-related folds within the sedimentary overburden could possibly affect the integrity of overlying fault-related folds. This could potentially cause failure of trap integrity and seal breach leading to potential escape of hydrocarbon traps.
- In cases where the deformational style within the basal detachment succession cannot be clearly resolved using seismic reflection data, calculating the volume of shale that moved together with rate and duration that shale moved could provide insights into whether the succession is deforming by ductile or brittle deformation mechanisms.

- The structural style in down-dip compressional settings is characterised by a series of complex duplexes and ductile layers that display significant lateral variations in thickness. As a consequence deformation within the cores of detachment folds cannot necessarily be adequately represented by end-member models (e.g. detachment folds, fault-bend folds, fault-propagation folds) as the structural complexity is overly simplified or masked.
- The variability in the deformational response within the basal detachment succession is likely controlled by a variety of factors, which include 1) the distribution of overpressured pore-fluids, 2) the magnitude of overpressure, 3) variations in lithology.
- It is proposed that the basal detachment succession is better represented as a heterogeneous multilayered succession with individual beds exhibiting different deformation responses. Beds that fracture are likely to be relatively strong and those that deform in a ductile manner are probably relatively mechanically weak.
- Rheological plastic flows that involve a complete loss of shear strength probably do characterise a portion of the deformation style. Withdrawal of material within the basal detachment succession has lead to the development of shale welds.
- Ductile deformation appears to have preferentially occurred beneath the synclines of detachment folds and has occurred in conjunction with a brittle thickening of strata. This apparent ductility maybe a consequence of the vertical resolution of the seismic reflection data.
- Despite the overpressured signature of basal detachment successions composed of argillaceous sediments overpressure is not necessarily synonymous with wide-spread ductile deformation, as evidence for multiple examples of brittle deformation styles have been found within the Niger Delta. As a result, the term mobile shale is fundamentally misleading in implying the type and style of deformation that occurs within these successions.

8 Appendices

8.1 Appendix 1

This chapter includes a glossary of terms

List of symbols

Acoustic impedance	Defined by density and seismic velocity (Brown, 2004).
Agbada Formation	Lithologic unit of the Niger Delta. Overlies the Akata formation, and is composed of alternating successions of sands and shales and constitutes the sedimentary overburden in deep-water regions (Avbovbo, 1978).
Akata Formation	Lithologic unit of the Niger Delta. Composed of pro-delta argillaceous, siliciclastic sediments (clays, silts and sand stones) and some carbonate interbeds. (Often referred to as - or composed of - mobile shale) (Avbovbo, 1978).
Argillaceous sediments	Sediments that are clay-rich.
Basal detachment unit	Composed of mechanically weak overpressured, argillaceous sediments or salt and forms a regionally extensive décollement that underlies the sedimentary overburden.
Basal detachment succession	See basal detachment unit
Benin Formation	Lithologic unit of the Niger Delta. Overlies the Abgbada Formation and is composed of continentally sourced channels sands. Only present in landward regions (Avbovbo, 1978).

Cataclastic flow	A process that fractures and shears the rock. Breaking of the rock particles occurs by rotation and mechanical moving of the particles (Ramsey and Huber, 1997).
Compaction	Encompasses the mechanical and chemical processes that change the physical properties of sediments that occur during progressive burial (Mondol et al., 2007).
Critical state deformation	Continuous shear failure for homogeneous sediments that behave in a perfectly plastic manner at a particular combination of porosity, pore-fluid pressure (effective stress) and differential stress (Roscoe, 1970; Yassir, 1989).
Detachment	Describes the apparent depth that brittle deformation ceases to penetrate within a sedimentary succession or to mark the separation of brittle-ductile regimes at the point of the fault zone in lithospheric crustal models (Lister and Davis, 1989; Briggs et al., 2006).
Detachment fault	A shallow dipping bedding parallel fault that mechanically links up-dip extension to down-dip contraction and can separate brittle from ductile deformation styles. A detachment fault is identified by the soling of numerous fault planes within the sedimentary overburden where displacement on the faults becomes zero (Lister and Davis, 1989; Briggs et al., 2006).

Detachment fold	Forms at the tip of a propagating bedding parallel thrust fault. Displacement is transferred from the thrust tip into an overlying mechanically weak detachment layer and induces buckling within an overriding mechanical competent layer (Jamison, 1987).
Detachment level	Refers to a basal fault (typically bedding parallel) along which numerous fault planes sole and separates brittle deformation styles from undeformed layers at the point of detachment (Briggs et al., 2006).
Detachment system	Describes the gross thin-skinned deformation style of a gravity-driven tectonic province where structural detachment occurs on a basal succession of overpressured argillaceous sediments or salt.
Diapir	Related to the presence of low reflectivity, chaotic discontinuous seismic reflections that on mass appear to rise into overlying laterally continuous reflections (Morley, 2003)
Differential stress	The difference between the maximum (σ_1) and minimum (σ_3) principal stress.
Disequilibrium compaction	A process that causes pore-fluids to become overpressured due to rapid burial of overlying sediments. Pore-fluids are unable to escape with burial and the lithostatic load is imposed onto the pore-fluids generating the overpressure.

Ductility	Describes the capacity of a material to a substantial strain without the tendency fracture (Rutter, 1986).
Effective stress	The proportion of an applied load that is sustained by the mineral skeleton (Terzaghi, 1923).
Fault-bend fold	Characterised by an upper and lower detachment level as a consequence of the propagating fault plane cutting-up section to the next mechanically incompetent layer (Suppe, 1983).
Fault-propagation fold	Related to a ramp in by a propagating fault plane where displacement at the upper tip line of the propagating fault tip is accommodated by folding (Suppe, 1985).
Fluidized flow	The entrainment of sediments within a flow where the moving sediment particles are supported by the upward motion of displaced pore-fluids (Maltman, 1994).
Fluid pressure ratio	The amount of excess pressure over the normal fluid pressure. Defined by the pore-fluid pressure / total burial pressure (Bilotti and Shaw, 2005).
Gravity gliding	Refers to sliding sedimentary strata where the majority of deformation is by translation (Schultz-Ela, 2001).

Gravity spreading	Refers to sedimentary strata that are collapsing vertically and extending laterally above a detachment surface (Schultz-Ela, 2001).
Hydraulic failure	Occurs when the pore-fluid pressure exceeds the minimum stress and tensile strength of the rock.
Hydrostatic pressure	The pressure exerted per unit area by the weight of a column of water to a given depth.
Incompetent successsion	A succession composed of mechanically weak strata typically overpressure argillaceous sediments or salt.
Liquefaction	Refers to the state within which sediments are entirely supporting an applied load through their pore-fluids. When in this state sediments have lost their ability to transmit a shear stress and effectively behaves as a fluid (Maltman, 1994).
Listric fault	A curved fault plane whose dip decreases with increasing depth. Listric normal fault contain a rollover anticline in adjacent hanging wall (Gibbs et al., 1984).

Master detachment fault	A kilometre-scale detachment fault that exerts the main control on hanging wall deformation. Can accommodate over tens of kilometres of displacement and mechanically links extension and contraction in gravitational settings (Lister et al., 1986).
Mobile shale	A term used to capture the large-scale, ductile deformation of thick accumulations of dominantly argillaceous sediments.
Normally consolidated sediments	Sediments that have been able to expel their pore-fluids during burial to remain at hydrostatic pressure (Maltman and Bolton, 2003).
Normal stress	The component of stress that acts perpendicular to a plane.
Overconsolid-ation	The ratio between the maximum effective vertical stress that sediments have been subjected to and the present effective vertical stress (Nygard et al., 2006).
Overpressure	Pore-fluid pressure that exceeds the hydrostatic pressure (Dickinson, 1953).

Plastic deformation	Where grains are internally distorted through dislocation of the crystal lattice (Rutter, 1986).
Pore-fluid pressure	The proportion of an applied load that is sustained by the pore-fluids (Terzaghi, 1923).
Regional hanging wall	Refers to all strata lying above an active master detachment fault.
Sediment mobilization	A term used to describe a process that involves a partial or complete loss of shear strength within a rock volume.
Sedimentary overburden	The sedimentary succession that overlies the basal detachment succession and is undergoing gravitational failure (e.g. Rowan et al., 2004).
Shale	Mud-rich, fine-grained laminated sedimentary rocks that are fissile (Potter et al., 1980).

Shale consolidation	The time-dependent mechanical reduction in sediment volume, which is related to sediment permeability, expulsion of pore-fluids with burial, mean effective stress and the differential stress (Yassir, 1989; Maltman and Bolton, 2003).
Shale tectonics	The large-scale deformation of argillaceous and siliciclastic sediments including clays, muds, silts and sandstones
Shear strength	The measure of a material's ability to resist undergoing deformation in response to a shear stress.
Shear stress	The component of stress that acts parallel to a plane
Tensile strength	The measure of a material's ability to resist deforming in response to a tensile stress.
Thin-skinned deformation	Refers to the fact that the basement is not involved in deformation.

Shale touchdown	Occurs when mobile shale withdraws from between two lithological successions, leaving the two originally separate lithologies juxtaposed against each other, forming what is described as the touchdown (Morley, 2003).
Shale weld	See ‘shale touchdown’
Undercompact-ion	Describes the state where a rock volume has been unable to expel its pore-fluids with burial and so contains elevated porosities and pore-fluids (Rowan et al., 2004).

List of symbols

2D	Two-dimensional
3D	Three-dimensional
τ	shear stress
C	cohesion
σ_n	normal stress
ϕ	angle of internal friction
S	vertical stress
z	thickness
ρ	density
g	gravitational acceleration
Pp	pore-fluid pressure
λ	fluid pressure ratio
σ'	effective stress
p'	mean effective stress
σ'_1	effective maximum principal stress
σ'_2	effective intermediate principal stress
σ'_3	effective minimum principal stress
q	differential stress
Z	acoustic impedance
R	reflection coefficient
v	velocity

f	frequency
t	one-way travel time
V°	initial velocity (ms)
k	the rate of change in velocity with increasing depth
f	present day porosity
$f_\circ$	the surface porosity
c	porosity-depth coefficient (km^{-1})
(A_x)	area of the a deformed shape
(la)	average restored bed length
$\sigma' min_{ob}$	minimum effective stress within the sedimentary overburden
T_{ob}	tensile strength of the overburden
T_h	tensile strength of sediment that acts parallel to bedding
$\sigma' h$	effective horizontal stress
σ'_v	effective vertical stress
T_v	tensile strength of sediments normal to bedding

8.2 Appendix 2

This appendix expands upon the data and methodologies as detailed in chapter 2.

This appendix includes:

- TWT maps of the laterally key horizons in each of the 3D seismic data sets, shows the seismic characteristic of each of the reflections, highlights structural features and seismic artefacts (if present) within each survey area.

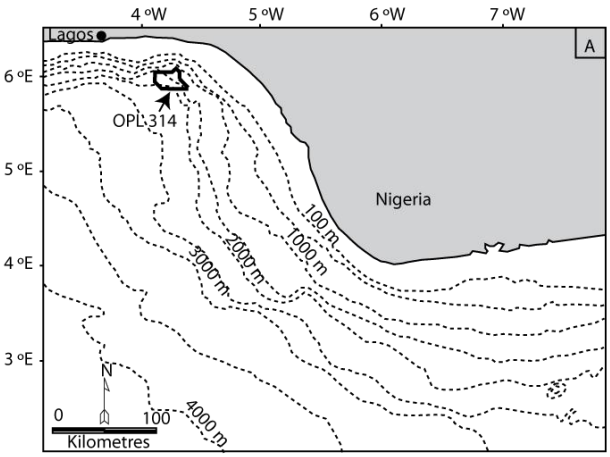

A) Location map of OPL 314 in the north-western Niger Delta.

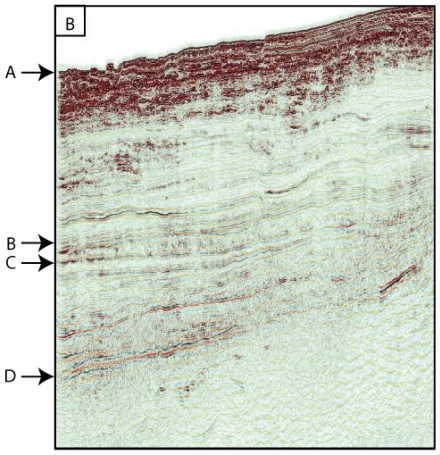

B) Seismic profile of the OPL 314 survey area. Labelled horizions are A = seabed, B= upper-Akata reflection, C = mid-Akata reflection, D = basement.

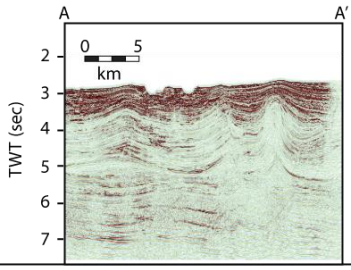

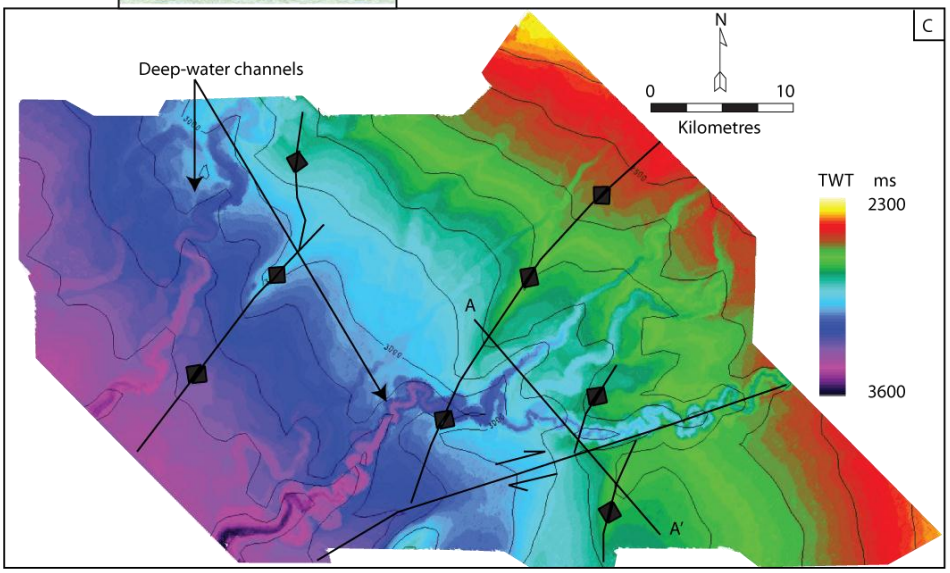

C) TWT map of the seabed with structural interpretation of features that are actively deforming the seabed. Detachment folds and a major dextral strike-slip fault are deforming the seabed. Contours are in100 ms intervals.

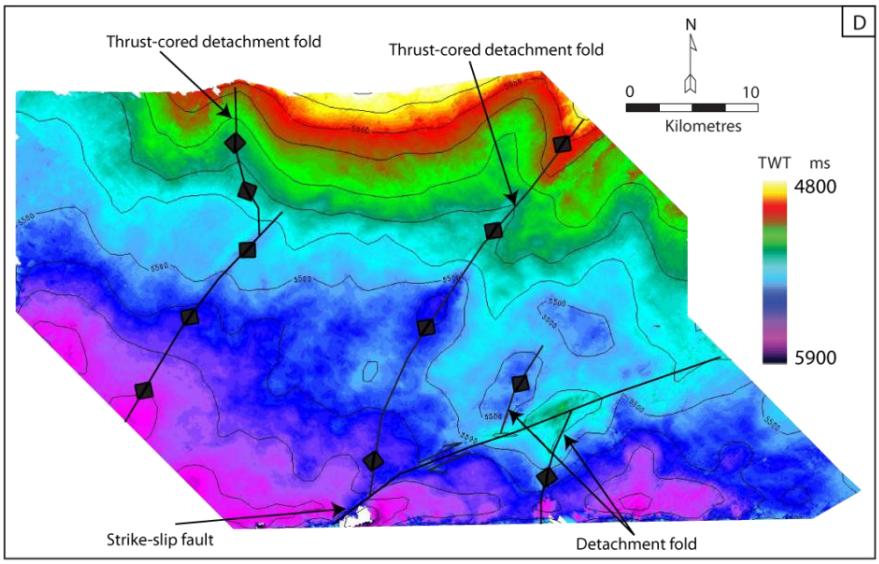

D) TWT map of the upper-Akata reflection with structural interpretation of compressional features. This reflection acts as a major detachment level for overlying structures inthe sedimentary overburden.

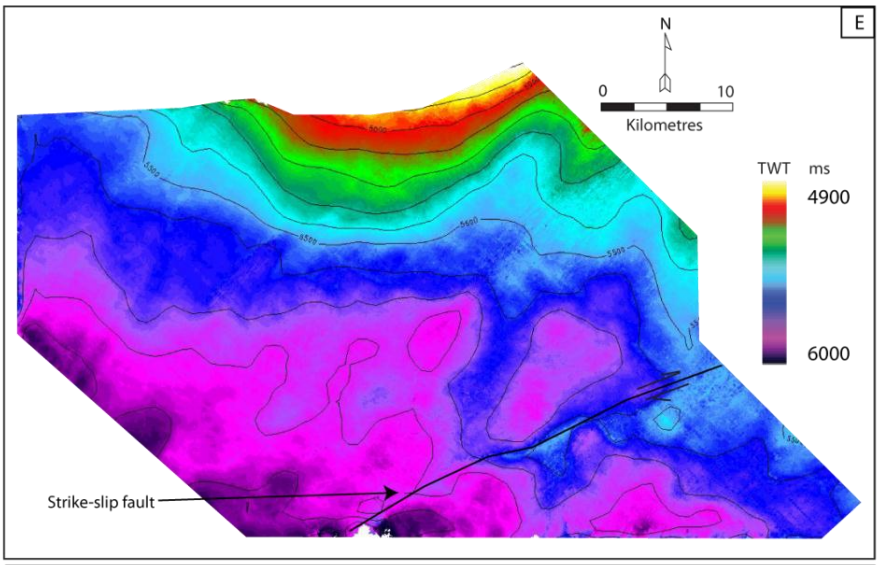

E) TWT map of the mid-Akata refecltion. The majority of deformation has detached upon the upper-Akata reflection apart from the major strike-slip fault which penetrates the basement. Small-scale thrust-related folds related to the compressional toes of slumps detach upon ths reflection.

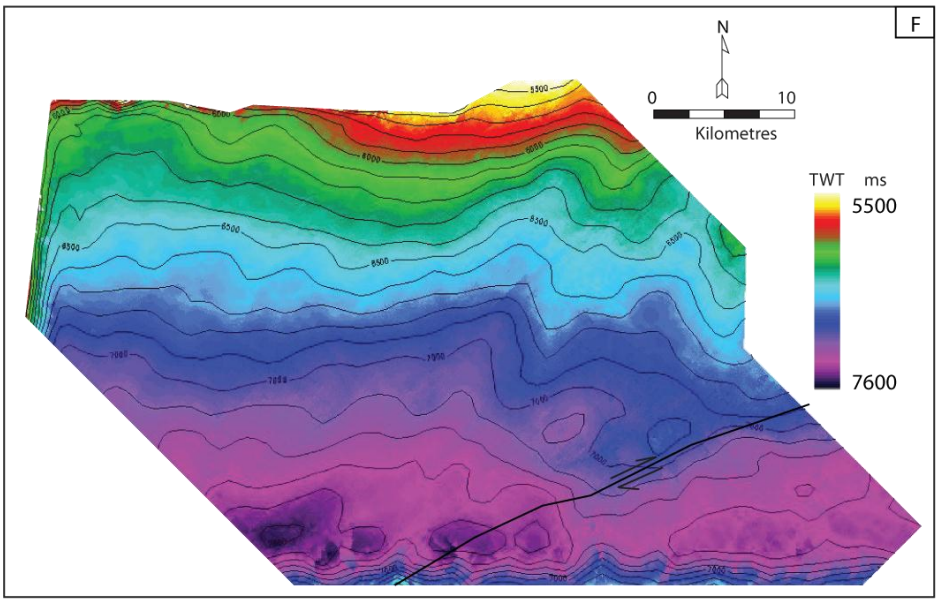

Fig. A1. A) Location map of OPL 314 in the north-western Niger Delta, B) seismic profile through the data set displaying the seismic characteristics of the data and C-F) TWT maps with structural interpretations of the key reflections.

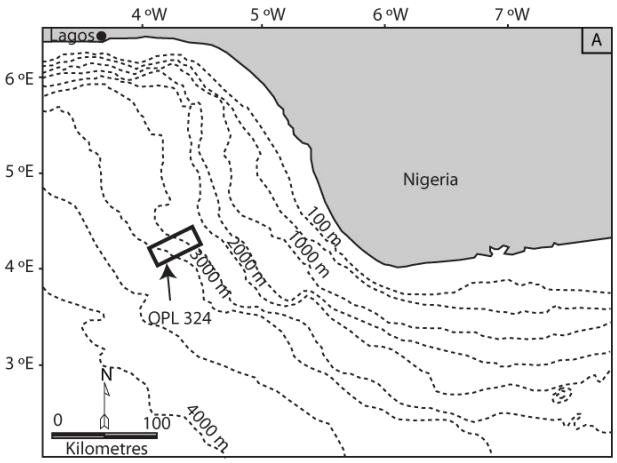

A) Location map of OPL 324 in the western Niger Delta.

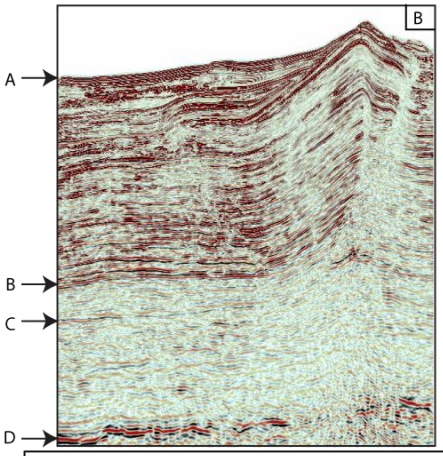

B) Seismic profile of the OPL 324 survey area. Labelled horizions are A = seabed, B= upper-Akata reflection, C = mid-Akata reflection, D = basement.

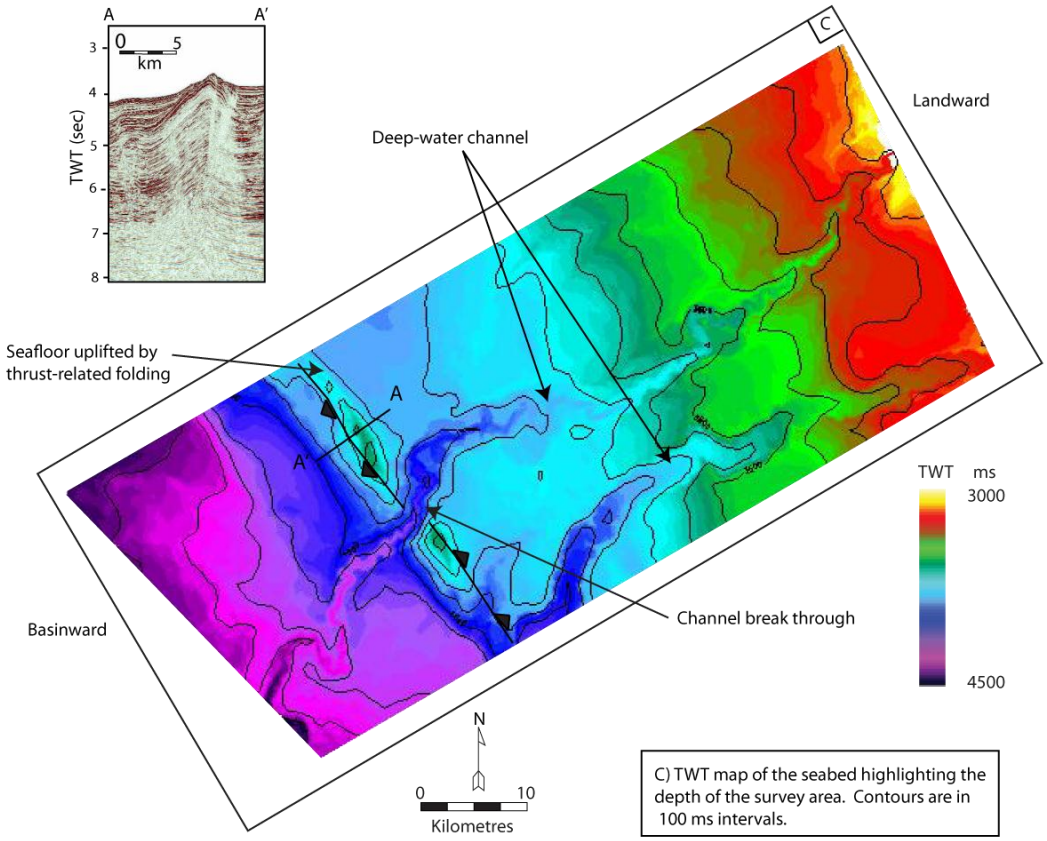

C) TWT map of the seabed highlighting the depth of the survey area. Contours are in 100 ms intervals.

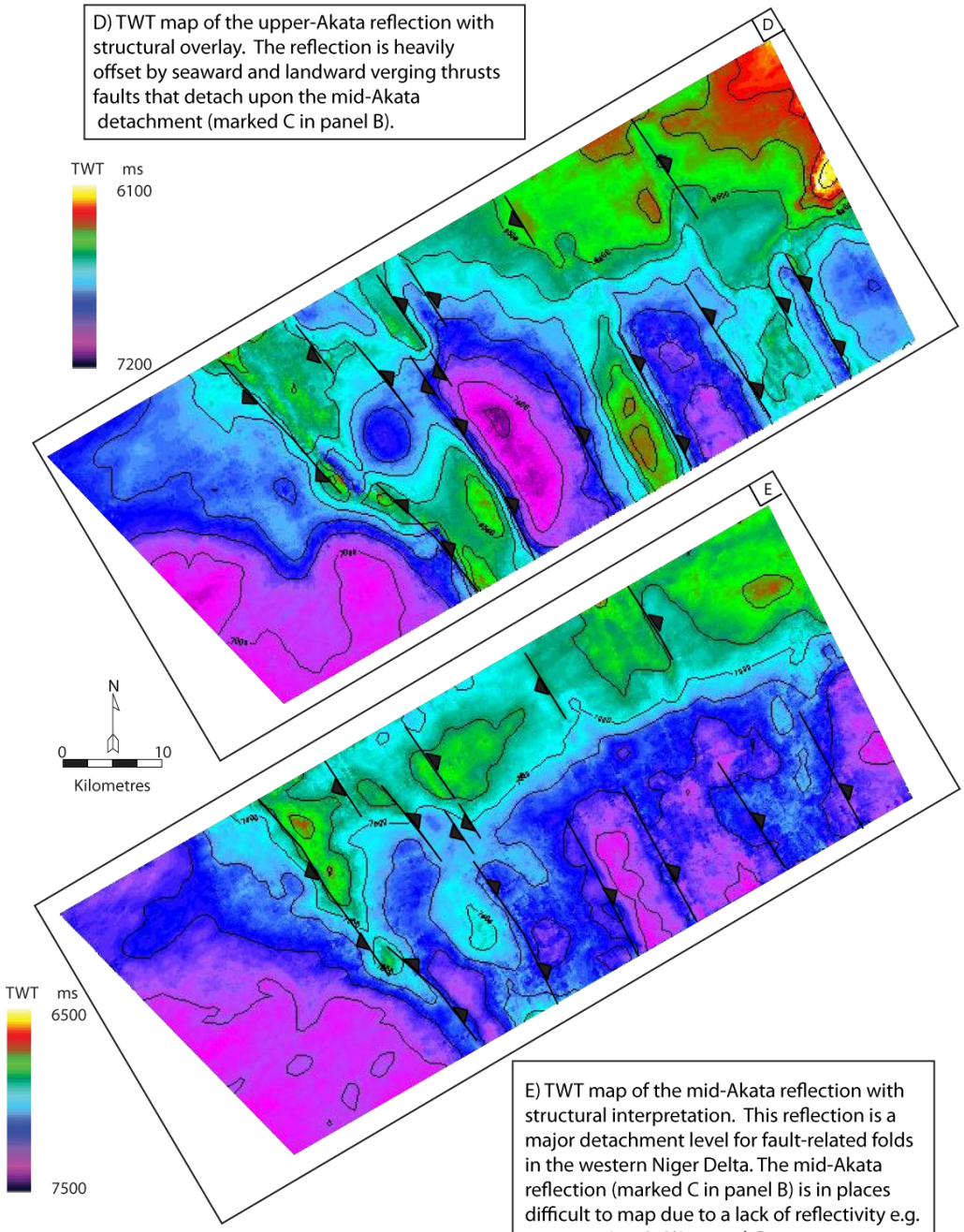

D) TWT map of the upper-Akata reflection with structural overlay. The reflection is heavily offset by seaward and landward verging thrusts faults that detach upon the mid-Akata detachment (marked C in panel B).

E) TWT map of the mid-Akata reflection with structural interpretation. This reflection is a major detachment level for fault-related folds in the western Niger Delta. The mid-Akata reflection (marked C in panel B) is in places difficult to map due to a lack of reflectivity e.g. cross-section A-A′ in panel C.

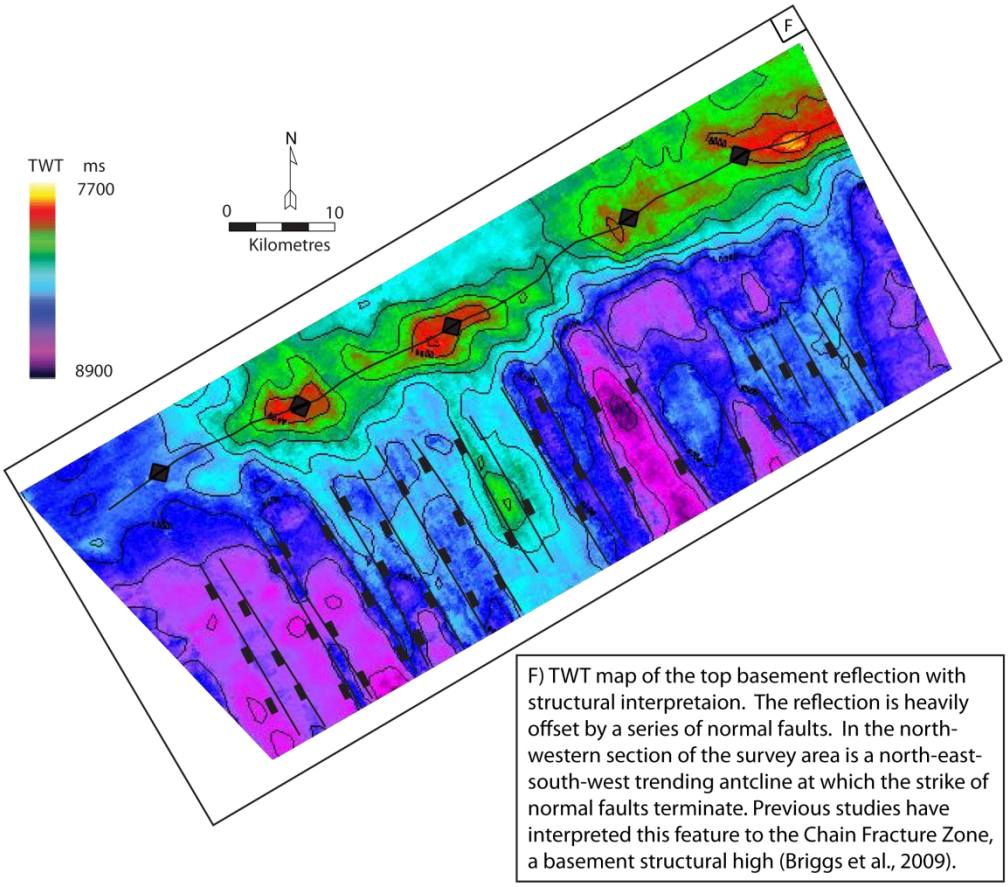

Fig. A2. A) Location map of OPL 324 in the western Niger Delta, B) seismic profile through the data set displaying the seismic characteristics of the data and C-F) TWT maps with structural interpretations of the key reflections.

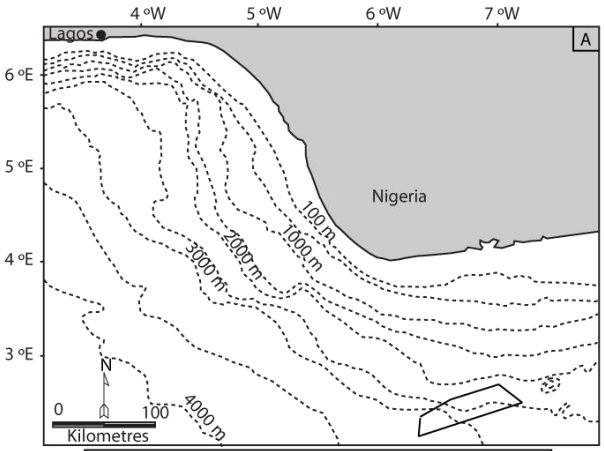

A) Location map of MC3D JDZ in the southern Niger Delta.

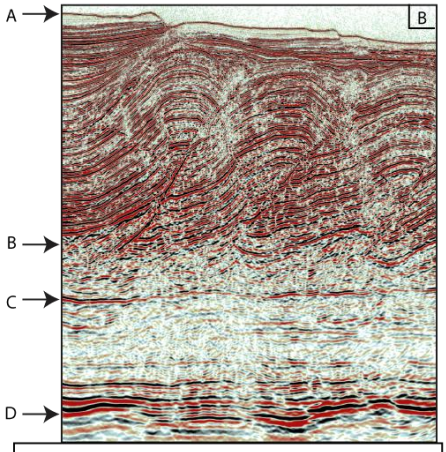

B) Seismic profile of the OPL 324 survey area. Labelled horizions are A = seabed, B= upper-Akata reflection, C = mid-Akata reflection, D = basement.

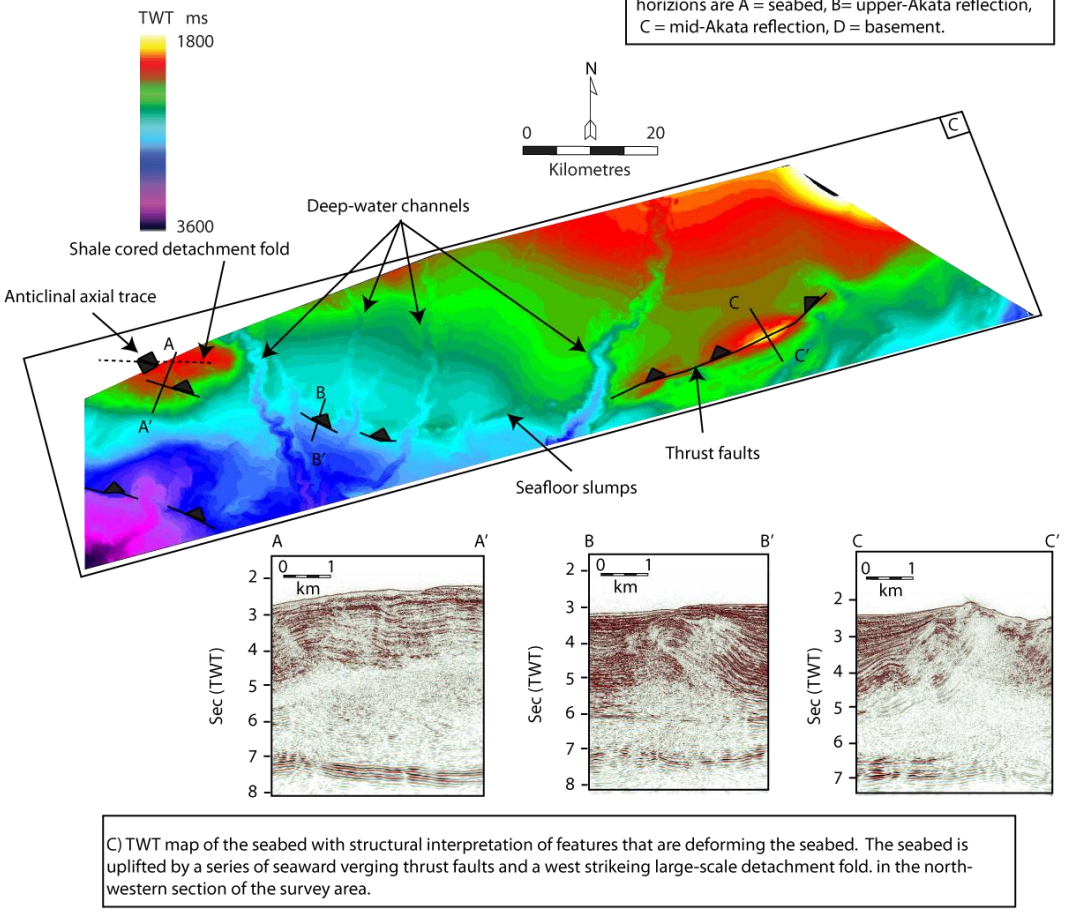

C) TWT map of the seabed with structural interpretation of features that are deforming the seabed. The seabed is uplifted by a series of seaward verging thrust faults and a west strikeing large-scale detachment fold. in the north-western section of the survey area.

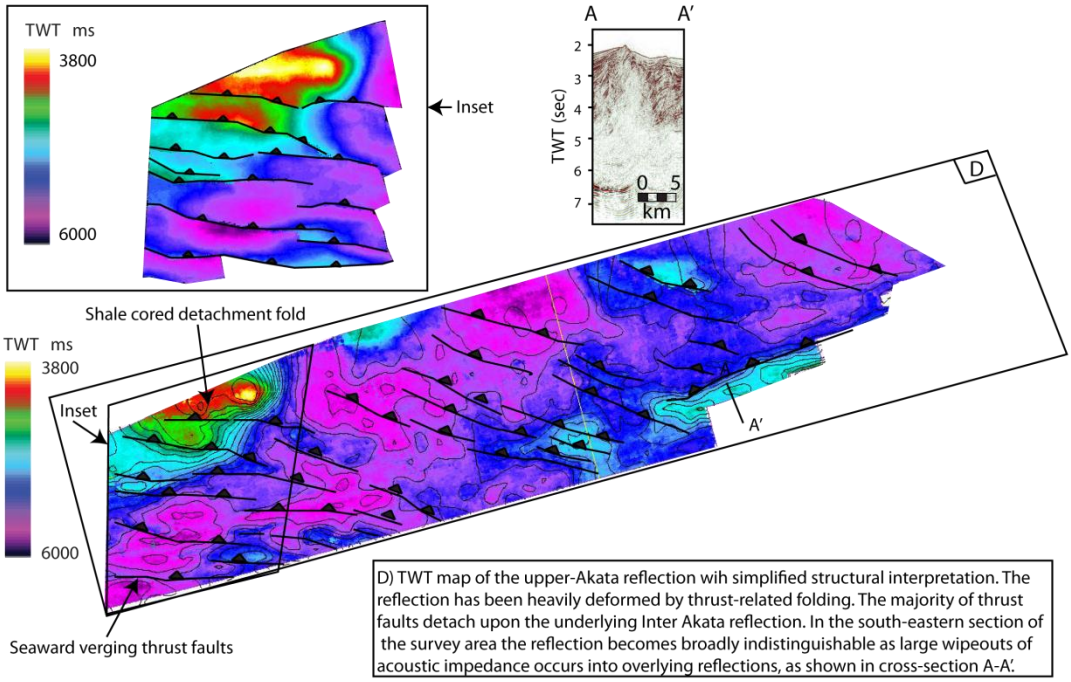

D) TWT map of the upper-Akata reflection wih simplified structural interpretation. The reflection has been heavily deformed by thrust-related folding. The majority of thrust faults detach upon the underlying Inter Akata reflection. In the south-eastern section of the survey area the reflection becomes broadly indistinguishable as large wipeouts of acoustic impedance occurs into overlying reflections, as shown in cross-section A-A′.

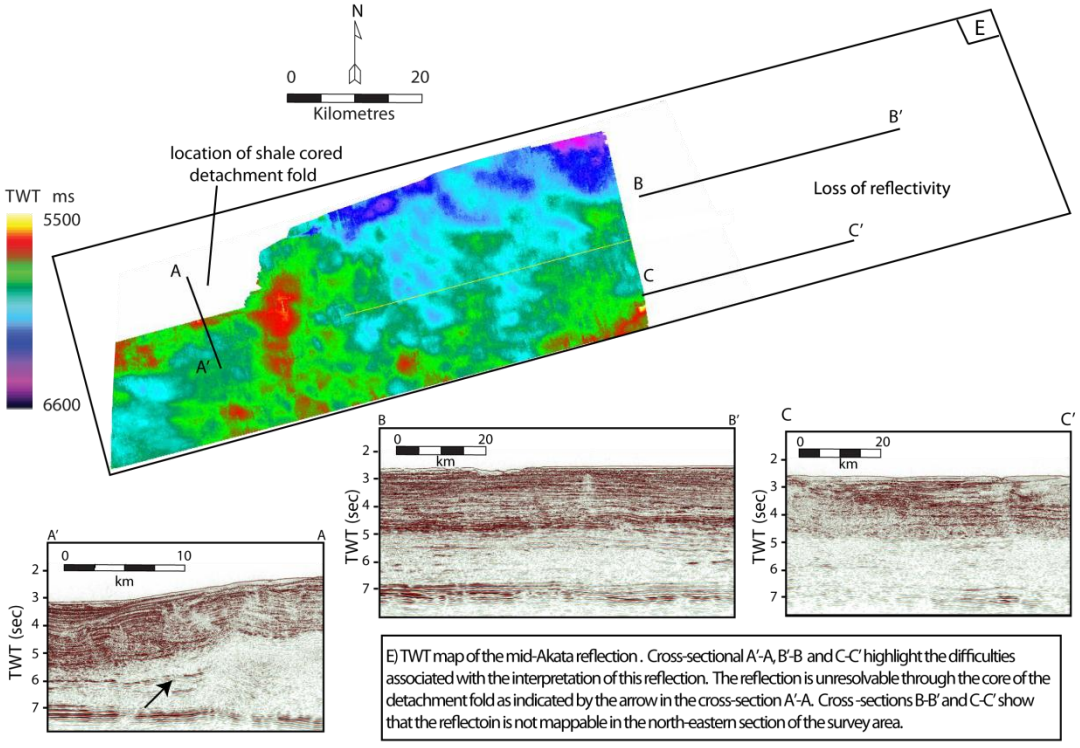

E) TWT map of the mid-Akata reflection . Cross-sectional A′-A, B′-B and C-C′ highlight the difficulties associated with the interpretation of this reflection. The reflection is unresolvable through the core of the detachment fold as indicated by the arrow in the cross-section A′-A. Cross -sections B-B′ and C-C′ show that the reflectoin is not mappable in the north-eastern section of the survey area.

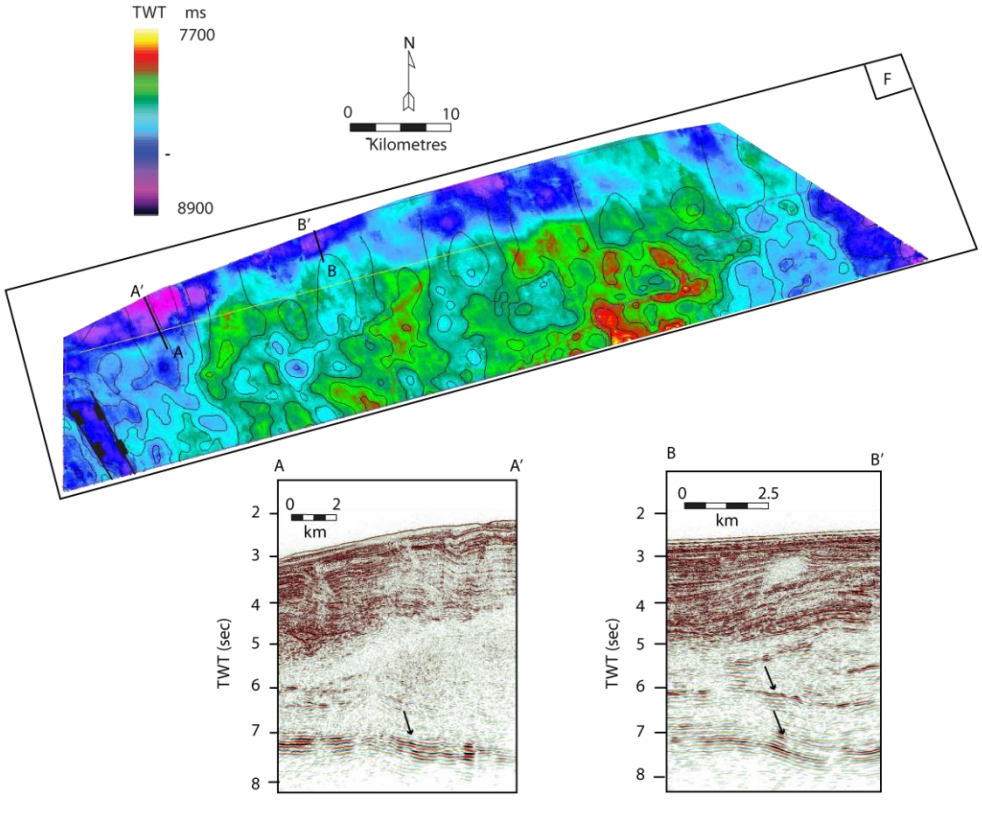

F) TWT map of the basement. The apparent synclinal depressions in the norh-western section of the survey area are the result of seismic "push down". A thickened succession of overpressured shale that has a low seismic velocity lies within the cores of overlying fault-related anticlines as shown by cross-sections A-A′ and B′B′. Arrows indicate the onset of reflections that have been pushed down.

Fig. A3. A) Location map of OPL 324 in the western Niger Delta, B) seismic profile through the data set displaying the seismic characteristics of the data and C-F) TWT maps with structural interpretations of the key reflections.

8.3 Appendix 3

This appendix provides supporting material for the in-house BG Group seismic data detailed in chapter 3.

This appendix includes a summary of

- Fault activity plots for the seismic profiles included in chapter 3

- A summary cartoon showing the development of a stacked detachment system.

Fig. A4. Fault activity plots for growth and post depositional faults in the sedimentary overburden. Plots were created with the assumption that differences between hanging wall and footwall growth strata relate to periods of fault slip upon individual faults. Fault activity plots in the following images are linked to seismic profiles shown in figures 3.5, 3.7, 3.9, 3.10 and 3.12.

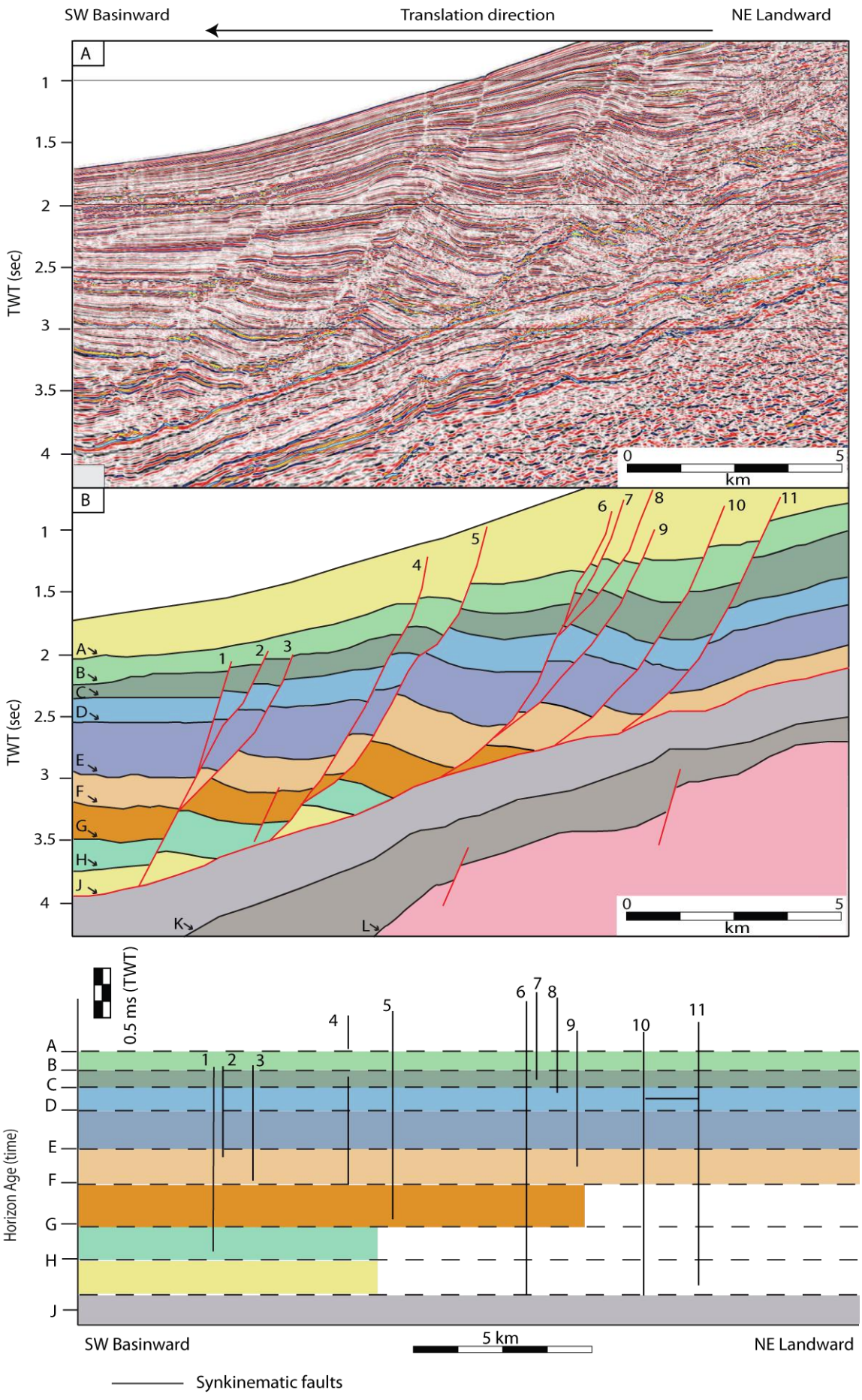
SW Basinward
Translation direction
NE Landward
A
B
TWT (sec)
1
1.5
2
2.5
3
3.5
4
0
5
km
A
B
C
D
E
F
G
H
J
K
L
1
2
3
4
5
6
7
8
9
10
11
0.5 ms (TWT)
Horizon Age (time)
5 km
SW Basinward
NE Landward
Synkinematic faults

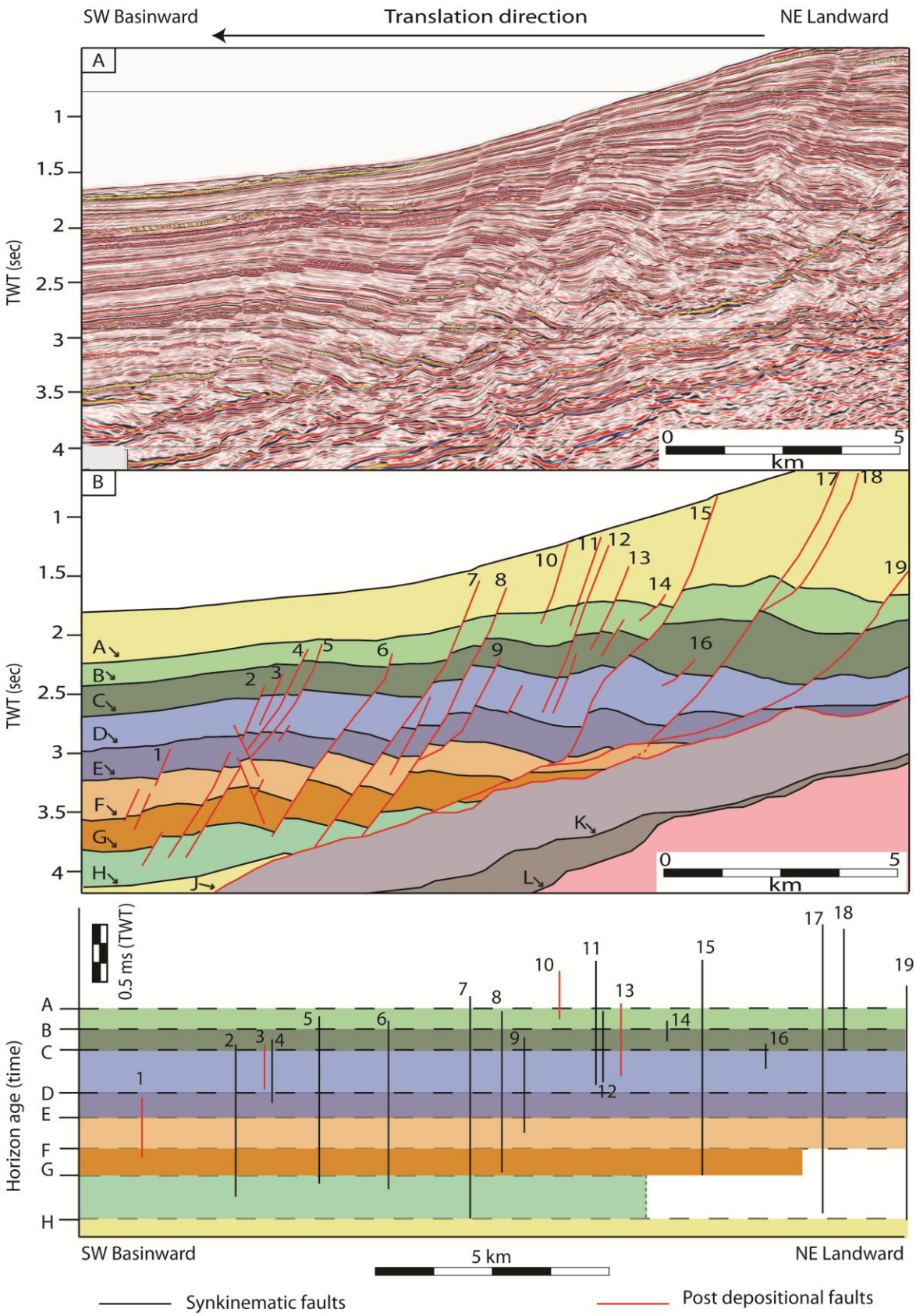
SW Basinward
Translation direction
NE Landward
A
B
TWT (sec)
1
1.5
2
2.5
3
3.5
4
0
5
km
A
B
C
D
E
F
G
H
J
K
L
1
2
3
4
5
6
7
8
9
10
11
12
13
14
15
16
17
18
19
0.5 ms (TWT)
Horizon age (time)
5 km
SW Basinward
NE Landward
Synkinematic faults
Post depositional faults

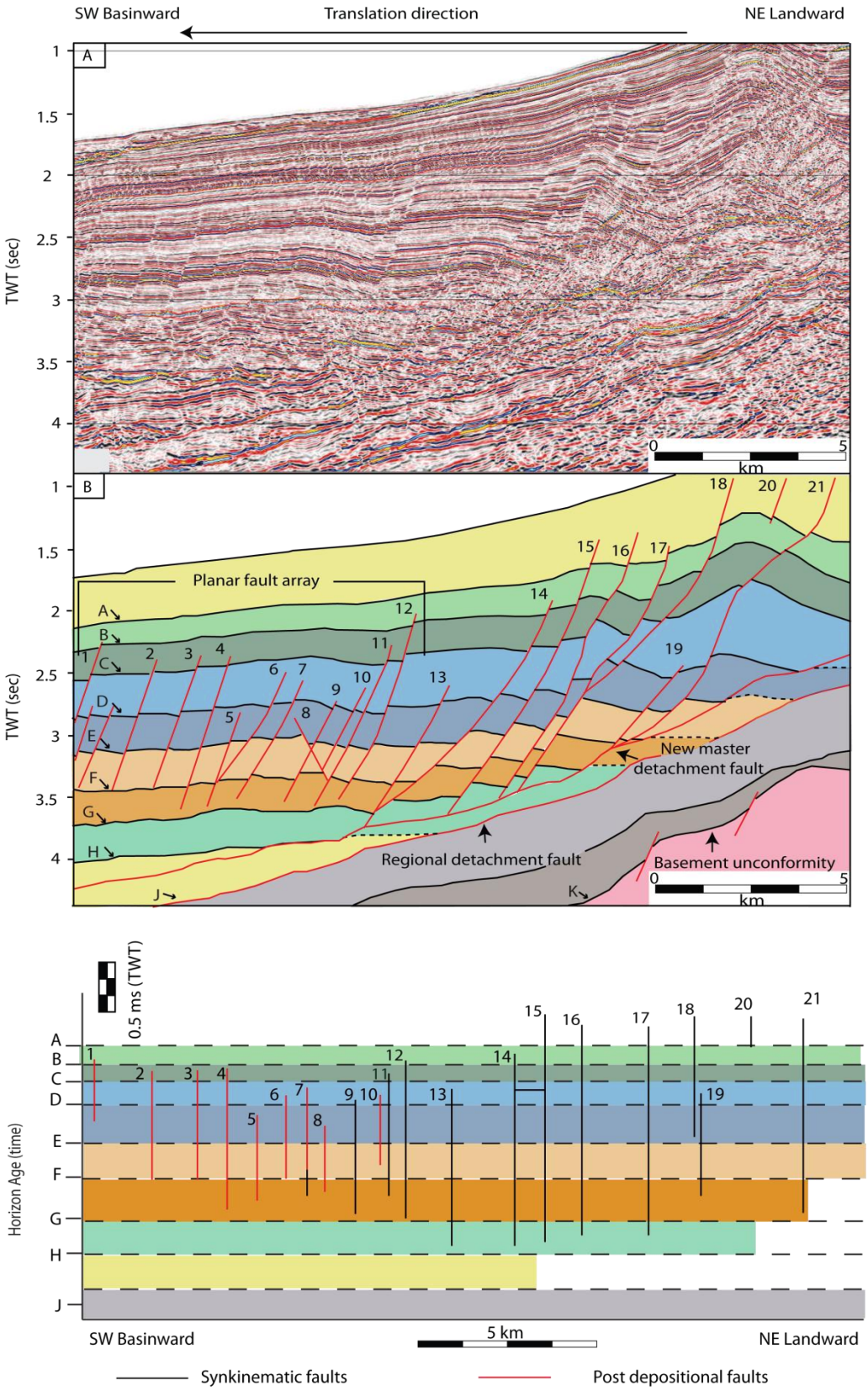
SW Basinward
Translation direction
NE Landward
A
B
TWT (sec)
Planar fault array
New master detachment fault
Regional detachment fault
Basement unconformity
0
5
km
0.5 ms (TWT)
Horizon Age (time)
5 km
Synkinematic faults
Post depositional faults

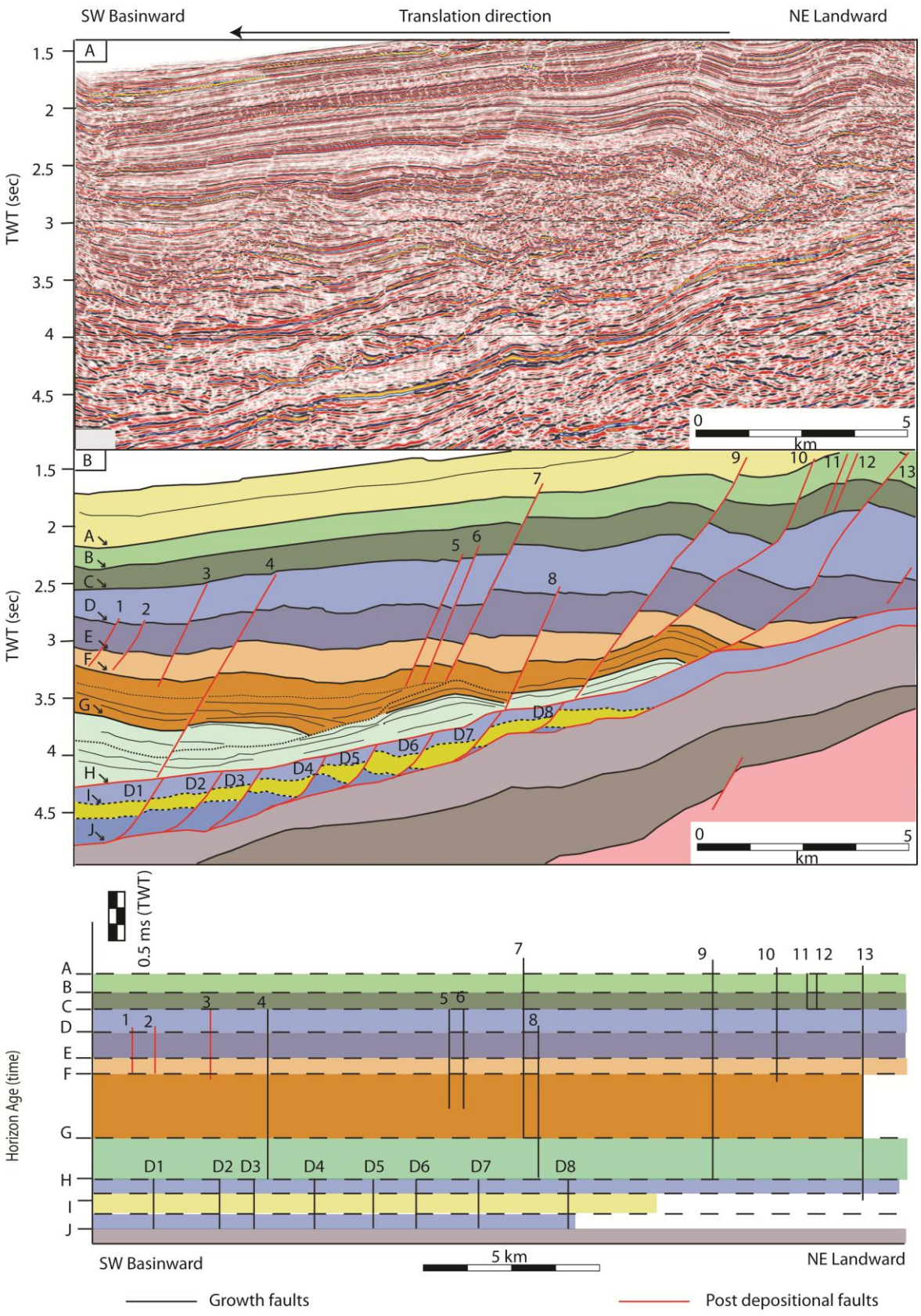
SW Basinward
Translation direction
NE Landward
A
B
TWT (sec)
1.5
2
2.5
3
3.5
4
4.5
0
5
km
A
B
C
D
E
F
G
H
I
J
D1
D2
D3
D4
D5
D6
D7
D8
1
2
3
4
5
6
7
8
9
10
11
12
13
0.5 ms (TWT)
Horizon Age (time)
5 km
Growth faults
Post depositional faults

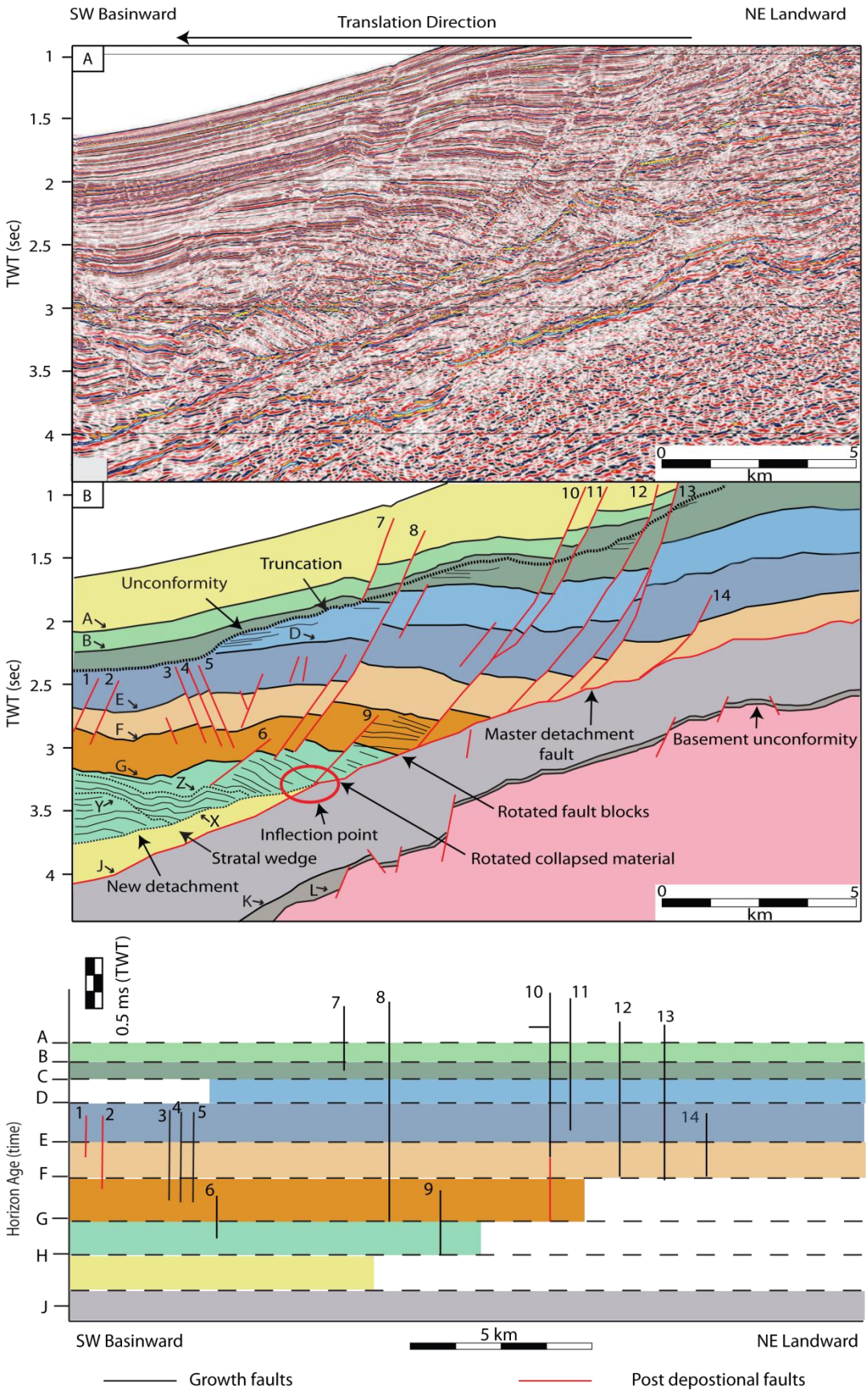
SW Basinward
Translation Direction
NE Landward
A
B
TWT (sec)
1
1.5
2
2.5
3
3.5
4
0
5
km
Unconformity
Truncation
Master detachment fault
Basement unconformity
Rotated fault blocks
Rotated collapsed material
Inflection point
Stratal wedge
New detachment
0.5 ms (TWT)
Horizon Age (time)
A
B
C
D
E
F
G
H
J
5 km
SW Basinward
NE Landward
Growth faults
Post depostional faults

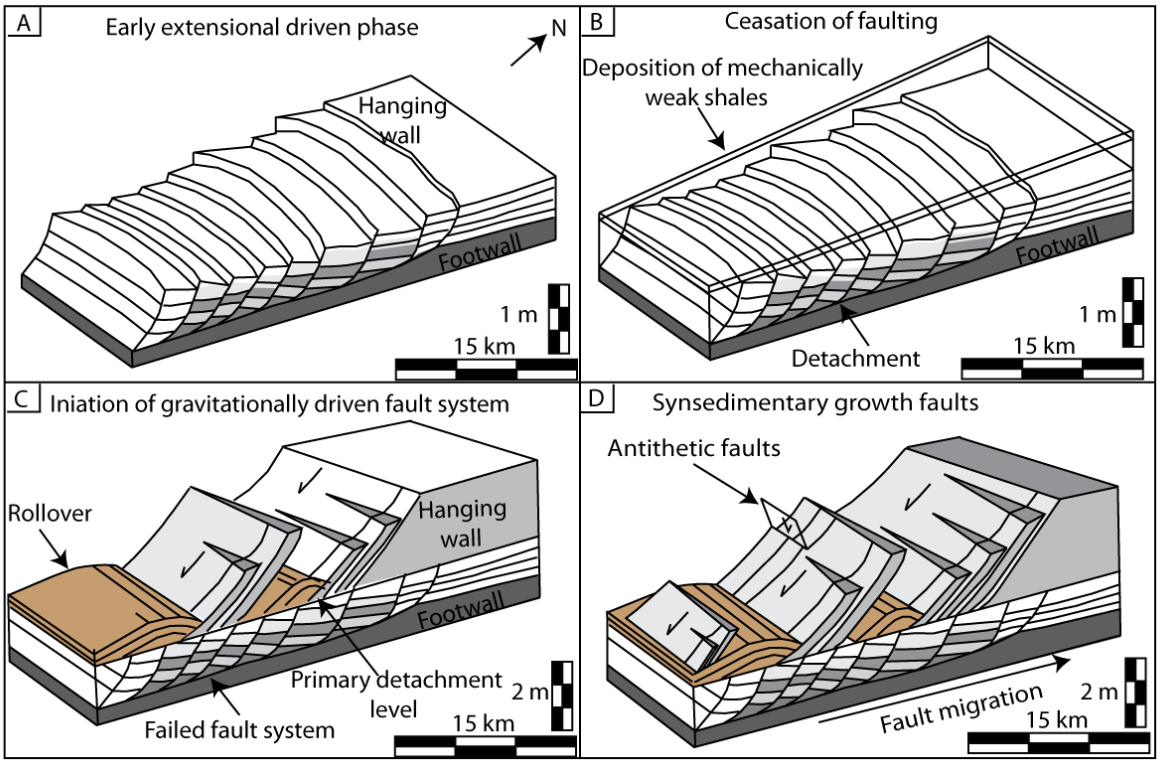

Fig. A5. Cartoon showing the preferred model for the evolution of the stacked detachment system in the north-western Niger Delta. A) An early stage of gravity-driven extension was potentially followed by B) cessation of deltaic progradation and deposition of mechanically weak clays. C) Gravitationally-driven extension then continued with the reinitiation of deltaic progradation and episodes of rapid deposition to from the present day geometries (D).

8.4 Appendix 4

This appendix provides supporting material for the research detailed in chapter 4.

The appendix includes:

- RMS amplitude maps of the upper- and mid-Akata reflection and of the basement.
- Isochron thickness maps of the upper- and lower Akata Formation.
- Depth conversion and sequential restoration of the shale weld (shale touchdown).
- Cross-sectional cartoon showing the structural architectures and geometries of the fault-related folding associated with the large-scale shale cored anticline.
- Davies et al. 2007 table 1.
- Flow diagram explaining how volumetric changes within the basal detachment unit were calculated.

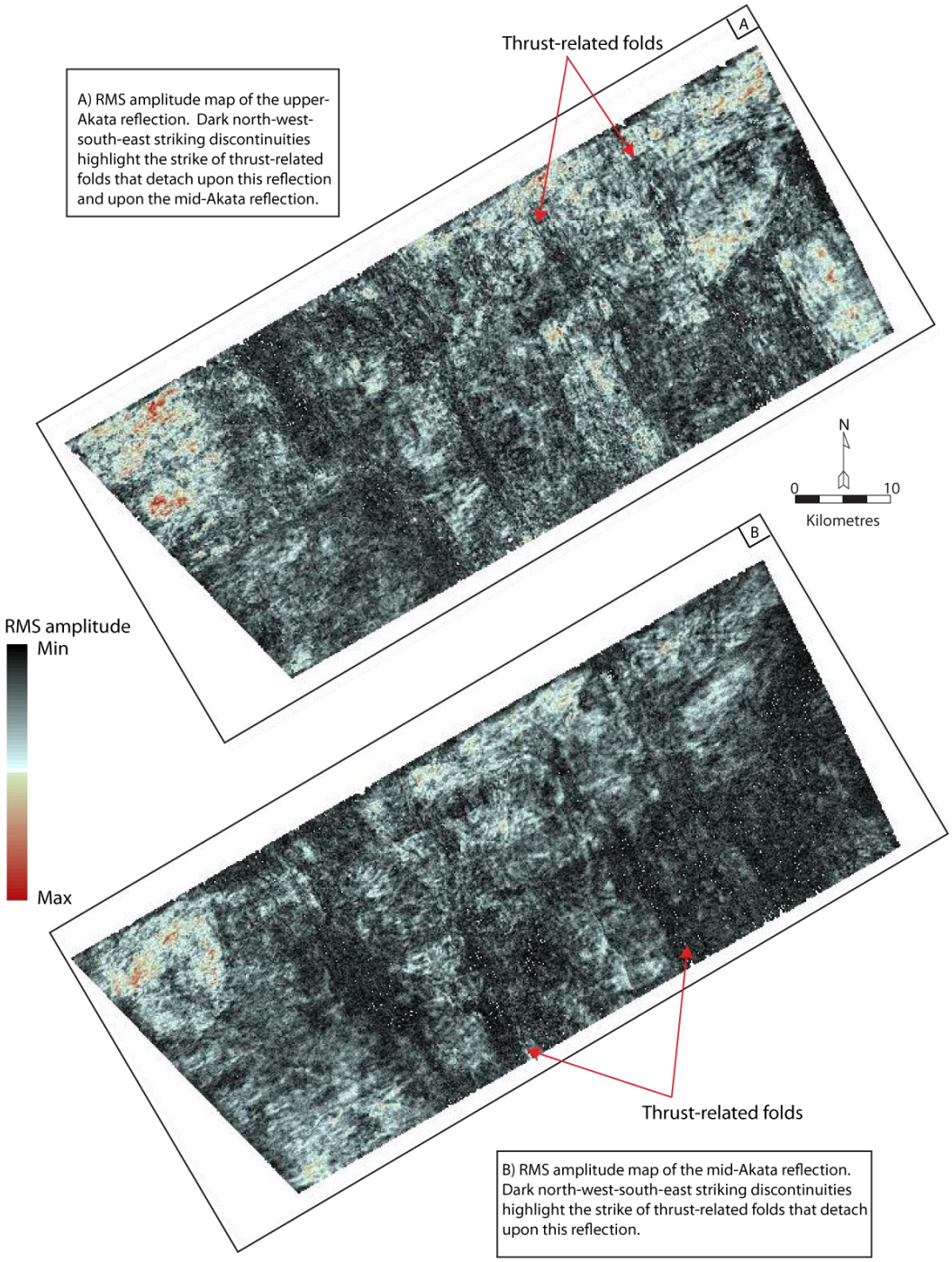
A
Thrust-related folds
A) RMS amplitude map of the upper-Akata reflection. Dark north-west-south-east striking discontinuities highlight the strike of thrust-related folds that detach upon this reflection and upon the mid-Akata reflection.
N
0
10
Kilometres
B
RMS amplitude
Min
Max
Thrust-related folds
B) RMS amplitude map of the mid-Akata reflection. Dark north-west-south-east striking discontinuities highlight the strike of thrust-related folds that detach upon this reflection.

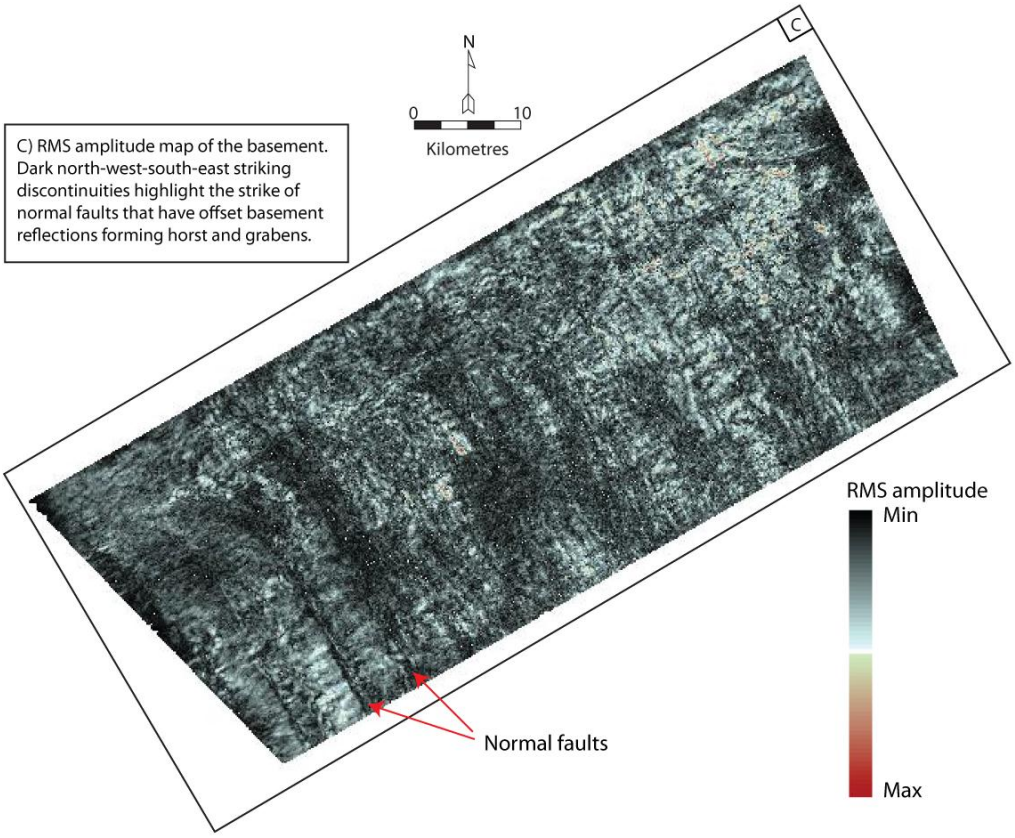

Fig. A6. RMS amplitude maps extracted from A) the upper-Akata reflection, B) the mid-Akata reflection C) the basement from the OPL 324 survey area. The majority of structures are north-west striking.

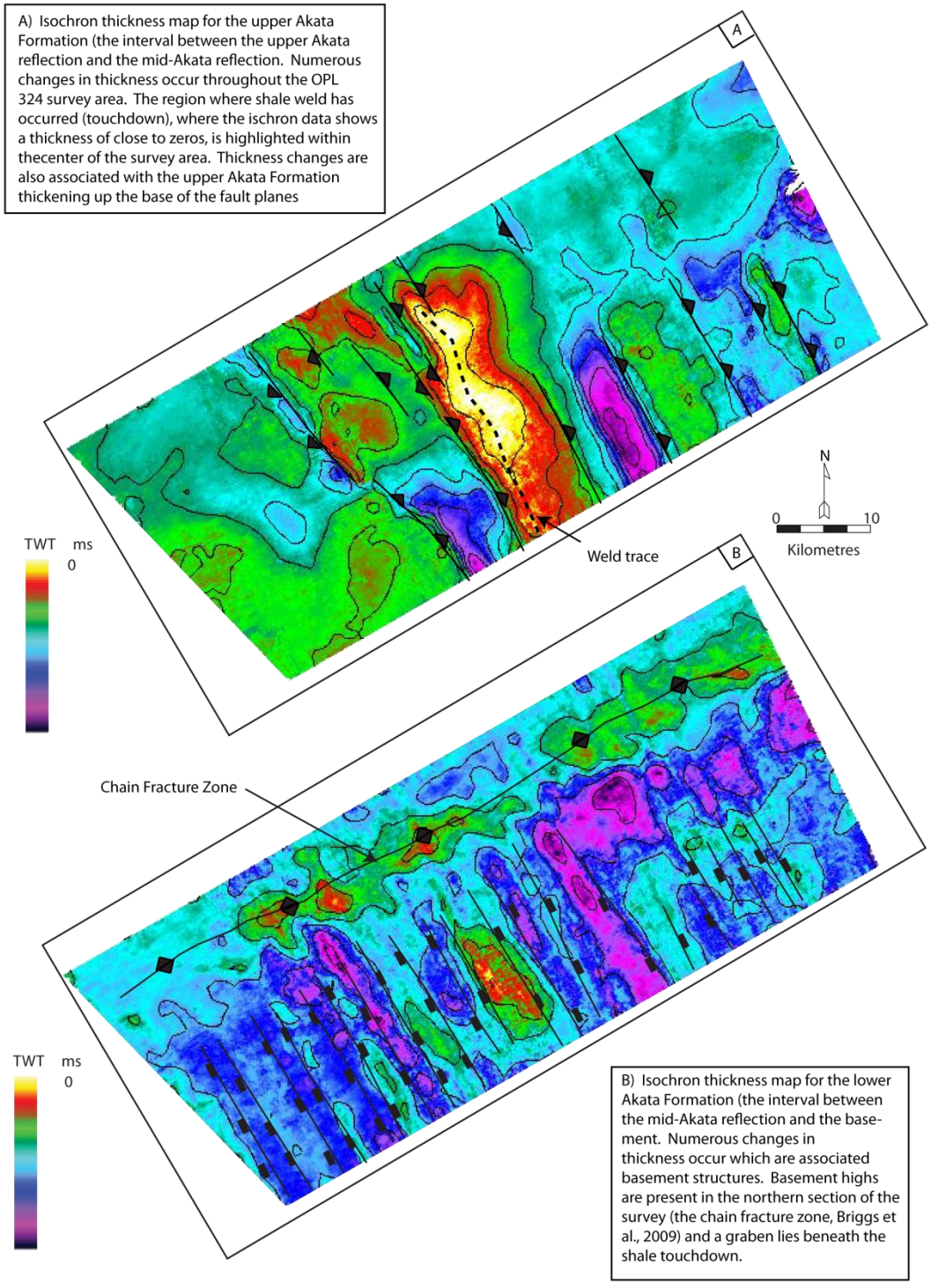

Fig. A7. Isochron thickness maps for A) the upper Akata Formation and B) the lower Akata Formation in the OPL 324 survey within the western Niger Delta.

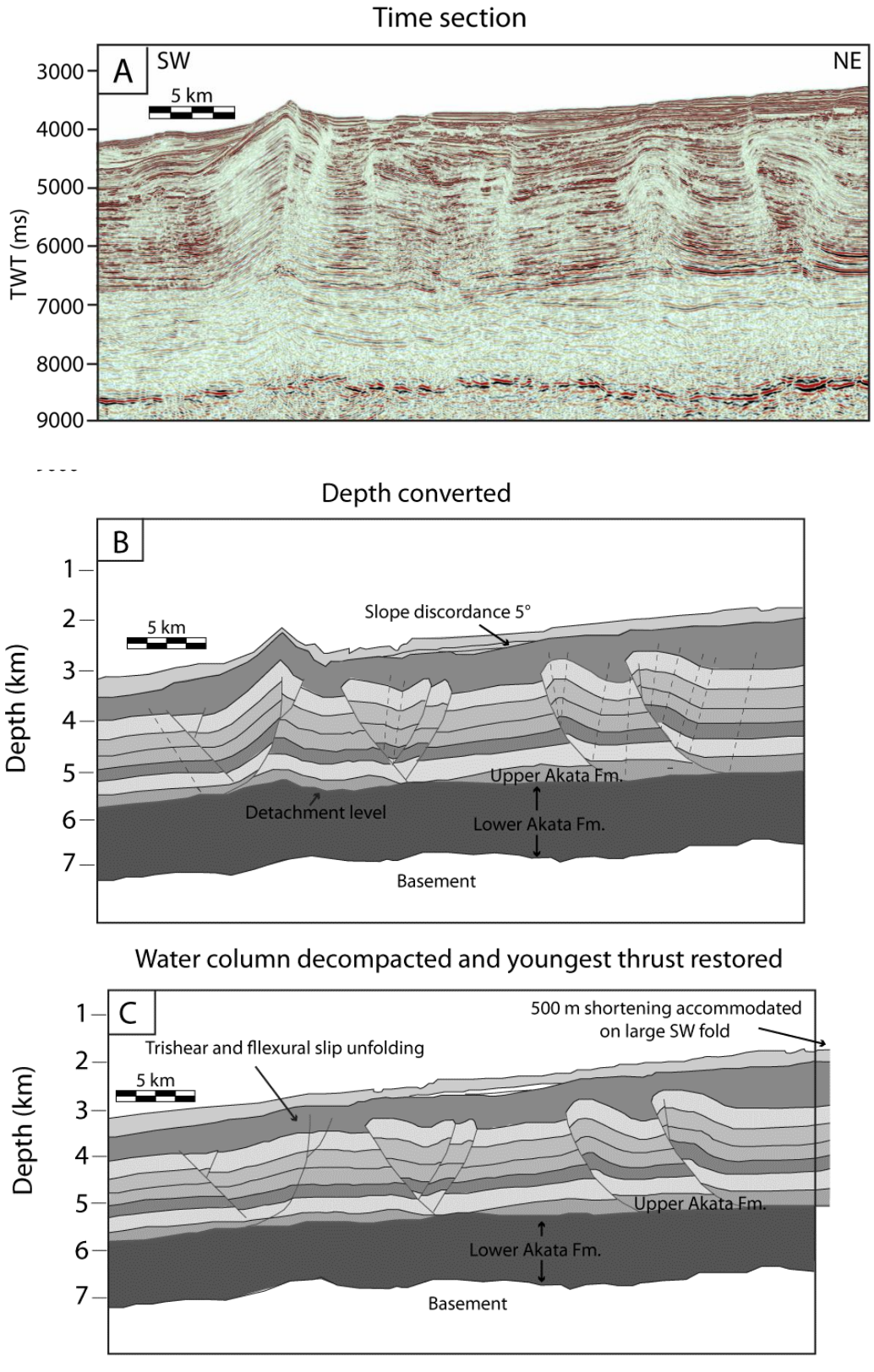
Time section
A
SW
NE
5 km
TWT (ms)
3000
4000
5000
6000
7000
8000
9000
Depth converted
B
5 km
Slope discordance 5°
Upper Akata Fm.
Detachment level
Lower Akata Fm.
Basement
Depth (km)
1
2
3
4
5
6
7
Water column decompacted and youngest thrust restored
C
500 m shortening accommodated on large SW fold
Trishear and fllexural slip unfolding
5 km
Upper Akata Fm.
Lower Akata Fm.
Basement
Depth (km)

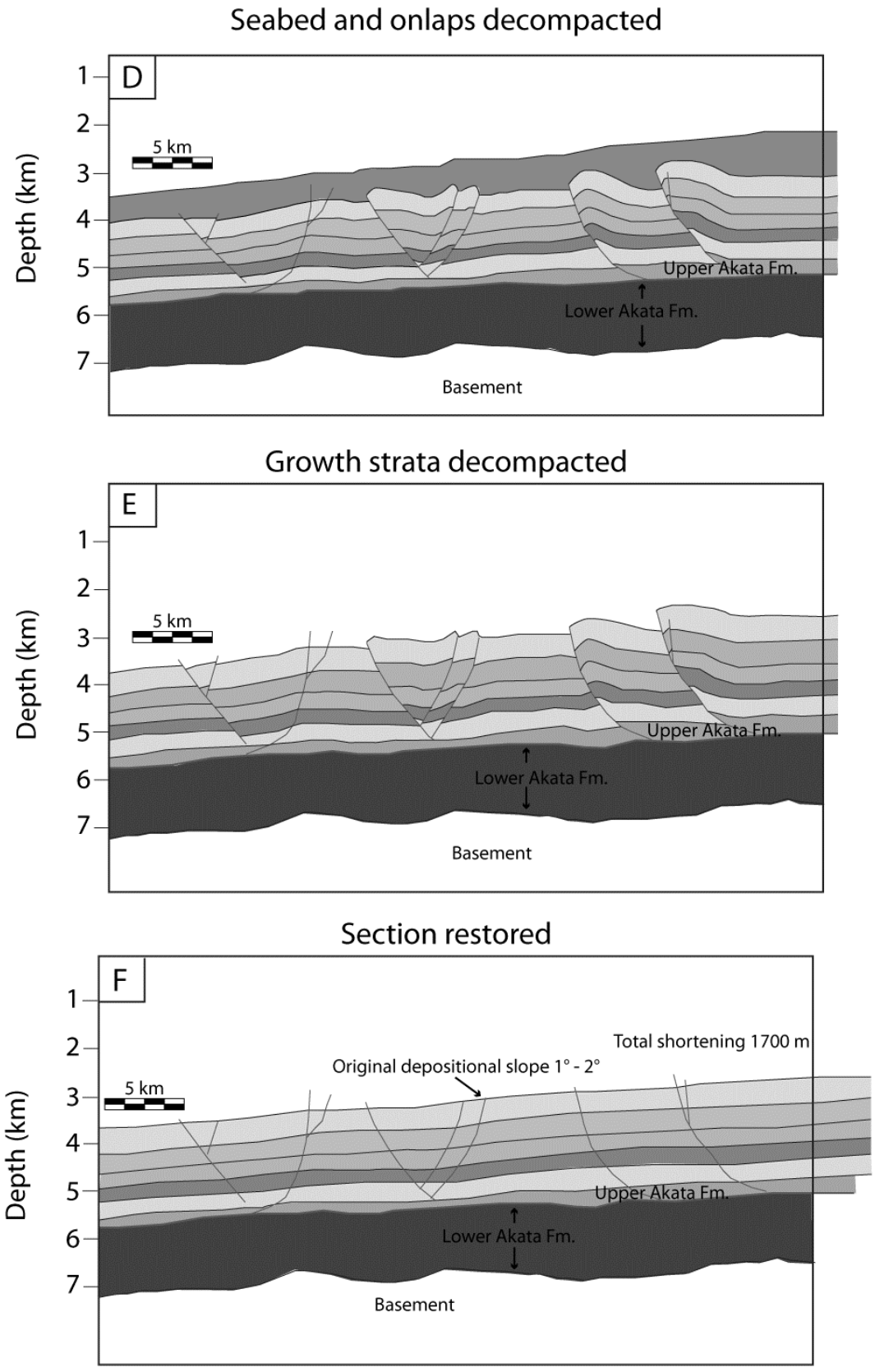
Seabed and onlaps decompacted
D
5 km
Depth (km)
1
2
3
4
5
6
7
Upper Akata Fm.
Lower Akata Fm.
Basement
Growth strata decompacted
E
5 km
Depth (km)
Upper Akata Fm.
Lower Akata Fm.
Basement
Section restored
F
Total shortening 1700 m
Original depositional slope 1° - 2°
5 km
Depth (km)
Upper Akata Fm.
Lower Akata Fm.
Basement

Fig. A8. Sequential restoration of the shale weld showing the evolution of this structure. The time section was depth converted using the velocity model of Morgan (2003) (Fig. 2.8) (panel B) and the present day slope angle was noted. The large backthrust was then resorted using trishear and flexural slip unfolding. Unfolding indicates that 500 m of extension was accommodated on this thrust fault. The seabed and growth strata were decompacted (panels D-E) and the remainder of the cross-section was restored. The section extended 1700 m within the sedimentary overburden and the angle of the original slope is estimated to be between 1-2. The restoration shows that there was not a significant pre-existing slope to be onlapped upon without withdrawal of shale and tilting of the overburden. Vertical scale is 2.5X the horizontal scale.

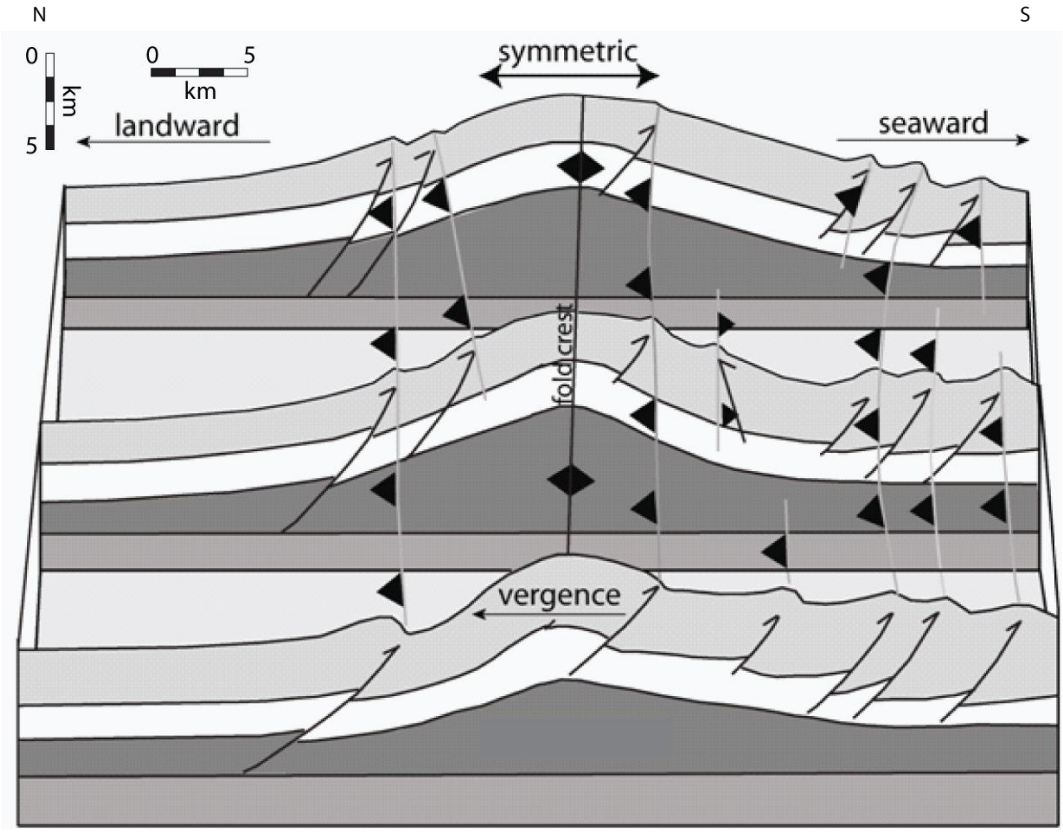

Fig. A9. Cross-sectional model of the detachment fold constructed from regional 2D lines. A series of seaward verging thrust faults are present on the limbs of the detachment fold.

	Lokbatan (Azerbaijan, 2001)	Koturdag (Azerbaijan, 1950-2007	Piparo (Trinidad, 2001)	Lusi (East Java, 2006)
Volume	0.0003 km^3	0.00045 km^3	0.025 km^3	0.012 km^3
Duration	30 minutes	18,200 days	1 day	173 days
Area	0.098 km^2	0.3 km^2	2.5 km^2	3.6 km^2
Average rate per day	0.0144 km^3	0.000000025 km^3	0.025 km^3	0.00007-0.0015 km^3
Average rate per Ma	52959600 km^3	9.13 km^3	9131250 km^3	25567.5 km^3 – 547875 km^3

Table. A1. Volume, duration, aerial coverage and rates of large-scale eruptions from mud volcanoes from the South Caspian Sea, Trinidad and Lusi mud volcano (from Davies et al., 2007).

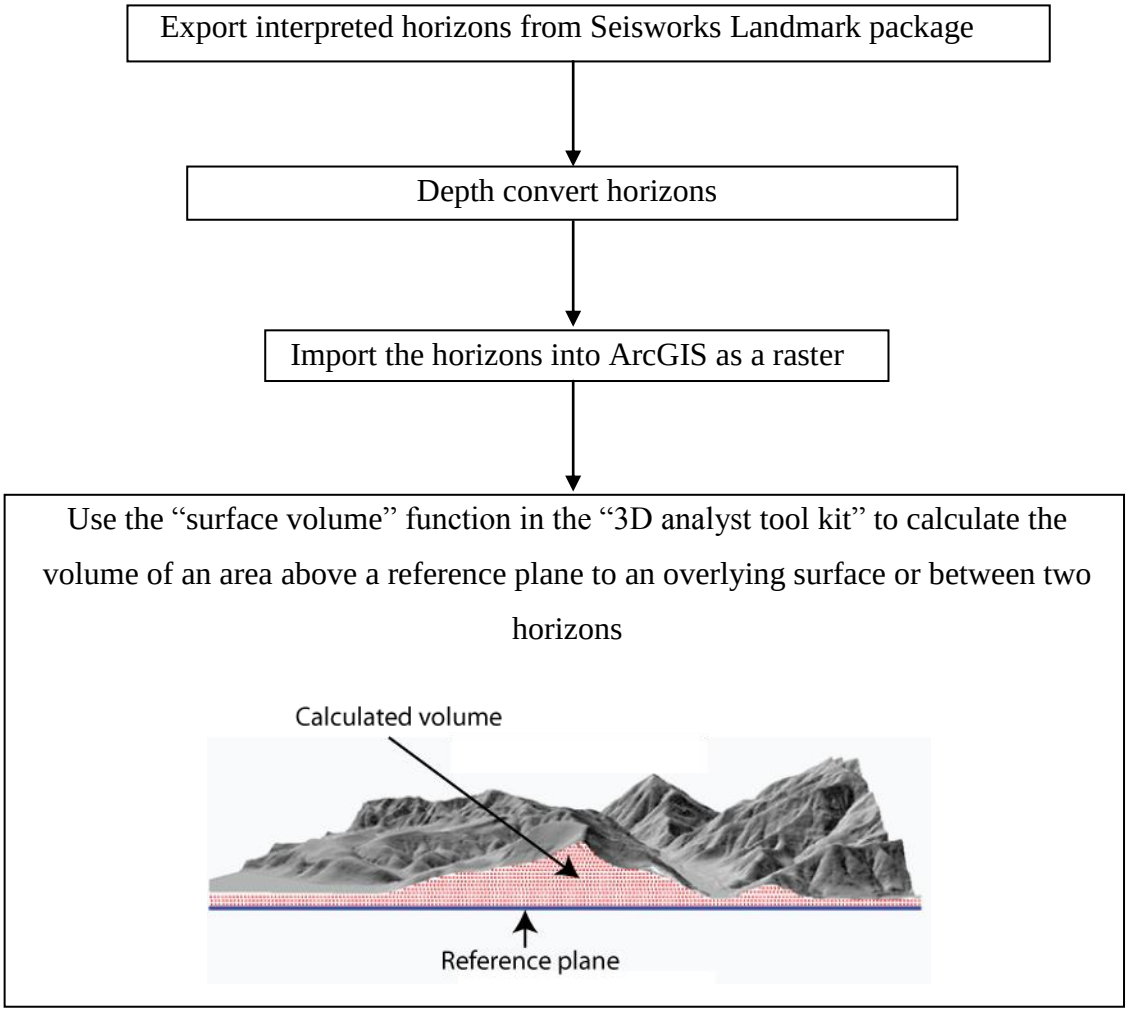

Fig. A10. Workflow and illustration of how volumetric changes were calculated within the casal detachment unit using ArcGIS (from ArcGIS Desktop 9.3 help).

8.5 Appendix 5

This appendix provides supporting material for the research done on the OPL 314 data detailed in chapter 5.

This appendix includes:

- Seismic profile showing the detachment of the strike-slip fault deep within the basement.
- TWT and RMS amplitude map of the mid-Akata reflection.
- Isochron map between the mid-Akata reflection and the basement.
- Detailed steps on the restoration techniques used for restoring the fault-related folds within the cores of the kilometre-scale anticlines.

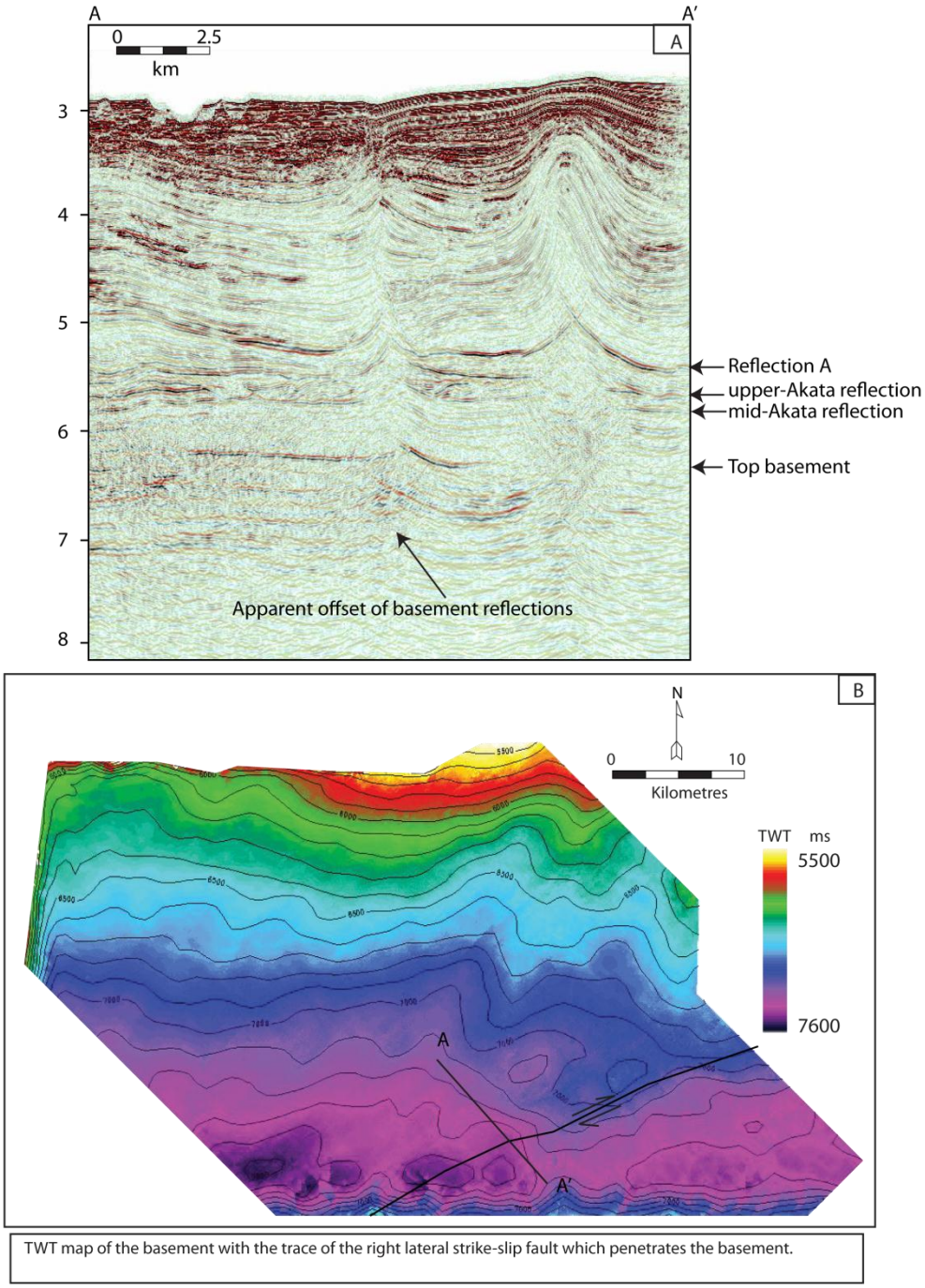

Fig. A11. A) Seismic cross-section through the right lateral strike-slip fault and an adjacent fault-related fold, which shows the apparent offset of deep-seated basement reflections. Reflections "curve upwards" and appear offset vertically across the trace of the strike-slip fault. B) TWT map of the basement reflection.

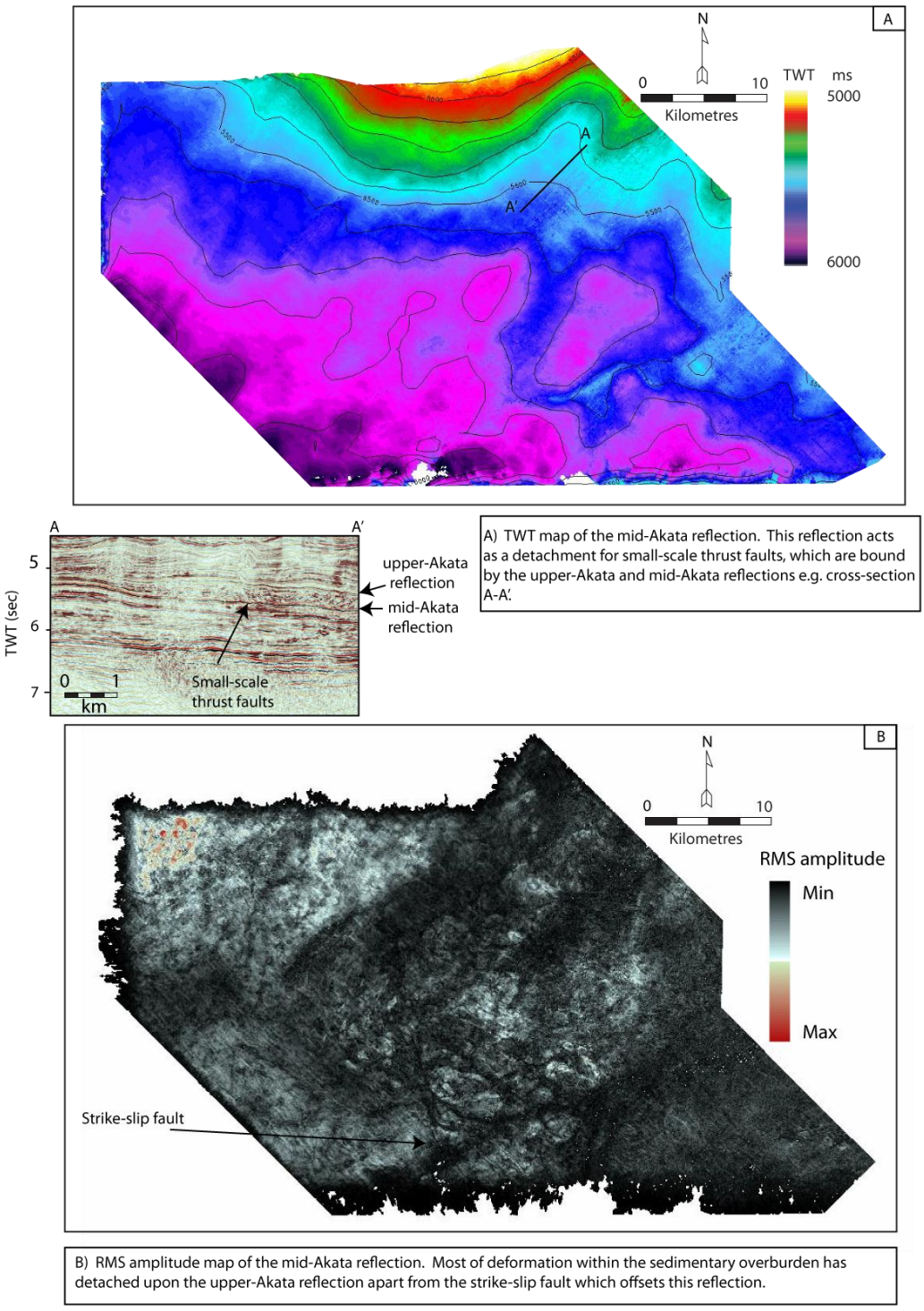

Fig. A12. A) TWT map of the mid-Akata reflection and, B) an RMS amplitude map extracted from the mid-Akata reflection. The dark north-east-south-west trending discontinuity in the south-eastern section of the survey area represents the strike-slip fault. Subtle north-west-south-east trending discontinuities represent the detachment of numerous small-scale thrust faults as shown in cross section A-A'. These thrust are bound between the mid- and upper-Akata reflections, which both act as detachment levels.

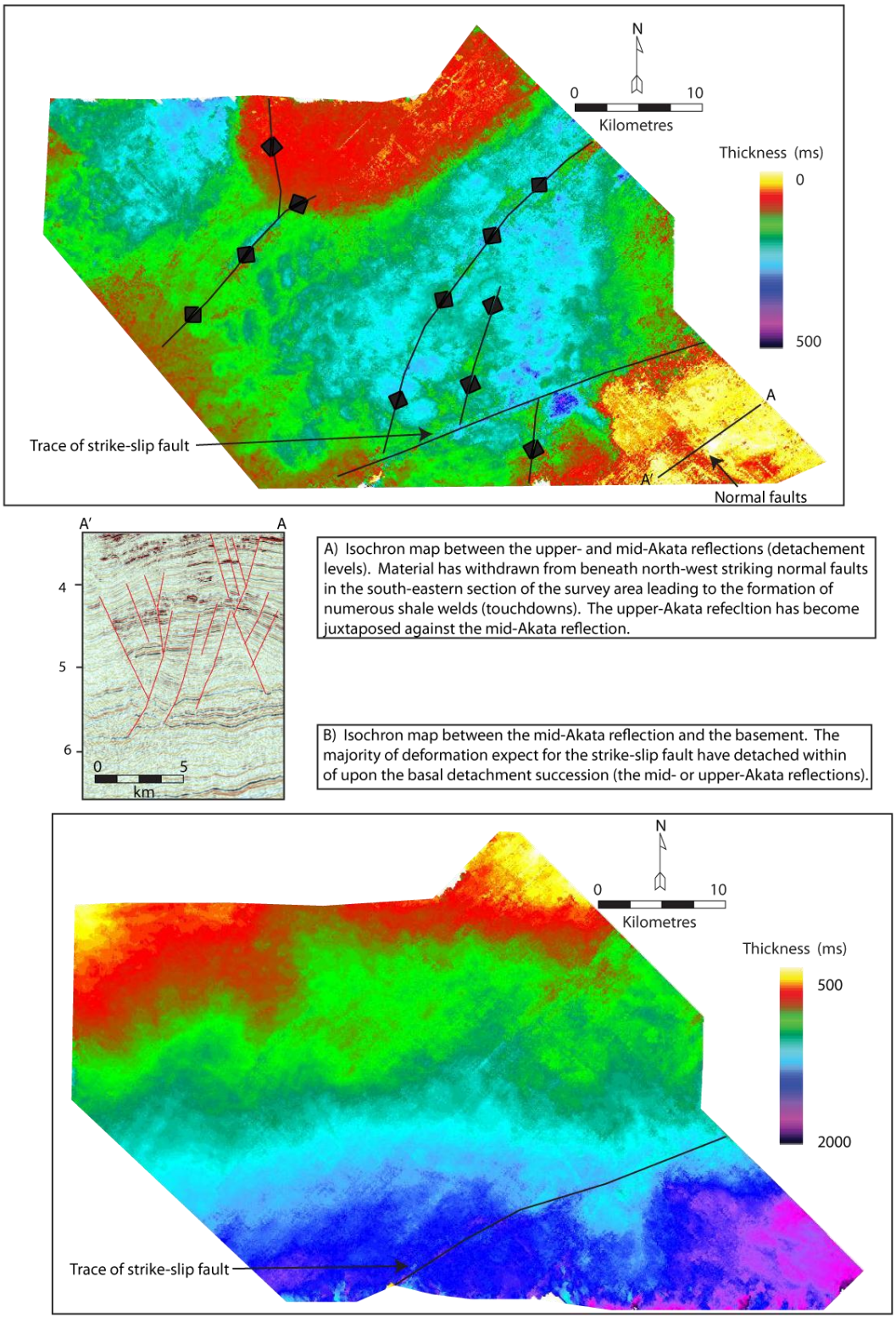

Fig. A13 Isochron maps for the upper Akata Formation (between the upper- and mid-Akata reflections) and the lower Akata Formation (between the mid-Akata reflection and the basement).

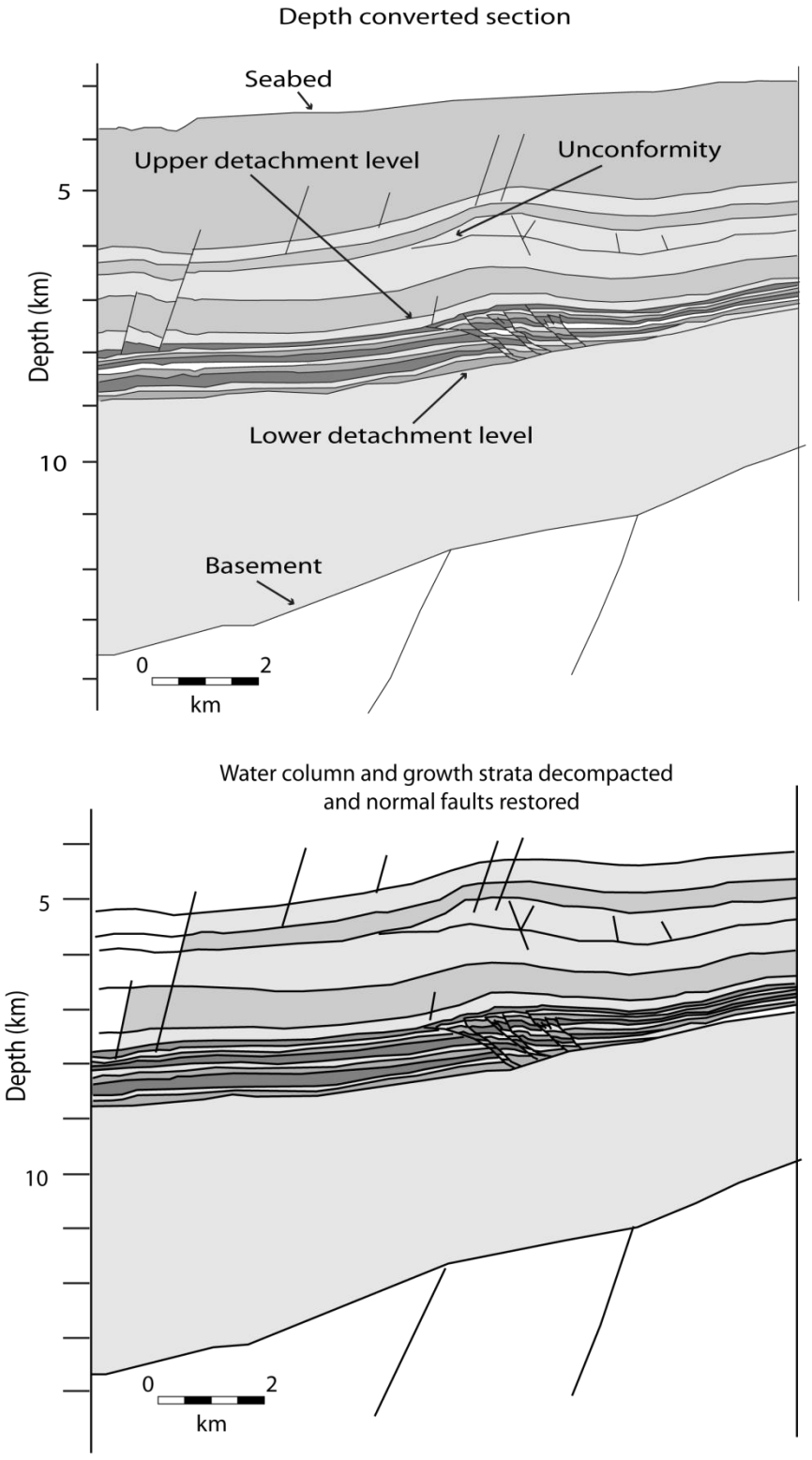
Depth converted section
Seabed
Upper detachment level
Unconformity
Lower detachment level
Basement
Depth (km)
5
10
0
2
km
Water column and growth strata decompacted
and normal faults restored
Depth (km)
5
10
0
2
km

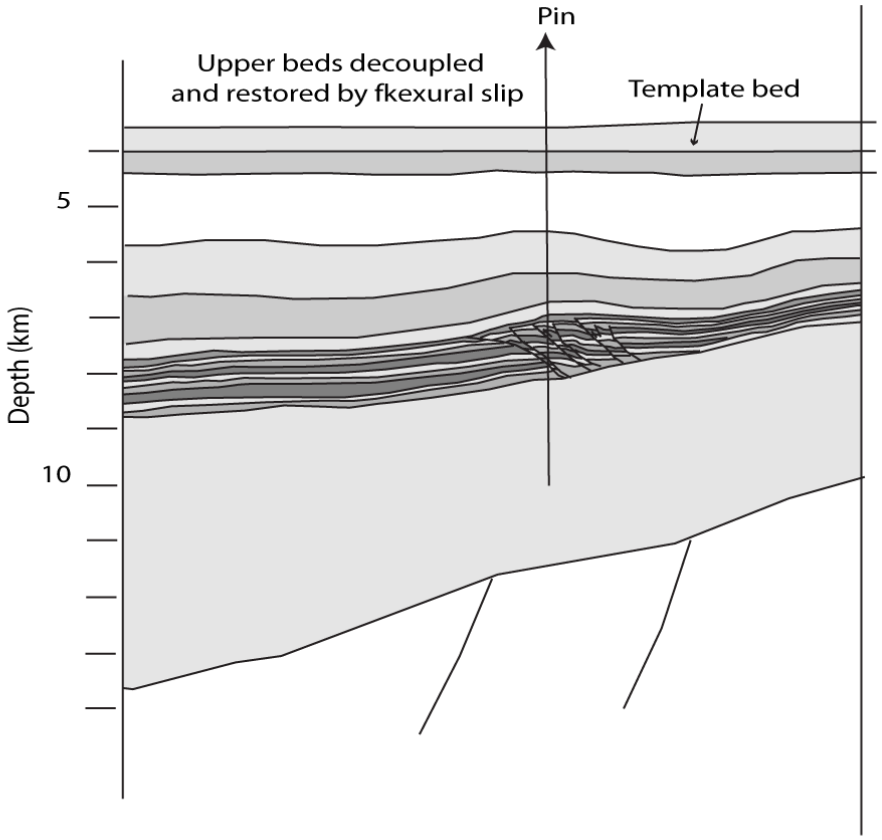
Pin
Upper beds decoupled
and restored by fkexural slip
Template bed
5
Depth (km)
10

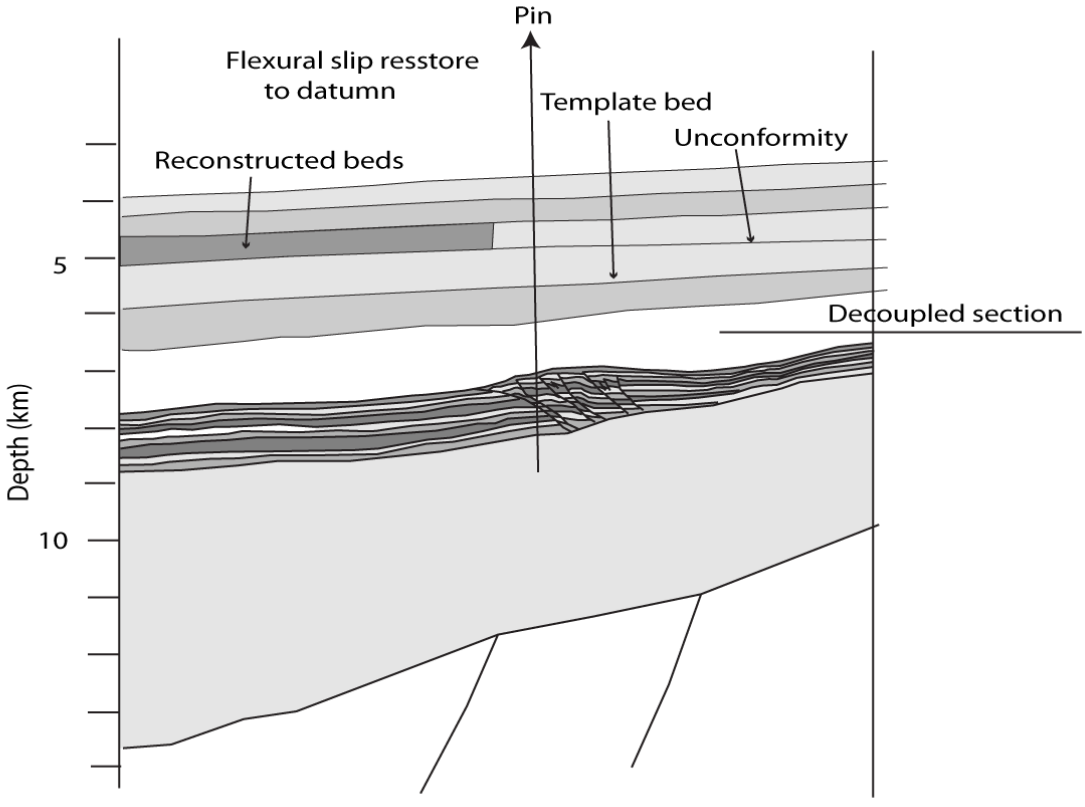
Pin
Flexural slip resstore
to datumn
Template bed
Unconformity
Reconstructed beds
5
Decoupled section
Depth (km)
10

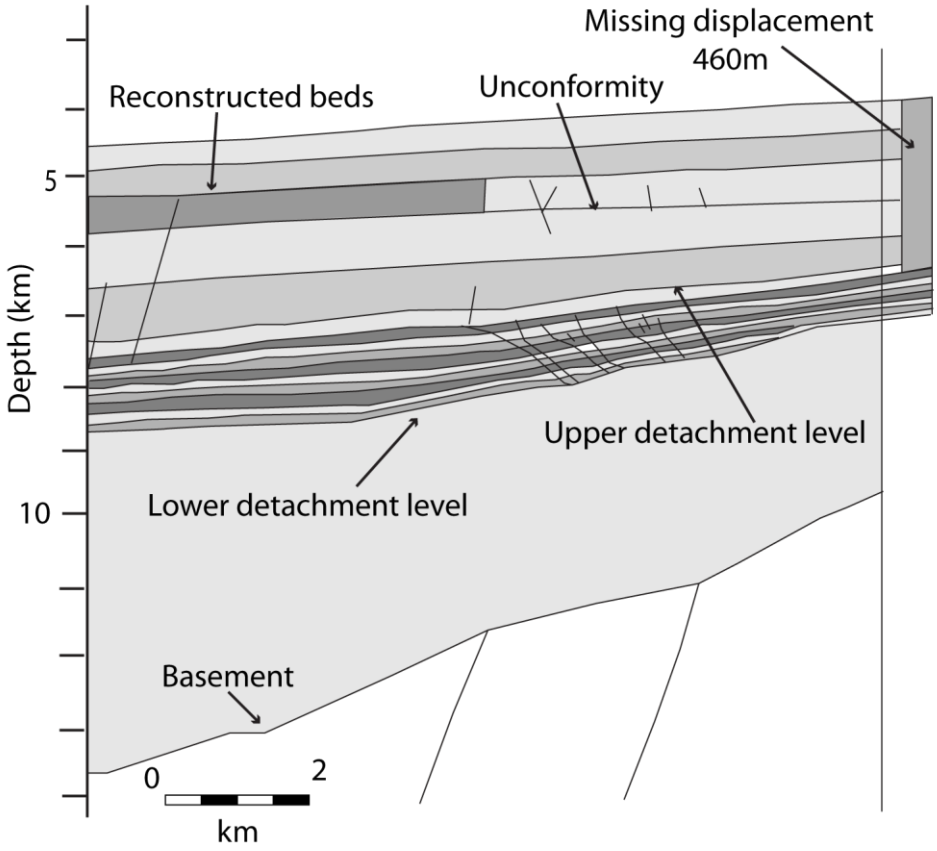

Fig. A14. Sequential restoration of the structural styles and geometries in detachment fold A. The TWT profile shown in figure 5.7 was depth converted, water column and growth strata were decompacted and the structure was subsequently restored. Bed removed by erosion were reconstructed. Vertical scale is equal to the horizontal scale.

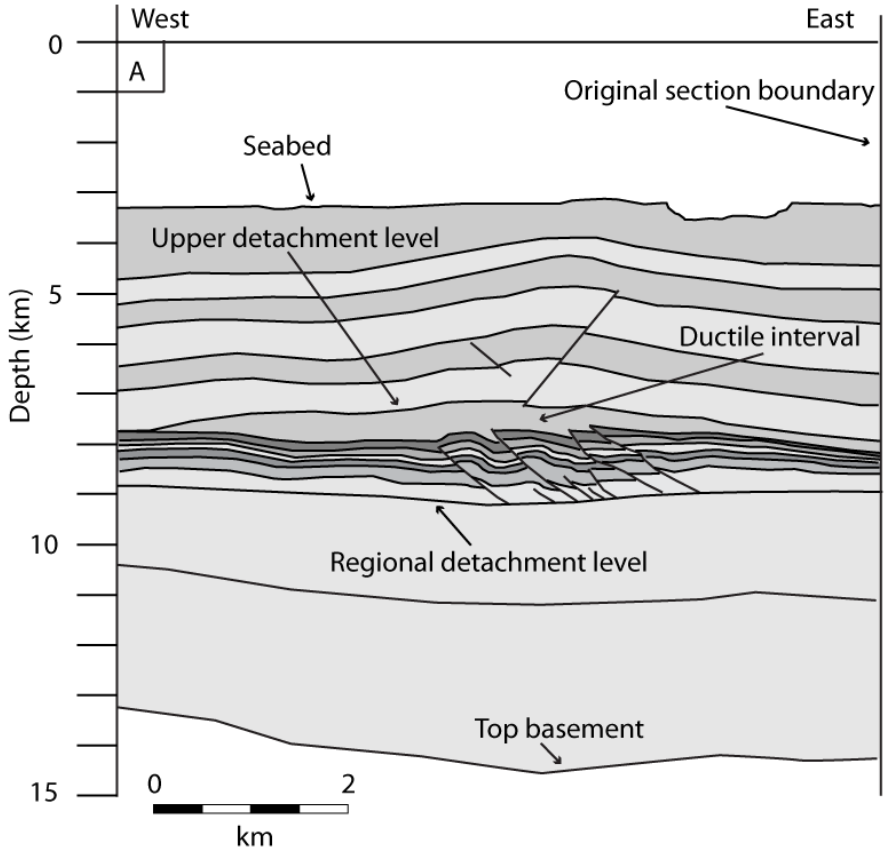
West
East
0
A
Original section boundary
Seabed
Upper detachment level
5
Depth (km)
Ductile interval
10
Regional detachment level
Top basement
15
0
2
km

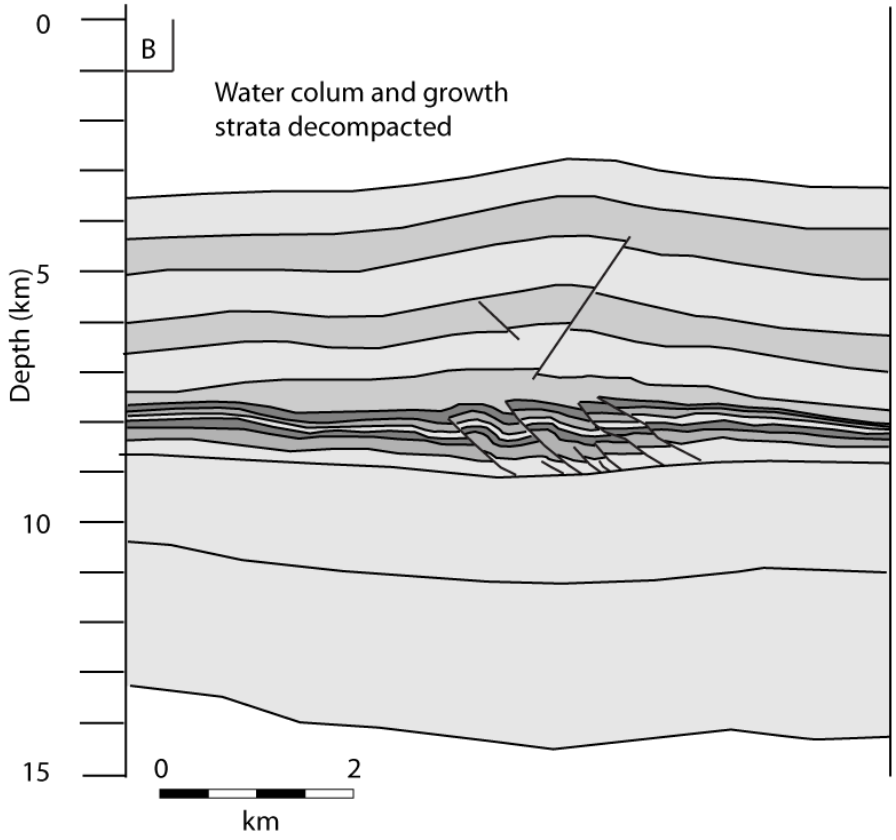
0
B
Water colum and growth
strata decompacted
5
Depth (km)
10
15
0
2
km

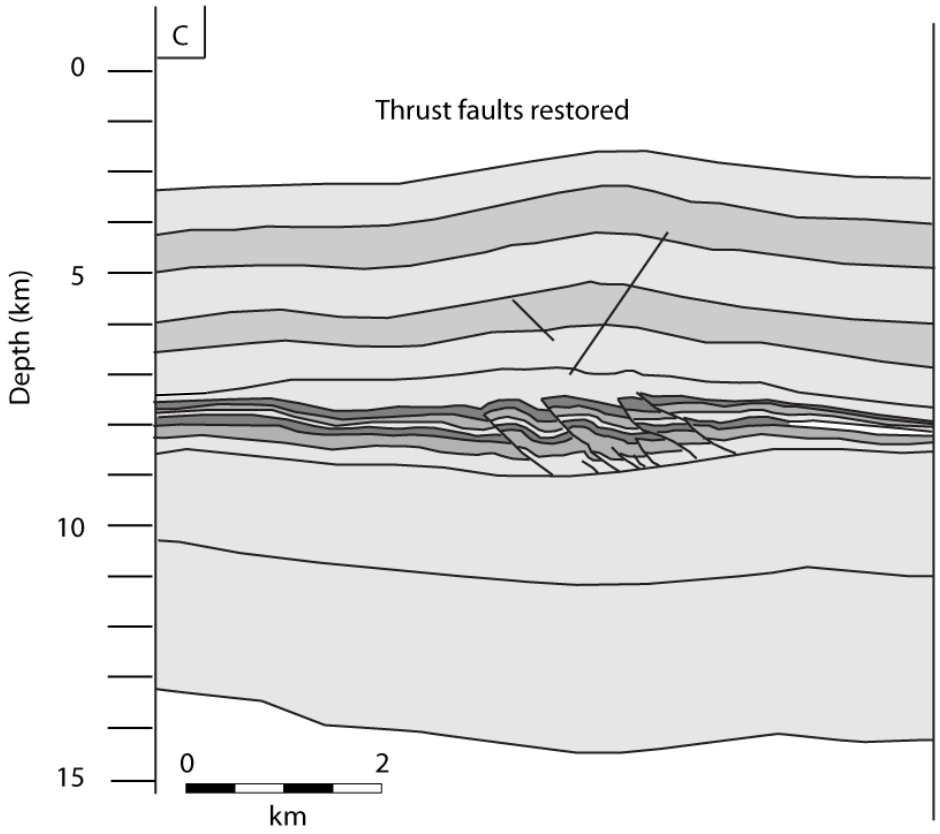
C
Thrust faults restored
Depth (km)
0
5
10
15
0
2
km

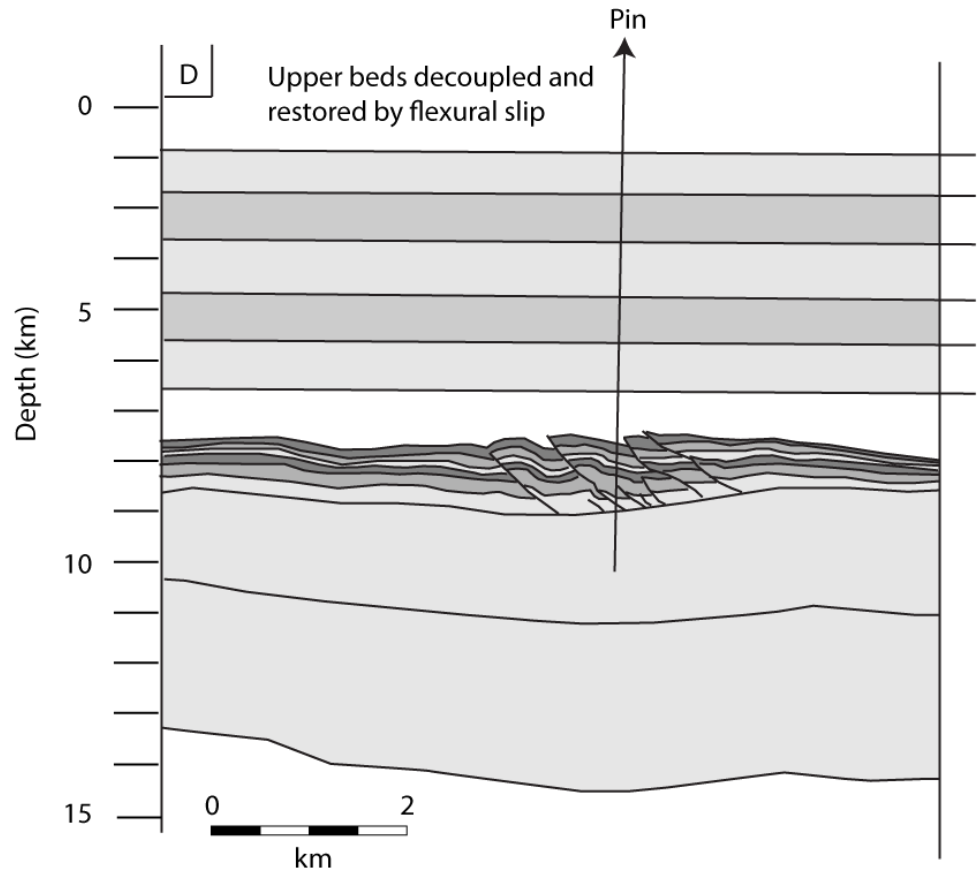
Pin
D
Upper beds decoupled and
restored by flexural slip
Depth (km)
0
5
10
15
0
2
km

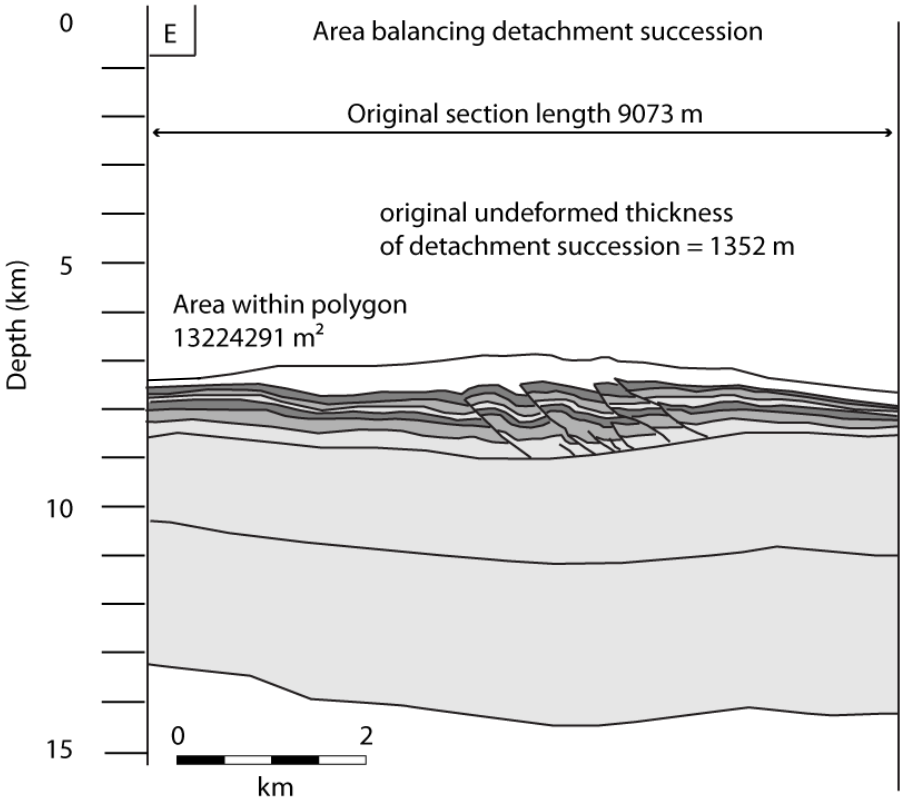
E
Area balancing detachment succession
Original section length 9073 m
original undeformed thickness
of detachment succession = 1352 m
Area within polygon
13224291 m²
Depth (km)
0
5
10
15
0
2
km

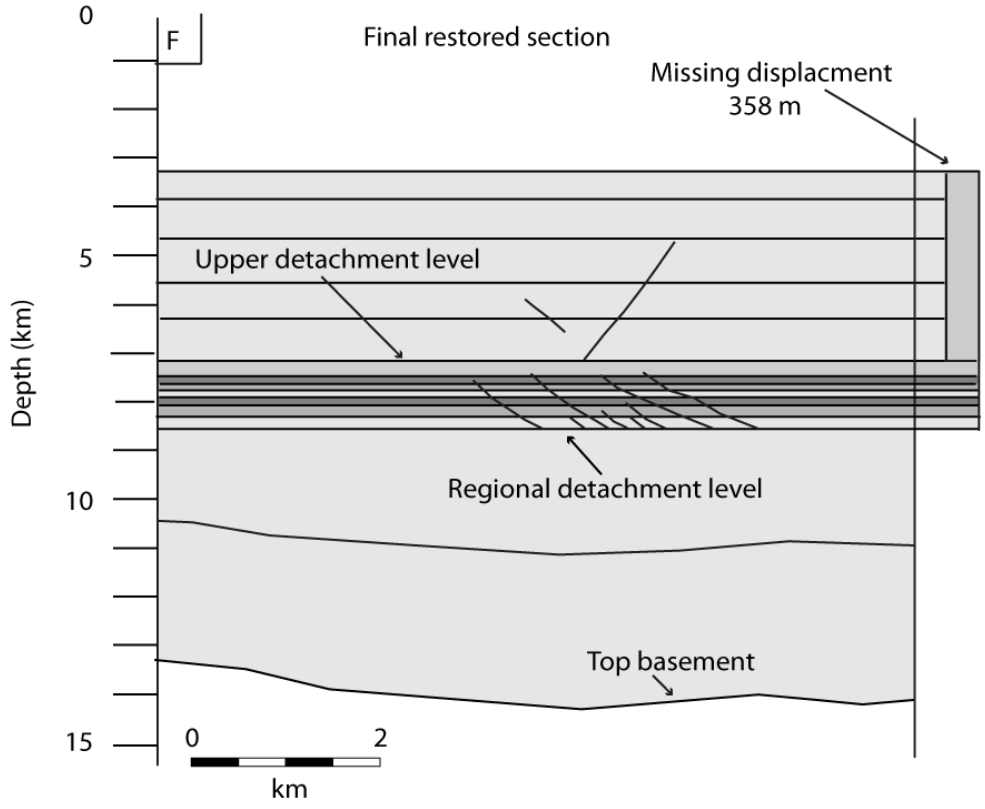
F
Final restored section
Missing displacment
358 m
Upper detachment level
Regional detachment level
Top basement
Depth (km)
0
5
10
15
0
2
km

Fig. A15. Restoration of the structural styles and geometries in detachment fold B. The TWT profile shown in figure 5.9 was depth converted, water column and growth strata were decompacted and the structure was subsequently restored. Vertical scale is approximately 2x the horizontal scale.

8.6 Digital appendix

This appendix includes paper reprints of

D.P., R.J. Davies, J. Imber, and S. King, 2011, Structure of the footwall of a fault system revealed by 3D seismic data from the Niger Delta: Basin Research, v. doi: 10.1111/j.1365-2117.2011.00514.x. (online preview version).

Maloney, D.P., R.J. Davies, J. Imber, S. Higgins, and S. King, 2010, New insights into deformation mechanisms in the gravitationally-driven Niger Delta deep-water fold and thrust belt: AAPG Bulletin, v. 94, p. 1401-1424.

PH.D. in digital format

9 References

ArcGIS Desktop 9.3 Help.

Ajakaiye, D. E., and A. W. Bally, 2002, Course Manual and Atlas of Structural Styles on Reflection Profiles from the Niger Delta. Continuing Education Course Note Series. v. 41, AAPG, Tulsa. Axen.

Atkinson, P. K., and W. K. Wallace, 2003, Competent unit thickness variation in detachment folds in the Northeastern Brooks Range, Alaska: geometric analysis and a conceptual model: Journal of Structural Geology, v. 25, p. 1751-1771.

Avbovbo, A. A., 1978, Tertiary Lithostratigraphy of Niger Delta: AAPG Bulletin, v. 62, p. 295-306.

Axen, G. J., 1987, The geometry of planar domino-style normal faults above a dipping basal detachment: Journal of Structural Geology, v. 10, p. 405-411.

Back, S., C. Höcker, M. B. Brundiers, and P. A. Kukla, 2006, Three-dimensional-seismic coherency signature of Niger Delta growth faults: integrating sedimentology and tectonics: Basin Research, v. 18, p. 323-337.

Badri, M. A., C. M. Sayers, R. Awad, and A. Graziano, 2000, A feasibility study for pore-pressure prediction using seismic velocities in the offshore Nile Delta, Egypt: The Leading Edge, v. 19, p. 1103-1108.

Barker, C., 1972, Aquathermal Pressuring: Role of Temperature in Development of Abnormal Pressure Zone: AAPG Bulletin, v. 56, p. 2068-2071.

Bahroudi, A., and H. A. Koyi, 2003, Effect of spatial distribution of Hormuz salt on deformation style in the Zagros fold and thrust belt: an analogue modelling approach: Journal of the Geological Society, London, v. 160, p. 719-733.

Bahroudi, A., H. A. Koyi, and C. J. Talbot, 2003, Effect of ductile and frictional décollements on extension style: Journal of Structural Geology, v. 15, p. 1401-1423.

Bally, A., W. Bernoulli, G. A. Davies, and L. Montadert, 1981, Listric normal faults: Oceanologica Acta, v. 4, supplement, p. 81-101.

References

Banks, C. J., and J. Warburton, 1986, 'Passive-roof' duplex geometry in the frontal structures of the Kirthar and Sulaiman Mountain belts, Pakistan: Journal of Structural Geology, v. 8, p. 229-237.

Barber, A. J., S. Tjokrosapoetro, and T. R. Charlton, 1986, Mud volcanoes, shale diapirs, wrench faults and melanges in accretionary complex, eastern Indonesia: AAPG Bulletin, v. 70, p. 1729-1741.

Bilotti, F., and J. H. Shaw, 2005, Deep-water Niger Delta fold and thrust belt modeled as a critical-taper wedge: The influence of elevated basal fluid pressure on structural styles: AAPG Bulletin, v. 89, p. 1475-1491.

Bolton, A., and A. Maltman, 1998, Fluid-flow pathways in actively deforming sediments: the role of pore fluid pressures and volume change: Marine and Petroleum Geology, v. 15, p. 281-297.

Bonini, M., 2003, Detachment folding, fold amplification and diapirism in thrust wedge experiement: Tectonics, v. 22, p. 1065, doi:10.1029/2002TC001458.

Bonini, M., 2007, Deformation patterns and structural vergence in brittle-ductile thrust wedges: An additional analogue modelling perspective: Journal of Structural Geology, v. 29, p. 141-158.

Booth, J. S., and A. G. Dahl, 1986, A note on the relationships between organic matter and some geotechnical properties of a marine sediment: Marine Geotechnology, v. 6, p. 281-297.

Bose, S., and S. Mitra, 2009, Deformation along oblique and lateral ramps in listric normal faults: Insights from experimental models: AAPG Bulletin, v. 93, p. 431-451.

Boyer, S. E., and D. Elliott, 1982, Thrust systems: AAPG Bulletin, v. 66, p. 1196-1230.

Briggs, S. E., J. Cartwright, and R. J. Davies, 2009, Crustal structure of the deep-water west Niger Delta passive margin from the interpretation of seismic reflection data: Marine and Petroleum Geology, v. 26, p. 936-950.

Briggs, S. E., R. J. Davies, J. A. Cartwright, and R. Morgan, 2006, Multiple detachment levels and their control on fold styles in the compressional domain of the deep-water west Niger Delta: Basin Research, v. 18, p. 435-450.

Boudin, C., J. Cartwright, 2008, Early stage evolution of growth faults: 3D seismic insights from the Levant Basin, Eastern Mediterranean: Journal of Structural Geology, v. 30, p. 888-898.

Brown, A.R., 2004, Interpretation of Three-Dimensional Seismic Data: AAPG Memoir 42, SEG Investigations in Geophysics.

Brown, L. F., R. G. Loucks, R. H. Trevino, and U. Hammes, 2004, Understanding growth-faulted, intraslope subbasins by applying sequence-stratigraphic principles: Examples from the south Texas Oligocene Frio Formation: AAPG Bulletin, v. 88, p. 1501–1522

Bruce, C. H., 1973, Pressured Shale and Related Sediment Deformation; mechanism for Development of Regional Contemporaneous Faults: AAPG Bulletin, v. 57, p. 878-886.

Brun, J. P., and T. P.-O. Mauduit, 2007, Rollovers in salt tectonics: The inadequacy of the listric fault model: Tectonophysics, v. 457, p. 1-11.

Bull, S., J. A. Cartwright, and M. Huuse, 2009, A review of kinematic indicators from mass-transport complexes using 3D seismic data: Marine and Petroleum Geology, v. 26, p. 1132-1151.

Burke, K., 1972, Longshore Drift, Submarine Canyons, and Submarine Fans in Development of Niger Delta: AAPG Bulletin, v. 56, p. 1975-1983.

Burst, J. K., 1969, Diagenesis of Gulf Coast Clayey Sediments and its Possible Relation to Petroleum Migration: AAPG Bulletin, v. 53, p. 73-93.

Buryakovsky, L. A., R. D. Djevanshir, and G. V. Chilingar, 1995, Abnormally-high formation pressures in Azerbaijan and the South Caspian Basin (as related to smectite <--> illite transformations during diagenesis and catagenesis): Journal of Petroleum Science and Engineering, v. 13, p. 203-218.

Butler, R. W. H., and W. D. McCaffrey, 2004, Nature of thrust zones in deep-water sand-shale sequences: outcrop examples from the Champsaur sandstones of SE France: Marine and Petroleum Geology, v. 31, p. 911-921.

References

Cartwright, J., R. Bouroullec, D. James, and H. Johnson,1998, Polycyclic motion history of some Gulf Coast growth faults from high-resolution displacement analysis: Geology, v. 26, p. 819-822.

Chamberlin, R. T., 1910, The Appalachian folds of central Pennsylvania: Journal of Geology, v. 18, p. 228-251.

Chapman, R. E., 1980, Mechanical versus thermal cause of abnormally high pore pressures in shales: AAPG Bulletin, v. 64, p. 2179–2183.

Chester, J. S., and F. M. Chester, 1990, Fault-propagation folds above thrusts with constant dip: Journal of Structural Geology, v. 12, p. 903-910.

Childs, C., A. Nicol, J. J. Walsh, and J. Watterson, 2003, The growth and propagation of synsedimentary faults: Journal of Structural Geology, v. 25, p. 633-648.

Clement, J., J. A. Cartwright, and J. Booth, 1997, Structural segmentation and the influence of basement structure on the Namibian passive margin: Journal of the Geological Society, London, v. 154, p. 477-482.

Cloos, E., 1968, Experimental analysis of Gulf Coast fracture patterns: AAPG Bulletin, v. 52, p. 420–444.

Cobbold, P. R., R. Mourgues, and K. Boyd, 2004, Mechanism of thin-skinned detachment in the Amazon Fan: assessing the importance of fluid overpressure and hydrocarbon generation: Marine and Petroleum Geology, v. 21, p. 1013-1025.

Cobbold, P. R., B. J. Clarke, and H. Løseth, 2009, Structural consequences of fluid overpressure and seepage forces in the outer thrust belt of the Niger Delta: Petroleum Geoscience, v. 15, p. 3–15.

Cohen, H. A., and K. McClay, 1996, Sedimentation and shale tectonics of the northwestern Niger Delta front: Marine and Petroleum Geology, v. 13, p. 313-328.

Corredor, F., J. H. Shaw, and F. Bilotti, 2005, Structural styles in the deep-water fold and thrust belts of the Niger Delta: AAPG Bulletin, v. 89, p. 753-780.

Costa, E., and B. C. Vendeville, 2002, Experimental insights on the geometry and kinematics of fold-and-thrust belts above weak, viscous evaporitic décollement: Journal of Structural Geology, v. 24, p. 1729-1739.

Cotton, J.T., and H. A. Koyi, 2000, Modelling of thrust fronts above ductile and frictional de´collements: application to structures in the Salt Range and Potwar Plateau, Pakistan: Geological Society of America Bulletin, 112, 351–363.

Couzens-Schultz, B. A., B. C. Vendeville, and D. V. Wiltschko, 2003, Duplex style and triangle zone formation: insights from physical modeling: Journal of Structural Geology, v. 25, p. 1623-1644.

Currie, J.B., H. W. Patnode, and R. P. Trump, 1962, Developments of folds in sedimentary strata: Geological Society of America Bulletin, v. 73, p. 655–674.

Dahlen, F. A., J. Suppe, D. M. Davis, 1984, Mechanics of fold-and-thrust belts and accretionary wedges: cohesive Coulomb theory: Journal of Geophysical Research, v. 89, p. 10,087- 10,101.

Dahlstrom, C. D. A., 1970, Structural geology in the eastern margin of the Canadian Rocky Mountains: Bulletin of Canadian Petroleum Geology, v. 18, p. 332-406.

Dahlstrom, C. D. A., 1990, Geometric constraints derived from the law of conservation of volume and applied to evolutionary models for detachment folding: AAPG Bulletin, v. 74, p. 336-344.

Damuth, J. E., 1994, Neogene gravity tectonics and depositional processes on the deep Niger Delta continental margin: Marine and Petroleum Geology, v. 11, p. 320.

Davis, D., J. Suppe, F. A. Dahlen, 1983, Mechanics of fold-and-thrust belts and accretionary wedges: Journal of Geophysical Research, v. 88, p. 1153-1172.

Davis, G.H., 1983a, Shear zone model for the origin of metamorphic core complexes: Geology, v. 11, p. 342–347.

Davis, G.H., 1983b, A shear zone model for the structural evolution of metamorphic core complexes in southeastern Arizona. In: Continental Extensional Tectonics (Ed. by M. P. Coward, J. F. Dewey, & P. L. Hancock), Geological Society, London, Special Publications, 28, 247–266.

Davis, D.M., and T. Engelder, 1985, The role of salt in fold and thrust belts: Tectonophysics, v. 119, p. 67-88.

Davies, R. J., 2003, Kilometer-scale fluidization structures formed during early burial of a deep-water slope channel on the Niger Delta: Geology, v. 31, p. 949-952.

Davies, R. J., and S. A. Srewart, 2005, Emplacement of giant mud volcanoes in the South Caspian Basin: 3D seismic reflection imaging of their root zones: Journal of the Geological Society London, v. 162, p. 1-4.

Davies, R. J., R. E. Swarbrick, R. J. Evans, and M. Huuse, 2007, Birth of a mud volcano: East Java, 29 May 2006: GSA Today, v. 17, p. 4-9.

de Vera, J, P., P. Granado, and K. McClay, 2010, Structural evolution of the Orange Basin gravity driven system, offshore Namibia: Marine and Petroleum Geology, v. 27, p. 223-237.

Deptuck, M. E., G. S. Steffens, M. Barton, and C. Pirmez, 2003, Architecture and evolution of upper fan channel-belts on the Niger Delta slope and in the Arabian Sea: Marine and Petroleum Geology, V. 20, p. 649-676.

Deville, E., S.-H. Guerlais, Y. Callec, R. Griboulard, P. Huyghe, S. Lallemant, A. Mascle, M. Noble, and J. Schmitz, 2006, Liquefied vs stratified sediment mobilization processes: Insight from the South of the Barbados accretionary prism: Tectonophysics, v. 428, p. 33-47.

Deville, E., S.-H. Guerlais, S. Lallemant, and F. Schbneider, 2010, Fluid dynamics and subsurface sediment mobilization processes: an overview from Southeast Caribbean: Basin research, v. 22, p. 361-379.

Dickenson, G., 1953, Geological aspects of abnormal reservoir pressures in Gulf Coast Louisiana: AAPG Bulletin, v. **37** p. 410–432.

Doust, H., and E. Omatsola, 1990 Niger Delta in divergent/passive margin basins, In: AAPG Memoir (Ed. by J.D. Edwards and P.A. Santogrossi), v. 48, p. 201-238.

Dula, W. F., 1991, Geometric models of Listric Normal Faults and Rollover Folds: AAPG Bulletin, v. 75, p. 1609-1825.

Einsele, G, R. Overbeck, H. U. Schwarz, and G. Unsöld, 1974, Mass physical properties, sliding and erodability of experimentally deposited and differentially consolidated clayey muds: Sedimentology, v. 21, p. 339-372.

Epard, J.-L., and R. H. Groshong, 1993, Excess area and depth to detachment: AAPG Bulletin, v. 77, p. 1291-1302.

Epard, J. L., and R. H. Groshong, 1995, Kinematic model of detachment folding including limb rotation, fixed hinges and layer-parallel strain: Tectonophysics, v. 247, p. 85-103.

Erickson, S. G., 1996, Influence of mechanical stratigraphy on folding vs faulting: Journal of Structural Geology, v. 18, p. 443-450.

Erslev, E. A., 1991, Trishear fault-propagation folding: *Geology, v.* 19, p. 617-620.

Espurt, N., J-P. Challot, J. Totterdell, H. Struckmeyer, and R. Vially, 2009, Interactions between continental breakup dynamics and large scale delta system evolution: Insights from the Cretaceous Ceduna delta system, Bight Basin, Southern Australian margin: Tectonics, v. 28, p. 1-16.

Evamy, B. D., J. Haremboure, P. Kamerling, W. A. Knaap, F. A. Molloy, and P. H. Rowlands, 1978, Hydrocarbon habitat of Tertiary Niger Delta: AAPG Bulletin, v. 62, p. 1-39.

Feinstein, S., Y. Eyal, and J. S. Bell, 1999, Implications of meso-structures for deformational history of the Moose Mountain structure, Canadian Rocky Mountain foothills: Journal of Structural Geology, v. 21, p. 55-66.

Finch, W. C., 1969, Abnormal Pressure in Antelope Field North Dakota: Journal of Petroleum Technology, v. 213, p. 170-179.

Fisher, M. P., and P. B. Jackson, 1999, Stratigraphic controls on deformation patterns in fault-related folds: a detachment fold example from the Sierra Madre Oriental, northeast Mexico: Journal of Structural Geology, v. 21, p. 613-633.

Fort, X., and J.-P. C. F. Brun, 2004, Salt tectonics on the Angolan margin, synsedimentary deformation processes: AAPG Bulletin, v. 88, p. 1523-1544.

Gamberei, R., and M. Rovere, 2010, Mud diapirs, mud volcanoes and fluid flow in the rear of the Calabrain Arc orogenic Wedge (southeastern Tryyhenian sea): Basin Research: v. 22, p. 452-464.

Gaullier, V., Y. Mart, G. Bellaiche, J. Mascle, B. Vendeville, T. Zitter, and the second leg 'PRISMED II' scientific party, 2000. Salt Tectonics in and around the Nile deep-sea fan: Insights from the 'PRISMED II' cruise. In the arctic to the Mediterranean: Salt, shale and igneous diapirs in and around Europe Geological Society Special Publication. pp. 111–129.

Gibbs, A. D., 1984, Structural evolution of extensional basin margins: Journal of Geological Society London, v. 141, p. 609-620.

Graue, K., 1999, Mud volcanoes in deep-water Nigeria: Marine and Petroleum Geology, v. 17, p. 959-974.

Grauls, D., 1999, Overpressures: Causal Mechanisms, Conventional and Hydromechanical Approaches: Oil & Gas Science and Technology – Rev. IFP, v. 54,, p. 667-678.

Groshong R. H., 1989, Half-graben structures: Balanced models of extensional fault-bend folds: Geological Society of America Bulletin, v. 101, p. 96–105.

Groshong, R. H., and J.-L. Epard, 1994, The role of strain in area-constant detachment folding: Journal of Structural Geology, v. 16, p. 613-618.

Guerlais, S. -H., 2000, Modélisation des règimes de pression dans le prisme d'accrétion de le Barbade à partir des données ODP. M.Sc. degree memoir., IFP report 55546.

Gutierrez, M., R. Nygård, K. Høeg, T. Berre, 2008, Normalized undrained shear strength of clay shales: Engineering Geology, v. 99, p. 31–39.

Guy, D. H. S., 2009, Influence of the mechanical behaviour of brittle-ductile fold-thrust belts on the development of foreland basins: Basin Research, v. 22, p. 139-156.

Hardy, S., and J. Poblet, 1994, Geometric and numerical model of progressive limb rotation in detachment folds: Geology, v. 22, p. 371-374.

Harrison, J. C., 1995, Tectonics and kinematics of a foreland folded belt influenced by salt, Arctic Canada, in M. P. A. Jackson, D. G. Roberts, and S. Snelson eds., Salt tectonics: a global perspective: AAPG Memoir 65, p. 379–412.

Hedberg, H. D., 1974, Relation of Methane Generation to Undercompacted Shales, Shale Diapirs, and Mud Volcanoes: AAPG Bulletin, v. 58, p. 668-673.

Heiniö, P. and R. J. Davies, 2006, Degradation of compressional fold belts: Deep-water Niger Delta: AAPG, v. 90, p. 753-770.

Higgins, S., R. J. Davies, and B. Clarke, 2007, Antithetic fault linkages in a deep-water fold and thrust belt: Journal of Structural Geology, v. 29, p. 1900-1914.

Homza, T. X., and W. K. Wallace, 1995, Geometric and kinematic models for detachment folds with fixed and variable detachment depths: Journal of Structural Geology, v. 17, p. 575-588.

Homza, T. X., and W. K. Wallace, 1997, Detachment folds with fixed hinges and variable detachment depth, northeastern Brooks Range, Alaska: Journal of Structural Geology, v. 19, p. 337-354.

Hooper, R. J., R. J. Fitzsimmons, N. Grant, and B. C. Vendeville, 2002, The role of deformation in controlling depositional patterns in the south-central Niger Delta, West Africa: Journal of Structural Geology, v. 24, p. 847-859.

Hubbert, M. K., and W. W. Rubey, 1959, Mechanics of Fluid Filled Porous Solids and its Application to Overthrust Faulting. 1, Role of Fluid Pressure in Mechanics of Overthrust Faulting: Geological. Society of America Bulletin, v. 70, p. 115-166.

Huuse, M., C. A.-L. Jackson, P. V. Rensenbergen, R. J. Davies, P. B. Flemings, and R. J. Dixon, 2010, Subsurface sediment remobilization and fluid flow in sedimentary basins: an overview: Basin Research, v. 22, p. 342-360.

Iacopini, D., and R. W. H. Butler, 2011, Imaging deformation in submarine fold and thrust belts using seismic attributes: Earth and Planetary Science Letter, v. 302, p. 414-422.

Ibanez, W. D., and A. K. Kronenberg, 1993, Experimental Deformation of Shale - Mechanical-Properties and Microstructural Indicators of Mechanisms: International

Journal of Rock Mechanics and Mining Sciences & Geomechanics Abstracts, v. 30, p. 723-734.

Imber, J., C. Childs, P. A. R. Nell, J. J. Walsh, D. Hodgetts, and S. Flint, 2003, Hanging wall fault kinematics and footwall collapse in listric growth fault systems: Journal of Structural Geology, v. 25, p. 197-208.

Jackson M. P. A., and C. Cramez, 1989, Seismic recognition of salt welds in salt tectonics regimes: Gulf Coast Section of the Society of Economic Palentologists and Mineralogists Tenth Annual Research Conference Program and Abstracts, Houston, TX, USA p. 66–71.

Jackson M. P. A., and B. C. Vendeville, 1994, Regional extension as a trigger for diapirism: Geological Society of America Bulletin, v. 106, p. 57-73.

Jaeger, J. C., N. G. W. Cook, and R. W. Zimmerman, 2007, Fundamentals of rock mechanics: Blackwell Publishing.

Janik, A. G., J. A. Hood, and M. V. Ask, 1998, Physical properties data at Hole 959D: Comparison of core and log measurements and a proposed revision of lithologic units: In, Proceedings of the Ocean Drilling Program, Scientific results (Ed. by J. Mascle, G. P. Lohmann, M. Moullade et al.,) v. 159: Collage Station, Texas, Ocean drilling Program, p. 241-248.

Jamison, W. R., 1987, Geometric analysis of fold development in overthrust terranes: Journal of Structural Geology, v. 9, p. 207-219.

Jolly, R. J. H., and L, Lonergan, 2002, Mechanisms and controls on the formation of sand intrusions: Journal of the Geological Society 2002; v. 159; p. 605-617.

kearey, P., M. Brooks, and I. Hill, 2002, An Introduction to Geophysical Exploration: Blackwell Science, third edition

Knox, G.J., and E. M.Omatsola, 1989, Development of the Cenozoic Niger Delta in terms of the "escalator regression" model and impact on hydrocarbon distribution. In, Proceedings of the symposium on Coastal lowlands; geology and geotechnology. (Eds, W.J.M. van der Linden et al..) Dordrecht, Kluwer, p. 181-202.

Latta, D. K., and D. J. Anastasio, 2007, Multiple scales of mechanical stratification and décollement fold kinematics, Sierra Madre Oriental foreland, northeast Mexico: Journal of Structural Geology, v. 29, p. 1241-1255.

Leduc, A., R. J. Davies, A. L. Densmore, and J. Imber, 2011, The lateral strike-slip domain in gravitational detachment delta systems: A case study of the northwest margin of the Niger Delta: AAPG Bulletin, In Review.

Lehner, P., and P. A. C. De Ruiter, 1977, Structural history of Atlantic margin of Africa: AAPG Bulletin, v. 61, p. 961-981.

Lister, G. S., M. A. Etheridge, and P. A. Symonds, 1986 Detachment faulting and the evolution of passive continental margins: Geology, v. 14, p. 246-250.

Lister, G. S. and G. Davis, 1989, The origin of metamorphic core complexes and detachment faults formed during Tertiary continental extension in the northern Colorade River region, U.S.A: Journal of Structural Geology, v. 11, p. 65-94.

Loncke, L., J. Mascle, and Fanil Scientific Parties, 2004, Mud volcanoes, gas chimneys, pockmarks and mounds in the Nile deep-sea fan (Eastern Mediterranean): geophysical evidences: Marine and petroleum Geology, v. 21, p. 669-689.

Lorenz, J.C., L.W. Teufel, and N. R. Warpinski, 1991, Regional fractures 1: a mechanism for the formation of regional fractures at depth in flat-lying reservoirs: AAPG Bulletin, v. 75, p. 1714–1737.

Maloney, D. P., R. Davies, J, Imber, and S. King, 2010, New insights into deformation mechanisms in the Niger Delta gravity driven fold and thrust belt: AAPG Bulletin, v. 94, p. 1401-1424.

Maltman, A., 1987, Shear zones in argillaceous sediments-an experimental study. In: Deformation of Sediments and Sedimentary Rocks (Ed. by M.E. Jones and R. M. F. Preston) Geological Society, London, Special Publications, v. 29, p. 77-87.

Maltman, A., 1994, The geological deformation of sediments (Ed. by A. Maltman): London; New York, N.Y: Chapman & Hall.

Maltman, A. J., and A. Bolton, 2003, How sediments become mobilized. In: Subsurface Sediment Mobilization (Ed. by P. V. Rensbergen, R. R. Hillis, A. J. Maltman, and C. K. Morley) Geological Society, London, Special Publications, v. 216, p. 9-20.

Martínez, A., L. Rivero, and A. Casas, 1997, Integrated gravity and seismic interpretation of duplex structures and imbricate thrust systems in the southeastern Pyrenees (NE Spain): Tectonophysics, v. 282, p. 303-329.

Matos, R. M. D., 1993, Geometry of the Hanging Wall above a System of Listric Normal Faults—A numerical solution: AAPG Bulletin, v. 77, p. 1839-1859.

McClay, K. R., 1990, Extensional fault systems in sedimentary basins: a review of analogue model studies: Marine and Petroleum Geology, v. 7, p. 206-233.

McClay, K. R., 1995, The geometry and kinematics of inverted fault systems: a review of analogue model studies: Geological Society, London, Special Publications, v. 88, p. 97-118.

McClay, K. R., D. A. Waltham, A. D. Scott, and A. Abousetta, 1991, Physical and seismic modelling of listric normal fault geometries: Geological Society, London, Special Publications, v. 56, p. 231-239.

McClay, K. R., T. Dooley, and G. Lewis, 1998, Analog modeling of progradational delta systems: Geology, v. 26, p. 771-774.

McClay, K. R., T. Dooley, and G. Zamora, 2003, Analogue models of delta systems above ductile substrates: In: Subsurface Sediment Mobilization (Ed. by P. V. Rensbergen et al.,) Geological Society, London, Special Publications, v. 216 p. 411-428.

Midland Valley, 2010, Midland Valley 2D Move Training Course.

Mills, P. C., 1983, Genesis and diagnostic value of soft-sediment deformation structures—A review: Sedimentary Geology, v. 2, p. 83-102.

Mitra, S., 1990, Fault-propagation folds; geometry, kinematic evolution, and hydrocarbon traps: AAPG Bulletin, v. 74, p. 921-945.

Mitra, S., 2002, Structural models of faulted detachment folds: AAPG Bulletin, v. 86, p. 1673–1894.

Mitra, S., 2003, A unified kinematic model for the development of detachment folds: Journal of structural Geology, v. 25, p. 1659-1673.

Mitra, S., and J. Namson, 1989, Equal-area balancing: American Journal of Science, v. 289, p. 563-599.

Mondol, N. H., K. Bjorlykke, J. Jahren, and K. Hoeg, 2007, Experimental mechanical compaction of clay mineral aggregates - Changes in physical properties of mudstones during burial: Marine and Petroleum Geology, v. 24, p. 289-311.

More, J. C., and A. Klaus, the scientific party, 1998, Consolidation patterns during initiation and evolution of a plate boundary decollement zone: Northern Barbados accretionary prism: Geology, v. 26, p. 811-814.

Morgan, R., 2001, Structural controls on the positioning of submarine channels on the lower slopes of the Niger Delta, in , Davies, R. J., j. A. Cartwright, S. A. Stewart, M. Lappin, and J. R. Underhill eds. 3D Seismic Technology: Application to the Exploration of Sedimentary Basins. Geological Society of London Memoir 29, p. 45-51.

Morgan, R., 2003, Prospectivity in ultradeep-water the case for petroleum generation and migration with the outer parts of the Niger Delta apron. In: Petroleum Geology of Africa: New Themes and Developing Technologies (Ed. by T. J. Authur, D. S. MacGregor & N. R. Cameron), Geological Society London, Special Publication, v. 207, p. 45-51.

Morley, C. K., 2003A, Mobile shale related deformation in large deltas developed on passive and active margins. In: Subsurface Sediment Mobilization (Ed. by P. V. Rensbergen, R. R. Hillis, A. J. Maltman, and C. K. Morley) Geological Society, London, Special Publications, v. 216, p. 335-357.

Morley, C. K., 2003B, Outcrop examples of mudstone intrusions from the Jerudong anticline, Brunei darussalam and inferences for hydrocarbon reservoirs. In, Subsurface Sediment Mobilization (Ed. by P. V. Rensbergen, R. R. Hillis, A. J. Maltman, and C. K. Morley) Geological Society, London, Special Publications, v. 216, p. 381-394.

Morley, C. K., 2009, Geometry of an oblique thrust fault zone in a deep-water fold belt from 3D seismic data: Journal of Structural Geology, v. 31, p. 1540-1555.

Morley, C, K., and G. Guerin, G, 1996, Comparison of gravity-driven deformation styles and behaviour associated with mobile shale and salt: Tectonics, v. 15, p. 1154-1170.

Morley, C. K., P. Crevello, and Z. H. Ahmad, 1998, Shale tectonics and deformation associated with active diapirism: the Jerudong Anticline, Brunei Darussalam: Journal of the Geological Society, v. 155, p. 475-490.

Moscardelli, L., L. Wood, and P. Mann, 2006, Mass-transport complexes and associated processes in the offshore area of Trinidad and Venezuela: AAPG Bulletin, v. 90, p. 1059-1088.

Musgrave, A. W., and W. G. Hicks, 1966, Outlining shale masses by geophysical methods: Geophysics, v. 31, p. 711–725,

Noack, T., 1995, Thrust development in the eastern Jura Mountains related to pre-existing extensional structures: Tectonophysics, v. 252, p. 419-431.

Nygard, R., M. Gutierrez, R. K. Bratli, and K. Hoeg, 2006, Brittle-ductile transition, shear failure and leakage in shales and mudrocks: Marine and Petroleum Geology, v. 23, p. 201-212.

Osborne, M. J., and R. E. Swarbrick, 1997, Mechanisms for generating overpressure in sedimentary basins; a reevaluation: AAPG Bulletin, v. 81, p. 1023-1041.

Owoyemi, A. O., and B. J. Willis, 2006, Depositional Patterns Across Syndepositional Normal Faults, Niger Delta, Nigeria: Journal of Sedimentary Research v. 76, p. 346-363.

Pennebaker, E.S. Jr., 1968, An engineering interpretation of seismic data: Journal Society of. Petroleum Engineers p. 2168 SPE.

Petley, D. N., 1999, Failure envelopes of mudrocks at high confining pressures: Geological Society, London, Special Publications 1999; v. 158; p. 61-71.

Plesch, A., J. H. Shaw, and D. Kronman, 2007, Mechanics of low-relief detachment folding in the Bajiaochang field, Sichuan Basin, China: AAPG Bulletin, v. 91, p. 1559-1575.

Price, N.J., and J. W. Cosgrove, 1990, Analysis of Geological Structures: Cambridge University Press, Cambridge.

Problet, J., and K. McClay, 1996, Geometry and kinematics of single-layer detachment folds: AAPG Bulletin, v. 80, p. 1085-1109.

Problet, J., K. McClay, F. Storti, and J. A. Muñoz, 1997, Geometries of syntectonic sediments associated with single-layer detachment folds: Journal of Structural Geology, v. 19, p. 369-381.

Problet, J., M. Bulunes, K. McClay, and S. Hardy, 2004, Plots of crestal structural relief and fold area verses shortening - A graphical technique to unravel the kinematics of thrust-related folds. In Thrust Tectonics and Hydrocarbon Systems (Ed. K. R. McClay): AAPG Memoir 82, p. 372-399.

Problet, J., and M. Bulnes, 2005, Fault-slip, bed-length and area variations in experimental rollover anticlines over listric normal faults: influence in extension depth to detachment estimations: Tectonophysics, v. 396, p. 97-117.

Potter, P. E., J. B. Maynard, and W. A. Pryor, 1980, Sedimentology of Shale: Study guide and reference source: Springer-Verlag, New York.

Ramsay, J. G., and M. I. Huber, 1987, The Techniques of Modern Structural Geology, Volume 2: Folds and Fractures. Academic Press, New York.

Roberts, K. S., R. J. Davies, and S. A. Stewart, 2010, Structure of exhumed mud volcano feeder complexes, Azerbaijan: Basin Research, v. 22, p. 439-451.

Roscoe, K. H., 1970, The influence of strains in soil mechanics: Tenth Rankine Lecture.

Rouby, D., and P. R. Cobbold, 1996, Kinematic analysis of a growth fault system in the Niger Delta from restoration in map view: Marine and Petroleum Geology, v. 13, p. 565-580.

Rowan, M. G., 1997, Three-dimensional geometry and evolution of a segmented detachment fold, Mississippi Fan foldbelt, Gulf of Mexico, Penrose conference on Fault-related folding. D. J. Anastasio, E. A. Erslev, D. M. Fisher and J. P. Evans, Pergamon, 19, p. 463-480.

Rowan, M. G., F. J. Peel, and B. C. Vendeville, 2004, Gravity-driven foldbelts on passive margins. In: Thrust tectonics and hydrocarbon systems(Ed. by K. R. McClay): AAPG Memoir 82, p. 159-184.

Rutter, E. H., 1986, On the nomenclature of failure transitions in rocks: Tectonophysics, v. 122, p. 381-387.

Salisbury, M. H., and C. E. Keen, 1993, Listric faults imaged in oceanic crust: Geology, v. 21, p. 117-120.

Sandwell, D. T., and W.H.F. Smith, 1997, Marine gravity anomaly from Geosat and ERS-1 satellite altimetry: Journal of Geophysical Research, v. 102, p. 10039–10050

Sclater, J. G., and P. A. F. Christie, 1980, Continental stretching: an explanation of the post-mid-Cretaceous subsidence of the Central North Sea basin: Journal of Geophysical Research, v. 85, p. 3711-3739.

Schöpfer, M. P. J., C. Childs, and J. J. Walsh, 2006, Localisation of normal faults in multilayer sequences: Journal of Structural Geology, v. 28, p. 816-833.

Schultz-Ela, D. D., 2001, Excursus on gravity gliding and gravity spreading: Journal of structural Geology, v. 23, p. 7 25-731.

Serra, S. and R. A. Nelson, 1988, Clay modeling of rift asymmetry and associated structures: Tectonophysics, v. 153, p. 307–312.

Shaw, J. H., E. Novoa, and C. D. Connors, 2004, Structural controls on growth stratigraphy in contractional fault-related folds. In: Thrust tectonics and hydrocarbon systems (Ed. by K. R. McClay): AAPG Memoir 82, p. 400 – 412.

Shelton, J. W., 1984, Listric normal faults: an illustrated summary: AAPG Bulletin, v. 86, p. 801-815.

Sheriff, R., and L. Geldart, 1995, Exploration seismology: Cambridge.

Short, K. C., and A. J. Stäuble, 1967, Outline of geology of Niger Delta.: AAPG Bulletin, v. 51, p. 761-779.

Sibson, R.H., 1985, A note on fault reactivation: Journal of Structural Geology, v. 7, p. 751-754.

Sibson, R.H., 2003, Brittle-failure controls on maximum sustainable overpressure in different tectonic regimes: AAPG Bulletin, v. 87, p. 901-908.

Simm, R., and R. White, 2002, Tutorial: Phase, polarity and the interpreter's wavelet: First Break, v. 20, p. 277-281.

Smith, D.K., J. R. Cann, and J. Escartin, 2006, Widespread active detachment faulting and core complex formation near 13N on the Mid-Atlantic Ridge: Nature, v. 442, p. 440–443.

Song, T., and P. A. Cawood, 2001, Effects of subsidiary faults on the geometric construction of listric normal fault systems: AAPG Bulletin., v. 85, p. 221-232.

Stewart, S. A., 1996, Influence of detachment layer thickness on style of thin-skinned shortening: Journal of Structural Geology, v. 18, p. 1271-1274.

Stewart, S. A., and J. D. Argent, 2000, Relationship between polarity of extensional fault arrays and presence of detachments: Journal of Structural Geology, v. 22, p. 693-711.

Stewart, S. A., and R. J. Davies, 2006, Structure and emplacement of mud volcano systems in the South Caspian Basin: AAPG Bulletin, v. 90, p. 771-786.

Suppe, J., 1983, Geometry and kinematics of fault-bend folding: American Journal of Science, v. 283, p. 684-721.

Suppe, J., 1985, Principles of structural geology: Englewood Cliffs, New Jersey, Prentice Hall.

Suppe, J., and D. A. Medwedeff, 1990, Geometry and kinematics of fault-propagation folding: Eclogae Geologicae Helvetiae, v. 83, p. 409–454.

Suppe, J., G. T. Chou, and S. C. Hook, 1992, Rates of folding and faulting determined from growth strata, In K. R. McClay ed., Thrust Tectonics, p. 105-121.

Suppe, J., C. D. Connors, and Y. Zhang, 2004, Shear Fault-bend Folding, In K. R. McClay, ed., Thrust tectonics and hydrocarbon systems: AAPG Memoir 82, p. 303-323.

Swan, G., J. Cook, S. Bruce, and R. Meehan, 1989, Strain Rate Effects in Kimmeridge Bay Shale: International Journal of Rock Mechanics and Mining Sciences & Geomechanics Abstracts, v. 26, p. 135-149.

Swarbrick R., and Osborne, 1998, Mechanisms that generate abnormal overpressures: an Overview. In, law, B. E., G. F. Ulmishek, and V. I. Slavin eds., Abnormal pressures in hydrocarbon environments: AAPG Memoir, v. 70, p, 13-34.

Swarbrick, R. E., M. J. Osborne, and G. S. Yardley, 2002, Comparison of Overpressure Magnitude Resulting from the Main Generating Mechanisms. In: Pressure regimes in sedimentary basins and their prediction (Ed. A. R. Huffman and G. L. Bowers, eds): AAPG Memoir, v. 76, p. 1–12.

Terzaghi, 1925, Principles of soil mechanics: I-phenomena of cohesion of clays. IV-settlement and consolidation of clay: Engineering News-Record, v. 95, p. 742-746, 874-878.

Tingay, M. R. P., R. R. Hillis, R. E. Swarbrick, C. K. Morley, and A. R. Damit, 2009, Origin of overpressure and pore-pressure prediction in the Baram province, Brunei: AAPG Bulletin, v. 93, p. 51-74.

Totterdell, J. M., and A. A. Krassay, 2003, The role of shale deformation and growth faulting in the Late Cretaceous evolution of the Bight Basin, offshore southern Australia. In: Subsurface Sediment Mobilization (Ed. by P. V. Rensbergen, R. R. Hillis, A. J. Maltman, and C. K. Morley) Spec. Publ. Geol Soc London., v. 216, p. 429-442.

Van Rensbergen, P., C. K. Morley, D. W. Ang, T. Q. Hoan, and N. T. Lam, 1999, Structural evolution of shale diapirs from reactive rise to mud volcanism: 3D seismic data from the Baram delta, offshore Brunei Darussalam: Journal of the Geological Society, v. 156, p. 633-650.

Van Rensbergen, P., and C. K. Morley, 2000, 3D Seismic study of a shale expulsion syncline at the base of the Champion delta, offshore Brunei and its implications for the early structural evolution of large delta systems: Marine and Petroleum Geology, v. 17, p. 861-872.

Van Rensbergen, P., R. R. Hillis, A. J. Maltman, and C. K. Morley, 2003, Subsurface sediment mobilization: introduction: In: Subsurface Sediment Mobilization (Ed. by P. V. Rensbergen, R. R. Hillis, A. J. Maltman, and C. K. Morley) Geological Society, London, Special Publications, v. 216, p. 1-8.

Van Rensbergen, P., and C. K. Morley, 2003, Re-evaluation of mobile shale occurrences on seismic sections of the Champion and Baram deltas, offshore Brunei: In: Subsurface Sediment Mobilization (Ed. by P. V. Rensbergen, R. R. Hillis, A. J. Maltman, and C. K. Morley) Geological Society, London, Special Publications, v. 216, p. 395-409.

Vendeville, B. C., and M. P. A. Jackson, 1992, The rise of diapirs during thin-skinned extension: Marine and Petroleum Geology, v. 17, p. 937-958.

Waltham, D., 1997, Why does salt start to move?: Tectonophysics, v. 282, p. 117-128.

Wernicke, B., 1981, Low-angle normal faults in the Basin and Range province: Nappe tectonics in an extended orogen: Nature, v. 291, p. 645-648.

Wheeler, J., 1987, Variable models of deformation above listric normal faults: the importance of area conservation: Journal of Structural Geology, v. 9, p. 1047-1049.

Weijermars, R., M. P. A. Jackson, and B. C. Vendeville, 1993, Rheological and tectonic modelling of salt provinces: Tectonophysics, v. 217, p. 143-174.

Weimer, P., and R. T. Buffler, 1992, Structural Geology and Evolution of the Mississippi Fan Fold Belt, Deep Gulf of Mexico: AAPG Bulletin, v. 76, p. 225-251.

White, N. J., 1992, A method for automatically determining normal fault geometry at depth: Journal of Geophysical Research, v. 97 (B2), p. 1715-1733.

White, N. J., and G. Yielding, 1991, Calculating normal fault geometries at depth: theory and examples. In: The Geometry of Normal Faults (Ed. by A. M. Roberts, G. Yielding & B. Freeman,), Geological Society London Special Publication 56, pp. 251-260.

White, N. J., J. A. Jackson, and D. P. McKenzie, 1986, The relationship between the geometry of normal faults and that of sedimentary layers in their hanging walls: Journal of Structural Geology, v. 8, p. 897-909.

William, G. and I. Vann, 1987, The geometry of listric normal faults and deformation within their hangingwalls: Journal of Structural Geology, v. 9, p. 789-795.

Withjack, M. O., and E. T. Peterson, 1993, Prediction of normal-fault geometries—a sensitivity analysis: AAPG Bulletin, v. 77, p. 1860-1873.

Wood, L. J., 2000, Chronostratigraphy and Tectonostratigraphy of the Columbus Basin, Eastern Offshore Trinidad: AAPG Bulletin, v. 84, p. 1905-1928.

Woodward, N. B., 1997, Low-amplitude evolution of break-thrust folding. In Penrose conference on Fault-related folding (Eds. D. J. Anastasio, E. A. Erslev, D. M. Fisher, and J. P. Evans), v. 19, Pergamon, p. 293-301

Yamada, Y., and K. R. McClay, 2003A, Application of geometric models to inverted listric fault systems in sandbox experiments. Paper 1: 2D hanging wall deformation and section restoration: Journal of Structural Geology, v. 25, p. 1551-1560.

Yamada, Y., and K. R. McClay, 2003B, Application of geometric models to inverted listric fault systems in sandbox experiments. Paper 2: insights for possible along strike migration of material during 3D hanging wall deformation: Journal of Structural Geology, v. 25, p. 1331-1336.

Yassir, N. A. 1989. Mud volcanoes and the behaviour of overpressured clays and silts. Ph.D. thesis, University of London.

Yassir, N., 2003, The role of shear stress in mobilizing deep-seated mud volcanoes: geological and geomechanical evidence from Trinidad and Taiwan. In: Subsurface Sediment Mobilization (Ed. by P. V. Rensbergen, R. R. Hillis, A. J. Maltman, and C. K. Morley) Geological Society, London, Special Publications, v. 216, p. 461-474.